Final Report
June 15, 2005

Critical Factors for the Transition from Chromate to Chromate-Free Corrosion Protection

PP-1119
ARO contract number DACA72-99-C-0002.

A research program conducted by:

The Ohio State University
Air Force Research Laboratory
Army Research Laboratory

Report Prepared by The Ohio State University

For:

The Strategic Environmental Research and Development Program

CLEARANCE REQUEST FOR PUBLIC RELEASE OF DEPARTMENT OF DEFENSE INFORMATION

(See Instructions on back.)

(This form is to be used in requesting review and clearance of DoD information proposed for public release in accordance with DoDD 5230.9.)

TO: Director, Freedom of Information & Security Review, Rm. 2C757, Pentagon

1. DOCUMENT DESCRIPTION

a. TYPE Final Report	b. TITLE Critical Factors for the Transition from Chromate to Chromate-Free Corrosion Protection (PP-1119)
c. PAGE COUNT 182	d. SUBJECT AREA Strategic Environmental Research & Development Program (SERDP)

2. AUTHOR/SPEAKER

a. NAME *(Last, First, Middle Initial)* Buchheit, Rudolph	b. RANK	c. TITLE
d. OFFICE Ohio State University		e. AGENCY Ohio State University

3. PRESENTATION/PUBLICATION DATA *(Date, Place, Event)*

Posting on the SERDP web site.

CLEARED
For Open Publication
DEC 28 2005 3
Office of Freedom of Information
and Security Review
Department of Defense

4. POINT OF CONTACT

a. NAME *(Last, First, Middle Initial)* Rusk, Jennifer	b. TELEPHONE NO. *(Include Area Code)* 703-326-7801

5. PRIOR COORDINATION

a. NAME *(Last, First, Middle Initial)*	b. OFFICE/AGENCY	c. TELEPHONE NO. *(Include Area Code)*
Smith, Bradley	SERDP Executive Director	703-696-2121
Pellerin, Charles	SERDP Pollution Prevention Program Manager	703-696-2128

6. REMARKS

THE INFORMATION CONTAINED IN THIS REPORT FALLS UNDER THE PURVIEW OF THIS OFFICE.

WHEN CLEARED, PLEASE FAX DD-1910 TO 703-478-0526. ATTN: Jennifer Rusk (phone: 703-326-7801)

if mailed: ATTN: Jennifer Rusk, 1155 Herndon Parkway, Suite 900, Herndon, VA 20170

7. RECOMMENDATION OF SUBMITTING OFFICE/AGENCY

a. THE ATTACHED MATERIAL HAS DEPARTMENT/OFFICE/AGENCY APPROVAL FOR PUBLIC RELEASE *(qualifications, if any, are indicated in Remarks section)* AND CLEARANCE FOR OPEN PUBLICATION IS RECOMMENDED UNDER PROVISIONS OF DODD 5320.9. I AM AUTHORIZED TO MAKE THIS RECOMMENDATION FOR RELEASE ON BEHALF OF:

Strategic Environmental Research & Development Program

b. CLEARANCE IS REQUESTED BY 20051208 *(YYYYMMDD).*

c. NAME *(Last, First, Middle Initial)* Smith, Bradley P.	d. TITLE Executive Director, Strategic Environmental R&D Program
e. OFFICE SERDP	f. AGENCY USD (AT&L)
g. SIGNATURE	h. DATE SIGNED *(YYYYMMDD)* 20051118

DD FORM 1910, MAR 1998 (EG) PREVIOUS EDITION MAY BE USED. WHS/DIOR, Mar 98

Table of Contents

Principal Investigator Contact Information	1
List of Figures	2
List of Tables	9
Acknowledgements	10
Executive Summary	11
Objective	13
Background	15
Results and Accomplishments Part I: Corrosion Inhibition of Al and Al Alloys by Soluble Chromates, Chromate Coatings, and Chromate-Free Coatings	16
Results and Accomplishments Part II: Corrosion Protection of Aluminum 2024-T3 by Vanadate Conversion Coatings	66
Results and Accomplishments Part III: Active Corrosion Protection and Corrosion Sensing in Chromate-Free Organic Coatings	97
Results and Accomplishments Part IV: Integrated Coating System Evaluation	119
List of Technical Publications	159
Appendix	164

Principal Investigator Contact Information

For information regarding the content of this report contact:

Rudolph G. Buchheit
Professor-Materials Science and Engineering
Department of Materials Science and Engineering
477 Watts Hall
2041 College Rd.
Columbus, Ohio 43210

buchheit.8@osu.edu
Tel. (614) 292-6085
FAX (614) 292-9857

List of Figures

Research and Accomplishments Part I:

Figure 1. Relative concentration of the oxo-Cr^{6+} species as a function of pH for a total Cr^{6+} concentration of (a) 10^{-6} M and (b) 1 M. (c) 0.075M, a typical concentration for a conversion coating.

Figure 2. Relative piezo-electrokinetic response (unitless) as a function of pH for 0.01F oxo-Cr^{6+} and 0.01 M sodium nitrate or hydroxide.

Figure 3. Cathodic polarization curves on 2024-T3 in actively oxygen -sparged 1M NaCl solution with (a) dichromate additions, and (b) 0.3 vol% peroxide and dichromate additions.

Figure 4. Polarization response of a Cu RDE in 5% NaCl solution with Cr(VI) and Ce(III) inhibitor additions.

Figure 5. Dependence of the pitting potential of Al on the chloride: chromate ratio. H. Kaesche, Localized Corrosion III, p. 516, NACE, Houston, TX (1971).

Figure 6. Relative concentration of the oxo-Cr^{6+} species as a function of pH in the pH 0-3 range for a total Cr^{6+} concentration of 0.01 M.

Figure 7. Current vs. time for 600 grit polished Al 1100 polarized at $-0.500V_{sce}$ in 1M chloride solution at (a) pH ~1 and (b) pH ~0.

Figure 8. The ratio of steady state current at $-0.500V_{sce}$ in the presence to that in the absence of oxo-Cr^{6+} as a function of pH.

Figure 9. AFM image for a freshly polished (0.01 micron) Al 2024-T3 surface exposed for 3 seconds to Alodine solution at 5° C.

Figure 10. (a) Schematic representation of the hydrolysis-polymerization-precipitation mechanism for $Cr(OH)_3$ "backbone formation. (b) Condensation of Cr(VI) on the Cr(III) backbone by nucleophilic attack of hydroxyl ligands in the backbone.
L. Xia, R.L. McCreery, J. Electrohem. Soc., 145, 3083 (1998).

Figure 11. Normalized intensity of the $859cm^{-1}$ Cr^{3+}-O-Cr^{6+} scattering band as a function of coating time. A representative current versus time trace is shown for comparison. Electrode area was $0.008cm^2$.

Figure 12. Transmission electron micrograph of a CCC stripped from a 99.98% pure Al substrate. CCC was formed by a 5 s immersion in $Cr_2O_7^{2-}/F^-$ solution at sub-ambient temperature. Local Cr-rich deposits (location b) are located on grain boundaries or pre-

existing metal ridge. Microchemical analysis of regions away from nodules (location a) suggest non-uniform CCC formation across the surface. G.M. Brown, K. Shimuzu, K. Kobayashi, G.E. Thompson, G.C. Wood, Corrosion Sci., 33, 1371 (1992).

Figure 13. (a) Optical micrograph of a conversion coated S phase particle colony in 2024-T3. The dashed line approximates the boundaries of the particle colony. (b) Intensity map of the 859cm^{-1} Cr^{3+}-O-Cr^{6+} Raman band over the region in (a). The absence of intensity over the location of the particle indicates atypical CCC formation on the S phase particle.

Figure 14. Periodic Table of the elements, compounds of which (shaded) have been considered as alternatives for oxo-Cr^{6+} inhibitors.

Figure 15. Pourbaix diagrams for Cr, Mn, Tc and Mo, elements that have soluble hypervalent oxo-anions that reduce to form insoluble oxide. Note that the pH region of stability for the insoluble oxides is very broad for Cr, Mn, and Tc, but not Mo.

Research and Accomplishments Part II:

Figure 1. (a) Photograph of the simulated scratch cell. (b) Schematic cross section of the cell.

Figure 2. Anodic polarization curves for 2024-T3 exposed to aerated 0.124 M NaCl solution pH 6 with and without additions of 0.1M $NaVO_3$.

Figure 3. Cathodic polarization curves for 2024-T3 exposed to aerated 0.124 M NaCl solution pH 6 with and without additions of 0.1M $NaVO_3$.

Figure 4. Complex plane plots of EIS data collected from 2024-T3 exposed to aerated 0.1M NaCl plus 0.1M $NaVO_3$ for various lengths of time.

Figure 5. Variation of R_c with exposure time for 2024-T3 exposed to aerated 0.1M NaCl with additions of vanadate, chromate, or with no inhibitor additions.

Figure 6. A summary of the effect of VCC bath chemistry on coating corrosion resistance. Corrosion resistance is characterized by R_c determined from EIS data collected after exposure to aerated 0.1M NaCl for 24 hours. VCC bath pH was varied from 1 to 8.5. Coatings were also made with and without additions of NaF and $K_3Fe(CN)_6$. (a) 10mM $NaVO_3$ + 3mM NaF + 2mM $K_3Fe(CN)_6$, (b) 10mM $NaVO_3$ + 3mM $K_3Fe(CN)_6$, (c) 10mM $NaVO_3$ + 2mM NaF.

Figure 7. Scanning electron micrographs of (a, b, and d) vanadate and (c) chromate conversion coatings. Micrographs c and d show the two coatings at identical magnifications for comparison.

Figure 8. Composition depth profiles for Al, O, and V through a VCC collected by Auger electron spectroscopy. Sputtering rate is estimated to by 10 nm/minute based on SiO_2 standard.

Figure 9. XANES of a VCC at the vanadium K absorption edge. The absorption spectrum includes a pre-edge peak due to the presence of V^{5+} in the coating.

Figure 10. Photographs of a VCC on 2024-T3 in the (a) as-coated condition, (b) after 168 hours of salt spray exposure, and (c) bare 2024-T3 after 168 hours of salt spray exposure. Coupon sizes are approximately 50 x 100mm.

Figure 11. .VCC corrosion resistance determined by EIS testing. R_c values, indicated by data points scatter bands, were determined after exposure to aerated 0.5M NaCl solution. The upper band indicates the range of R_c values measured for CCCs in this environment. The lower band indicates the range in R_c values measured for uncoated Al alloys.

Figure 12. Anodic polarization curves for VCC coated 2024-T3 collected in aerated 0.5M NaCl. The time notations refer to the length of time the samples were immersed in the coating bath. The “bare” sample was uncoated.

Figure 13. Cathodic polarization curves for VCC coated 2024-T3 collected in aerated 0.5M NaCl. The time notations refer to the length of time the samples were immersed in the coating bath. The “bare” sample was uncoated.

Figure 14. Corrosion resistance of bare 2024-T3 surfaces exposed in a simulated scratch cell with VCC, CCC or uncoated 2024-T3 surfaces. Corrosion resistance is expressed as R_c determined by EIS. The cells were filled with 0.1M NaCl solution. 2024-CCC refers to a cell constructed with a bare 2024-T3 surface and a chromate conversion coated 2024-T3 surface. 2024-VCC refers to a cell constructed with a bare 2024-T3 surface and a vanadate conversion coated 2024-T3 surface. 2024-2024 refers to a cell constructed with two bare 2024-T3 surfaces.

Figure 15. Evolution of the vanadium and chromium concentrations in the simulated scratch cell solutions as determined by ICP-OE. 2024-CCC refers to a cell constructed with a bare 2024-T3 surface and a chromate conversion coated 2024-T3 surface. 2024-VCC refers to a cell constructed with a bare 2024-T3 surface and a vanadate conversion coated 2024-T3 surface. 2024-2024 refers to a cell constructed with two bare 2024-T3 surfaces.

Figure 16. Possible reaction processes involved in VCC formation. (a) water addition to the primary coordination sphere for $VO(OH)_3$ to form $VO(OH)_3(OH_2)_2$. (b) Olation reaction that leads to vanadium oxide gel formation. The octahedra in (b) represent octahedrally coordinated V^{5+}.

Figure 17. Equilibrium speciation of soluble V^{5+} ions in aqueous solutions at millimolar concentrations. Adapted from C.F. Baes, Jr., R. E. Mesmer, Hydrolysis of Cations, p. 210, Robert E. Krieger Publishing Co., Malabar FL (1986).

Research and Accomplishments Part III:

Figure 1. X-ray diffraction patterns for Al-Zn-decavanadate and Al-Zn-chloride hydrotalcite compounds. The approximate ratio of Zn to Al in these compounds is 2 to 1. Gallery heights are calculated from the difference between the basal plane spacing and the thickness of the Al-Zn-hydroxide layer (4.77Å).

Figure 2. Schematic illustration of the layered structure in hydrotalcite compounds. The structure consists of alternating layers of positively charged mixed metal hydroxide sheets and anions.

Figure 3. Schematic illustration of anion exchange in hydrotalcite compounds.

Figure 4. Concentration as a function of exposure time for vanadium and zinc in 0.5M NaCl solution in contact with an excess of Al-Zn-decavanadate hydrotalcite powder.

Figure 5. Optical macrographs of 2024-T3 coupons coated with PVA with and without HT-V inhibitors before and after exposure to ASTM B117 salt spray.

Figure 6. R_c (R_{coat}) for PVA coated 2024-T3 substrates as a function of exposure time to aerated 0.5M NaCl solution. (PVA/V-HT) PVA resin containing 3 wt.% Al-Zn-decavanadate particulate additive, (PVA/V) PVA resin with 3wt.% $NaVO_3$ added, (PVA only) PVA resin with no additives.

Figure 7. (a) Anodic and (b) cathodic polarization curves for 2024-T3 in 0.124M NaCl solution open to air with and without additions of 0.1M $NaVO_3$.

Figure 8. Cathodic polarization curve for 2024-T3 in aerated 0.124M NaCl solution with increasing amounts of Zn^{2+} added as $ZnCl_2$.

Figure 9. Optical macrographs of coated and scribed samples exposed to aerated 0.5M NaCl solution for 400 hours. Exposed circular areas are 32 cm^2.

Figure 10. X-ray diffraction patterns from Al-Zn-decavanadate hydrotalcite powder specimens. (a) unexposed. (b) exposed to deionized water for 22 days. (c) exposed to 0.5M NaCl solution for 22 days. (d) exposed to saturated NaCl solution for 22 days. Boxed region contains the HT-V 006 reflection at about 16° and the 003 HT-chloride reflection at about 12°.

Figure 11. X-ray diffraction patterns from HT-V dispersed in epoxy resin and exposed to aerated 0.5M NaCl solution for 450 hours.

Research and Accomplishments Part IV:

Figure 1. Optical macrographs of the chromate-coated positive control samples at selected times during the salt spray exposure experiment. Three replicate panels are shown. Exposure times are noted under each set of replicates.

Figure 2. Optical macrographs of the samples with the HT-V-pigmented primer over a Ce/Mo conversion coating at selected times during the salt spray exposure experiment. Three replicate panels are shown. Exposure times are noted under each set of replicates.

Figure 3. Optical macrographs of the samples with an HT-V-pigmented primer over a Ce conversion coating at selected times during the salt spray exposure experiment. Three replicate panels are shown. Exposure times are noted under each set of replicates.

Figure 4. Optical macrographs of the neat epoxy negative control samples at selected times during the salt spray exposure experiment. Three replicate panels are shown. Exposure times are noted under each set of replicates.

Figure 5. Optical macrographs of the HT-V-pigmented epoxy coatings applied to deoxidized 2024-T3 surfaces at selected times during the salt spray exposure experiment. Three replicate panels are shown. Exposure times are noted under each set of replicates.

Figure 6. Optical macrographs of HT-V-pigmented epoxy over a vanadate conversion coating at selected times during the salt spray exposure experiment. Three replicate panels are shown. Exposure times are noted under each set of replicates.

Figure 7. Optical macrographs of neat epoxy coatings applied to vanadate conversion coated samples at selected times during the salt spray exposure experiment. Three replicate panels are shown. Exposure times are noted under each set of replicates.

Figure 8. Optical macrographs of the HT-V-pigmented epoxy over a silane pretreatment at selected times during the salt spray exposure experiment. Three replicate panels are shown. Exposure times are noted under each set of replicates.

Figure 9. Optical macrographs of HT-V-pigmented epoxy coatings applied to Ce-inhibited silane pretreated 2024-T3 surfaces at selected times during the salt spray exposure experiment. Three replicate panels are shown. Exposure times are noted under each set of replicates.

Figure 10. Optical macrographs of CCC-$SrCrO_4$-epoxy coating after selected exposure times during UV exposure. Three replicate panels are shown. Exposure times are noted under each set of replicates.

Figure 11. Optical macrographs of HT-V-pigmented epoxy coatings applied to Ce-Mo conversion coated 2024-T3 surfaces after selected times during the UV exposure

experiment. Three replicate panels are shown. Exposure times are noted under each set of replicates.

Figure 12. Optical macrographs of HT-V-pigmented epoxy coatings applied to Ce conversion coated 2024-T3 surfaces at selected times during the UV exposure experiment. Three replicate panels are shown. Exposure times are noted under each set of replicates.

Figure 13. Optical macrographs of neat epoxy coatings applied to deoxidized 2024-T3 surfaces at selected times during the UV exposure experiment. Three replicate panels are shown. Exposure times are noted under each set of replicates.

Figure 14. Optical macrographs of HT-V-pigmented epoxy coatings applied to deoxidized 2024-T3 surfaces at selected times during the UV exposure experiment. Three replicate panels are shown. Exposure times are noted under each set of replicates.

Figure 15. Optical macrographs of HT-V-pigmented epoxy coatings applied to mandate conversion coated 2024-T3 surfaces at selected times during the UV exposure experiment. Three replicate panels are shown. Exposure times are noted under each set of replicates.

Figure 16. Optical macrographs of neat epoxy coatings applied to vanadate conversion coated 2024-T3 surfaces at selected times during the UV exposure experiment. Three replicate panels are shown. Exposure times are noted under each set of replicates.

Figure 17. Optical macrographs of HT-V-pigmented epoxy coatings applied to silane pretreated 2024-T3 surfaces at selected times during the UV exposure experiment. Three replicate panels are shown. Exposure times are noted under each set of replicates.

Figure 18. Optical macrographs of HT-V-pigmented epoxy coatings applied to Ce-inhibited silane pretreated 2024-T3 surfaces at selected times during the UV exposure experiment. Three replicate panels are shown. Exposure times are noted under each set of replicates.

Figure 19. Schematic illustration of the pull-off adhesion test apparatus.

Figure 20. Pull-off adhesion strengths of coating system used in this study. Coating systems are identified by the pretreatment and organic coating used.

Figure 21. Variation of total impedance, $|Z|$, with time for salt spray tested coatings.

Figure 22. Variation of pore resistance, R_p, with time for salt spray tested coatings.

Figure 23. Variation of low frequency phase angle, $-\theta$, with time for salt spray tested coatings.

Figure 24. Variation of coating capacitance, C, with time for salt spray tested coatings.

Figure 25. Variation of total impedance, |Z|, with time for UV-exposed coatings.

Figure 26. Variation of pore resistance, R_p, with time for UV-exposed coatings.

Figure 27. Variation of low frequency phase angle, $-\theta$, with time for UV-exposed coatings.

Figure 28. Variation of coating capacitance, C, with time for UV-exposed coatings.

List of Tables

Research and Accomplishments Part I:

Table 1. Summary of the Chemistry in Key Intellectual Property Related to Non-Chromate Coatings.

Research and Accomplishments Part II:

Table 1. VCC Color and corrosion resistance as a function of bath pH. Corrosion resistance is reported as R_c determined by EIS after a 3 h exposure in 0.1M NaCl solution.

Research and Accomplishments Part IV:

Table 1. Average scribe failure rating for AA2024-T3 with various pretreatments and HTV primer (ASTM D 1654 Procedure A).

Table 2. Average unscribed area failure for AA2024-T3 with various pretreatments and HTV primer (ASTM D1654 Procedure B).

Table 3. Summary of corrosion observations from salt spray exposure testing. “x” indicates a positive indication.

Acknowledgements

The following organizations and individuals have provided important sources of support for research closely related to the work carried out under this project. These organizations are Air Force Office of Scientific Research, Maj. Hugh DeLong and Lt. Col. Paul Trulove program managers, The U.S. Army Corrosion Control Office (Dr. Joe Argento, Mr. John Theis, and Mr. Don Skelton) and Concurrent Technologies Corporation, Largo, FL (Mr. Larry Gintert). We are most grateful for their support.

Scientific collaborators we have had the good fortune to work with over the course of this project include Dr. C. Jeffcoate, and Dr. H. Isaacs, Brookhaven National Laboratory, Prof. J. Olesik, Ohio State University, Prof. R. Taylor University of Mississippi Medical Center, Dr. M. Kendig, Rockwell Science Center, Dr. K. Ogle, Usinor-Irsid. We wish to thank them for their discussions and insights on many different aspects of this project.

Students and investigators who worked directly on this project are:

Satyendra Mamidipally (MS 2000)
Richard Boger (MS 2001)
Ryan Leard (MS 2001)
William McGovern (MS 2001)
Natasha Voevodin (PhD 2002)
Jeremy Ramsey PhD (2002)
Wenping Zhang (PhD 2003)
Qiajing Meng (PhD 2003)
Belinda Hurley (PhD 2004)
Yuhchae Yoon (PhD 2004)
Syadwad Jain (PhD 2005)
Valerie Laget (Post-doct. researcher)
Christian Paglia (Post-doct. researcher)
A. Sehgal (Post-doct. researcher)
Hong Guan (Staff scientist)
Prof. Gerald Frankel
Prof. Richard McCreery
Prof. Hamish Fraser
Dr. Michael Donley
Dr. John Beatty

Their effort, insight and intellect were the foundation for the success of this project.

Finally, we would like to thank the Strategic Environmental Research and Development Program for their support of research at the Fontana Corrosion Center. We would particularly like to than Mr. Charles Pellerin, who has been a staunch supporter of this work since its beginning in 1999, and the SERDP and HydroGeologic support staff for making the administrative matters remarkably manageable for us.

Rudolph G. Buchheit
Professor-Materials Science and Engineering
The Ohio State University

Executive Summary

Because of increasing regulatory pressure to eliminate chromium from surface finishing, the Department of Defense (DOD) and Department of Energy (DOE) have committed to replace chromate-based metal finishing in present and next generation systems. At issue is whether this change will occur in a timely manner without performance or cost penalties that could compromise operational readiness. Additionally, undue delay in determining and implementing new corrosion protection practices poses enormous risk for existing assets. To facilitate this transition an understanding of important functions of chromate corrosion protection that must be replicated in new surface finishing methods is needed. This study was carried out to address those needs.

The results of this and related studies show that the oxoanions of hexavalent chromium uniquely inhibit the corrosion of many metals and alloys and have been particularly useful for protecting the high strength aluminum alloys against corrosion. Part of the usefulness of hexavalent chromium lies in its ability to react with metallic surfaces to form an inert Cr^{3+} oxide barrier with retained, releasable Cr^{6+}. The ability of absorbed and reduced Cr^{6+} (forming Cr^{3+} hydroxide) to inhibit the reduction of oxygen represents its main role in inhibiting corrosion though other components of corrosion protection do exist. For example, speciated as an oxoanion, Cr^{6+} appears to have an ability to inhibit pit initiation. Chromate conversion coatings offer an especially attractive mix of characteristics including ease of application on a wide range of substrates, good corrosion resistance, and good adhesion. Supplemental bath ingredients such as F^- and $Fe(CN)_6^{3-}$ are essential in making robust conversion coatings. Coating formation can be appropriately understood in the context of a sol-gel process. Freshly formed conversion coating gels are well hydrated, and coating properties change dramatically as the gel dries. This has a range of practical consequences ranging from loss in corrosion resistance to loss of adhesion.

In follow-on work, an idea for a Cr-free conversion coating involving vanadate chemistry was devised and demonstrated. This approach was based on the fundamental understanding of chromate corrosion protection developed over the past 10 years. Electrochemical testing was used to confirm earlier reports of Al corrosion inhibition by soluble vanadates. In near-neutral solutions vanadate increased the pitting potential and decreased the oxygen reduction reaction rate on 2024-T3. Impedance experiments suggested that slow film formation occurred on Al in contact with vanadate-bearing solutions. Vanadate conversion coatings were produced by immersion in a $NaVO_3/K_3Fe(CN)_6/NaF$ solution with a pH of about 1.7. Coatings formed spontaneously at room temperature in a matter of minutes. Coating formation appeared to involve hydrolysis, condensation and polymerization to produce a hydrated vanadium oxide, which is triggered by a slight increase in the pH of the metal-solution interface. The resulting coating was yellow in appearance and continuous across the sample surface. The coating was non-crystalline and consisted of vanadium in several oxidation states as well as other ingredients in the coating bath. Coating formation was very sensitive to bath pH and the presence of $K_3Fe(CN)_6$. VCCs provided excellent corrosion protection in salt spray and constant immersion tests. Polarization experiments showed that VCCs

increased resistance to pitting and suppressed oxygen reduction reactions. Simulated scratch cell experiments suggested that VCCs were also self-healing in a manner that closely resembles this characteristic in chromate conversion coatings.

In yet another phase of this work, a new idea for a Cr-free pigment for organic coatings was devised and demonstrated based on the understanding developed with respect to chromate-bearing organic coatings. The basic aspects of corrosion protection, enabled by Al-Zn-decavanadate hydrotalcite pigments in epoxy, were demonstrated. In these coatings, corrosion protection originated from release of vanadates and Zn^{2+}, which are anodic and cathodic inhibitors respectively for Al alloys. Corrosion protection due to leaching of these two inhibitors was sufficient to suppress corrosion in scribes exposing underlying bare metal during exposure to salt spray testing. Corrosion sensing consists of detection of electrolyte permeation into coatings, which is often a prelude to corrosion under coatings. This is achieved by exploiting the change in basal plane spacing in hydrotalcites that accompanies ion exchange. In this case, inhibiting decavanadate ion is exchanged for chloride or sulfate contained in the attacking electrolyte. Inhibitor is released, attacking ions are taken up and nucleate a new hydrotalcite phase with different basal plane spacing. The presence of this new phase can be detected remotely by x-ray diffraction. Taken together, these results showed that the use of hydrotalcite pigments in organic coatings may lead to new coatings with useful levels of corrosion protection for Al alloys and can enable a new means for determining when coating replacement is warranted.

Overall, these studies have demonstrated that high levels of coating performance can be achieved with novel coatings systems. Corrosion resistance and adhesion levels of these simple and rudimentary coatings approach that of incumbent chromate-bearing coating systems. It should be noted that no attempts to optimize coating formulation or application were made in this study. Optimization in this regard can be expected to result in considerable improvements in coating performance.

Future efforts dedicated towards optimization of formulations and application using chemistries based on those examined here appear to have a high likelihood of achieving chromate-like coatings system performance.

Objectives

This project was carried out in two phases. The objectives for each phase were as follows.

The objectives of this program were to develop the understanding and information required to 1) leave behind mature, familiar, and trusted chromate-based corrosion protection technologies; 2) understand the key functional attributes of chromate coatings and devise strategies for duplicating these attributes using environmentally friendly chemistries; and 3) develop the information to confidently match chromate-free processes with application given the myriad of technologies currently vying for acceptance. These program objectives were addressed by:

- Explicitly recognizing, understanding, and mitigating the effects of *microstructural heterogeneity* in aluminum alloys on chromate and chromate-free conversion coating.

- Establishing the *structure, chemistry, and performance profiles* for chromate coatings as applied in military depots, and associated OEM facilities so that chromate-free coating formulators have realistic processing and performance goals to work towards.

- Determining the extent to which application method, coating age, and alloy substrate chemistry affect the self-healing nature of chromate coatings

- Developing rapid, quantitative, and predictive *diagnostic tests* to stimulate the rate of chromate free coating development and implementation

This project was carried out as a four-year collaborative effort involving investigators from Ohio State University (OSU), the Air Force Research Laboratories (AFRL), and the Army Research Laboratory (ARL).

The objectives of the second phase of the program were to demonstrate one or more completely Cr-free coating systems suitable for high-performance military applications where thin coat corrosion protection is required.

Coating systems, as studied in this program, consisted of surface cleaning, conversion coating and corrosion inhibiting organic coating. Suitability for high-performance applications were determined by performance in standardized tests for chromated coating systems described in MIL-P-23377 "Performance Specification, Primer Coatings: Epoxy, High-Solids", with a special focus on the corrosion resistance requirement established in this specification. To meet this overall program objective, several supporting objectives also needed to be met:

- Demonstration of conversion coatings with robust corrosion protection derived from anodic inhibition, cathodic inhibition and self-healing, and/or

- Demonstration of conversion coatings with exceptional adhesion promoting capabilities for subsequently applied primers and paints.

- Development of Cr-free inhibiting pigments for primer coatings that are sufficiently soluble to provide high corrosion resistance, but do not promote osmotic blistering.

Project Background

The Department of Defense (DOD) and Department of Energy (DOE) have committed to replace chromate-based metal finishing in present and next generation systems. At issue is whether this change will occur in a timely manner without performance or cost penalties that could compromise operational readiness. Additionally, undue delay in determining and implementing new corrosion protection practices poses enormous risk for existing assets. Faced with the request from the user community for chromate-free corrosion protection, the coatings science and technology community has been unable to deliver. This situation exists, in part, because chromate corrosion protection has some rare, and perhaps unique attributes. It also exists because chromates have been used on many different metals and alloys in a vast range of applications. Consequently, the understanding of chromate corrosion protection is broad but, arguably, not deep. The chromate-replacement problem has clearly exposed the lack of depth in our understanding. For example, we cannot account for, or predict in any quantitative way, the effect of alloy-to-alloy microstructural variations in the effectiveness of chromate or chromate-free corrosion protection. We do not understand how to duplicate self-healing action thought to be key in chromate corrosion protection. We do not understand the range in performance exhibited by chromate coatings as applied in the field. We do not have a suite of test methods that permit quantitative, discriminating, and predictive evaluation suitable for both chromate and chromate-free corrosion protection. Sound, strategic investments in chromate elimination research and development have been made, but these issues require special attention to successfully cross the chromate-free corrosion protection threshold. This proposal is offered as an attempt to address these issues in a way that will permit timely and effective chromate replacement without risk to valuable assets.

Results and Accomplishments Part I:

Corrosion Inhibition of Al and Al Alloys by Soluble Chromates, Chromate Coatings, and Chromate-Free Coatings[1]

ABSTRACT

In this review, aspects of corrosion protection of aluminum and aluminum alloys by soluble chromate inhibitors, chromate conversion coatings and selected Cr-free conversion coatings are presented. The review covers the aqueous chemistry of chromium, and the origins of chromium toxicity. Evidence from older and more recent studies is presented showing that inhibition of Al corrosion is derived from both inhibition of oxygen reduction, and inhibition of metal dissolution reactions due mainly to a delay in the onset of pitting. Inhibition of corrosion by chromates appears to be closely linked to their ability to irreversibly adsorb on to metal and oxide surfaces. With respect to chromate conversion coatings (CCCs), the evolution of modern coating formulations is presented with a focus on key advances that led to process simplification, and improved coating performance. The current understanding of CCC formation, protection and aging is presented. In the last section of the paper, processing and properties of selected chromate-free conversion coating chemistries is discussed. This discussion focuses on coatings that offer particularly attractive attributes such as self-healing, excellent adhesion.

INTRODUCTION

The unique chemical and electronic properties of the oxo-compounds of chromium, Cr (valence electronic structure $3d^5\ 4s^1$ [1]), gives them a seemingly unique ability to inhibit corrosion in ferrous and non-ferrous materials. The electronic properties of Cr allow for very different behaviors for the oxo- and hydroxo-compounds of Cr^{6+} and Cr^{3+}. The tetrahedral, d^0, hexavalent oxoanion compounds of chromium (chromate, dichromate, bichromate and chromic acid) dissolve as stable complexes in water, transport easily and adsorb on oxide surfaces. The octahedral, d^3, trivalent compounds of Cr form very stable, kinetically inert refractory oxides. Bulk Cr^{3+} hydroxides form by sol-gel polymerization, giving rise to well hydrated amorphous materials [2]. Chromate conversion coatings form on aluminum through reduction of Cr^{6+} (dichromate) in solution. Conversion coating solutions are usually acidic with solution pH in the range of 1.6. Coating formation is assisted by sodium fluoride additions, which activate the Al surface and by an "accelerator", often potassium ferricyanide, which increases the coating formation rate. The subsequent film formation probably proceeds by this sol-gel route [3]. The chemical and electronic variety found in Cr chemistry leads to the ability of Cr^{6+}oxoanions to inhibit corrosion. Unfortunately, the mobility of aqueous Cr^{6+} within

[1] Published in Corrosion, 59, 379-400 (2003).

biological systems and its reactivity with biochemical oxidation mediators make it both highly toxic and carcinogenic. As such, there is a high motivation to eliminate Cr^{6+} from the manufacturing environment despite its technical utility as a corrosion inhibitor.

Cr^{6+} compounds find use for protecting structural materials and functional materials for electrical service. Cr^{6+} compounds protect aluminum and other light alloys used in the aircraft and aerospace industry and are contained in deoxidizers, conversion coatings, sealants and paints. Cr^{6+} also forms protective coatings on high-strength steel fasteners used in both the aerospace and automotive industries. Rinses for phosphate coatings and paints used as primers for ferrous and aluminum alloys also contain Cr^{6+}. Identification of ways to eliminate or reduce the use of Cr^{6+} compounds in corrosion protection schemes requires a comprehensive understanding of the corrosion inhibition mechanism of hexavalent chromium in the context of its history and prospective replacements. The corrosion protection of aluminum alloys and the current consensus on the mechanisms by which Cr^{6+} provides corrosion protection for aluminum alloys will form the framework for this review.

AQUEOUS CHEMISTRY

Cr^{6+} is readily hydrolyzed in aqueous solution and exists as an oxoanion in all but the most acidic conditions. Hydrolysis of Cr^{6+} is directly related to corrosion inhibition because it affects speciation, adsorption, transport, and condensation processes, which all have roles in chromate corrosion protection. Unfortunately, hydrolysis and subsequent speciation of Cr^{6+} oxoanions compounds is often neglected in studies of inhibition. Even if pH is maintained constant for a particular experiment, interpretation is complicated because the relative distribution of Cr^{6+} between the mononuclear bichromate anion, $HCrO_4^-$, and binuclear dichromate anion, $Cr_2O_7^{2-}$, varies with concentration **[4]**. Corrosion inhibition of Al and Al alloys is detected in chromate solutions with widely varying pH and it is likely that each of the oxo-Cr^{6+} oxoanions that exist provide some level of corrosion protection. A possible exception to this is the fully protonated H_2CrO_4, which exists in strongly acidic solutions. Evidence suggests that this species exists in active pits, but does not inhibit because it is not charged and cannot adsorb of interact with the corroding surface [5]. Clearly, a detailed understanding of the complex Cr^{6+} oxoanion equilibria becomes important when interpreting corrosion kinetic data obtained as a function of total Cr^{6+} concentration. Hence, a summary of the aqueous Cr^{6+} chemistry follows.

The speciation of Cr^{6+} oxoanions in aqueous solution involves the following equilibria [6-9]:

$$H_2CrO_4 \rightleftharpoons H^+ + HCrO_4^- \qquad K_1 = 0.18 \qquad \text{(eq. 2)}$$

$$HCrO_4^- \rightleftharpoons H^+ + CrO_4^{2-} \qquad K_2 = 3.2 \times 10^{-7} \qquad \text{(eq. 3)}$$

$$2HCrO_4^- \Longleftrightarrow Cr_2O_7^{2-} + H_2O \qquad K_3 = 98 \qquad \text{(eq. 4).}$$

Letting x = $[H_2CrO_4]$ and h = $[H^+]$:

$$[HCrO_4^-] = \frac{K_1 x}{h} \qquad \text{(eq. 5)}$$

$$[CrO_4^{2-}] = \frac{K_1 K_2 x}{h^2} \qquad \text{(eq. 6)}$$

$$[Cr_2O_7^{2-}] = \frac{K_3 K_1^2 x^2}{h^2} \qquad \text{(eq. 7).}$$

Mass balance requires all the Cr^{6+} in the respective species sum to the total concentration of Cr^{6+}, C:

$$x + \frac{K_1 x}{h} + \frac{K_1 K_2 x}{h^2} + 2\left[\frac{K_3 K_1^2 x^2}{h^2}\right] - C = 0 \qquad \text{(eq. 8).}$$

For a given pH and total chromate concentration, C, the concentrations of the individual species may be determined by solving Eq. 8 for $[H_2CrO_4]$ and substituting this concentration into equations 5 through 7. Eq. 8 is a quadratic equation of the form $ax^2 + bx + c = 0$, whose roots are given by:

$$x = \frac{-b \pm \sqrt{(b^2 - 4ac)}}{2a} \qquad \text{(eq. 9)}$$

where x = $[H_2CrO_4]$, and

$$a = \frac{2K_3K_1^2}{h^2}$$

$$b = 1 + \frac{K_1(1+K_2)}{h}$$

$$c = -C$$

The real root of Eq. 9 has physical meaning, and is used to calculate the relative concentration of the various Cr^{6+} oxoanion species as a function of total chromium concentration, C, and pH. The calculation will be as accurate as the equilibrium

constants, which actually depend to a degree on the ionic strength of the solution. K_3, for example, approaches 33 as the ionic strength approaches 0 [6-9]. However, it is quite reasonable to use the constants expressed in Eqs. 2-4 for solutions with ionic strengths between 0.01 and 0.5 M.

Figures 1a-b show the calculated concentrations of the respective Cr^{6+} species involved in the reaction equilibria shown in Eqs. 2-4. The key results from this analysis are the following:

- In acidic environments (pH 2-4) $HCrO_4^-$ dominates for low total Cr^{6+} concentrations (10^{-6} M) (Fig. 1a); whereas $Cr_2O_7^{2-}$ dominates for higher concentrations of total chromium (Fig. 1b).
- The chromate anion, CrO_4^{2-} , dominates at pH greater than 7 (Figs. 1a-b).
- At very low pH, $HCrO_4^-$ anion protonates to form H_2CrO_4.

Results from Raman spectroscopic experiments confirm the validity of these calculations [5, 10, 11]. The concentration of $HCrO_4^-$ in pits and adsorption on aluminum corrosion product surfaces has been reported [10]. Recent analysis of anodized Al 1100 using a piezo-electrokinetic (PEK) method shows that $HCrO_4^-$ absorbs on anodized oxide surfaces at near neutral solution pH values to lower the charge. The PEK method uses an acoustic pulse to shear the double layer adjacent to the internal surface of the pores in anodized aluminum. The magnitude and sign (phase) of the voltage response depends on the fixed charge on the surface within the pore. In the absence of chromate, the PEK signal at neutral pH is high and positive. The addition of chromate lowers this charge as a result of specific adsorption as seen in the decrease in the PEK signal at neutral pH and its reversal in sign above pH 8. However, with decreasing pH, the following reaction shifts to the left increasing the concentration of $HCrO_4^-$:

$$3HCrO_4^- \leftrightarrow CrO_4^{2-} + Cr_2O_7^{2-} + H^+ + H_2O \qquad \text{(eq. 10).}$$

With decreasing pH, the PEK response is not diminished as strongly as in neutral solution (Figure 2) [12]. This result suggests that $HCrO_4^-$ and eventually H_2CrO_4, which forms under very acidic conditions, do not adsorb extensively on oxide surfaces and may not be contributing strongly to corrosion inhibition. Figure 1c shows the Cr^{6+} oxoanion distribution for a solution having a concentration of Cr^{6+} typical of that of a commercial conversion coating (0.050 - 0.075M). As can be seen from Figure 1c, in the bath pH region around pH 2, $Cr_2O_7^{2-}$ (80%) and CrO_4^{2-}(20%) oxoanions dominate.

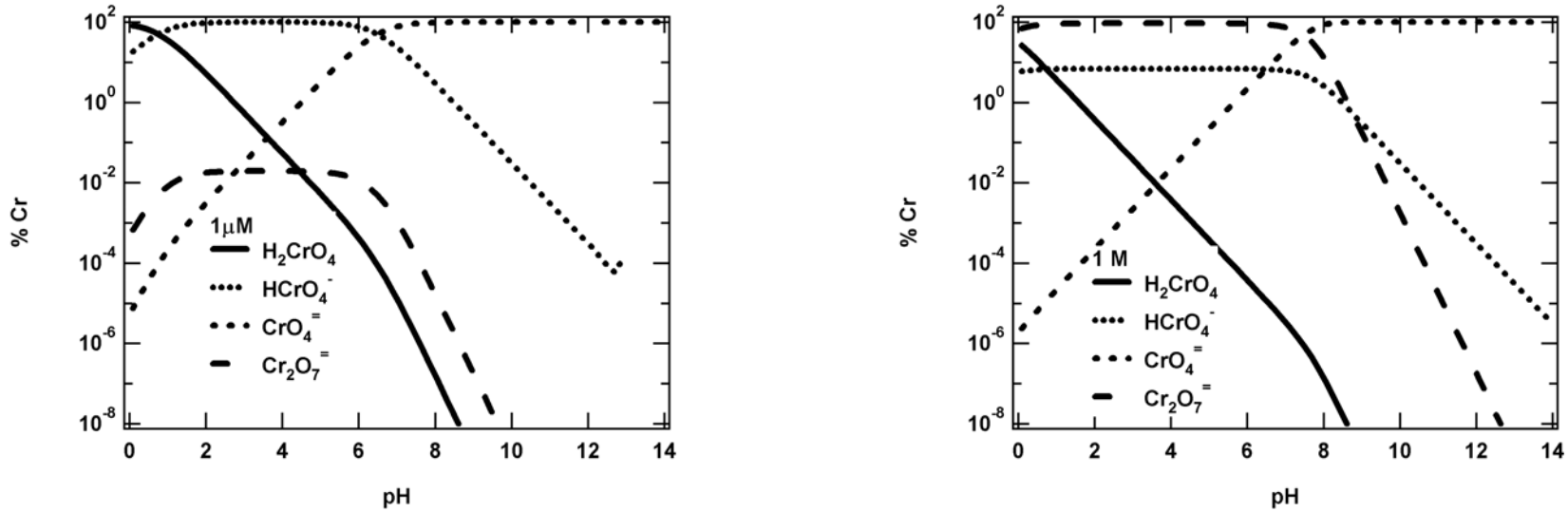

(a) (b)

Figure 1. Relative concentration of the oxo-Cr(VI) species as a function of pH for a total Cr(VI) concentration of (a) 10^{-6} M and (b) 1 M.

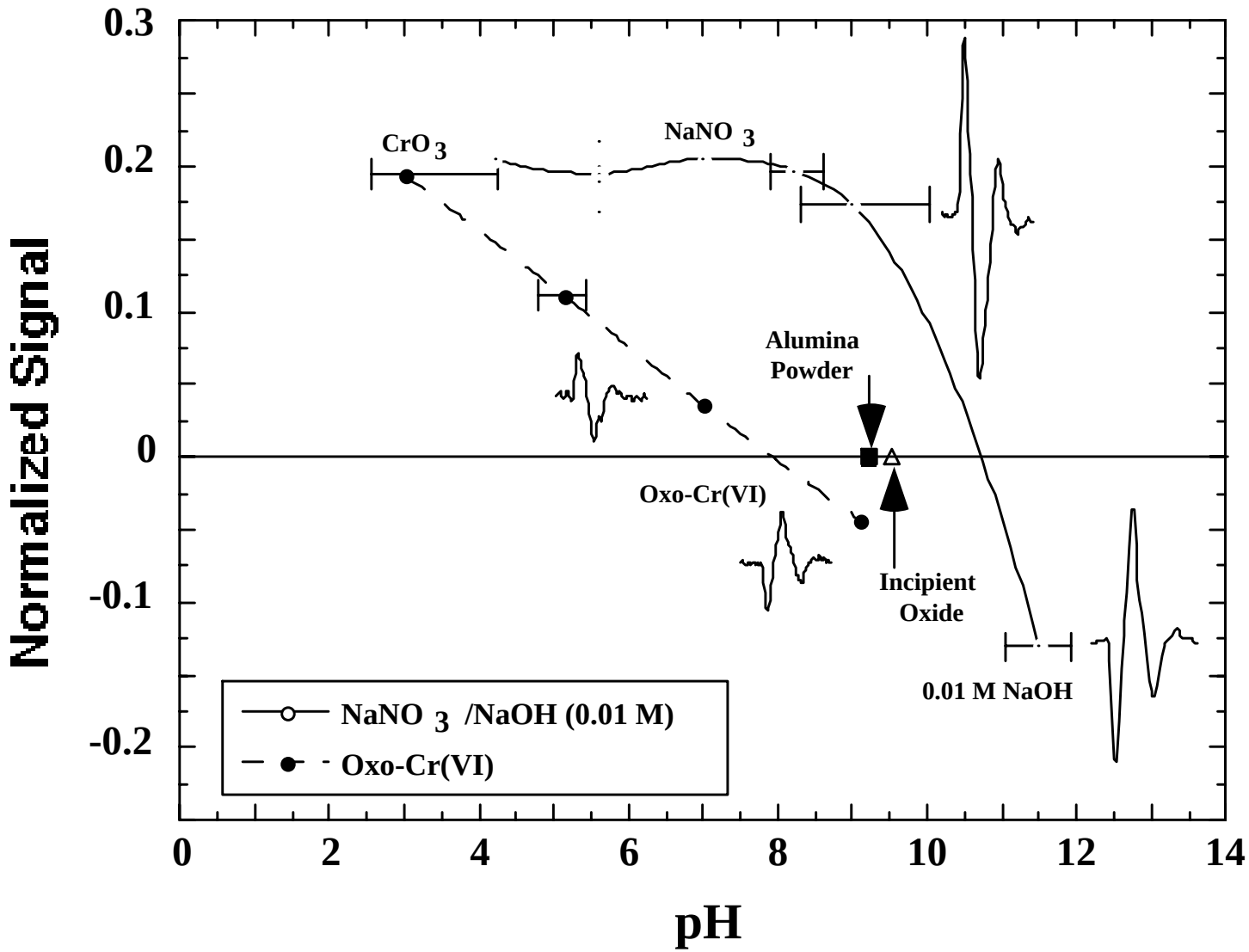

Figure 2. Relative piezo-electrokinetic response (unitless) as a function of pH for 0.01F oxo-Cr^{6+}, and 0.01 M sodium nitrate or hydroxide.

TOXICITY

A recent review [13] cites earlier studies [14] that document Cr^{6+} as a human carcinogen associated with lung cancer. It is not the static presence of Cr^{3+}or Cr^{6+} that contributes directly to the DNA damage that leads to cancer. Rather, the molecular debris associated with the process of Cr^{6+} to Cr^{3+} reduction induces the critical changes in DNA. Evidence supporting this idea comes from *in vitro* studies showing that chromate alone does not damage DNA in the absence of reducing agents [13]. In fact, it is the biological anti-oxidants, such as ascorbate, glutathione, and L-cystine that lead to DNA damage [15, 16]. One mechanistic hypothesis for Cr^{6+}-induced DNA damage entails a Fenton-type reaction that lowers Cr oxidation state and catalyzes the formation of $^{*}OH$ radical from H_2O_2:

$$Cr(n\text{-}1) + H_2O_2 \rightarrow {}^{*}OH + OH^{-} + Cr(n) \qquad \text{(eq. 11).}$$

The intracellular reaction of Cr^{6+} in the presence of reducing agents produces Cr^{5+}, Cr^{4+}, Cr^{3+}, free radicals, and reactive oxygen; all of which are potentially genotoxic. A specific example of this process involves reaction of Cr^{6+} with ascorbic acid to form Cr^{5+}, Cr^{4+}, and carbon-based free radical. This illustrates the idea that oxidation mitigation provided by small intracellular molecules, such as ascorbic acid, actually contributes to damage of DNA [17].

Alternative mechanisms to the Fenton-type interaction have been proposed by Lay et al. [18], who suggest that the DNA-damaging species are the peroxo-complexes of Cr^{4+} and Cr^{5+}. This mechanism does not require the formation of the $^{*}OH$ radical. These authors do not rule out the direct oxidation of DNA by Cr^{4+} or Cr^{5+} species. The presence of intracellular alpha hydroxy-carboxylic acids R-C(OH)COOH tends to stabilize Cr^{5+}.

Although there is no general agreement on the details for the Cr^{6+} induced damage to DNA, the following points are clear:

- Cr^{6+} is highly water soluble and passes through cell membranes.

- Small molecule antioxidants such as ascorbate, glutathione and L-cystine appear to form highly reactive intermediates such as Cr^{5+} stabilized by alpha hydroxy carboxylates and Cr^{4+}, which in turn react either directly or through free radical intermediates to damage DNA.

A relation between the mechanism of Cr^{6+} toxicity to corrosion inhibition mechanisms is not obvious or expected. However, the existence of Cr^{4+} and Cr^{5+} complexes in the aqueous intercellular environment leads to the question of the significance of such species in corrosion inhibition. For example, are similar species responsible for the very rapid deactivation of cathodic sites on metallic surfaces during the reduction of Cr^{6+} to the passivating Cr^{3+} oxide? Are traces of Cr^{4+} and Cr^{5+} present in conversion coatings or chromate-containing paint films? Do they have any role in

corrosion protection? The authors know of no active research considering the role of these intermediate-valent Cr species. Definition of the role of corrosion inhibition by Cr^{6+} will not be complete until the importance of these organic-stabilized intermediate-valence state species are considered. Such considerations could have important implications for the mechanism of inhibition by chromate pigments in paints. Stable Cr^{5+} can be synthesized [19] and used for such investigations.

MECHANISM OF INHIBITION

Recent investigation [20-24] of corrosion protection by chromates and chromate conversion coatings has focused on a number of specific working hypotheses regarding the mechanisms of inhibition. They can be condensed to the following statements. Cr^{6+} oxoanions:

- being highly soluble and very mobile in solution, are transported to sites of localized corrosion where they are reduced to Cr^{3+} and irreversibly adsorbed at metal surfaces where they inhibit oxygen reduction.

- inhibit pit initiation of Al and dissolution of active intermetallic phases in Al alloys.

- modify the chemical composition of the surface of passive oxides and passivated intermetallic phases by adsorption and buffering.

- adsorb on aluminum oxides, lowering the zeta potential, thereby discouraging adsorption of anions such as chloride, which promote dissolution and destabilization of protective oxides.

Chromate conversion coatings:

- provide good, hydrophobic Cr^{3+} hydroxide barrier with adhesion-promoting chemical and mechanical properties.

- store Cr^{6+} oxoanions that can be slowly released into an attacking solution. Released ions can migrate to and interact at defects to stifle corrosion.

- inhibit anodic and cathodic reactions, at least temporarily, leading to corrosion inhibition.

Some of these hypotheses are better established than are others. There appears to be very good agreement that chromate conversion coatings not only contain [25-30], but also release [29, 31, 32] hexavalent chromium to repair defects and damage of the conversion coating. Since chromium hydroxide coatings are already very good barriers on light alloys [33], the addition of active corrosion protection by release of stored inhibitor makes for a highly corrosion resistant coating.

Recent research has focused on several key issues in chromate corrosion inhibition including the relative contributions of anodic and cathodic inhibition to overall protection, the effect of chromates on the compositional and morphological changes in the vicinity of intermetallic phases in Al 2024-T3, the effect of chromate on dealloying of Cu-rich intermetallic phases, and slow release of Cr^{6+} by coatings and the subsequent "self-healing" effect that occurs. The following sections highlight relevant aspects of research in these areas.

Microstructure of 2024-T3. Much of the recent research on chromate inhibition has been carried out in the context of corrosion and inhibition of Al alloy 2024-T3. The nominal composition of this alloy is 4.4%Cu, 1.5%Mg, 0.6%Mn, and lesser amounts of Fe, Si and impurity element allowables [34]. The balance of the alloy is aluminum. The "T3" designation indicates that the alloy was solution annealed, quenched and aged at ambient temperatures to a substantially stable condition [35]. This alloy is of interest because it is a main alloy used in aircraft fuselage structures. It is important to recognize that in most modern aircraft an "Alclad" variant of the 2024-T3 is used. Alclad 2024-T3 has a thin layer of commercially pure Al applied to enhance corrosion resistance [36]. The Alclad layer is easily removed exposing the underlying 2024-T3 core in maintenance operations where grinding-out of cosmetic corrosion surfaces is routine. Corrosion protection of the 2024-T3 core then becomes an issue, especially for older aircraft that have experienced many depot maintenance cycles.

In recent years, the metallurgical characteristics of 2024-T3 that affect the localized corrosion behavior have been studied in some detail [37-45]. Several important highlights are discussed here. Alloy 2024 contains a distribution of constituent particles that range in size from about 0.1 to a few micrometers in diameter. These second phase particles are enriched in the various alloying elements. These particles form during the original solidification of the cast billet and are not dissolved to any great extent during subsequent thermomechanical processing. The predominant chemical types present in 2024 are Al-Cu-Mn-Fe particles whose chemistry ranges from Al_7Cu_2Fe to $Al_{20}Cu_3Mn$. Constituent θ phase, Al_2Cu, and S phase, Al_2CuMg can also be present in the alloy. The θ phase tends to be the more predominant of the two phases in alloys with a higher Cu:Mg ratio. S phase predominates at lower Cu;Mg ratios [46].

These particles are usually noble with respect to the surrounding matrix, and tend to localize corrosion to the matrix phase at the particle periphery during exposure to aggressive aqueous environments. These particles support reduction reactions at enhanced rates, which leads to this localized dissolution; perhaps assisted by local alkalinization that occurs near the particle due to the cathodic activity at the particle [45].

Localized corrosion at S phase particles is more complex [38, 39, 45]. S phase particles are initially active with respect to the surrounding matrix phase. These particles will dealloy, become enriched with Cu and ennobled to such an extent that their galvanic relationship to the matrix is reversed. Under certain conditions, these particles have been observed to dealloyed to such an extent that they appear to be selectively dissolved [45].

Alloy 2024-T3 also contains homogenous distribution of Cr, Mn and Si dispersoids [47]. It also contains a dispersion of S phase laths that form during natural or artificial aging [47]. None of these phases has been directly implicated in localized corrosion phenomena in the alloy in the T3 temper.

Inhibition of the oxygen reduction reaction (ORR). Inhibition of cathodic kinetics has been recognized for sometime, but recently this issue has gained increased attention. Chromates are excellent inhibitors of oxygen reduction in near neutral and alkaline solutions. In these environments, they can stifle corrosion by suppressing this cathodic partial reaction. The inhibition mechanism appears to involve reduction of Cr^{6+} to Cr^{3+} at a metal surface and formation of an irreversibly absorbed Cr^{3+} hydroxide surface layer of near-monolayer thickness [48].

Chromate is a very powerful cathodic inhibitor even at high chloride:chromate ratios. Cathodic polarization curves collected for 2024-T3 in a base solution of oxygen-sparged 1.0M NaCl, oxygen reduction reaction rate is reduced by about an order of magnitude (at $-0.80V_{sce}$) by addition of 10^{-5} M $Na_2Cr_2O_7$ (Figure 3) [49]. In similar experiments where 0.3% H_2O_2 was added as a cathodic depolarizer, 10^{-4}M dichromate additions had no effect on the oxygen reduction reaction rate. However, additions of 10^{-3} M chromate reduced the cathodic reaction rate by an order of magnitude.

The results of these experiments show that chromate inhibits the cathodic reaction at chloride:chromate concentration ratios of 10^5:1. This value is much higher than the 1:1 to 10:1 ratio where increases in the pitting potential during anodic polarization experiments are observed [50]. The curves in Figure 3 also suggest that hydrogen and water reduction are inhibited at the lowest measured potentials. It is usually the case that the cathodic polarization response of Al alloys is affected by cathodic corrosion. In Cu-bearing alloys this leads to Cu surface enrichment and an increase in cathodic kinetics. However, the data of Figure 3 suggest that dichromate is a potent enough to inhibit cathodic kinetics and suppress cathodic corrosion and attendant Cu surface enrichment, even at very large cathodic overpotentials.

In high strength Al alloys, Cu-rich intermetallic particles support the oxygen reduction reaction (ORR) in aerated solutions. Reduction of Cr^{6+} to Cr^{3+} and subsequent adsorption at these sites inhibits the ORR. In neutral sulfate solutions, a Cu rotating disk electrode (RDE) shows a rotation rate-dependent cathodic current [44, 51, 52]. In the presence of chromate, the rotation rate dependence disappears as a result of the inhibition of the ORR by chromate. Furthermore, the inhibition is nearly irreversible. Upon removal of chromate from solution, the ORR remains inhibited. This supports the idea of a strongly adsorbed species from the chromate-containing electrolyte that subsequently inhibits the ORR.

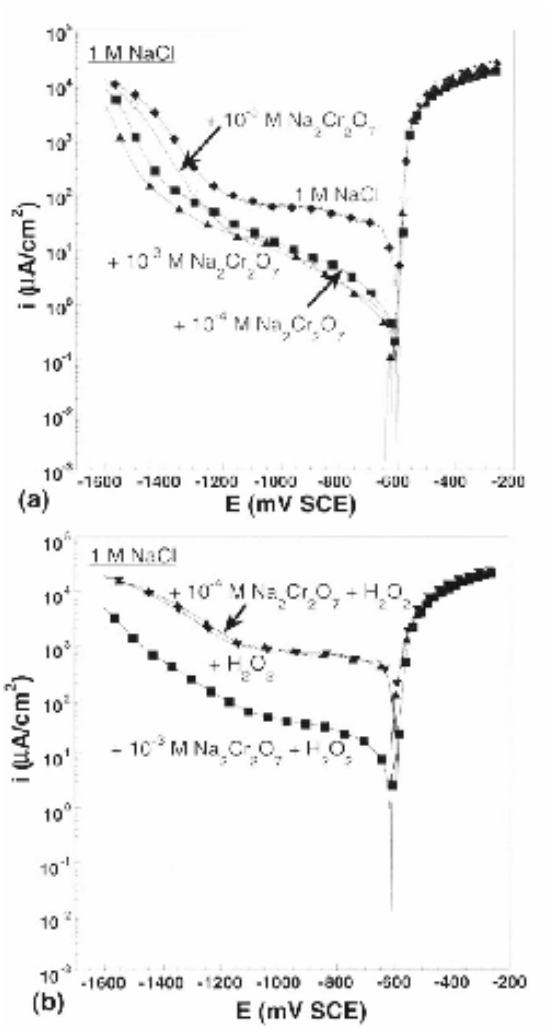

Figure 3. Cathodic polarization curves on 2024-T3 in actively oxygen -sparged 1M NaCl solution with (a) dichromate additions, and (b) 0.3 vol% peroxide and dichromate additions.

A. Sehgal, G. S. Frankel, B. Zoofan, S. Rokhlin, J. Electrochem. Soc., 147, 140 (2000).

This result has also been reproduced in neutral sodium chloride solutions, a detailed analysis of which shows hexavalent chromium to inhibit both the ORR and further Cr^{6+} reduction [48, 53]. The current-voltage behavior for a rotating Cu electrode (2000rpm) in Figure 4 illustrates this point for a 5% NaCl solution at pH 6 [53]. With the addition of chromate, the current in the -0.60 to -0.85V_{sce} region decreases due to the inhibition of oxygen reduction. However, at potentials below -0.85V_{sce}, the chromate contributes to a current plateau as its reduction proceeds under diffusion control. The extremely large overvoltage required for the diffusion limited Cr^{6+} reduction attests to the self-inhibition of Cr^{6+} reduction.

A more detailed study [48] shows that the inhibition of ORR involves the adsorption and rapid reduction of Cr^{6+}oxoanions to form an inhibiting Cr^{3+} hydroxide, which is probably bound strongly to the surface. The Cr^{3+} hydroxide surface may also contain co-adsorbed Cr^{6+} oxoanions. It has been suggested that such a surface film would form a bipolar barrier that would inhibit electron transfer in a manner not explained by a monolayer barrier alone [48]. The reduction of Cr^{6+} may also have significance to the corrosion process since it appears to be coupled to an induced anion adsorption [54].

Anodic inhibition. Anodic inhibition of Al alloys by soluble chromate has been studied using both electrochemical and non-electrochemical techniques. The effectiveness of chromates as anodic inhibitors has been questioned [49], but it is now generally regarded that modest anodic inhibition by chromates does in fact occur. The extent of inhibition depends on environmental factors such as chloride:chromate ratio, pH, and degree of aeration. It also depends on alloy substrate chemistry and temper. Whether inhibition is detected in any laboratory experiment appears to depend on an interplay among environmental conditions, Al alloy type, test technique, and protocol.

Pitting potential data from Kaesche determined for 99.99% Al in mixed chloride-chromate solutions provide a useful benchmark for this discussion [50]. Figure 5 shows the dependence of the pitting potential in solutions with chloride and chromate ion concentrations ranging from 10^{-6} to 10^{-2} M. In general, the pitting potential begins to be ennobled when the chloride:chromate ratio is below about 10:1 to 1:1. Studies conducted over the past several years have shed light on the action of chromate in the various stages of pit initiation and growth.

In near neutral 1.0 mM chloride solutions, 25 to 50 μM chromate additions have been observed to suppress metastable pitting on high purity Al wire loop electrodes [55]. Suppression of metastable pitting occurs at chloride:chromate ratios that are somewhat larger than those established by Kaesche based on critical pitting potential measurements. Under potentiostatic control, soluble chromate appears to decrease the metastable pitting rate, the magnitude (peak current) of metastable pitting events, the growth rate of individual pits, and the apparent pit current density. These factors decrease the chances that metastable pits will develop into stable pits before repassivating.

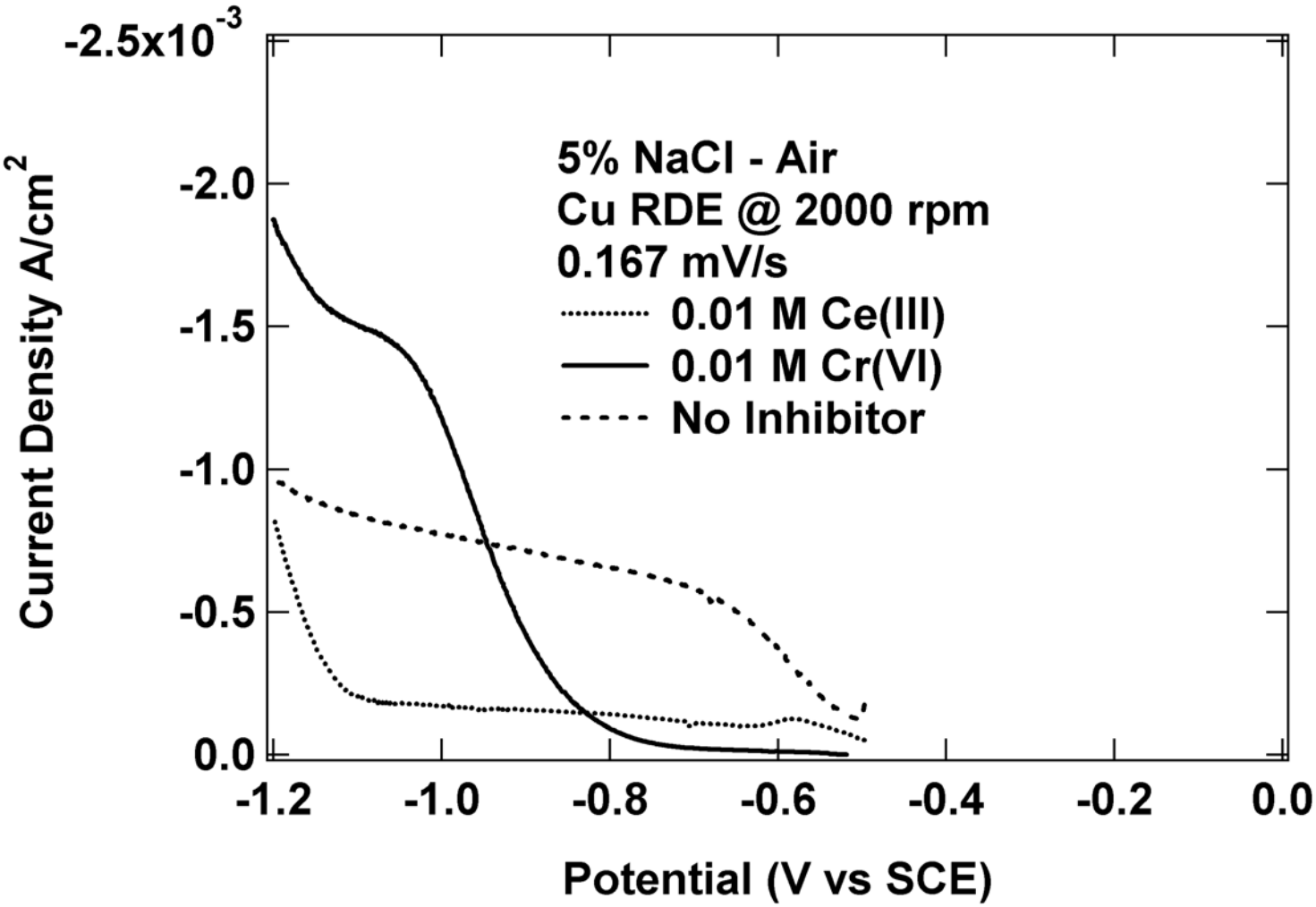

Figure 4. Polarization response of a Cu RDE in 5% NaCl solution with Cr(VI) and Ce(III) inhibitor additions.

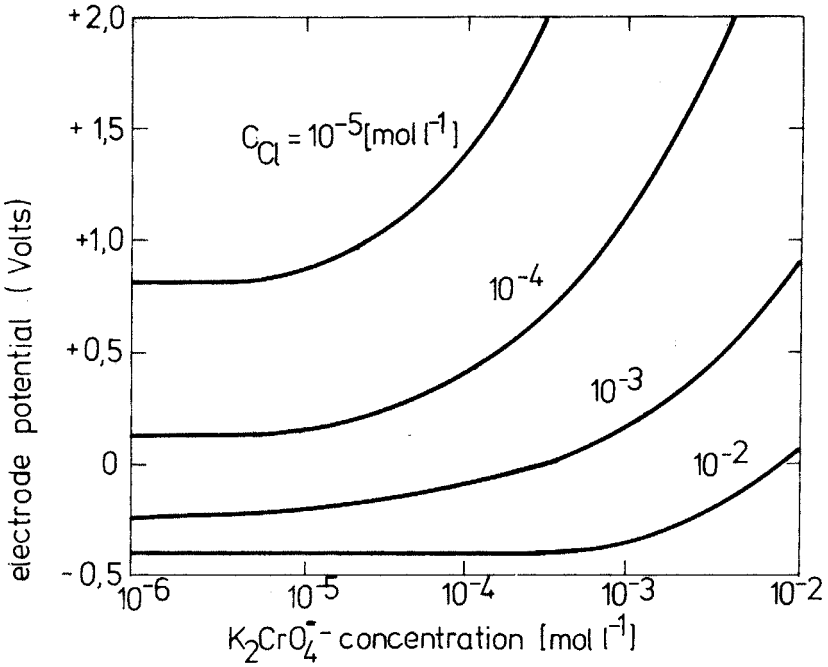

Figure 5. Dependence of the pitting potential of Al on the chloride: chromate ratio.

H. Kaesche, Localized Corrosion III, p. 516, NACE, Houston, TX (1971).

Chromate in near-neutral bulk chloride solutions will inhibit the growth kinetics of pits and crevices, but only at chloride:chromate concentration ratios much lower than those established by Kaesche from pitting potential measurements [56]. In thin film pitting experiments conducted under potentiostatic control, additions of 50 mM $Na_2Cr_2O_7$ to 1.0 M NaCl solution had virtually no effect on pit growth kinetics or the pit repassivation potential. Dichromate additions of 500mM elevated the repassivation potential by about 90 mV. A 2000mM $Na_2Cr_2O_7$ addition was required to stifle pit propagation completely. Dichromate ions are expected to become enriched in propagating crevices due to electromigration, which may lead to inhibition. However, in artificial crevice electrode experiments, additions of either 10 or 100 mM $Na_2Cr_2O_7$ to a bulk solution of comprised of 100mM NaCl was found not to inhibit crevice propagation kinetics [57]. It has also been found that chromate additions to neutral chloride solutions will accelerate the kinetics of repassivation, and suppress reactivation of aluminum [58].

Kendig has argued that in experiments conducted under potential control, extremely acidic conditions develop on the working electrode surface because a large component of the cathodic reaction is displaced to the counter electrode [5]. Chromate becomes increasingly protonated with decreasing pH, and as suggested by PEK measurements, less likely to adsorb on oxide covered surfaces to promote corrosion resistance. For a total dissolved concentration in the millimolar range, Cr^{6+} is speciated almost entirely as the neutral, potentially non-inhibiting H_2CrO_4 species as the pH approaches 0 (Figure 6). Figures 7a and b show current versus time behavior of Al 1100 during potentiostatic polarization at $-0.500V_{sce}$ in 1.0M chloride solution at pH 0 and 1. At pH 0, the steady state dissolution current is about 45 A/cm^2. The dissolution rate is not lowered by addition of 0.01M CrO_3 indicating no inhibition. At pH 1, addition of 0.01M CrO_3 lowers the dissolution rate from about 0.17 A/cm^2 to less than 0.05 A/cm^2 indicating an improvement in the inhibiting efficiency. These results support the notion that the ability of Cr^{6+} to inhibit is associated with how it is speciated in solution, and that H_2CrO_3 does not inhibit corrosion because is does not adsorb on metal or oxide covered surfaces.

Inhibition by chromate adsorption. The precise nature of anodic inhibition by chromates is not clear. As suggested by PEK measurements, it may involve non-reductive adsorption rather that adsorption and reduction that seems to underlie ORR inhibition. Evidence that Cr^{6+} oxoanions on their own impart corrosion inhibition to oxide covered surfaces without reduction to the Cr^{3+} oxide was recognized in 1966 by Cartledge [59]. More recently, absorption of Cr^{6+} oxoanions on the corrosion product in growing pits [10], and adsorption of Cr^{6+} oxoanions in the porous layer of anodized aluminum [12] have been suggested to provide inhibition without being reduced. Adsorption on anodized aluminum lowers the normally positive zeta potential of the oxide within the porous layer. Using a model similar to that described by Sato [60] for ferrous oxide films, the adsorption of the negatively charged chromate will hinder adsorption of chloride. McCafferty, Natishan and co-workers [61, 62] make similar arguments with regard to the role of chromate and other inhibiting oxoanions for increasing the pitting potential on aluminum alloys.

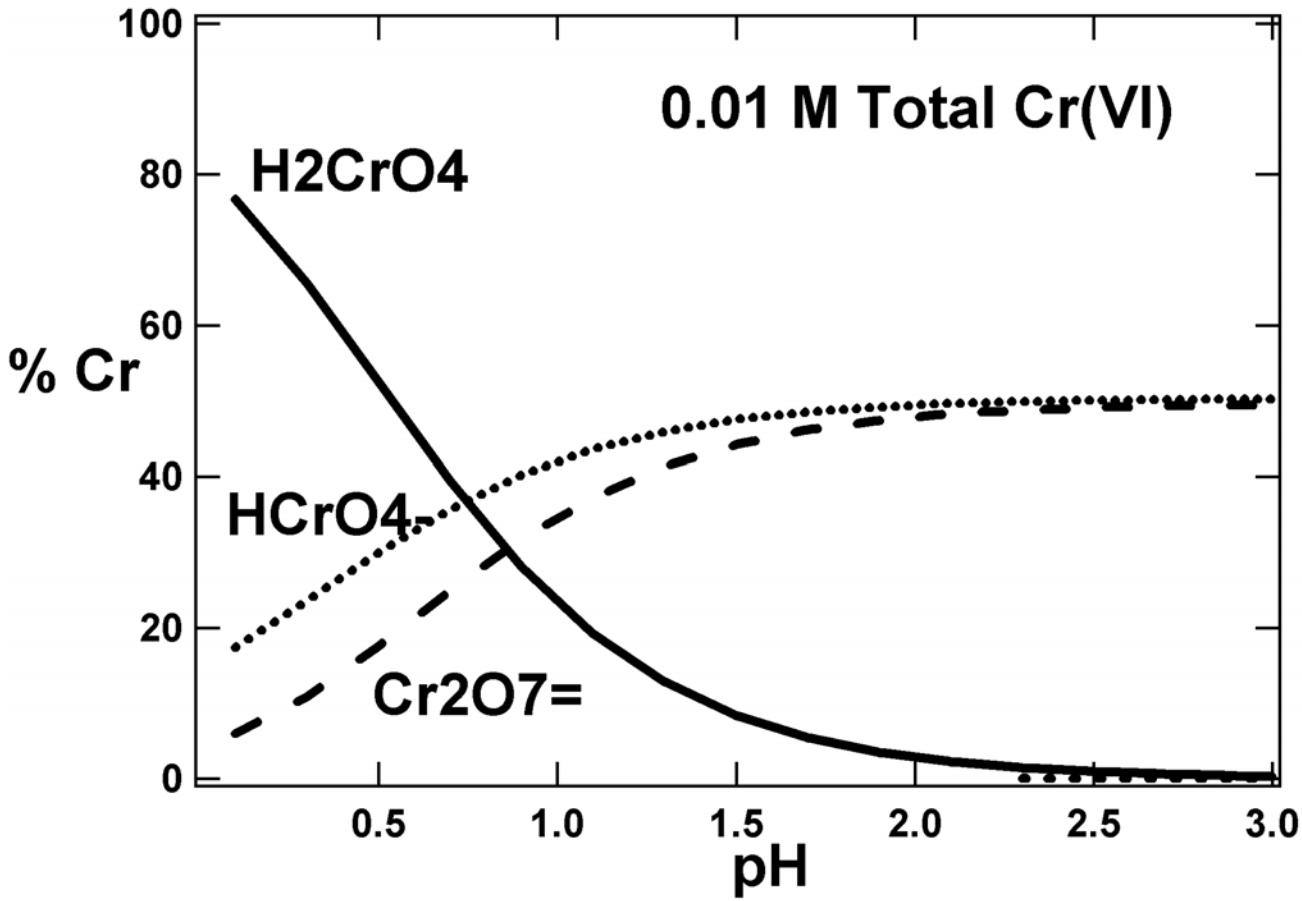

Figure 6. Relative concentration of the oxo-Cr^{6+} species as a function of pH in the pH 0-3 range for a total Cr^{6+} concentration of 0.01 M.

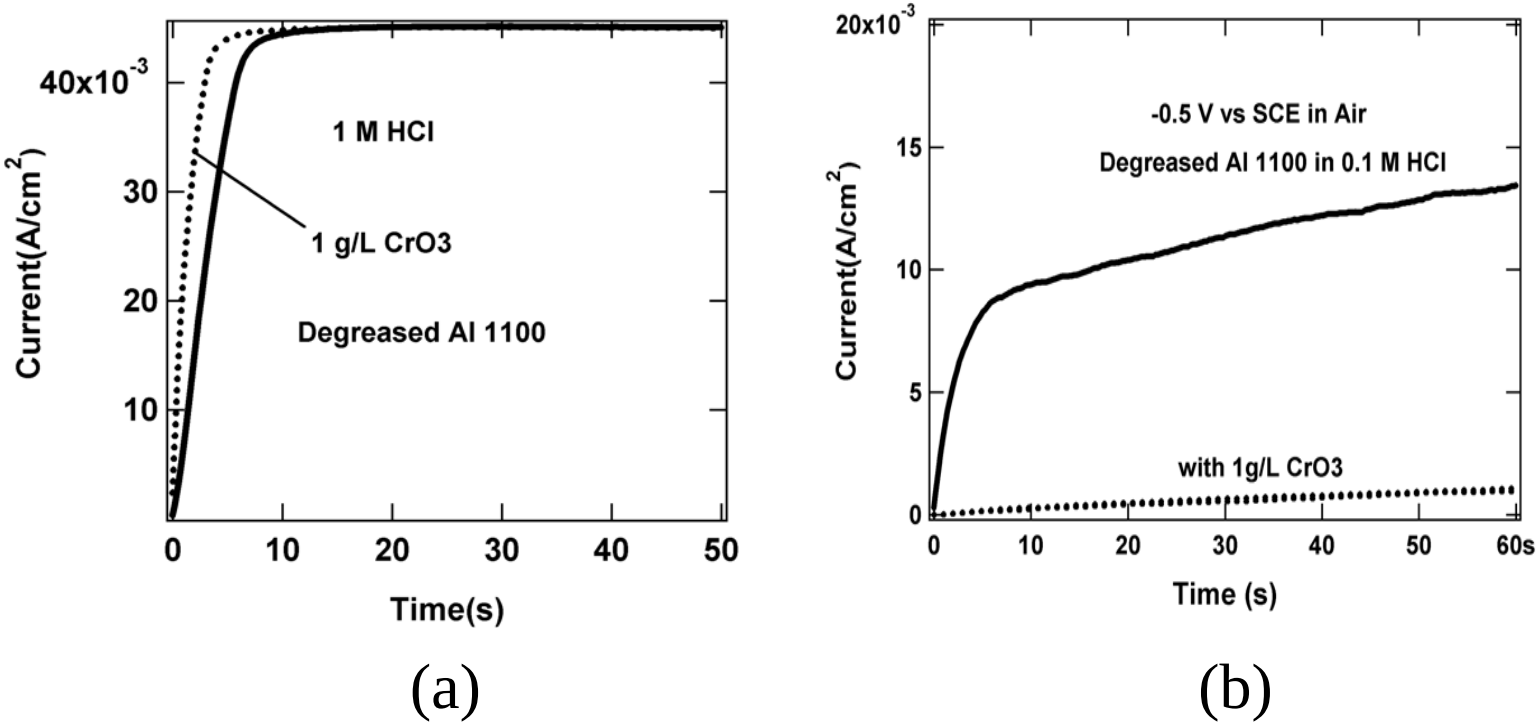

Figure 7. Current vs time for 600 grit polished Al 1100 polarized at –0.500V_{sce} in 1M chloride solution at (a) pH ~1 and (b) pH ~0.

Inhibition at intermetallic particles. The interaction of the chromate inhibitor with intermetallic particles in Al alloys is essential for understanding the mechanism of corrosion inhibition. Hence, consideration of the relative role of anodic and cathodic inhibition by chromate must take into account the electrode processes taking place on the intermetallic phases. Arguments can be made that inhibition of ORR at Cu-rich cathodes alone cannot explain the inhibition of corrosion of 2024-T3 by chromate in near neutral solutions [44, 52, 53, 63, 64], and that it is necessary to account for other components of corrosion protection.

Passivation of the Cu-rich intermetallic phases and other cathodically active sites by chromate conversion films appears likely although details of the interaction are still being studied. Initiation of chromate conversion coating formation on 99.99% Al by reductive deposition of Cr^{3+} oxide at cathodic sub-grain boundaries has been shown by TEM of microtomed sections [65]. Atomic force microscopy (AFM) of the nucleation of chromate films from dilute, cold (5°C) Alodine on Al 2024-T3 shows preferential deposition of a film of undetermined composition on the cathodic Fe, Cu, Mn aluminide phase (see Figure 9 and [66]). The use of a cold solution was necessary to catch the very earliest stages of nucleation. Even at this temperature complete coverage of the surface occurred within 10 seconds of exposure. Shorter times allowed evaluation of the partial coverage. Several groups have shown the Al-Cu-Fe-Mn phase to be relatively noble [67-69], which would account for enhanced chromate reduction.

Whether the mechanism of chromate inhibition of the Cu-rich intermetallic phases in 2XXX alloys is as simple as the rapid absorption-reduction passivation process observed on pure Al remains to be determined. Guillaumin, et al. [70] have shown that nucleation of chromate films on the various intermetallics of 2024-T3 from dilute dichromate in 0.5 M NaCl depends on the initial conditions of the surface. A surface that is abraded with an AFM Si tip shows selective deposition of chromate on the Al-Cu-Fe-Mn phase, but an 'as-polished' surface (1200 grit SiC, diamond paste, final ethanol rinse) of the more active Al_2CuMg phase showed a thicker coating deposit. In studies of chromate conversion coating formation from ferricyanide-accelerated solutions, it has been observed that the relative intensity of the an 860 cm^{-1} Raman band associated with a Cr^{3+}/Cr^{6+} complex unique to chromate conversion coating virtually disappears over Cu-rich intermetallic phases [71]. These authors hypothesize that $Fe(CN)_6^{-3}$ is preferentially adsorbed on Cu-rich intermetallic particles, which passivates these regions with respect to the film-forming Cr^{6+} to Cr^{3+} reduction reaction. This results in a locally thinner coating. In other studies based on the use of microchemical surface techniques (SERS, XANES, SIMS) on Al 2024-T3 and synthetic Cu-rich intermetallics, a relative depletion of Cr^{6+} on intermetallic surfaces is also observed [72]. Recently published work describing chromate conversion coating of various intermetallic phases coupled to Al seems to confirm the idea that $Fe(CN)_6^{-3}$ interferes with CCC formation at IMCs. Surface analysis suggests a rather slower rate of coating formation on intermetallic compounds as a result of ferricyanide reduction to ferrocyanide ($Fe(CN)_6^{-4}$), and adsorption of $Fe(CN)_6^{-4}$ on the particle site [73]. Whether the Cu-rich intermetallics catalyze a complete conversion of Cr^{6+} to Cr^{3+}, or whether they inhibit conversion coating formation due to unintended

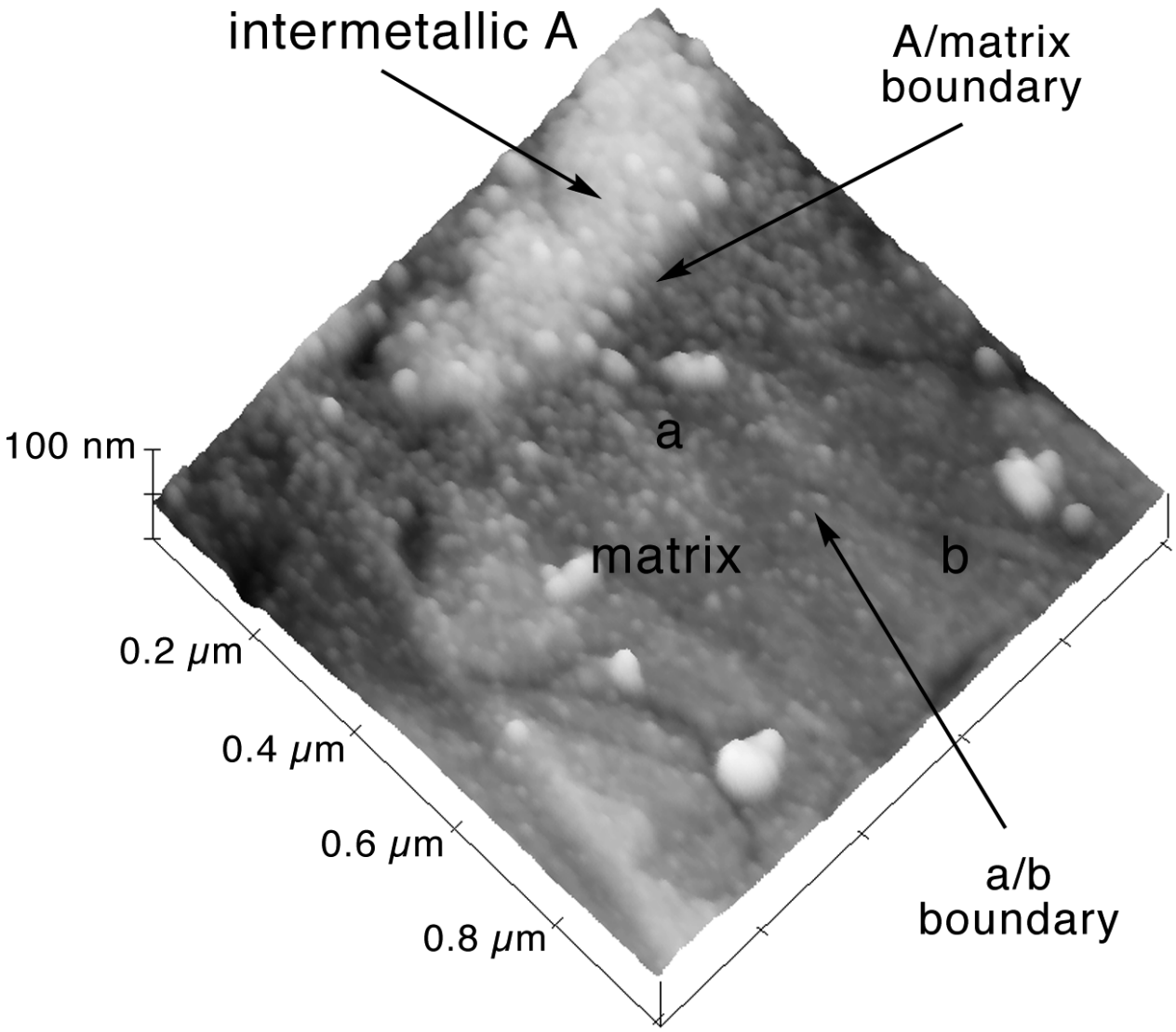

Figure 9. AFM image for a freshly polished (0.01 micron) Al 2024-T3 surface exposed for 3 seconds to Alodine solution at 5° C.

interaction with supplemental bath ingredients is a critical question that remains to be more fully resolved.

Slow Release of Cr^{6+} from filmed surfaces. Recent work has shown that the form of the residual Cr^{6+} in chromate films and conversion coatings differs from both the solution phase chromate and dichromate. It is most likely a compound reversibly bound to Cr^{3+} hydroxide polymer "backbone" [11] that can be released and transported to unprotected surfaces in a manner leading to self-healing [32].

New findings [74] based on reexamination of older studies [75, 76] suggest that the Cr^{6+} release characteristic is temporary. Consequently, self-healing might also be a temporary phenomenon. Dehydration of chromate surface films due to ambient or elevated temperature exposure immobilizes Cr^{6+} in the conversion coating structure. This results in a loss of Cr^{6+} leachability [31, 74-76], and probably eliminates self-healing. Exposure of filmed surfaces at ambient and modestly elevated temperatures ($60^{o}C$ is often cited as a critical temperature in this regard [77]) causes a loss in corrosion resistance, which is probably in part due to loss in self-healing ability.

Environmental conditions provide the driving force for release of Cr^{6+}. For example, local alkalinization resulting from oxygen reduction at a coating surface serves to release the inhibiting anion $HCrO_4^-$[31]. A recent XANES study showed that reducing conditions, such as those produced by additions of sodium sulfite, also promotes the release of Cr^{6+} [78]. These experimental results beg the question as to whether chromate coatings are not only ‘active’ but also ‘smart’ in the sense that they release the inhibitor only when the coating is coupled to an anodic defect which cathodically polarizes the coating causing both reduction and alkaline hydrolysis.

CHROMATE CONVERSION COATINGS

Overview. The use of chromate conversion coatings to increase the corrosion resistance and paintability of aluminum alloys can be traced to the early part of the twentieth century [79]. The state of the art has advanced considerably since then, and many different coating formulations involving chromates have come and gone. Overall, the evolution of chromate conversion coatings on aluminum has been characterized by several distinct innovations, some of which are easily recognized in modern coating formulations. Throughout this evolution, ease and versatility in processing and bath maintenance, and demand for increased corrosion resistance and paintability have been the primary drivers for process innovation.

Chromate conversion coatings of today are easily applied, offer excellent corrosion resistance, including a self-healing ability. CCCs are also easily paintable. However, they are produced using hazardous chemical ingredients, and environmentally friendly replacement technologies are desired. Matching the ease of application and high performance of chromate coatings using non-chromate formulations has been difficult. While chromate replacement has occurred in some applications, widespread replacement

will depend on further advances in chromate-free coating processing and coating performance.

Evolution of alkaline carbonate-chromate chemistries. The earliest inorganic conversion coatings specifically for Al alloys, which were just emerging as engineering materials in the early 1900s, were formed using alkaline carbonate-chromate solutions [79, 80]. In certain processes, coatings were subsequently sealed in a dichromate solution [81]. Work pieces were immersed in hot (90 – 95°C) potassium carbonate (0.1 to 0.5 M) - potassium (di)chromate† (< 0.1 M) († in alkaline solutions, chromate is the predominant chromium species in solution independent of the form in which is was added). Contact times ranged from tens of minutes to 4 hours. Over this time period, hard polycrystalline coatings up to 6 micrometers in thickness were formed. Little quantitative information on corrosion resistance has been reported, although resistance to mildly aggressive aqueous environments was noted. In these chemistries, the primary film forming reaction was hydrothermal Al oxide film growth, and contributions to film formation due to chromate were secondary.

In the late 1920s, researchers discovered that the processing time of alkaline carbonate-chromate formulations could be shortened to 3 – 5 minutes by controlling the carbonate/chromate ratio in solution [82]. For the first time, sodium metasilicate and sodium fluoride were used in millimolar concentrations to produce clear coatings [82]. Post-coating silicate treatments were used to increase corrosion resistance on Al-Cu alloys [83]. Interestingly, fluoride additions are reported to have been added to solution to complex with Cr and keep it *out* of the coating so that clear coats could be produced.

The use of small additions (millimolar) of phosphate and inhibiting transition metal oxoanions (permanganate) in the alkaline carbonate-chromate solutions was reported in the early 1930s [84]. In some of these formulations, chromate was not used at all [85]. Baths of these formulations were easier to maintain, and active ingredients could be added to restore effective coating formation characteristics. These coatings performed well as a base for paint, and provided good protection for emerging high-Cu aluminum alloys.

Acidic formulations. In the 1940s, acid chromate-phosphate-fluoride formulations arose [86]. These chemistries were distinguished by the fact that they were acid-based (pH < 1.8), and produced thin amorphous coatings with excellent corrosion resistance. Total phosphate concentrations ranged from 0.2 to 1.0 M, chromic acid ranged from 0.06 to 0.2 M, and fluoride ranged from 0.1 to 0.3 M. Coatings formed in a matter of minutes during immersion or during spray at ambient temperatures, although elevating the temperature up to about 50°C accelerated the formation rate. Phosphate-based chromate coating formulations of this type are still in use today. They are believed to consist of predominantly amorphous $CrPO_4 \cdot 4H_2O$ with a small amount of hydrated Cr_2O_3. As such, they are distinct from polycrystalline phosphate coatings in structure, chemistry and performance. These coatings have been used primarily as a base for painting, but boric acid additions were introduced in the late 1950s to limit film formation to promote appearance, weldability and corrosion resistance.

The demand for corrosion protection of various metal parts in military systems used in tropical and marine climates during World War II stimulated widespread use and increased experience with chromate metal finishing. After the war, this experience was adapted and applied to commercial manufacturing. Acid chromate-fluoride formulations, in which (di)chromate was the primary film forming agent, came into widespread use in the late 1940s and early 1950s. Typical bath formulations consisted of 30 –70 mM chromic acid, 10-30 mM dichromate, and 10-20 mM fluoride [87, 88]. Solution pH values ranged from 1.2 to 1.8 and contact times required to complete film formation ranged from 2 to 5 minutes at 30 to 35°C. These processes produced the familiar yellow to brown coatings associated with chromating of aluminum using modern formulations. The coatings could be as thick as one micrometer or more. Corrosion resistance was high, though not as high as with sealed anodized coatings, and corrosion resistance on different alloys scaled with the intrinsic corrosion resistance of the alloy substrate. In this regard, the corrosion resistance of chromate conversion coatings varied inversely with the Fe and Cu content of the alloy. These coatings were thin and provided for low electrical contact resistance, which made them well suited for electronics packaging and electrical connector applications. These coatings were also a minimal impediment in welding operations. An added advantage to this coating process was that there was virtually no dimensional change associated with coating formation, and coatings could be applied to carefully machined parts.

Modern accelerated chromate formulations. In the late 1960s and 1970s, the use of accelerants in chromate conversion coating formulations was initiated [89]. Accelerants increased coating weight and shortened coating time. Many different accelerants were used including a variety of organic and transition metal compounds [90]. However, the predominant accelerant in modern commercial formulations is ferricyanide, $Fe(CN)_6^{3-}$, which is added to acid chromate-fluoride chemistries in concentrations ranging from 2 to 5 mM. The original claim was only that the use of the compound increased coating weight. No special claims for enhanced corrosion resistance or paint adhesion were directly given. Several studies have been dedicated to characterizing $Fe(CN)_6^{3-}$ in conversion coatings and determining its role in stimulating coating growth and determining its influence on coating properties. The two primary theories for the action of $Fe(CN)_6^{3-}$ are 1) formation of mixed metal cyanide compounds [27, 91, 92], and 2) acceleration of the film-forming Cr^{6+} to Cr^{3+} reduction reaction by $Fe(CN)_6^{3-/4-}$ redox mediation [27].

Recent Developments. Chemistry modifications continue to be made to optimize coatings for special situations such as application to specific alloy type [90], or reduction of cracking due to drying [93]. Several new processes have been developed based on Cr^{3+} rather than Cr^{6+} chemistry [94]. In these processes, film formation is carried out in an acidic Cr^{3+} salt bath. Usually, an oxidizing treatment in applied to the coating after it is formed to improve corrosion resistance. This likely oxidizes some of the Cr^{3+} to Cr^{6+} and imparts some Cr^{6+}-leachability and self-healing to the coating. It may also increase the toxic hazard of the coating during any removal or maintenance operations. Nonetheless,

the resulting coatings offer corrosion resistances approaching that of the accelerated chromium chromate conversion coatings.

Self-healing. "Self-healing", discussed briefly above, refers to the distinctive ability of a chromate conversion coating to heal small chemical or mechanical defects that expose unprotected underlying metal. The process involves 1) liberation of latent Cr^{6+} into an attacking aqueous environment, 2) migration of the Cr^{6+} to an incipient defect, and 3) reduction to insoluble Cr^{3+} hydroxide or interaction with the corrosion product gel to stifle further corrosion. Self-healing was recognized as a component of chromate coating protection in acidic chromate-fluoride formulations no later than the early 1950s [95]. The literature does not ascribe self-healing characteristics to the earlier alkaline carbonate-chromate, or acidic chromate-phosphate-fluoride formulations.

Opinions vary on how important a component self-healing is to overall corrosion resistance. Chromate conversion coatings also offer excellent barrier protection, and freshly formed coatings do not support reduction reactions very well. In many applications, the conversion coating is protected by a primer coat heavily loaded with leachable chromate. Chromate leached from the primer is expected to play a more important role in corrosion protection than chromate leached from conversion coatings. However, results from exposure corrosion testing show that aluminum surfaces prepared with a chromate conversion coating and a chromate-free primer perform much better than a chromate-free sol-gel type conversion coating with the same chromate-free primer [96]. This observation suggests that inhibition by leachable chromate in the conversion coating is important to substrate corrosion protection.

Recent experiments using a simulated scratch cell clearly demonstrate self-healing by chromate conversion coatings [32]. In these experiments, a conversion coated Al alloy surface and a bare alloy surface (the simulated scratch) are placed a few millimeters apart facing one another. Solution is then introduced into the gap. After several hours, Cr^{6+} leached from the coating can be detected in the solution. Hydrated chromium-containing deposits are observed on the originally bare surface, and its corrosion resistance is observed to increase. Altogether, these observations suggest that self-healing in conversion coatings is an important attribute of chromate conversion coatings.

Chromate conversion coatings today. Chromate conversion coating technology is exceptionally versatile; coatings may be applied by immersion, spray or by rolling. Coatings with useful properties can be applied in a matter of seconds. Coating properties may be tailored by chemistry selection, or by controlling contact time. Coatings may be applied to a wide range of aluminum alloys and other metals. Over the years, capital investment in chromate metal finishing equipment has been extensive in many industries, although regulatory pressures have caused some abandonment of facilities. The investment in education and training of personnel on fabrication, use and maintenance of chromate conversion coatings has been correspondingly large. In essence, the technology is robust, mature, and trusted. Nonetheless, chromate is a potent human carcinogen, and its use is accompanied by intense scrutiny from both the public and private sectors. As a

result, this technology is becoming increasingly costly to use, and identification and implementation of replacement technologies is highly desirable.

The future. Examination of the total history of conversion coatings shows slow, but steady evolution in the technology, with occasional changes that have had widespread impact. Since the late 1980s there has been increased attention to the chromate-replacement issue, and there is good reason to expect that chromate-based surface pretreatment will eventually be eliminated. Investment in research and development related to this problem has been steady, particularly by the U.S. Department of Defense and the defense industries. The implementation of chromate-free technologies has already begun to occur, although perhaps more slowly than modern patience levels have been able tolerate. A detailed discussion of the trends in developing replacement technologies appears in a subsequent section of this review.

CONVERSION COATING FORMATION

Chromium-chromate coatings. Soluble chromate present in very minute quantities (< 1 µg/mL) will adsorb on metal surfaces and inhibit oxygen reduction [48]. However in aggressive solutions, small amounts of soluble chromate either have no effect or a slight accelerating effect on corrosion of ferrous [97], and aluminum alloys [56]. At concentrations greater than about 10^{-3} M over a fairly broad range of pH, chromate stimulates film formation, which is the basis for conversion coating. Modern coating chemistries typically consist of 50mM CrO_3, 30 to 40 mM mixture of fluoride and fluoro salts, and 2 to 5mM potassium ferricyanide. Commercial formulations often include other minor ingredients and may have alternate activators and accelerators. These reagents are added to a basis solution consisting of nitric acid whose pH is usually very close to 1.6.

The overall formation reaction for chromium-chromate conversion coatings on Al is typically given as [98, 99]:

$$Cr_2O_7^{2-} + 2Al + 2H^+ + H_2O \rightarrow CrOOH_{(s)} + 2AlOOH_{(s)} \qquad \text{(eq. 12).}$$

This reaction recognizes the all-important electrochemical component of film growth. However, it does not describe very well an equally important chemical component of growth, or the action of the F^- activator and $Fe(CN)_6^{3-}$ accelerator. For example, XPS analysis confirms that the bulk of the coating contains mixtures of CrOOH and Cr_2O_3 with significant levels of F^- and Fe, the latter implying the presence of ferricyanide throughout the coating [99]. Additionally, chromium-chromate conversion coatings are usually more Cr-rich than the stoichiometry of Eq. 11 suggests [25, 29].

Newer interpretations of CCC formation on Al are based on a sol-gel mechanism [11, 100]. According to this mechanism, coating formation involves hydrolysis, polymerization and condensation of Cr^{3+} (Figure 10a). This process is triggered by reduction of Cr^{6+} at the metal surface and near-surface pH increases due to hydrogen reduction on the activated Al surface. Fluoride prevents rapid passivation of the Al

Precipitation of Cr(III) hydroxide

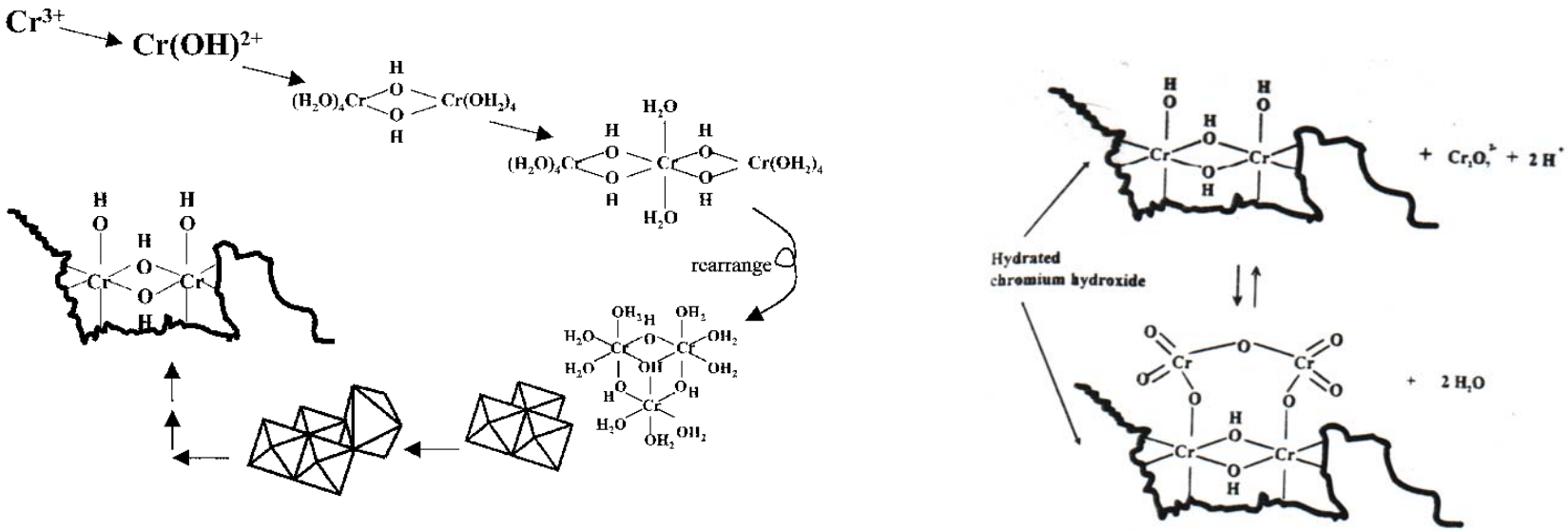

Figure 10. (a) Schematic representation of the hydrolysis-polymerization-precipitation mechanism for $Cr(OH)_3$ "backbone formation. (b) Condensation of Cr(VI) on the Cr(III) backbone by nucleophilic attack of hydroxyl ligands in the backbone.

L. Xia, R.L. McCreery, J. Electrohem. Soc., 145, 3083 (1998).

surface allowing Cr^{6+} to Cr^{3+} reduction to proceed longer than it would otherwise. Ferricyanide functions as a mediator between Al oxidation and chromate reduction and accelerates the redox reaction, which is normally quite sluggish.

This process yields a $Cr(OH)_3$ polymer "backbone" which consists of edge and corner-sharing Cr^{3+} octahedral units. The labile Cr^{6+} reservoir builds up in the coating simultaneously with backbone formation. This occurs by nucleophilic attack of the hydroxyl ligands in the $Cr(OH)_3$ backbone [101] leading to characteristic Cr^{3+}--O--Cr^{6+} bonds, which are readily detected by Raman spectroscopy [11] (Figure 10b).

When coating formation is observed on electrode arrays that permit current flow among electrode array elements to be measured, the growth occurs in two recognizable stages as shown in Figure 11[64]. The first stage, which lasts for about 30 seconds, is characterized by intense measurable electrochemical activity (current flow among electrodes in the array). First-stage coating growth results in the formation of round nanometer-sized nodules that nucleate quickly cover the surface [102]. Preferential nucleation and growth on local cathodic sites defined by local impurity element enrichment, and second phase particle inclusions has also been reported [65, 66, 103]. Coatings formed in just several seconds do confer useful levels of corrosion resistance, but are not as corrosion resistant as coatings formed by longer immersion times.

The second stage of coating growth occurs under electrochemically quiescent conditions, as net current flow among electrodes in an electrode array coating experiments is undetectable. It is possible that this stage of coating growth is also largely electrochemical in nature, but measurable net currents do not flow. Conversely, it is possible that this stage of coating growth is predominantly chemical in nature and follows the sol-gel formation mechanism described earlier. In any case, coatings grown through this stage exhibit an increase in the Cr:Al and Cr^{6+}:Cr^{3+} ratio [25, 29]. These coatings are also gelatinous and fragile when first formed, and can be damaged by the slightest touch.

If a CCC is to be used for stand-alone corrosion protection, it is usually allowed to harden for at least 24 hours before any further handling [104]. However, as CCCs harden, they become decreasingly receptive to organic overcoats. Therefore, it is common for conversion coated surfaces to be painted within the first 24 hours after coating application [77].

Chromium-phosphate coatings. Chromium-phosphate conversion coatings (CPCCs) are widely used in aluminum coil coating operations for the good corrosion resistance and paint adhesion properties conferred by short contact time spray application. CPCCs are formed by contact with acidic solutions containing CrO_3, H_3PO_4, and NaF as the primary ingredients. Fluoride serves to dissolve the air formed oxide and activate the surface, while $CrPO_4$ and H_3PO_4 are the primary film forming agents. Coating formation occurs by reduction of Cr^{6+} to Cr^{3+} and precipitation of hydrated $CrPO_4$, Cr^{3+} and Al^{3+} hydroxides [105]. Depending on the bath formulation, substrate type, contact time and temperature, CPCCs can be either amorphous [106], or crystalline [107]. Chromium phosphate is often the predominant compound in the coating comprising up to 80% of

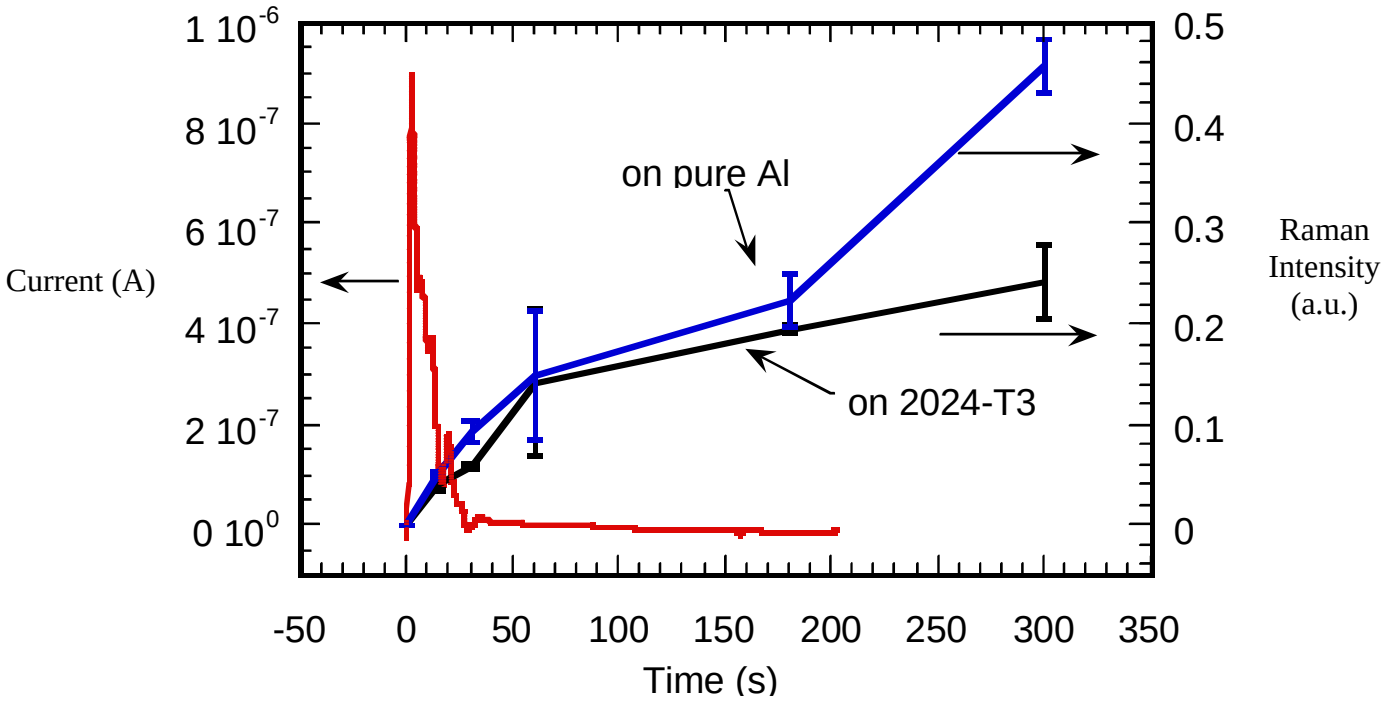

Figure 11. Normalized intensity of the 859cm^{-1} Cr^{3+}-O-Cr^{6+} scattering band as a function of coating time. A representative current versus time trace is shown for comparison. Electrode area was 0.008cm^2.

freshly formed films [108-110]. Most or all of the Cr in CPCCs is present in an insoluble Cr^{3+} form. Little or no Cr^{6+} is present in the coating. As such, these coatings do not possess the self-healing characteristics of CCCs and provide corrosion resistance by barrier protection only.

Cr^{6+} and Cr^{6+} speciation. Cr^{6+} speciation in coating baths is an important variable in CCC formation. Cr^{6+} in solution can rapidly speciate via hydrolysis and dimerization to form chromate, CrO_4^{2-}, dichromate, $Cr_2O_7^{2-}$, or bichromate $HCrO_4^-$ [4]. As described previously, the predominant species present in solution depends on Cr^{6+} concentration and pH, and not on the form of the salt or acid added to solution. Corrosion resistant films can be formed over a wide range of pH suggesting that all three of these species are film formers to some extent. However, modern chromium chromate and chromium phosphate processes are operated at chromate concentrations and pH values where dichromate is the predominant soluble species. As indicated earlier, solution concentrations of 50 mM Cr^{6+} and a pH of 1.6 are typical. Under these conditions, the total chromate concentration may vary by a factor of two or more without a significant impact on film formation rate [111].

Activators and Accelerators. CCC formation is greatly aided by "activating" species such as fluoride, sulfate, nitrate, formate and acetate, and others [111]. Fluoride is particularly effective in promoting film growth and is often added to both chromium chromate and chromium phosphate bath formulations. Fluoride is typically added as NaF and mixed metal fluoride salts whose total concentration is in the 30 to 40 mM range. Fluoride attacks existing surface films, particularly on aluminum. It readily complexes Al^{3+} in solution and has the effect of lowering the Al content in CCCs. Consequently, CCCs are found to be enriched in Cr, and are of greater thickness when F^- is added to the bath [28].

Accelerators used in commercial CCC formulations include: ferricyanides, acetates, formates, and chlorides, among others [111]. Of these, potassium ferricyanide, $K_3Fe(CN)_6$, has been most widely studied and described in the literature. Potassium ferricyanide is added to CCC formulations in 2 to 5 mM concentrations to increase coating weight. The active component in this compound is the ferricyanide anion, which increases chromate reduction reaction kinetics that are normally slow on oxide covered surfaces [112]. On aluminum, ferricyanide, $Fe(CN)_6^{3-}$, is readily reduced to ferrocyanide, $Fe(CN)_6^{4-}$. Ferrocyanide is oxidized by chromate, which is subsequently reduced to its trivalent form contributing to film formation. Coupling substrate oxidation to chromate reduction through this ferri-/ferrocyanide mediation mechanism increases the film formation rate, which results in a more corrosion resistant coating. Ferricyanide is also incorporated into the CCC [28], and Fe:Cr ratios of 1:10 have been reported in at least two studies [27, 112], and ferricyanide has been proposed to exist as mixed metal cyanide in CCCs [91, 113, 114]. It is now becoming clear that both F^- and $Fe(CN)_6^{3-}$ have a direct positive effect on coating corrosion resistance.

Coating formation on metallurgical and microstructural defects. CCC bath chemistries tend to optimized for coating formation on the basis metal of an alloy, e.g.,

Al, Zn or Fe. Alloying element additions, particularly when segregated into second phase particles, alter CCC formation locally. Some of these alterations have been characterized, but none are well understood. In Al alloys for example, CCC formation from accelerated bath formulations has been reported to be both enhanced [103, 115], and inhibited [27, 66, 73, 99, 116] at impurity-enriched grain and cell boundaries (Figure 12), and intermetallic particles such as Al_2Cu, Al_2CuMg, Al_3Fe, Al_7Cu_2Fe, and $Al_{12}Si(Fe,Mn)$. Film formation enhancement has been attributed to facile electron transfer at these sites, which permits reductive formation of a chromate film, and an increase in local pH with promotes condensation and precipitation of hydrolyzed Cr^{3+}. Film formation inhibition in the case of Cu-rich intermetallic particles such as Al_2Cu, and Al_2CuMg is attributed to the formation of a thin chemisorbed cyano-rich film that prevents proper CCC formation locally [71, 72]. This results in a thinner, chromium-deficient coating at these locations (Figure 13). For longer immersion times coating defects of this type appear to be diminished [27].

Recently, Brown and Kobayashi [117] used ultramicrotome sample preparation in conjunction with atomic force microscopy and transmission electron microscopy on 2024-T3 surfaces to generate a detailed description of the chromating process at surface heterogeneities. Their work confirms the heterogeneous nucleation of hydrous chromium oxide films at sub-grain boundaries and $(Al,Cu)_5Mn$ particles, and the growth of hydrous deposit halos around $Al_6(Cu,Fe,Mn)$ and Al_2CuMg. The halo around the $Al_6(Cu,Fe,Mn)$ results from the driving force provided by anodic dissolution of a supposed Cu depleted region adjacent to the intermetallic.

ALTERNATIVE CHEMISTRIES

For perhaps the last 20+ years, a considerable effort has focused on uncovering non-chromate corrosion inhibiting compounds for use as 'drop-in' replacements for protection of aluminum alloys. A number of reviews focusing on this subject alone have been written in the past several years [118-121]. Rather than providing an exhaustive review of all non-chromate alternatives, this section points to the general trends under investigation by citing a few examples. We consider both the traditional inorganic chemistry approach as well as the new concepts using conducting organic polymers.

What are the alternative inorganic chemistries that have been suggested for chromate conversion coatings? Figure 14 shows a periodic table with the elements whose compounds have been considered as alternative reagents shaded. Figure 14 has been prepared primarily in consideration of a review of the patent literature (Appendix 1). The inorganic species considered for replacement can be divided into the following categories:

- Reducible hypervalent transition metals (compounds of Mo, V, Mn, Tc). Like Cr, the high valent oxoanions of these elements exist in aqueous solution.

- Difficult to reduce transition metal oxides (Zr, Hf, Ta, Ti, Y) and covalent oxides (oxides and mixed oxides of Si, Ge, P, Te). Both the former and latter can be processed using sol-gel methods.

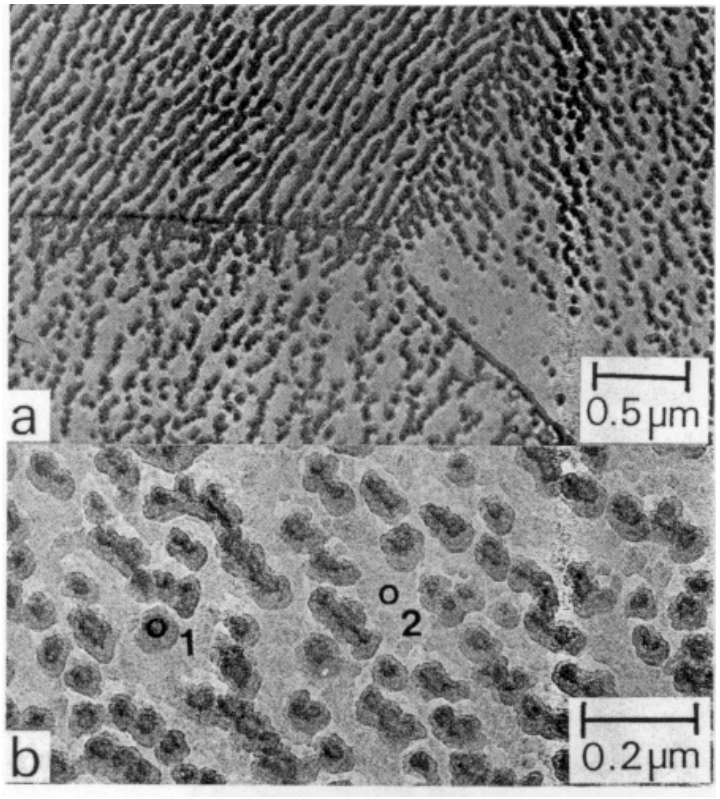

Figure 12. Transmission electron micrograph of a CCC stripped from a 99.98% pure Al substrate. CCC was formed by a 5 s immersion in $Cr_2O_7^{2-}/F^-$ solution at sub-ambient temperature. Local Cr-rich deposits (site 1) are located on grain boundaries or pre-existing metal ridge. Microchemical analysis of regions away from nodules (site 2) suggest non-uniform CCC formation across the surface.

G.M. Brown, K. Shimuzu, K. Kobayashi, G.E. Thompson, G.C. Wood, Corrosion Sci., 33, 1371 (1992).

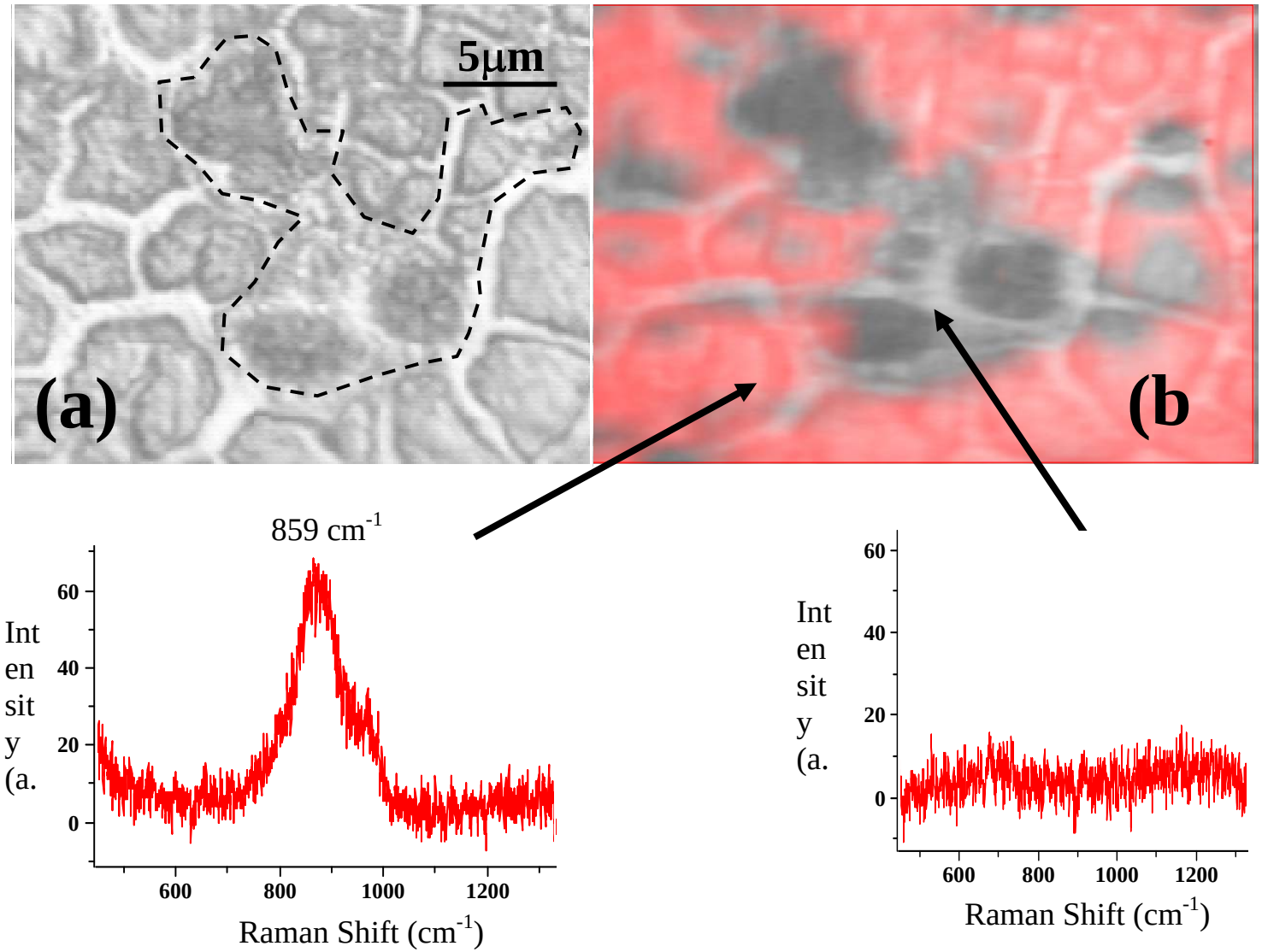

Figure 13. (a) Optical micrograph of a conversion coated S phase particle colony in 2024-T3. The dashed line approximates the boundaries of the particle colony. (b) Intensity map of the 859cm^{-1} Cr^{3+}-O-Cr^{6+} Raman band over the region in (a). The absence of intensity over the location of the particle indicates atypical CCC formation on the S phase particle.

Figure 14. Periodic Table of the elements, compounds of which (shaded) have been considered as alternatives for oxo-Cr^{6+} inhibitors.

- Precipitated coatings including boehmite and hydrotalcite coatings, and rare earth metal (REM) coatings.

If one draws a diagonal line across the transition metal portion of the periodic table, the elements above and to the left of this line provide relatively stable oxides, hence their logical consideration as replacements for chromium oxide conversion coatings.

Hypervalent transition metal oxoanions. The term 'hypervalent' as used here refers to the 'highest' valence state of the oxoanion which is typically is not thermodynamically stable in aqueous solution. Many of the metals that form oxo-metallates, such as Mn, Tc, Mo, and V, have soluble hypervalent oxoanions that reduce to form insoluble oxides in the same way as Cr. This can be better seen from schematic Pourbaix diagrams showing regions of stability of the oxoanions and the respective oxides (Figure 15). Note, however, that Mn, Cr, Tc exhibit very broad ranges in pH around neutral where their reduced oxides are stable. V and Mo, on the other hand, exhibit relatively narrow ranges in pH where the reduced oxides are stable (Figure 15). The vanadium oxide is relatively more stable toward high pH and the Mo oxide is stable toward lower pHs. Solely as oxides, the elements of Mo and V will never give the same stability as seen in analogous Cr^{3+} oxide. On the other hand, the oxo-compounds of these elements (Mo and V) can form very stable polyoxometallates (POMs) with each other, phosphates and tungstates. These metals are also gel-formers under the proper conditions. Hence, they should not be ruled out completely as chromate replacements. It should also be noted that vanadates and molybdates provide significant inhibition for aluminum [122], particularly in concert with other compounds [123]. Other reports have shown the inhibiting properties of molybdates and tungstates [124] and molybdates and permanganates [125] for aluminum.

In recent years, a process using permanganate has been commercialized [126], and a direct permanganate-based conversion coating approach has been described [127]. Unlike oxoanions of Cr and Tc, the oxoanion of hypervalent Mn, permanganate, is thermodynamically unstable with respect to the oxidation of water although in sufficiently alkaline solutions it remains kinetically inert [128].

The hypervalent Tc behaves like chromate and forms a stable oxide film over a much broader pH range. Indeed, the technetates have been shown to actually exceed the corrosion inhibiting behavior of chromate with regard to corrosion of ferrous materials [129]. Cotton and Wilkinson in their classic text on inorganic chemistry point out the corrosion inhibiting properties of technetates [1]. Unfortunately for the search for chromate alternatives, technetate hardly offers a practical alternative to chromate. Nuclei for all of its isotopes are unstable with respect to β decay, the Tc^{99} being the most stable with a 2.12×10^5 year half-life decaying via a 0.29 MeV β emission.

Refractive metal oxide precursors. The elements such as Nb, Hf, Ti, Zr and Ta form very stable oxides in their highest oxidation state. Unfortunately, soluble and mobile precursors of these oxides remain difficult to stabilize in aqueous solution. Peroxo complexes and acid fluorides of Nb, Hf, Ti, and Zr exist at low pH. They form the basis

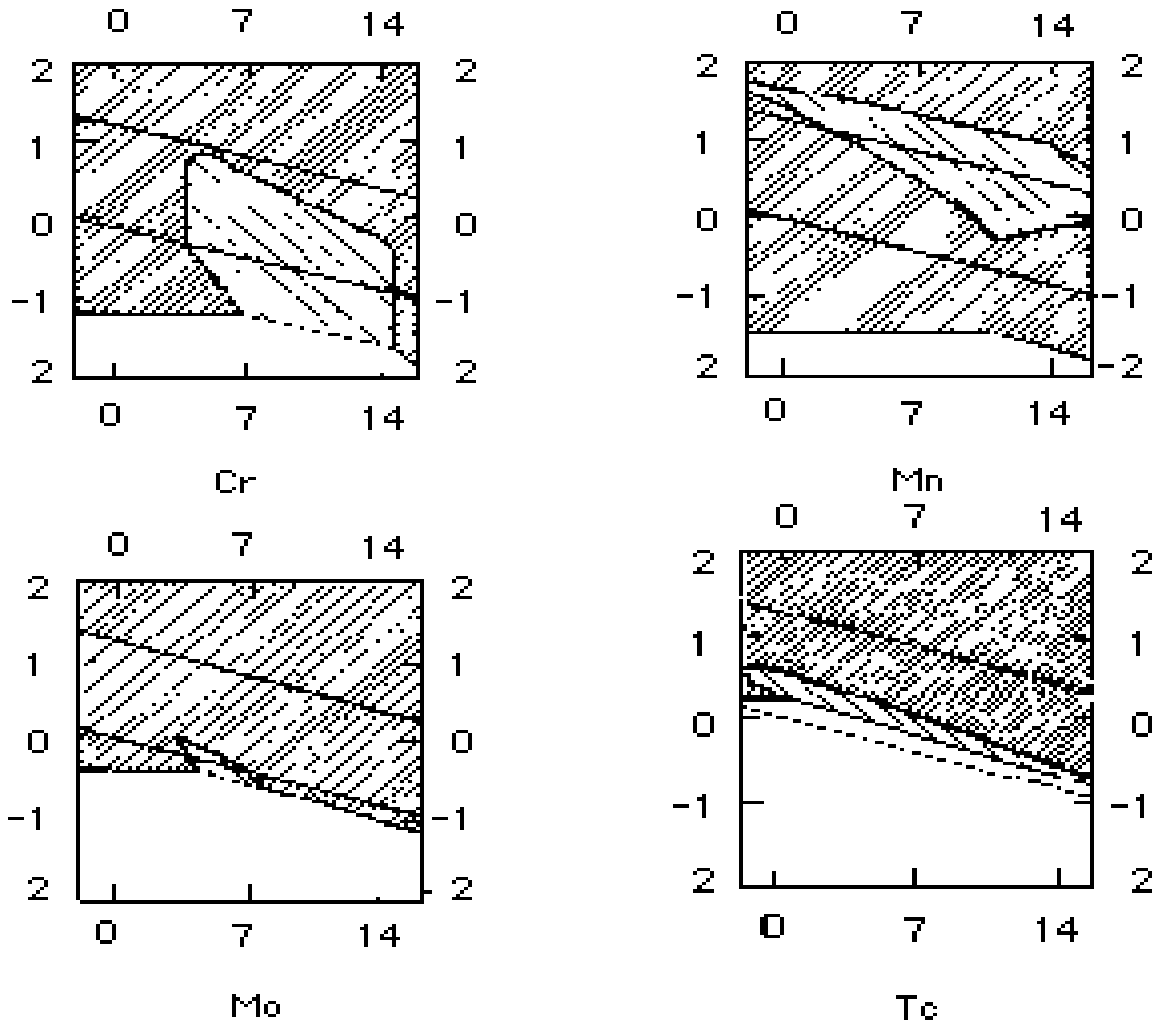

Figure 15. Pourbaix diagrams for Cr, Mn,Tc and Mo, elements that have soluble hypervalent oxo-anions that reduce to form insoluble oxide. Note that the pH region of stability for the insoluble oxides are very broad for Cr, Mn, and Tc, but not Mo.

of a number of patents (see Appendix 1). Thin Zr coatings have been shown to rapidly form a very thin self-limiting layer [130]. Alkoxides of these species can also be used to form stable dispersions (sols) leading to sol-gel routes for coating formation. How such active precursors could be retained in the resulting film in a manner analogous to the retention of Cr^{6+} by Cr conversion coatings is difficult to imagine.

Rare earths. In recent years, the use of rare earth compounds as corrosion inhibitors has become quite fashionable, primarily as a result of successful work by Hinton and his co-workers in Australia [131]. The mechanism for the rare earth inhibition seems to arise from the alkaline precipitation of protective oxide films at active cathodes. Ce cations also appear to work well in conjunction with molybdates and hydrothermal treatment to form very passive films on aluminum and its alloys [132], and as a seal for anodized aluminum [133]. Ce^{3+} reversibly adsorbs on anodized aluminum, but it acts at much different sites than the Cr^{6+} oxoanions. Whereas the adsorption of chromate on anodized aluminum lowers the zeta potential of the oxide, adsorption of Ce^{3+} increases the zeta potential [134]. It is highly likely that Ce does not protect by a rapid surface adsorption, but requires cathodic precipitation of a bulk oxide. The fact that low concentrations of Ce^{3+} increase the zeta potential on anodized Al provides more evidence that its inhibition mechanism differs considerably from that of Cr^{6+}. Although the elements in the lanthanide series are chemically similar, Ce species appear to offer the most effective corrosion inhibition. It has been speculated that this observation is related to the fact that Ce is the only lanthanide element that exhibits a tetravalent oxidation state that is stable in aqueous solution [135]. The solubility and stability (hence transportability) of Ce^{4+} in an alkaline solutions and the comparative insolubility of Ce^{3+} compounds in the same environment may go a long way towards explaining the ability of cationic solutions of Ce to inhibit active cathodic sites on Al and its alloys. In this sense, Ce^{4+} behaves somewhat like Cr^{6+}. The reduction product, Ce^{3+}, however is not nearly as stable in the case of the as compared to Cr^{3+}. It should be noted that the thermodynamic solubility of Ce^{4+} is lower than that of Ce^{3+}. However, Ce^{4+} is extensively hydrolyzed and readily complexed by a range of ligands, giving rise to a much greater apparent solubility [136]. Additional information on the lanthanide inhibitors can be found in a recent review [137].

Sol-gel chemistry. Sol-gel chemistry involves the hydrolytic polymerization POM ion solutions to form polymeric sols dispersed in water. Upon drying, POMs gel; that is they go from a solid phase dispersed in a liquid to liquid (water) dispersed in a three-dimensional solid network [2]. As pointed out in the Introduction, new descriptions of CCC formation closely follow a sol-gel mechanism [3, 11]. Recent Cr^{3+} technology developed by the Navy involves the polymerization of oxo-Cr^{3+} in sulfate solution to form a sol which in turn gels on the surface of aluminum alloys to dry as a protective coating [94].

Alkaline earth chemistries and hydrotalcite coatings. Synthetic hydrotalcites, also known as layered double hydroxides, mixed metal hydroxides, or anion-exchanging clays, are layered compounds derived from gibbsite and brucite[138, 139]. The archetypical hydrotalcites are the naturally occuring minerals hydromagnesite, $Mg_6Al_2(OH)_{16}{\cdot}CO_3{\cdot}4H_2O$, and pyroaurite, $Mg_6Fe_2(OH)_{16}{\cdot}CO_3{\cdot}4H_2O$. These compounds

consists of postively charged layered sheets of brucite in which Al^{3+} , or Fe^{3+} cations occupy octahedral sites. Layers of anions and water reside between, and electrostatically bind together the positively charged brucite sheets. Many synthetic hydrotalcites conforming to the generic formula: $M_x^{II}M_y^{III}(OH)_{2(x+y)}{\cdot}A_{y/n}{\cdot}nH_2O$ have been synthesized [140, 141].

Hydrolithisite, $Li_2[Al_2(OH)_6]_2{\cdot}A{\cdot}nH_2O$, forms spontaneously and rapidly as a coating on metallic aluminum and aluminum alloy surfaces when contacted with alkaline lithium salt solutions [142, 143]. Under the proper conditions, in a matter of minutes, a compact polycrystalline mass forms as a thin inorganic coating on alloy surfaces [144]. The resulting coating provides useful levels of corrosion protection, and renders an otherwise uncompatible surface receptive to organic coatings [145].

Under hot, alkaline, and oxidizing conditions hydrotalcite coatings with corrosion resistance sufficient to pass 168 hours of salt spray exposure testing without pitting can be formed [146]. To maximize corrosion resistance these coatings can be sealed with a variety of transition metal –based solutions or sealants used on anodized coatings. Sealed coatings offer enough corrosion resistance to protect 2024-T3 from pitting in salt spray exposure for times up to 336 hours [147].

Corrosion Inhibiting Pigments. The chromate-containing, corrosion-inhibiting pigments include the sparingly soluble chromates of the alkaline earths, Ca, Sr, Ba and Zn. They provide a source for active inhibiting Cr^{6+} compounds. A number of chromate alternatives have been considered, including molybdates, phosphates, metaborates, ZnO, vanadates, and silicates [148]. The patent literature suggests use of sol-gel technology for generating an endless variety of non-chromate pigments [149, 150]. In addition to their borate salts, organic acid salts of Ba have been considered as corrosion inhibitors. Although Ba metaborate as it exists at pH 10 provides very good inhibition for the Cu-rich intermetallics of Al 2024, its ability to inhibit decreases with decreasing pH [148].

Sinko notes that effective replacement of hexavalent Cr for the inhibition of high-strength alloys requires an inhibitor for both the ORR, and anodic dissolution of the active material of the intermetallic. Accordingly he proposes the concept of providing both of these functions, inhibition of ORR and inhibition of anodic dissolution/pitting, through the use using of ‘hybrid’ formulations [151-153] in which an organic (typically) ORR inhibitor is included with environmentally benign anodic inhibiting anions. Such anodic inhibitors might include ox-compounds of Mo, P and B. The organic ORR inhibitor takes over the role otherwise provided by Cr^{6+}.

Conducting Polymer Films. In 1985, DeBerry observed that like certain oxidizing inorganic compounds, conducting organic compounds could also anodically inhibit steel under certain conditions [154]. Since that time, a great deal of effort has been spent applying conducting organic polymers as corrosion protective films culminating in a number of recent patents [155-159]. Some work has been specifically directed at corrosion protection of aluminum and aluminum alloys [160-163]. A very recent patent claims the formation of a composite metal oxide conducting polymer anodic film [163].

Reports have claimed that electrochemically deposited polyanaline (PANI) improves the corrosion resistance of Al 2024-T3 by three orders of magnitude [164].

Parallels that exist between conducting polymer films and chromate may reveal the corrosion inhibition mechanism of such films. The doped and oxidized form of conducting polymers, such as PANI, conduct electrons. Upon reduction, these films become non-conducting [165]. Hence, they maintain oxides in the passive condition, while suppressing cathodic activity [166]. Scanning vibrating electrode measurements show that exposed metal in a large defect in a conducting polymer film do not corrode significantly during exposure to sulfate-chloride solutions [167].

Recent work has demonstrated another important property of doped and oxidized forms of conducting polymers. Materials doped with an inhibiting anion release the anion upon reduction. Both the release of an anionic pitting inhibitor and the decrease in conductivity of the cathode contribute to the inhibition [157, 168]. Others suggest that the negative potential of Al dominates the mixed PANI/Al potentials and that PANI coupled to Al 2024-T3 reduces to form a poor cathode [166]. This latter work also notes that CSA-doped PANI appears to inhibit pitting of a manufactured defect and that the inhibition process does not result from anodic stabilization. This supports the hypothesis that inhibiting anions play a role in pitting inhibition.

A hypothesis for the role of conducting polymer films emerges as the following:

- Conducting polymer films maintain passivity (anodically protects as per DeBerry [154] and Wessling [157]).

- Conducting polymer films short circuit the oxygen reduction reaction and become a non-conducting ‘poor’ cathode [166].

- Conducting polymer films release an inhibiting anion [168, 169].

This proposed model for corrosion inhibition by conducting polymers suggests investigating easily-processed materials doped in the oxidized state by a suitable corrosion (pitting) inhibiting anion. The choices for environmentally benign anions could include those oxoanions of molybdenum, or tungsten [124], permanganate [127], phosphate, borate and a number of heteropolyanions comprised of the oxo- compounds of Mo, W, Si, Al, Zr, V and P, and combinations thereof [122]. The possible combinations of inorganic anionic inhibitors as anion dopants for conducting polymer cations represent a large class of compounds.

As a final comment on the application of conducting polymers for chromate replacement, conducting polymer duplex films comprised of the reduced and oxidized form may lead to the same electron transfer inhibiting structures suggested by Clarke and McCreery [48] for inhibiting electron transfer at cathodes.

FUTURE TRENDS

Smart Coatings. Chromate conversion coatings are effectively smart coatings in that they release a corrosion-inhibiting compound, Cr^{6+}, when called upon to do so by the presence of a corrosive environment. Given the recent advances in nano-technology, self-organizing chemistries and biomemetic technologies, advances in the development of smart, self-diagnosing corrosion protective coatings represent a fruitful area research effort.

Inhibitor/Coating Discovery. As suggested in preceding section, inorganic oxoanions or organic oxygen reduction inhibitor chemistries represent a diverse of chemistry. Conventional corrosion testing of any one of these tens of thousands of possibilities would consume an inordinate amount of effort. Thus, development of methods for forming and screening large 'libraries' of potential corrosion inhibitors could identify that unique combination of properties as provided by chromate. In the past, pharmaceutical companies have used combinatorial methods to synthesize and screen classes of chemical compounds for a particular drug application. Recently those in materials science have begun to use such methods for materials discovery including identification of electrocatalysts and even corrosion inhibitors in microelectronic processes [170]. It may be appropriate to use this methodology to discover compounds that would inhibit corrosion of key aerospace alloys.

SUMMARY AND CONCLUSIONS

The oxoanions of hexavalent chromium uniquely inhibit the corrosion of many metals and alloys and have been particularly useful for protecting the high strength aluminum alloys against corrosion. Part of the usefulness of hexavalent chromium lies in its ability to react with metallic surfaces to form an inert Cr^{3+} oxide barrier with retained, releasable Cr^{6+}. The ability of absorbed and reduced Cr^{6+} (forming Cr^{3+} hydroxide) to inhibit the reduction of oxygen represents its main role in inhibiting corrosion though other components of corrosion protection do exist. For example, speciated as an oxoanion, Cr^{6+} appears to have an ability to inhibit pit initiation. While corrosion inhibition by Cr^{6+} is well characterized, the details of Cr^{6+} deposition are not. Chromate conversion coatings offer an especially attractive mix of characteristics including ease of application on a wide range of substrates, good corrosion resistance, and good adhesion. Supplemental bath ingredients such as F^- and $Fe(CN)_6^{3-}$ are essential in making robust conversion coatings. Coating formation can be appropriately understood in the context of a sol-gel process. Freshly formed conversion coating gels are well hydrated, and coating properties change dramatically as the gel dries. This has a range of practical consequences ranging from loss in corrosion resistance and loss of adhesion. A coating chemistry and technology for replacing chromate conversion still does not exist. Approaches to successfully replace chromate from current coating and inhibitor formulations will have to rely on the use of several chemistries engineered to play in concert the role of the unique Cr^{6+} oxoanions.

REFERENCES

1. F.A. Cotton, G. Wilkinson, *Advanced Inorganic Chemistry*, 2nd p. 818, New York, Wiley Interscience, 1966.
2. C.J. Brinker, G.W. Sherer, *Sol-Gel Science*, p. 272 Academic Press, New York, 1990.
3. J. Osborne, Observations on the Formation and Function of Chromate Conversion Coatings, p. in Proceedings of the Workshop on Advanced Metal Finishing Technologies for aerospace Applications, Air Force Office of Scientific Research, Keystone, CO, 1998.
4. C.F. Baes, R.E. Mesmer, *Hydrolysis of Cations*, p. 211, Malabar, FL, Robert E. Kreiger Publishing Co., 1986.
5. M.W. Kendig, J. Ramsey, R.L. McCreery, L. Xia, p. in Localized Corrosion III, PV 99-27, Electrochemical Society, Pennington, NJ, 1999.
6. J.D. Neuss, W. Reiman, *J. Am. Chem. Soc.*, 56, 2238 (1934).
7. R.K. Tandon, P.T. Crisp, J. Ellis, R.S. Baker, *Talanta*, 31, 227 (1984).
8. J.Y. Tong, E.L. King, *J. Am. Chem. Soc.*, 75, 6180 (1953).
9. S.-Y. Tong, K.-A. Le, *Talanta*, 33, 775 (1986).
10. J. Ramsey, R.L. McCreery, *J. Electrochem. Soc.*, 146, 4076 (1999).
11. L. Xia, R.L. McCreery, *J. Electrochem. Soc.*, 145, 3083 (1998).
12. M. Kendig, R. Addison, S. Jeanjaquet, *J. Electrochem. Soc.*, 146, 4419 (1999).
13. P.O. O'Brien, A. Kortenkamp, *Transition Metal Chemistry*, 20, 636 (1995).
14. *Chromium and Nickel Welding*, Lyon, International Agency for the Research on Cancer, 1990.
15. Y. Suzuki, *Ind. Health*, 28, 9 (1990).
16. Y. Suzuki, K. Fukuda, *Arch. Toxicol.*, 64, 169 (1990).
17. D. Stearns, K. Wetterhahn, *Chem. Res. Toxicol.*, 7, 219 (1994).
18. P. Lay, A. Levina, *J. Am. Chem. Soc.*, 120, 6704 (1998).
19. M. Krumploc, J. Rocek, *J. Am. Chem. Soc.*, 101, 3206 (1979).
20. G.S. Frankel, *Mechanism of Al Alloy Corrosion and the Role of Chromate Inhibitors*, First Annual Report, Contract No. F49620-96-1-0479, Ohio State University, Columbus, OH, 1997.
21. G.S. Frankel, *Mechanism of Al Alloy Corrosion and the Role of Chromate Inhibitors*, Second Annual Report, Contract No. F49620-96-1-0479, Ohio State University, Columbus, OH, 1998.
22. G.S. Frankel, *Mechanism of Al Alloy Corrosion and the Role of Chromate Inhibitors*, Third Annual Report, Contract No. F49620-96-1-0479, Ohio State University, Columbus, OH, 1999.
23. G.S. Frankel, *Mechanism of Al Alloy Corrosion and the Role of Chromate Inhibitors*, Fourth Annual Report, Contract No. F49620-96-1-0479, Ohio State University, Columbus, OH, 2000.
24. G.S. Frankel, *Mechanism of Al Alloy Corrosion and the Role of Chromate Inhibitors*, Final Report, Contract No. F49620-96-1-0479, Ohio State University, Columbus, OH, 2001.

25. K. Asami, M. Oki, G.E. Thompson, G.C. Wood, V. Ashworth, *Electrochim. Acta*, 32, 337 (1987).
26. T. Drozda, E. Maleczki, *Radioanal. Nucl. Chem. Lett.*, 95, 339 (1985).
27. P.L. Hagans, C.M. Haas, *Surface and Interface Analysis*, 21, 65 (1994).
28. A. Katzman, G. Malouf, R. Bauer, G.W. Stupian, *Applications of Surface Science*, 2, 416 (1979).
29. M.W. Kendig, A.J. Davenport, H.S. Isaacs, *Corrosion Sci.*, 43, 41 (1993).
30. Z. Yu, H. Ni, G. Zhang, Y. Wang, *Applications of Surface Science*, 62, 217 (1992).
31. L. Xia, E. Akiyama, G. Frankel, R. McCreery, *J. Electrochem. Soc.*, 147, 2556 (2000).
32. J. Zhao, G.S. Frankel, R.L. McCreery, *J. Electrochem. Soc.*, 145, 2258 (1998).
33. F. Pearlstein, V.S. Agarwala, p. 199 in Corrosion Protection by Coatings and surface Modification, PV 93-28, The Electrochemical Society, Pennington, NJ, 1993.
34. J.E. Hatch, *Aluminum: Properties and Physical Metallurgy*, p. 354, Metals Park, OH, American Society for Metals, 1984.
35. J.E. Hatch, *Aluminum: Properties and Physical Metallurgy*, p. 136, Metals Park, OH, American Society for Metals, 1984.
36. J.E. Hatch, *Aluminum: Properties and Physical Metallurgy*, p. 301, Metals Park, OH, American Society for Metals, 1984.
37. M.A. Alodan, W.H. Smyrl, *J. Electrochem. Soc.*, 145, 1571 (1998).
38. R.G. Buchheit, R.P. Grant, P.F. Hlava, B. McKenzie, G.L. Zender, *J. Electrochem Soc.*, 144, 2621 (1997).
39. R.G. Buchheit, M.A. Martinez, L.P. Montes, *J. Electrochem. Soc.*, 147, 119 (2000).
40. G.S. Chen, M. Gao, R.P. Wei, *Corrosion*, 52, 8 (1996).
41. N. Dimitrov, J.A. Mann, M.B. Vukmirovic, K. Sieradzki, *J. Electrochem. Soc.*, 146, 98 (1999).
42. R.G. Ford, R.W. Carpenter, K. Sieradzki, *Microsc. Microanal.*, 4, Suppl. 2, 754 (1998).
43. M. Gao, C.R. Feng, R.P. Wei, *Metall. Mater. Trans. A*, 29, 1145 (1998).
44. G.O. Ilevbare, J.R. Scully, *J. Electrochem. Soc.*, 148, B196 (2001).
45. M.B. Vukmirovic, N. Dimitrov, K. Sieradzki, *J. Electrochem. Soc.*, 149, B428 (2002).
46. L.F. Mondolfo, *Aluminum Alloys: Strucutre and Properties*, p. 698, London, Butterworths, 1976.
47. J.E. Hatch, *Aluminum: Properties and Physical Metallurgy*, p. 70, Metals Park, OH, American Society for Metals, 1984.
48. W.J. Clark, R.L. McCreery, *J. Electrochem. Soc.*, 149, B379 (2002).
49. A. Sehgal, G. S. Frankel, B. Zoofan, S. Rokhlin, *J. Electrochemc. Soc.*, 147, 140 (2000).
50. H. Kaesche, Pitting Corrosion of Aluminum and Intergranualr Corrosion of Al Alloys, p. 516 in Localized Corrosion, 3, NACE, Houston, TX, Williamsburg, VA, 1971.

51. G.O. Ilevbare, C. Jeffcoate, J.R. Scully, Passivity and Localized Corrosion, p. 269 in Sato Symposium, PV 99-27, The Electrochemical Society, 1999.
52. G.O. Ilevbare, J.R. Scully, *Corrosion*, 57, 134 (2001).
53. M. Kendig, S. Jeanjaquet, *J. Electrochem. Soc.*, 149, B47 (2002).
54. J. Horanyi, *Solid State Electrochem.*, 4, 153 (2001).
55. S. T. Pride, J. R. Scully, J.L. Hudson, *J. Electrochem. Soc.*, 141, 3028 (1994).
56. A. Sehgal, D. Lu, G.S. Frankel, *J. Electrochem. Soc.*, 145, 2834 (1998).
57. E. Akiyama, G.S. Frankel, *J. Electrochem. Soc.*, 146, 4095 (1999).
58. R.J. Cinderey, G.T. Burstein, *Corrosion Sci.*, 33, 493 (1992).
59. G.H. Cartledge, *J. Electrochem. Soc.*, 4, 328 (1966).
60. N. Sato, *Corrosion*, 5, 354 (1989).
61. E. McCafferty, *J. Electrochem. Soc.*, 133, 481 (1986).
62. E. McCafferty, *Corros. Sci.*, 37, 481 (1995).
63. A. Kolics, S. Besing, A. Wieckowski, *J. Electrochem. Soc.*, 8, B322 (2001).
64. W. Zhang, R.G. Buchheit, *J. Electrochem Soc.*, 149, B357 (2002).
65. K. Shimuzu, G.M. Brown, K. Kobyashi, P. Skeldon, G.C. Wood, *Corrosion Sci.*, 40, 1049 (1998).
66. J.R. Waldrop, M.W. Kendig, *J. Electrochem. Soc.*, 145, L11 (1998).
67. R.G. Buchheit, *J. Electrochem. Soc.*, 142, 3994 (1995).
68. A. Kolics, J.C. Polkinghorne, A. Wieckowski, *Chem. Materials*, 10, 812 (1998).
69. P. Schmutz, G.S. Frankel, p. in Proceedings of 8th International Conference on Passivity of Metals and semiconductors, to be published,
70. V. Guillaumin, P. Schmutz, G.S. Frankel, Scaning Kelvin Probe Force Microscopy and auger Electron Spectroscopy Studies of Passive Surfaces, p. in Proceedings of the Sato Symposium, to be published,
71. W.R. McGovern, P. Schmutz, R.G. Buchheit, R.L. McCreery, *J. Electrochem. Soc.*, 147, 4494 (2000).
72. G.P. Halada, C.R. Clayton, M.J. Vasquez, J.R. Kearns, M. Kendig, S. Jeanjaquet, G.G. Peterson, G.S. McCarthy, G.L. Carr, p. 139 in Critical Factors in Localized Corrosion (III), PV 98-17, The Electrochemical Society, Pennington, NJ, 1999.
73. L. Juffs, A.E. Hughes, P.J.K. Paterson, *Micron*, 32, 777 (2001).
74. V.N. Laget, C.S. Jeffcoate, R.G. Buchheit, H.S. Isaacs, *J. Electrochem Soc.*, January, submitted for publication (2002).
75. A. Gallacio, F. Pearlstein, M.R. D'Ambrosio, *Met. Finish.*, 64, 50 (1966).
76. A.L. Glass, *Mat. Prot.*, 7, 26 (1968).
77. U.S. Military Specification, MIL-C-5541E, Chemical Conversion Coatings on Aluminum and Aluminum Alloys, NAEC, Lakehurst, NJ, November, 1990.
78. C.S. Jeffcoate, H.S. Isaacs, A.J. Aldykiewicz, M.P. Ryan, *J. Electrochem Soc.*, 147, 540 (2000).
79. S. Wernick, R. Pinner, P.G. Sheasby, *Chemical Conversion Coatings*, p. 220 in *The Surface Treatment Treatment and Finishing of Aluminum and Its Alloys*, ASM International, Metals Park, OH, 1987.
80. O. Bauer, O. Vogel, German Patent Specification, 226 776, 1923.
81. J.D. Edwards, U. S. Patent, 1 946 153, 1934.

82. T. Biestek, J. Weber, *Electrolytic and Chemical Conversion Coatings*, p. 319 Portcullis Press Limited, Redhill, Surrey, UK, 1976.
83. R.P. Marshall, *Metal Industry*, 71, 93 (1947).
84. Pyrene Company Ltd., UK Patent, 441 088, 1936.
85. Unknown, French Patent, Continentale Parker, 698 699, 1931.
86. J. Spruance, U. S. Patent, 438 887, 1945.
87. W. Marchand, *Electroplating and Metal Finishing*, 14, 439 (1961).
88. S. Spring, K. Woods, *Metal Finishing*, 79, 49 (1981).
89. N.J. Newhard, *Metal Finishing*, 70, 69 (1972).
90. International Patent Application, Henkel Corporation, PCT/US92/04962, 1993.
91. J.A. Treverton, N.C. Davies, *Metals Technology*, 4, 480 (1977).
92. J.A. Treverton, N.C. Davies, *Surface and Interface Analysis*, 3, 194 (1981).
93. L.J. Bailin, Kostinko, U. S. Patent, 5 123 978, 1992.
94. F. Pearlstein, V.S. Agarwala, *Plating and Surface Finishing*, 81, 50 (1994).
95. G.W. Ostrander, *Plating*, 38, 1033 (1951).
96. J.H. Osborne, J. Du, A. Nercissiantz, S.R. Taylor, D. Bernard, G.P. Bierwagen, *Advanced Corrosion Resistant Aircraft Coatings*, prepared under contract no. F33615-96-C-5078, Air Force Materiel Command, Wright-Patterson AFB, OH, 2000.
97. H.H. Uhlig, A. Geary, *J. Electrochem. Soc.*, 101, 215 (1954).
98. P.L. Hagans, C.M. Haas, *Chromate Conversion Coatings*, p. 405 in *Surface Engineering*, ASM International, Metals Park, OH, 1987.
99. E. Hughes, R.J. Taylor, B.W.R. Hinton, *Surface and Interface Analysis*, 25, 223 (1997).
100. J.H. Osborne, *Prog. Org. Coatings*, 41, 280 (2001).
101. M. Henry, J.P. Jolivet, L. Livage, *Aqueous Chemistry of metal Cations: Hydrolysis Condensation, and Complexation*, p. 155 in *Structure and Bonding*, Springer-Verlag, Berlin, 1992.
102. D.J. Arrowsmith, J.K. Dennis, P. Sliwinski, *Trans. of the Institute of Metal Finishing*, 62, 117 (1984).
103. G.M. Brown, K. Shimuzu, K. Kobayashi, G.E. Thompson, G.C. Wood, *Corrosion Sci.*, 34, 1045 (1993).
104. DOE Specification, 9904151, Coating, Chromate on Aluminum, Department of Energy, 1989.
105. R.A. Haaksma, J.R. Weir, p. 1074 in Proceedings of the 27th International SAMPE Technical Conference, SAMPE, 1995.
106. J.A. Treverton, A. Bosland, J.M. Brown, *Corrosion Sci.*, 30, 1159 (1990).
107. L. Fedrizzi, F. Marchetti, *J. Materials Sci.*, 26, 1931 (1991).
108. N.J. Newhard, *Metal Finishing*, 70, 49 (1972).
109. N.J. Newhard, *Metal Finishing*, 70, 66 (1972).
110. L.A. Nimon, G.K. Korpi, *Plating*, 59, 421 (1972).
111. F.W. Eppensteiner, M.R. Jenkins, *Chromate Conversion Coatings*, p. 494 in *Metal Finishing*, Metals and Plastics Publications, Hackensack, NJ, 1999.
112. L. Xia, R.L. McCreery, *J. Electrochem. Soc.*, 146, 3696 (1999).
113. F.W. Lytle, R.B. Greegor, G.L. Bibbins, K.Y. Blohowiak, R.E. Smith, G.D. Tuss, *Corrosion Sci.*, 37, 349 (1995).

114. J.A. Treverton, M.P. Amor, *Trans. of the Institute of Metal Finishing*, 60, 92 (1982).
115. G.M. Brown, K. Shimuzu, K. Kobayashi, G.E. Thompson, G.C. Wood, *Corrosion Sci.*, 33, 1371 (1992).
116. M.J. Vasquez, J.R. Kearns, G.P. Halada, C.R. Clayton, *Surface and Interf. Analysis*, 33, 796 (2002).
117. G.M. Brown, K. Kobayashi, *J. Electrochem. Soc.*, 11, B457 (2001).
118. S.M. Cohen, *Corrosion*, 51, 71 (1995).
119. B.W.R. Hinton, *Metal Finishing*, 89, 55 (1991).
120. B.W.R. Hinton, *Metal Finishing*, 89, 15 (1991).
121. R.L. Twite, G.P. Bierwagen, *Prog. Org. Coatings*, 33, 91 (1998).
122. R.L. Cook, S.R. Taylor, *Corrosion*, 56, 321 (2000).
123. T. Yamamoto, p. in Proceedings of Advances in Corrosion Protection by Organic Coatings, PV 89-13, The Electrochemical Society, Christ's College, Cambridge, 1989.
124. S. Zein, *J. Appl. Electrochemistry*, 31, 711 (2001).
125. V. Moutarlier, M.P. Gigandet, L. Ricq, J. Pagetti, *Appl. Surf. Sci.*, 1-2, 1 (2001).
126. J. Bibber, Paper no. 392, p. in Corrosion/95, NACE International, Houston, TX, 1995.
127. I. Danilidis, J.M. Sykes, J.A. Hunter, G. Scamens, *Surf. Engineering*, 4, 401 (1999).
128. A. Cusanelli, U. Frey, D.T. Richens, A.E. Merbach, *J. Am. Chem. Soc.*, 118, 5265 (1996).
129. G.H. Cartledge, *J. Electrochem. Soc.*, 113, 328 (1966).
130. T. Schram, G. Goeminne, H. Terryn, *Trans. Inst. Met. Fin.*, 73, part 3, 91 (1995).
131. B.W.R. Hinton, *Metals Forum*, 4, 211 (1984).
132. F. Mansfeld, S. Lin, K. Kim, H. Shih, *Corrosion Sci.*, 27, 997 (1987).
133. D. Dull, C. Chen, F. Mansfeld, Abstract No. 100, p. in 193rd Society Meeting, PV98-1, San Diego, CA, 1998.
134. M. Kendig, R. Addison, S. Jeanjaquet, *Electrochemical Society Letters*, 3, 266 (2000).
135. R.G. Buchheit, S.B. Mmidipally, P.Schmutz, H. Guan, *Corrosion*, 58, 3 (2002).
136. C.F. Baes, R.E. Mesmer, *Hydrolysis of Cations*, p. 138, Malabar, FL, Robert E. Kreiger Publishing Co., 1986.
137. M. Bethancourt, F. Botana, J. Calvino, M. Marcos, M. Rodriguez-Chacon, *Corrosion Sci.*, 11, 1803 (1998).
138. S. Miyata, *Clay and Clay Miner.*, 23, 369 (1975).
139. H.F.W. Taylor, *Min. Mag*, 39, 377 (1973).
140. K. Itaya, H.-C. Chang, I. Uchida, 26, 624 (1987).
141. W.T. Reichle, *J. Catal.*, 94, 547 (1985).
142. R.G. Buchheit, G.E. Stoner, *Corrosion*, 50, 205 (1994).
143. R.G. Buchheit, G.E. Stoner, U. S. Patent, 5,266,356, 1993.
144. C.A. Drewien, M.O. Eatough, E.R. Tallant, C.R. Hills, R.G. Buchheit, *J. Mater. Res.*, 11, 1507 (1996).
145. R.G. Buchheit, C.A. Drewien, J.A. Finch, G.E. Stoner, Paper No. 542, NACE International, Houston, TX, 1994.

146. R.G. Buchheit, L.P. Montes, M.A. Martinez, R.J. Taylor, N. Cella, *NACE Research in Progress Symposium Abstracts*, NACE International, Houston, TX, 1998.
147. R.G. Buchheit, M.A. Martinez, U. S. Patent, 5,756,218, 1998.
148. M. Kendig, M. Cunningham, S. Jeanjaquet, D. Hardwick, *J. Electrochem. Soc.*, 11, 3721 (1997).
149. C.L. Kissle, U. S. Patent, 5158605, 1992.
150. C.L. Kissle, U. S. Patent, 5198487, 1993.
151. J. Sinko, Challenges of Chromate Inhibitor Pigments Replacement in Organic Coatings, p. 267-282 in XXV Athens Conference, 42, Prog. Org. Coatings, Athens, 1999.
152. J. Sinko, Considerations on the Chemistry and Action Mechanism of Corrosion Inhibitor Pigments in Organic Coatings, p. in 6th Biennial Conference on Organic Coatings, Hilton Head Island, SC, 2000.
153. J. Sinko, U.S. Patent, 6,139,610, 2000.
154. D. DeBerry, *J. Electrochem. Soc.*, 132, 1022 (1985).
155. P. Kinlen, U. S. Patent, 5532025, 1996.
156. MacDiarmid, N. Ahmad, U. S. Patent, 5645890, 1997.
157. B. Wessling, *Synthetic Metals*, 41-43, 907 (1991).
158. D.A. Wrobleski, B.C. Benicewicz, K.G. Thompson, C.J. Bryan, U. S. Patent, 5658649, 1997.
159. D.A. Wrobleski, *Polymer Preprints*, 1, 264 (1994).
160. M. Perucki, P. Chandrasekhar, *Synthetic Metals*, 119, 385 (2001).
161. R. Racicot, R. Brown, S.C. Yang, *Synthetic Metals*, 85, 1263 (1997).
162. R. Racicot, S.C. Yang, R. Brown, *Corrosion*, 53, 1 (1997).
163. J. Runge-Marchese, M. McNallan, U. S. Patent, 5980723, 1999.
164. K. Shah, Y.R. Zhu, G.S. Akundy, J.O. Iroh, O. Popoola, *Durable Surfaces*, 197, 111 (2001).
165. G. MacDiarmid, J. Chang, J. Richter, A. Somasiri, A. Epstein, *Conducting Polymers*, Holland, Reidel Publishing Co., 1987.
166. S.F. Cogan, M.D. Gilbert, G.L. Holleck, J. Ehrlich, M.H. Jillson, *J. Electrochem. Soc.*, 6, 2143 (2000).
167. J. He, V.J. Gelling, D. Tallman, G.P. Bierwagen, G. Wallace, *J. Electrochem. Soc.*, 10, 3667 (2000).
168. S.S. deSouza, J. Pereira, S.C.d. Torres, M. Temperini, R. Torresi, *Electrochemical and Solid State Letters*, 4, B27 (2001).
169. P. Kinlen, D. Silverman, *Corrosion*, to be published, (2002).
170. S. Affrossman, J. Daviot, D. Holmes, R.A. Pethrick, M. Wilson, *Corrosion Sci.*, 5, 939 (2001).

Table I. Summary of the Chemistry in Key Intellectual Property Related to Non-Chromate Coatings.

US04085063	nitrate and metasilicate inhibitor in cooling water
US04148670	Zr and/or Ti, fluoride and phosphate or polyhydroxy compounds having 6 or fewer carbon atoms.
US04222779	silicate, sulfuric acid H2O2, organo phosphonate, substituted ureas
US04225350	H2SO4,H2O2, silicate + cationic triarylmethane dye. organophosphorus
US04225351	H2O2, H2SO4, silicate, organo-phosphate
US04313769	Zr, Hf, Ti, F
US04370177	Zr, Hf, Ti, F
US04451304	nitrite post treatment
US04470853	acidicfluoro zirconic, fluoroboric, F, tannin, phosphates, Zn
US04545842	adhesion promotor based on fluorides of Zr, Si, Ti
US04921552	hexafluoro zirconate, HF, polyacrylic acid
US05052421	heteropoly vanadic acid deoxidation
US05077332	polyvinyl butyl resin+ anti-corrosive pigment from borate and phosphate salts. (wash primer)
US05129967	H2ZrF6 + polyacrylic + acid HF
US05294265	organophosphates or phosphonates and chloride or fluoride
US05298092	Oxide film cobalt conversion coating
US05328525	polyacrylic acid or homopolymers and copolymers thereof, a molybdate, and a dihydrohexafluo acid
US05378293	Al2O3,as the largest volume percent, and cobalt oxides CoO, Co3 O4,Co2O3
US05389405	cationic polymer, an alkaline aqueous,silicate and an organofunctional silane
US05411606	Oxide film cobalt conversion coating
US05415687	Aluminum oxide - Co oxide based
US05451431	aqueous solution of a cationic polymer, an alkaline aqueous,silicate and an organofunctional silane
US05463804	organophonic and phosphinic acid adhesion promotor
US05468307	Al2O3,as the largest volume percent, and cobalt oxides CoO, Co3 O4,Co2O3
US05472524	Co oxide conversion coating
US05487949	Co oxide conversion coating
US05496417	steam oxidation
US05551994	Co oxide
US05584946	acidic fluorides of Hf, Zr, Ti,
US05641542	polymeric composition
US05683816	phosphoric acid Mo(V)-Mo(VI)
US05693153	10% HNO3 and 3% NaBrO4 deoxidation + boiling water + Li nitrate Al silicate seal
US05759244	acidic oxy groupe IVA with no fluoride or solvent

US05843242	Co(II),Co(III) oxide with sodium decavanadate seal
US05866652	Ce oxide,vanadate,borate
US05873953	Co(II) oxide
US05897716	H2XF6 where X=Ti,Zr,Hf,Al,Si,Ge,Sn,B + hydroxy carboxylic acids + polymers + other
US05266356	Li and alkaline salt to form hydrotalcite
US05756218	reaction of an alkaline surface with soluble compounds of Al, Mg, Ca, Sr, Ti, Mo, Ce, Pr, Nd, Sm,Eu, Gd, Tb, Dy, Ho, Er, Tm, Yb, Lu, Mn, Fe, Co, Ni, and Bi

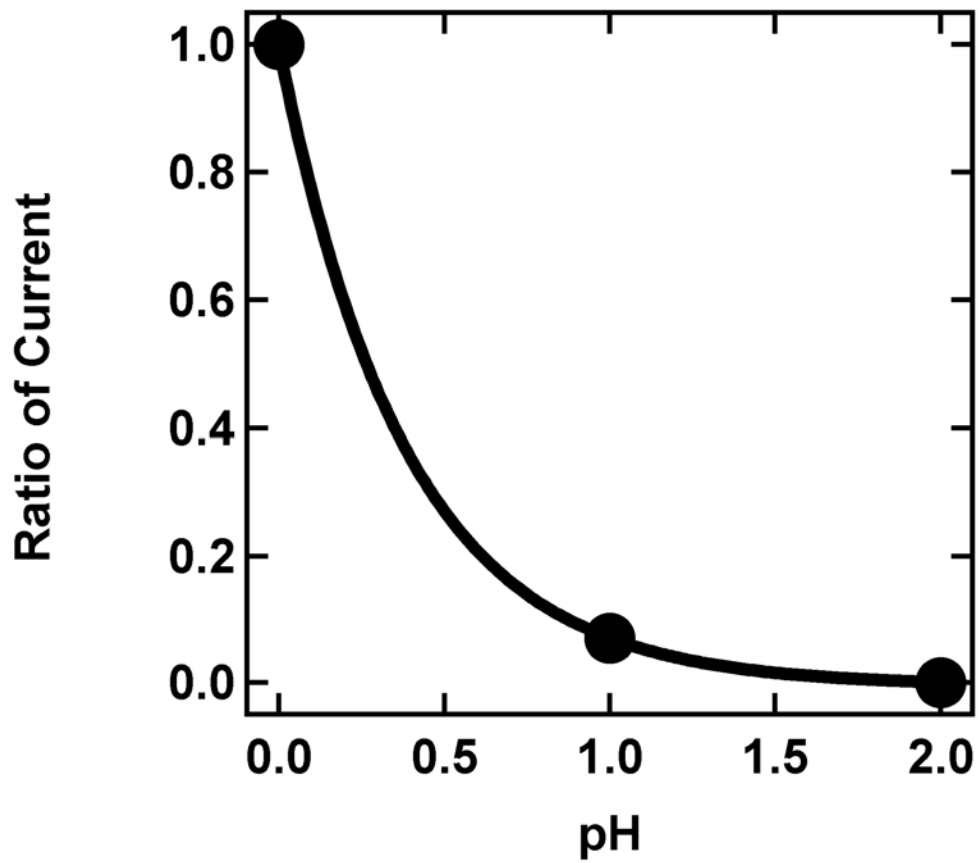

Figure 8. The ratio of steady state current at –0.500V_{sce} in the presence to that in the absence of oxo-Cr^{6+} as a function of pH.

Results and Accomplishments Part II:

Corrosion Protection of Aluminum 2024-T3 by Vanadate Conversion Coatings[2]

ABSTRACT

In this paper, the formation, chemistry, morphology and corrosion protection of a new type of inorganic conversion coating is described. This coating, referred to as a vanadate conversion coating (VCC), forms on Al alloy substrates in a matter of minutes during simple immersion in aqueous vanadate-based solutions at ambient temperatures. VCCs are yellow in color and conformal across the surface of Al alloy 2024-T3 substrates. Auger electron sputter depth profiles and x-ray absorption near edge spectroscopy shows that VCCs formed by a 3-minute immersion are 300 to 500nm thick and consist of a mixture of vanadium oxides and other components in the coating bath. In anodic polarization experiments conducted in aerated chloride solutions, VCCs increase the pitting potential and decrease the rate of oxygen reduction. When characterized by electrochemical impedance spectroscopy, VCCs demonstrate a low frequency impedance between 1 and 2 $M\Omega \cdot cm^2$ after 24 hours exposure to aerated 0.5M NaCl solutions. In salt spray testing conducted according to ASTM B117, VCCs suppress formation of large pits for more 168 hours. VCCs also appear to be self-healing. Analysis of solution in contact with VCCs by inductively coupled plasma emission spectroscopy indicates that vanadate is released into solution upon exposure. Vanadium deposits were identified by x-ray microchemical analysis on a bare alloy substrate held in close proximity to a vanadate conversion coated surface, and corrosion resistance of this bare surface was observed to increased during exposure. An important component of VCC formation appears to involve inorganic polymerization of V^{5+}, which leads to the build-up of a film that passivates the surface and inhibits corrosion.

INTRODUCTION

Vanadium compounds are versatile corrosion inhibitors, though they are not widely used to protect engineering materials at the present time. For example, additions of $NaVO_3$ in amounts of 0.1 to 0.2 wt.% have been observed to reduce the corrosion rate of carbon steel in boiling K_2CO_3 solutions saturated with CO_2 and H_2S from 340 mpy to less than 0.1mpy [1, 2]. Modest corrosion protection of aluminum alloy 2014 exposed to aerated 1mM NaCl has been demonstrated using 2mM $NaVO_3$ additions [3, 4]. Recent studies have shown potent inhibition of localized corrosion on 2024-T3 over a range of solution pH when 3.4mM $NaVO_3$ is added to aerated 0.6M NaCl solution [5].

Other studies have shown that vanadium can be alloyed with Fe or Al to promote corrosion resistance. Vanadium additions are known to increase the pitting resistance of

[2] Published in Corrosion 60 (3): 284-296 (2004)

both austenitic and ferritic stainless steels [6]. In ferritic stainless steels, V additions have been observed to increase the pitting potential measured in 3.5% NaCl solution to the same extent as equivalent additions of molybdenum [7]. Increases in pitting resistance appear to be due to a decrease in the rate of metastable pit nucleation and an increase in metastable pit salt film stability, which is proposed to increase the tendency for pit repassivation. In others studies, 1 to 4 wt. % additions of V to ferritic stainless steels were found to lower the critical current required for passivation and to increase the potential range over which passivity was detected in anodic polarization experiments [8]. Non-equilibrium Al-V alloys produced by sputter deposition exhibit an increase in pitting and repassivation potentials during anodic polarization in aerated 0.1M NaCl solution [9]. Additions of 10 to 20 wt.% V increased the pitting potential by more than 1.0V compared to pure Al. The repassivation potential was found to increase by nearly 0.5V in the same experiments.

Vanadium compounds have also been used to enhance the corrosion protection provided by coatings. Small amounts of vanadate added to sulfuric acid anodizing solutions have been found to make the anodized coating much more protective after hydrothermal sealing [10]. In other studies, vanadate compounds were used to seal thickened oxide layers on 6061-T6-alumina composites by direct application of a vanadate solution [11]. These vanadate-sealed surfaces promoted adhesion of subsequently applied fluoropolymer coatings and resulted in coating systems with very high levels of corrosion resistance in a range of environments.

Vanadium compounds have also been used as primary ingredients in several film formation processes. Solutions comprising vanadate, one of several other transition metal ions, and an acid-resistant organic resin will form protective films on Zn and Zn-Al alloys provided that the coating solution pH is less than 3 [12]. Corrosion resistant sol-gel coatings doped with vanadates have been demonstrated on steel and aluminum substrates [13, 14]. In other studies, acidic vanadate-phosphate coating chemistries have been developed to form corrosion resistant coatings on aluminum and aluminum alloy substrates [15].

Outside of the context of inhibitors and coatings, formation of hydrated vanadium oxide gels upon acidification of metavanadate salt solutions has been thoroughly studied and described [16]. The oxide formation process involves a hydrolysis-condensation-polymerization mechanism that is essentially a sol-gel process. Vanadium oxides produced in this way are used as reversible cathodes for lithium batteries and electrochromic devices.

A comparison of this vanadium oxide formation mechanism and recent interpretations of chromate conversion coating (CCC) formation on Al alloys suggest an approach that might be exploited to make a corrosion resistant vanadate conversion coating or "VCC". CCC formation involves electrochemical reduction of chromate followed by inorganic polymerization to build the conversion film [17-19]. Specifically, this process involves reduction of Cr^{6+} in solution to form hydrated $Cr(OH_2)_6^{3+}$. This species hydrolyzes in the locally alkaline region at the alloy-solution interface forming

hydrated chromium hydroxide, $Cr(OH_2)_3(OH)_3$. This hydrate then polymerizes by forming Cr(III)-OH-Cr(III) linkages forming a so-called polymer "backbone". Simultaneously, chromate binds via oxygen ligands forming Cr(VI)-O-Cr(III) linkages, which are characteristic of chromium chromate conversion coatings [18].

Chromate by itself is not a potent film former [19]. Exposure of pure Al to an acidified chromate solution does not impart much latent corrosion protection. What does form is a very thin strongly adsorbed layer of hydrated chromium hydroxide with near-monolayer thickness [20]. This layer stifles further chromate film formation, but is not robust enough to confer lasting corrosion protection in aggressive aqueous chloride environments. Fluoride additions to acidic chromate baths delay chromate passivation of Al surfaces for about 20 to 30 seconds. This delay, often referred to as "activation", appears to be sufficient to generate enough Cr^{3+} by electrochemical reduction to fuel the hydrolysis and polymerization process leading to formation of coatings with thicknesses approaching one micrometer when dried. In the chromate conversion coating formation process, ferricyanide is used as a redox mediator [21]. Ferricyanide enhances the Cr^{6+} to Cr^{3+} reduction reaction kinetics, which are normally sluggish on Al, thereby stimulating coating growth. Electrochemical testing of conversion coatings formed in the presence and absence of fluoride and ferricyanide additions shows that these supplemental ingredients play an essential role in the formation of conversion coatings with high levels of corrosion resistance [19].

The ability of Cr and V to form hydrated oxides by sol-gel processes combined with the well known stimulating effects of ferricyanide and fluoride in chromate coating processes suggests an approach for developing a chromate-free conversion coating process based on vanadium oxide film formation. To explore the utility of this approach, we have attempted to induce the formation of vanadate coatings on Al alloys by inorganic polymerization stimulated by additions of fluoride and ferricyanide.

EXPERIMENTAL PROCEDURES

Materials and preparation. Coating formation was carried out on samples prepared from commercial 2.0 mm thick 2024-T3 sheet (3.8-4.9Cu, 1.2-1.8 Mg, 0.3-0.9 Mn, 0.5 Si and Fe, 0.15 Zn and Ti, and 0.1 Cr on a weight percentage basis). Sample surfaces were prepared for examination by electron microscopy and electrochemical corrosion testing by mechanical polishing using silicon carbide paper and ethanol, starting at 600 grit and finishing with 1200 grit. The specimens were ultrasonically cleaned in ethanol before further use. All the electrolytes were made from reagent grade chemicals and 18MΩ·cm deionized water.

Vanadate conversion coating (VCC) formation. Vanadate conversion coating was carried out in a manner analogous to chromate conversion coating (CCC). Coatings were formed on 50mm x 100mm x 2mm 2024-T3 sheet stock. Prior to coating, all samples were washed with an alkaline detergent, degreased in a sodium silicate ($NaSiO_3$)/sodium carbonate (Na_2CO_3) solution, then deoxidized in a nitric acid (HNO_3)/sodium bromate

($NaBrO_3$)-based solution. Samples were rinsed in overflowing deionized water between each step. VCC coatings were formed by immersion in a bath containing a mixture of sodium metavanadate, $NaVO_3$ (10 to 100mM), potassium ferricyanide, $K_3Fe(CN)_6$ (3mM), and sodium fluoride, NaF (2mM) at room temperature. The bath pH was adjusted using concentrated nitric acid, HNO_3. After the coatings were formed, the coated surfaces were rinsed in overflowing deionized water, then soaked for an additional 3 minutes in deionized water. Coatings were air-dried and aged for 24 hours before any further handling or analysis.

XANES, AES, and SEM. X-ray absorption near edge spectroscopy (XANES) measurements at the V K edge (E_0 = 5480eV) were made at the National Synchrotron Light Source on beam line X19A following well-established procedures for conversion coatings [22, 23]. The fluorescent intensity was recorded with a 13-element detector at right angles to the incoming beam and the sample tilted at 45° with respect to the incident beam. Spectra were background subtracted and normalized so that the absorption coefficient, defined as fluorescent intensity over incident beam intensity was equal to 1.0 at E = 5505eV. A good estimation of the ratio of V^{5+} over total V was then directly given by the height of a pre-edge peak characteristic of vanadium in the +5 oxidation state [24, 25].

Scanning electron microscopy (SEM) and Auger electron spectroscopy (AES) were used to characterize surface morphologies and surface chemistries. AES measurements were made with a PHI 680 Auger spectrometer equipped with a field emission gun. A range of operating beam conditions were used depending on which spectral regions were being investigated. Areas of interest were identified by secondary electron imaging. For depth profiling, a 1 keV/0.5mA argon ion beam was used. The sputter rate was 10 nm/min for SiO_2. Quantitative AES results were determined from derivative spectra using elemental sensitivity factors.

Electrochemical and exposure characterization techniques. The corrosion resistance of conversion coated surfaces was evaluated using electrochemical impedance spectroscopy (EIS). EIS was carried out using a Princeton Applied Research model 273 potentiostat combined with a Solartron 1250 Frequency Response Analyzer controlled by Zplot™ EIS software. EIS spectra were collected from 10kHz to 10mHz using a 10mV amplitude sinusoidal voltage perturbation superimposed on a DC potential set at the sample open circuit potential. Spectra were collected at a rate of 10 points per decade frequency. EIS data were fitted to an equivalent circuit model using a complex least squares fitting routine.

Anodic and cathodic inhibition by soluble vanadate was assessed by potentiodynamic polarization. A Princeton Applied Research model 273 potentiostat controlled by Corrware™ software was used to conduct the potentiodynamic polarization scans. The experiments were carried out using a three-electrode configuration (saturated calomel electrode (SCE) as a reference electrode) with $1.0cm^2$ exposure area of working electrode. The anodic polarization scans were initiated 30mV negative to the steady-state open circuit potential (OCP) and ramped in the positive direction at 0.2mV/s until the current density reached 1000 $\mu A/cm^2$. The direction of the scan was then reversed and

continued until a potential of 30 mV negative of the open circuit potential was reached. At a minimum, all polarization experiments were run in duplicate. Cathodic polarization scans were initiated at the sample OCP and were measured to a potential –1500mV negative of that potential.

Salt spray testing was conducted according to ASTM B117, which specifies chamber exposure of coated panels at 35°C (95°F) to a fog generated by atomizing a 5% NaCl solution. After exposure, samples were rinsed in deionized water and visually inspected for evidence of corrosion damage.

A “simulated scratch cell” was used to test for elements of self-healing [26]. The cell shown in Figure 1, was constructed of two 2024-T3 samples separated by a 5mm thick rubber O-ring gasket with a diameter of 50mm. One side of the cell was a 2024-T3 surface coated with a VCC, the other side of the cell was a cleaned but uncoated surface. The exposure area for each panel was 15.9cm^2 and the volume of the cell between the surfaces was about 8ml giving a VCC surface area to solution volume ratio of 2cm^{-1}. A 5mm diameter hole was made on the top panel (the coated surface) to fill the gap with 0.1M NaCl solution and to accommodate a saturated calomel reference electrode (SCE). A Pt counter electrode was inserted into the cell to enable EIS measurements to be made in situ. EIS measurements of the bare side of the cell were collected and analyzed to check for increases in corrosion resistance that might indicate self-healing. Solution was extracted from the cell periodically to check for the presence of vanadium leached from the VCC. X-ray microchemical analysis by energy dispersive spectroscopy was performed on the originally bare side of the cell to check for the presence of vanadium that migrated from the VCC.

RESULTS

<u>Corrosion inhibition by metavanadate</u>. Additions of $NaVO_3$ to aerated chloride solutions inhibit both anodic and cathodic kinetics on 2024-T3 electrodes. Figure 2 shows anodic polarization curves of 2024-T3 in aerated 0.124M NaCl solution at pH 6. Duplicate polarization curves are shown for the chloride-only solution, and triplicate curves are shown for solutions to which 0.1M $NaVO_3$ was added. At this pH, vanadium is speciated as $VO(OH)_3$, $VO_2(OH)_2^-$, and $(VO3)_x^{x-}$ where x ranges from 1 to 4. These species are referred to collectively as "metavanadates" [27]. Comparison of the two sets of curves shows that metavanadates are modest anodic inhibitors. A region of imperfect passivity exists over a range of about 100mV positive of the (OCP). Passive behavior ends abruptly giving rise to a pitting potential. Repassivation potentials were not detected in solutions with or without metavanadate additions over the range of potentials examined in these experiments. Yellow deposits were observed on the alloy surface after testing. The yellow deposits, presumably a vanadate compound, were adsorbed in corrosion product in the vicinity of pits that had formed. Figure 3 shows replicate cathodic polarization curves in 0.124M NaCl with and without additions of 0.1M $NaVO_3$. A comparison of these curves shows that metavanadates reduce slightly the cathodic kinetics in the range where oxygen reduction is expected to occur. They also increase the cathodic overpotential required for water reduction.

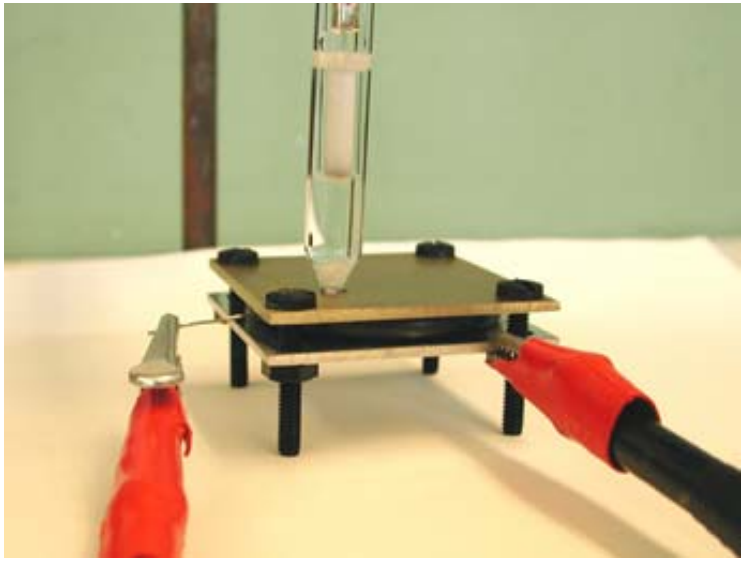

(a)

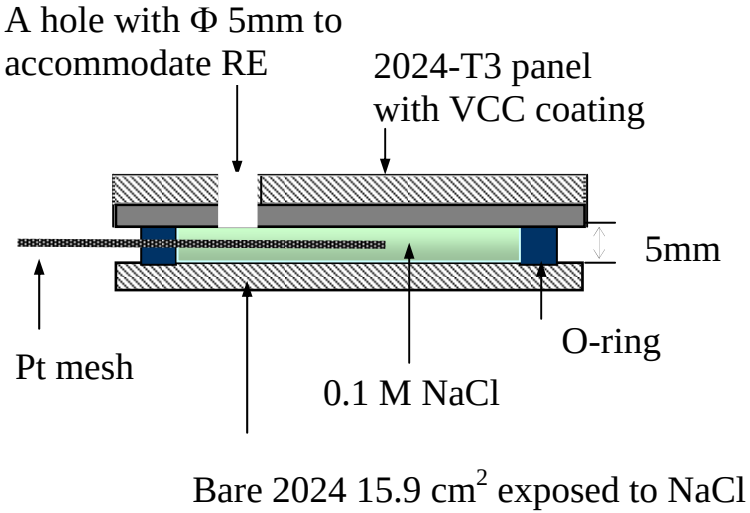

(b)

Figure 1. (a) Photograph of the simulated scratch cell. (b) Schematic cross section of the cell.

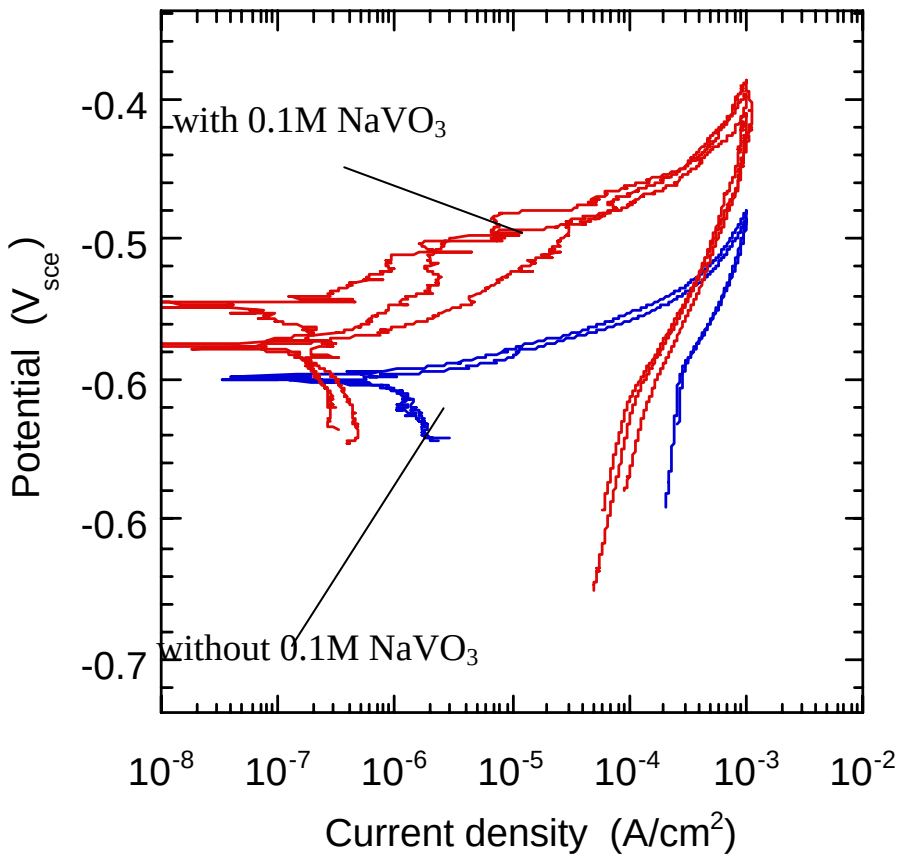

Figure 2. Anodic polarization curves for 2024-T3 exposed to aerated 0.124 M NaCl solution pH 6 with and without additions of 0.1M $NaVO_3$.

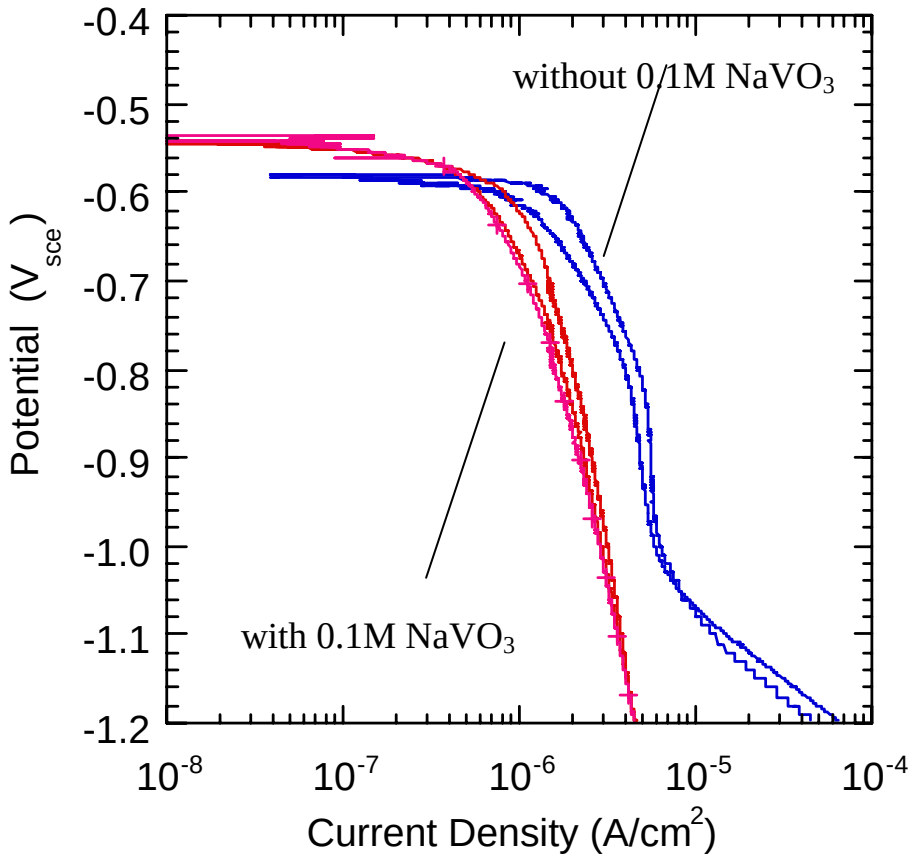

Figure 3. Cathodic polarization curves for 2024-T3 exposed to aerated 0.124 M NaCl solution pH 6 with and without additions of 0.1M $NaVO_3$.

Over the span of about a day the impedance of a 2024-T3 electrode exposed to 0.1M NaCl plus 0.1M $NaVO_3$ will gradually increase suggesting slow growth of a protective film. Once formed, this coating resists localized corrosion for long exposure times. Figure 4 is a complex plane plot showing impedance spectra collected over the span of 24 hours. During the first 5 hours, the total impedance increases by about 10-fold and does not increase further up to 24 hours. Figure 5 shows the variation with time of the total resistance of the sample surface, R_c, determined over much longer periods of time. For comparison, the R_c data for 2024-T3 were determined in 0.1M NaCl with and without additions of 0.1M K_2CrO_4. R_c values were obtained from fitting spectra to a simplified Randles circuit model consisting of a parallel combination of a resistor (R_c) and constant phase element, which represented the impedance response of the sample. This network was in series with a solution resistance. Overall, the corrosion resistance measured here is one to two orders of magnitude lower than that of a surface exposed to chromate-containing solution, but more that one order of magnitude greater than R_c measured in the inhibitor-free NaCl solution. This result shows inhibition by metavanadates, and provides a useful comparison to chromate inhibition.

VCC formation. Vanadate conversion coating bath chemistries and application methods were generally modeled after chromate conversion chemistries and processes. A range of bath chemistries were examined. The many individual permutations of ingredient concentrations that were explored are not listed for brevity, but coating baths chemistry ranges included: 10 or 100mM $NaVO_3$, 0-2mM NaF, and 0-3mM $K_3Fe(CN)_6$. Bath pH was varied from 1.0 to 9.0 using additions of HNO_3 and NaOH. The coating bath was operated at ambient temperatures (23°-26^oC) and immersion times used ranged from 1 to 10 minutes. The film forming ability of a given coating bath chemistry could be qualitatively judged by visual inspection. Vanadate coatings are yellow in color due to the presence of V^{5+}. After some experimentation, it became apparent that coatings with a pronounced yellow coloration provided the best corrosion resistance.

In terms of corrosion resistance measured during constant immersion in aerated chloride solutions, coatings formed from baths with 10 – 100mM $NaVO_3$, 3 mM $K_3Fe(CN)_6$, 0-2mM NaF with a pH near 1.7 yielded the best results. There was some tendency for coating corrosion resistance to diminish as immersion time in the coating bath increased beyond 5 minutes. Figure 6 shows the variation in R_c determined from EIS spectra collected after 3 hours immersion in aerated 0.1M NaCl solution. The plot shows the variation in corrosion resistance as a function of coating bath pH and the presence and absence of 3mM $K_3Fe(CN)_6$ and 2mM NaF. The coating time in all these experiments was 3 minutes. These data show that the formation of a corrosion resistant coating strongly depends on pH and the presence of $K_3Fe(CN)_6$. Coating in baths with a pH of about 1.7 results in the greatest corrosion resistance.

Characterization of VCCs formed under conditions leading to maximum corrosion resistance. VCCs formed on 2024 by a 3-minute immersion in a 100mM $NaVO_3$, 3mM $K_3Fe(CN)_6$ and 2mM NaF at pH 1.7 M bath exhibited a yellow integral surface layer that was apparently continuous across the sample surface. Figure 7 shows scanning electron micrographs of such a VCC at several different magnifications. A micrograph of a

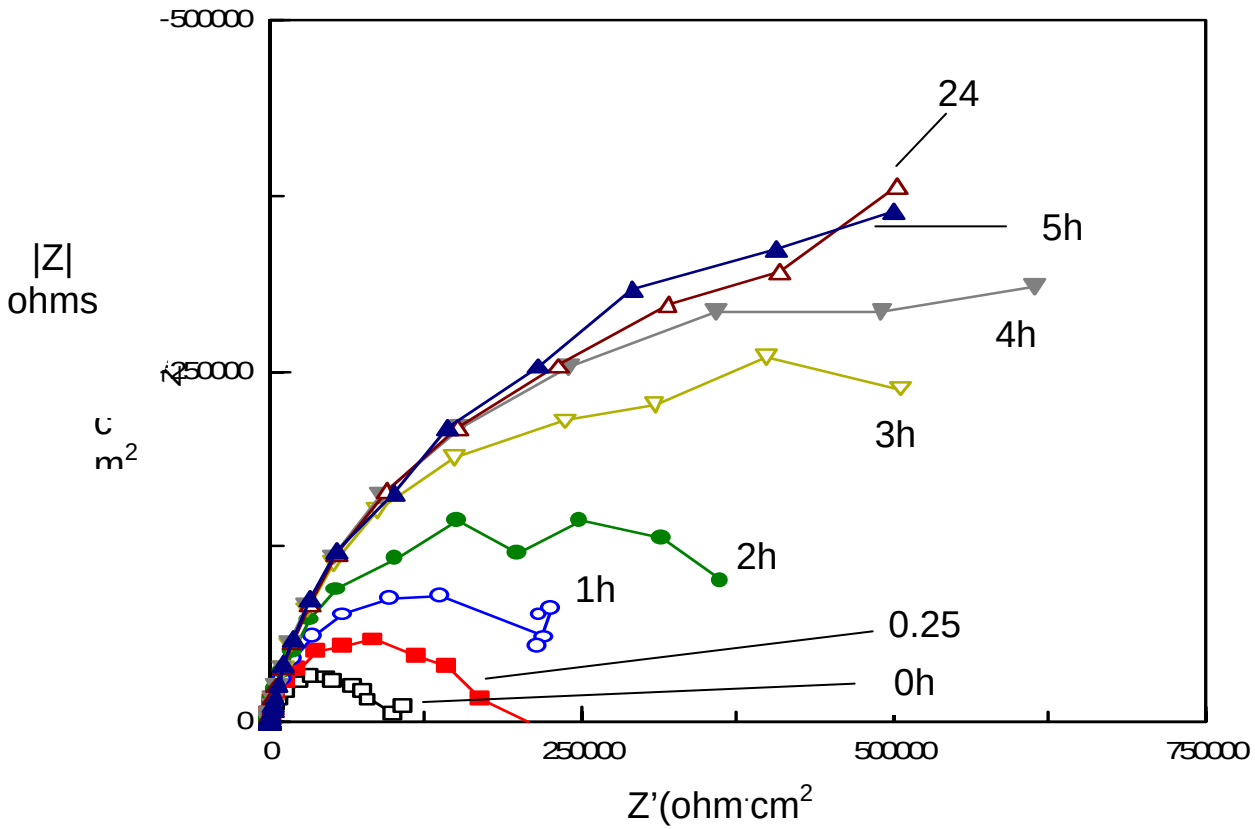

Figure 4. Complex plane plots of EIS data collected from 2024-T3 exposed to aerated 0.1M NaCl plus 0.1M $NaVO_3$ for various lengths of time.

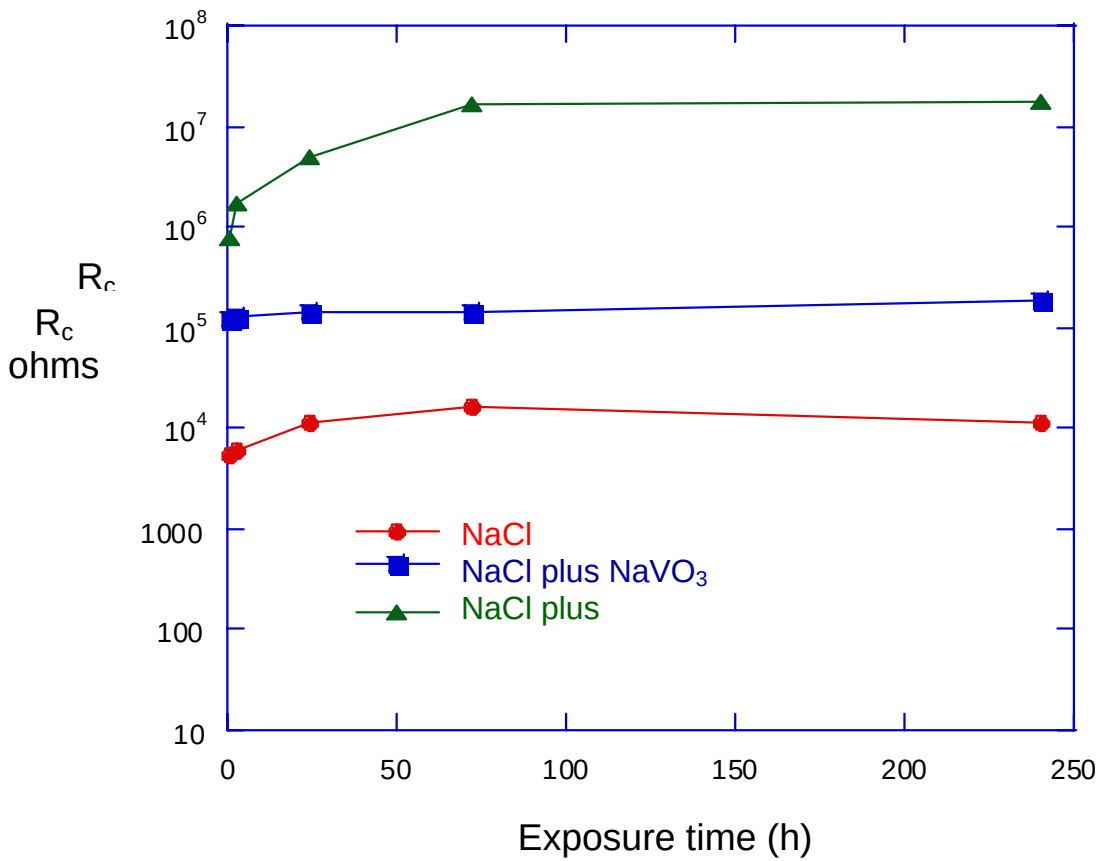

Figure 5. Variation of R_c with exposure time for 2024-T3 exposed to aerated 0.1M NaCl with additions of vanadate, chromate, or with no inhibitor additions.

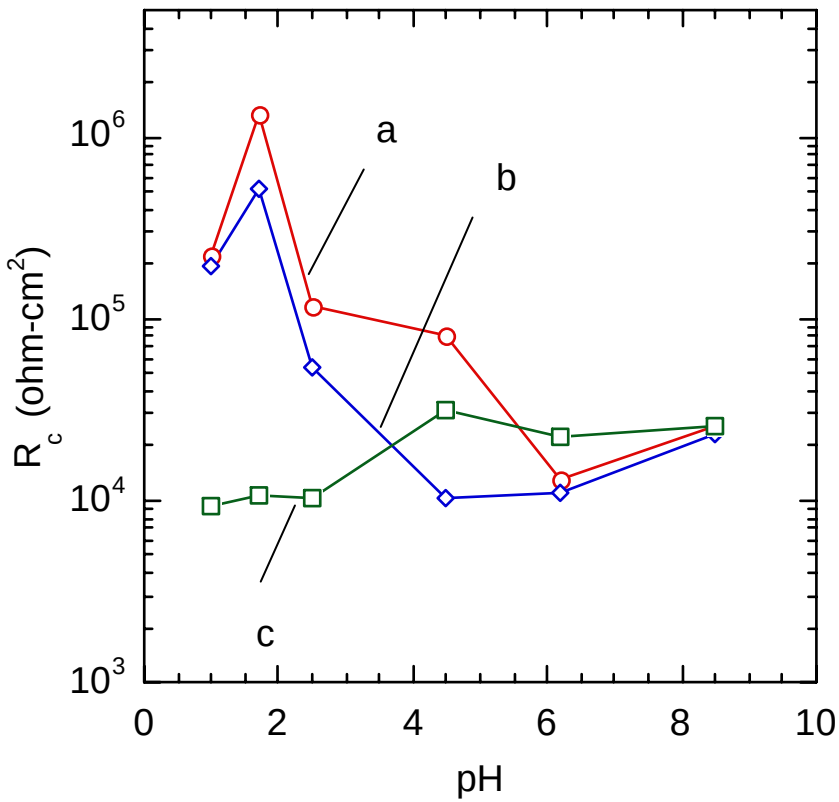

Figure 6. A summary of the effect of VCC bath chemistry on coating corrosion resistance. Corrosion resistance is characterized by R_c determined from EIS data collected after exposure to aerated 0.1M NaCl for 24 hours. VCC bath pH was varied from 1 to 8.5. Coatings were also made with and without additions of NaF and $K_3Fe(CN)_6$. (a) 10mM $NaVO_3$ + 3mM NaF + 2mM $K_3Fe(CN)_6$, (b) 10mM $NaVO_3$ + 3mM $K_3Fe(CN)_6$, (c) 10mM $NaVO_3$ + 2mM NaF.

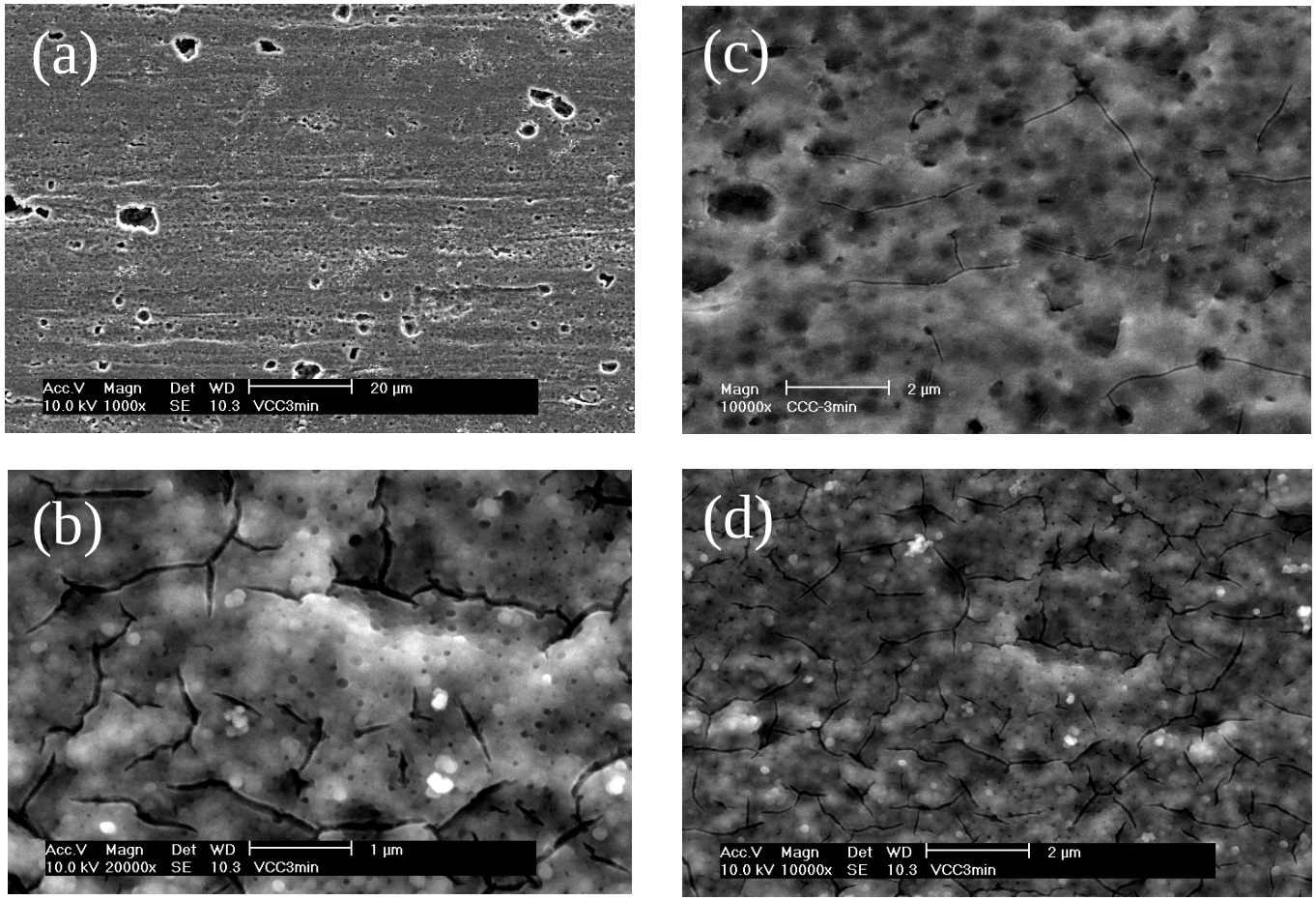

Figure 7. Scanning electron micrographs of (a, b, and d) vanadate and (c) chromate conversion coatings. Micrographs c and d show the two coatings at identical magnifications for comparison.

chromium chromate conversion coating formed in a ferricyanide-accelerated bath is shown for comparison. In terms of coating morphology, VCCs appear to be quite similar to CCCs. The VCC forms in and over pits that are formed during deoxidation and etching treatments. The coating forms over intermetallic particles and inclusions present in the alloy. The coating itself contains small nodular features. There is no faceting or structure to suggest a crystalline component to the coating. In fact, no crystalline compounds were detected by x-ray diffraction of the coated surface. The VCC does contain a network of cracks that appear to be shrinkage cracks, which are known to develop in CCCs. It is likely that the cracks in the VCC develop due to coating dehydration; analogous to the situation with CCCs.

Figure 8 shows composition depth profiles for Al, V, and O determined by Auger electron spectroscopy and sputter depth profiling. Vanadium is present through the full thickness of the coating, which is estimated to be about 300 to 400nm based on a 10nm/min. sputter rate for SiO_2. This agrees well with direct measurements of thickness made by measuring the step height between coated and uncoated regions of a 2024-T3 surface. The data show that this VCC contained between 15 and 20 at. % vanadium in the outer region of the coating. Diminishing amounts of vanadium were observed in the inner region of the coating. Fe, C and N were present through the thickness of the coating at a maximum concentrations of about 10at.%. The composition profiles for these elements were not shown in Figure 8 for clarity. A rigorous analysis for fluorine was not carried out.

Figure 9 shows x-ray absorption from a VCC in the region near the K absorption edge for vanadium. Like chromium, vanadium exhibits a pre-absorption edge peak [25]. This is associated with the presence of V^{5+} in the coating. Established methods were used for estimating V^{5+} content based on the ratio of the normalized and background corrected pre-edge peak height to the edge height. Reported pre-edge peak intensities (normalized to edge height) range from 0.4 to 0.79 for a pure V^{5+} sample (e.g., V_2O_5) [25, 28]. Lower intensities are reported for hydrated forms of V_2O_5. On the basis of these reports, it is estimated that this coating contains 30 to 55% V^{5+}. The remainder of the vanadium in the coating exists at lower, as yet undefined oxidation states.

<u>Overall VCC corrosion resistance</u>. To evaluate overall corrosion resistance of VCCs, coated 2024-T3 panels were subjected to salt spray testing, which was carried out according to ASTM B 117. Six samples of coated 2024-T3 were tested. No pitting damage was found on any of the samples after 24 hours of exposure. A few pits appeared on four of the sample surfaces in 72 hours, but no further pitting damage developed up to the end of the test at 168 hours. Figure 10 shows VCCs on 2024-T3 before and after exposure. An uncoated 2024-T3 control panel is shown for comparison. VCCs on 2024-T3 are not as protective as CCCs in this test. However, the difference in the amount of corrosion observed on the control sample and the coated sample is a visual indication of the substantial increase in corrosion protection provided by VCCs.

Electrochemical impedance spectroscopy was used to quantitatively characterize the corrosion resistance of VCCs. Coated 2024-T3 samples were exposed to aerated 0.5M

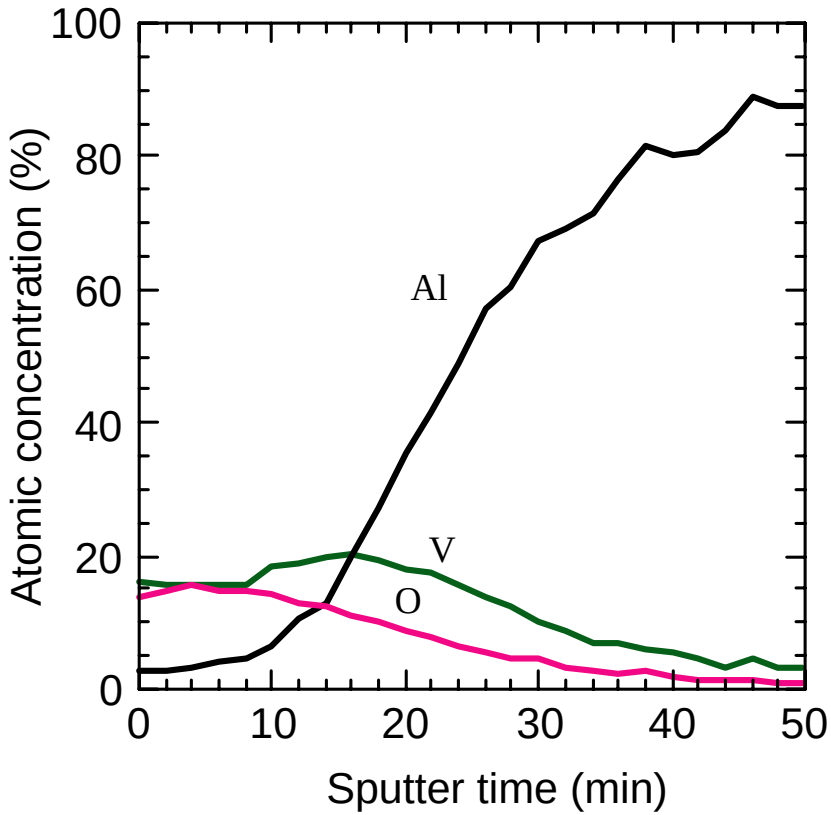

Figure 8. Composition depth profiles for Al, O, and V through a VCC collected by Auger electron spectroscopy. Sputtering rate is estimated to by 10 nm/minute based on SiO_2 standard.

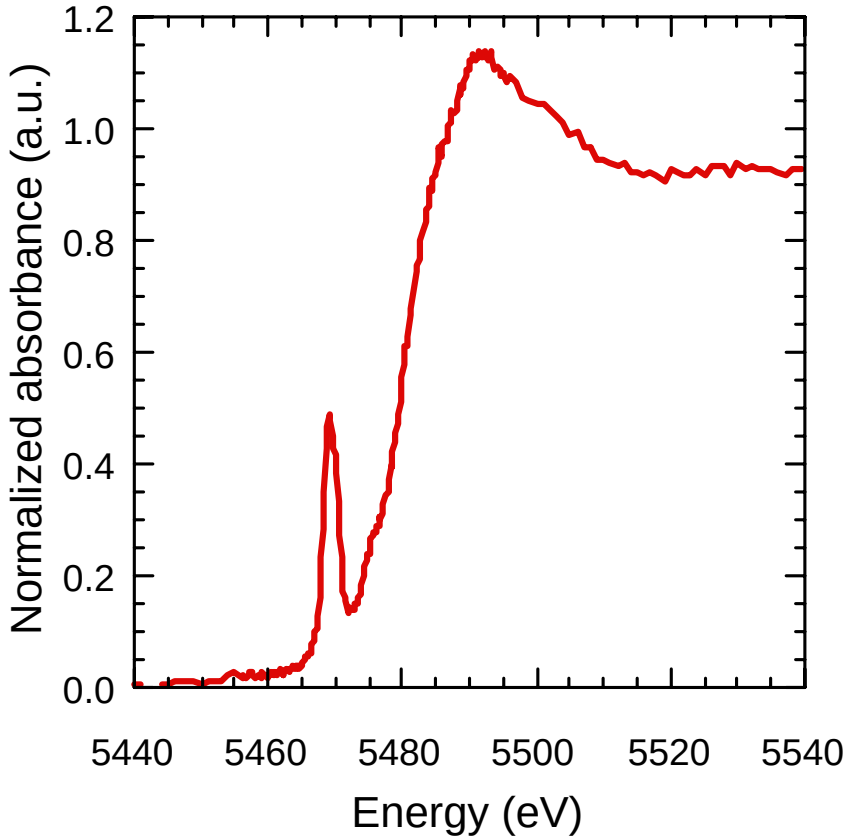

Figure 9. XANES of a VCC at the vanadium K absorption edge. The absorption spectrum includes a pre-edge peak due to the presence of V^{5+} in the coating.

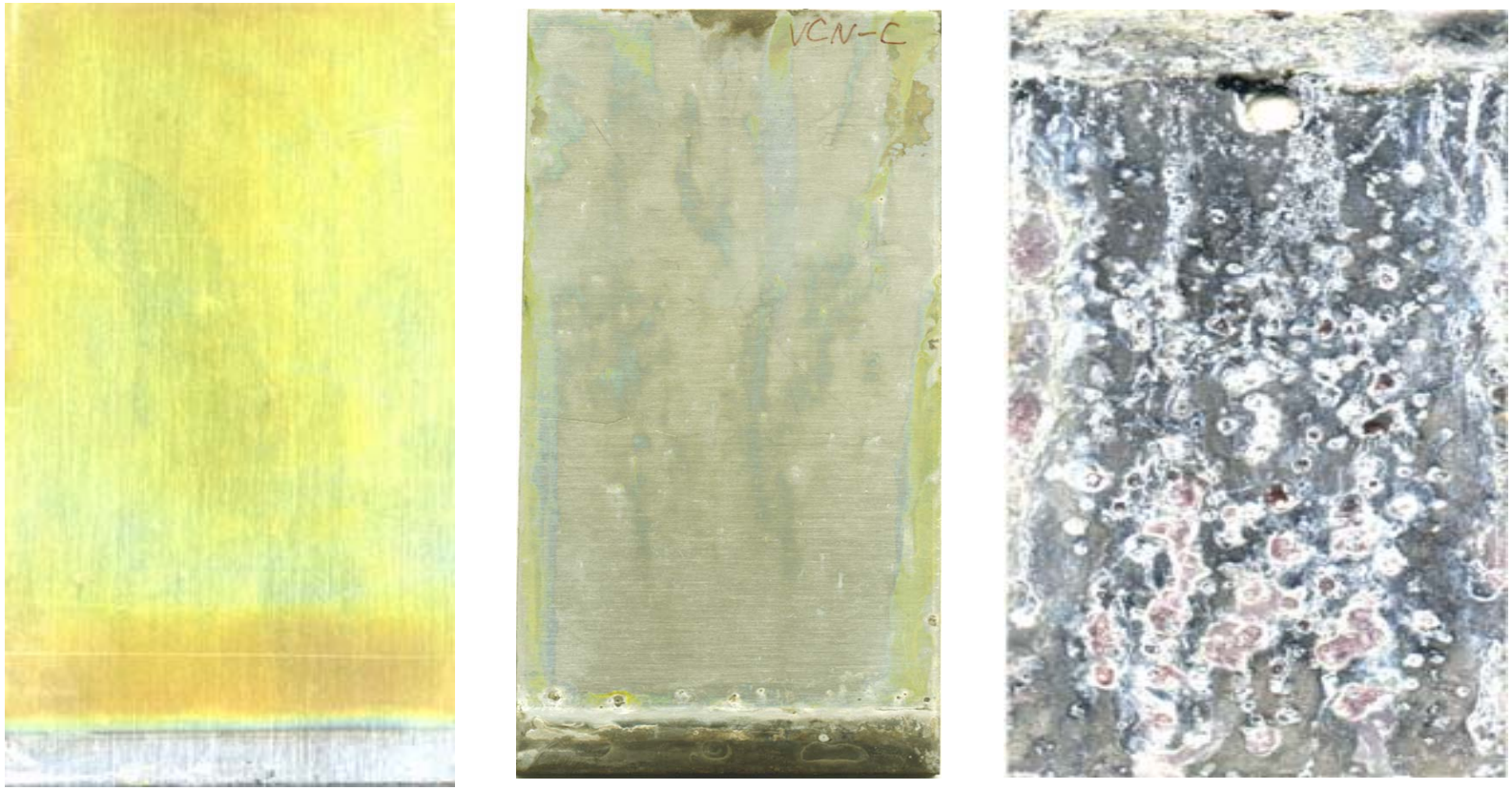

(a) (b) (c)

Figure 10. Photographs of a VCC on 2024-T3 in the (a) as-coated condition, (b) after 168 hours of salt spray exposure, and (c) bare 2024-T3 after 168 hours of salt spray exposure. Coupon sizes are approximately 50 x 100mm.

NaCl solution using a flat cell exposing $1cm^2$ of the coated surface. Impedance spectra were collected at different exposure times. Figure 11 shows that the coating resistance of VCCs was steady at about 10^6 $\Omega \cdot cm^2$ during 120h immersion in solution. These values of coating resistance are within the range of values commonly observed for chromate coatings on 2024-T3 when tested under similar conditions. The range of R_c values observed for uncoated Al alloys in this test is also shown for comparison.

Components of VCC corrosion resistance. Figure 12 shows anodic polarization curves for 2024-T3 samples with VCCs formed by immersion in the coating bath for 3, 5 and 10 minutes. The curves were collected during exposure to aerated 0.5M NaCl solution. A polarization curve for uncoated 2024-T3 is shown for comparison. The uncoated alloy exhibits no passive region in this environment. However, when a VCC is present on the alloy spontaneous passivity is observed. At sufficiently positive potentials, passivity breaks down as pitting on the electrode occurs. Dispersion in pitting potential measurements has not been characterized, however this figure suggests that coatings formed by immersion in the coating bath for 3 to 5 minutes are more resistant to pitting than coatings formed by a 10 minute immersion. These results open the possibility that VCC corrosion protection is degraded by immersion in the coating bath for times beyond 5 minutes.

Figure 13 shows cathodic polarization curves for 2024-T3 samples also coated for 3, 5 and 10 minutes in the VCC bath. These measurements were made during exposure to aerated 0.5M NaCl solution. In the potential region where mass transport limited oxygen reduction occurs, the limiting current density is reduced by as much as an order of magnitude compared to that of an uncoated control sample. Inhibition of oxygen reduction appears to increase as coating immersion time decreases, supporting the idea that over-coating degrades VCC corrosion protection. The form of all of the curves in Figure 13 indicates that oxygen reduction is occurring mainly under mass transport control. One interpretation of this observation is that oxygen reduction is occurring locally on the electrode surface, and VCC formation serves to decrease the fractional area supporting this reaction.

To determine if VCCs exhibit self-healing characteristics, simulated scratch cell experiments were carried out according to the methods described in the Procedures section [26]. In these experiments, a vanadate conversion coating was formed on 2024-T3 by immersion for 3 minutes in the coating bath. About 5 ml of 0.1M NaCl solution was introduced into the cell gap and impedance spectra were collected periodically over 200 hours to assess changes in the corrosion resistance of the uncoated side of the cell. Figure 14 shows R_c data plotted as a function of exposure time in the cells. The data show that the surface exposed in the simulated scratch cell with the VCC exhibits R_c values nearly an order of magnitude greater than that of a surface exposed only to another bare surface. This result suggests that the bare surface in the simulated scratch cell has been protected from corrosion by release of vanadium from the VCC coating.

As a test for vanadium release from the VCC, the composition of the solution in the cell was analyzed by inductively coupled plasma-optical emission spectroscopy (ICP-OES). Solution

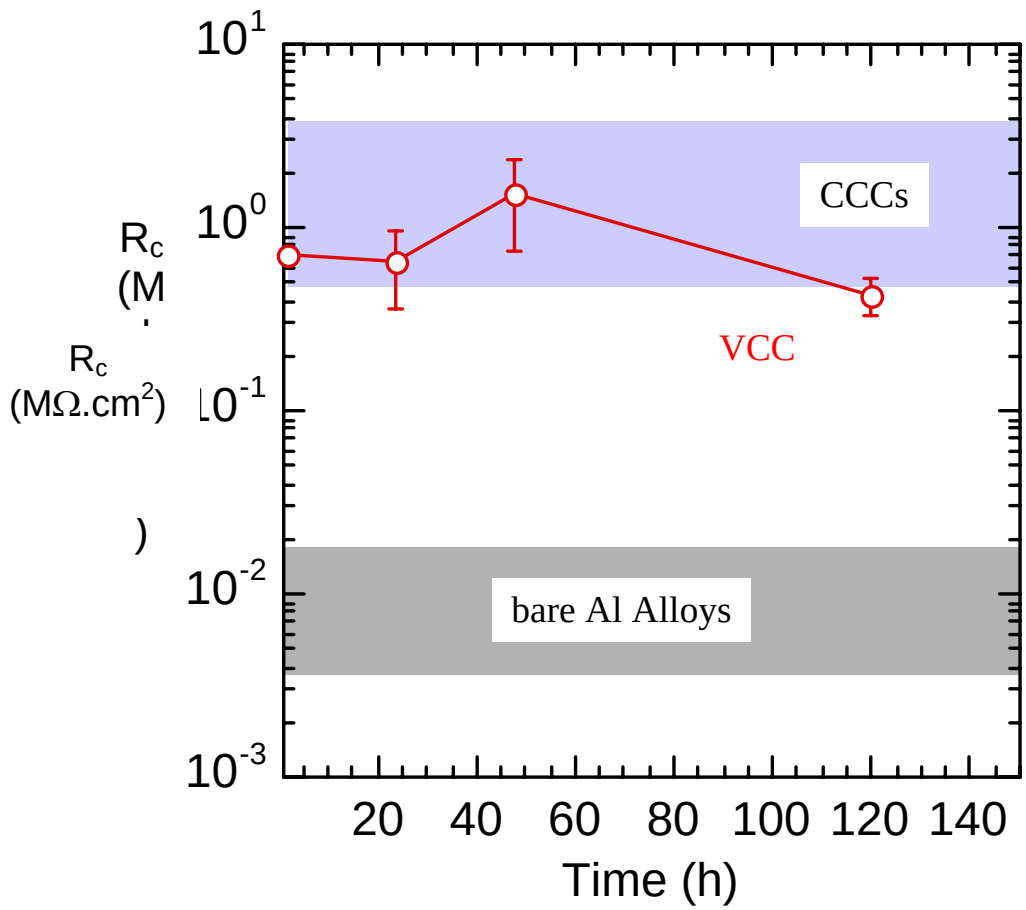

Figure 11. .VCC corrosion resistance determined by EIS testing. R_c values, indicated by data points scatter bands, were determined after exposure to aerated 0.5M NaCl solution. The upper band indicates the range of R_c values measured for CCCs in this environment. The lower band indicates the range in R_c values measured for uncoated Al alloys.

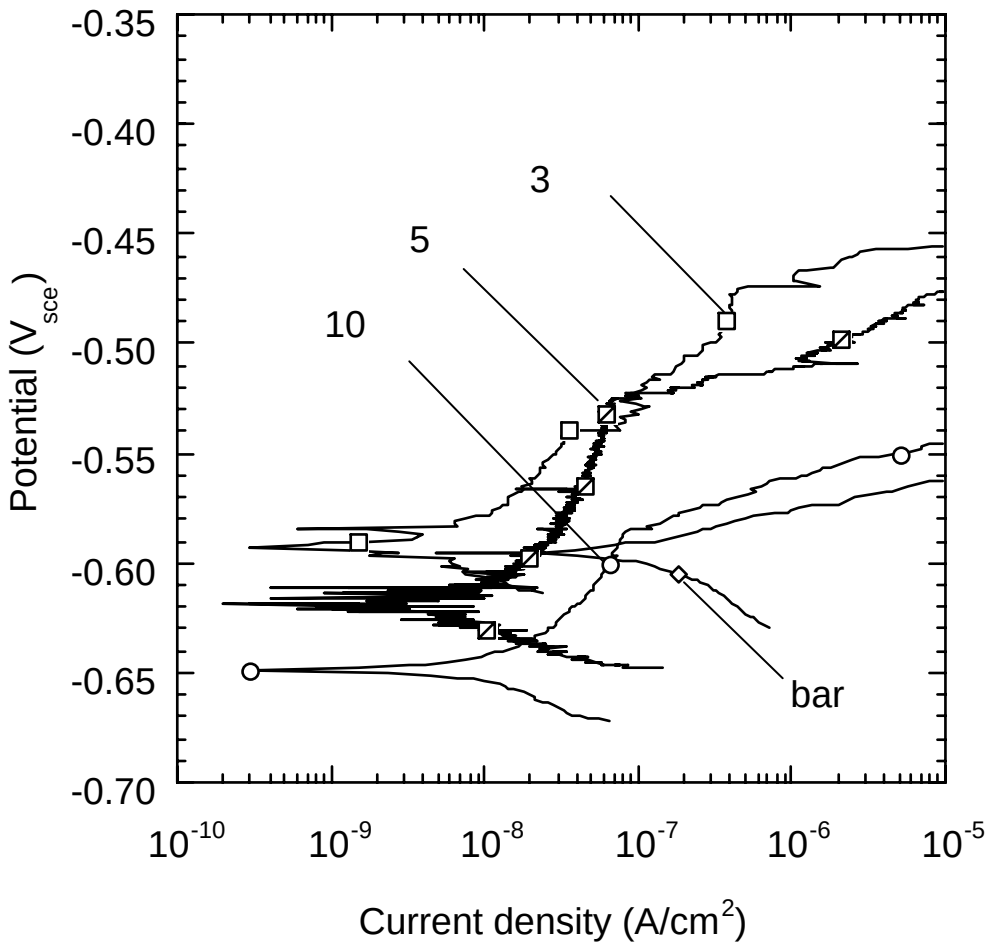

Figure 12. Anodic polarization curves for VCC coated 2024-T3 collected in aerated 0.5M NaCl. The time notations refer to the length of time the samples were immersed in the coating bath. The "bare" sample was uncoated.

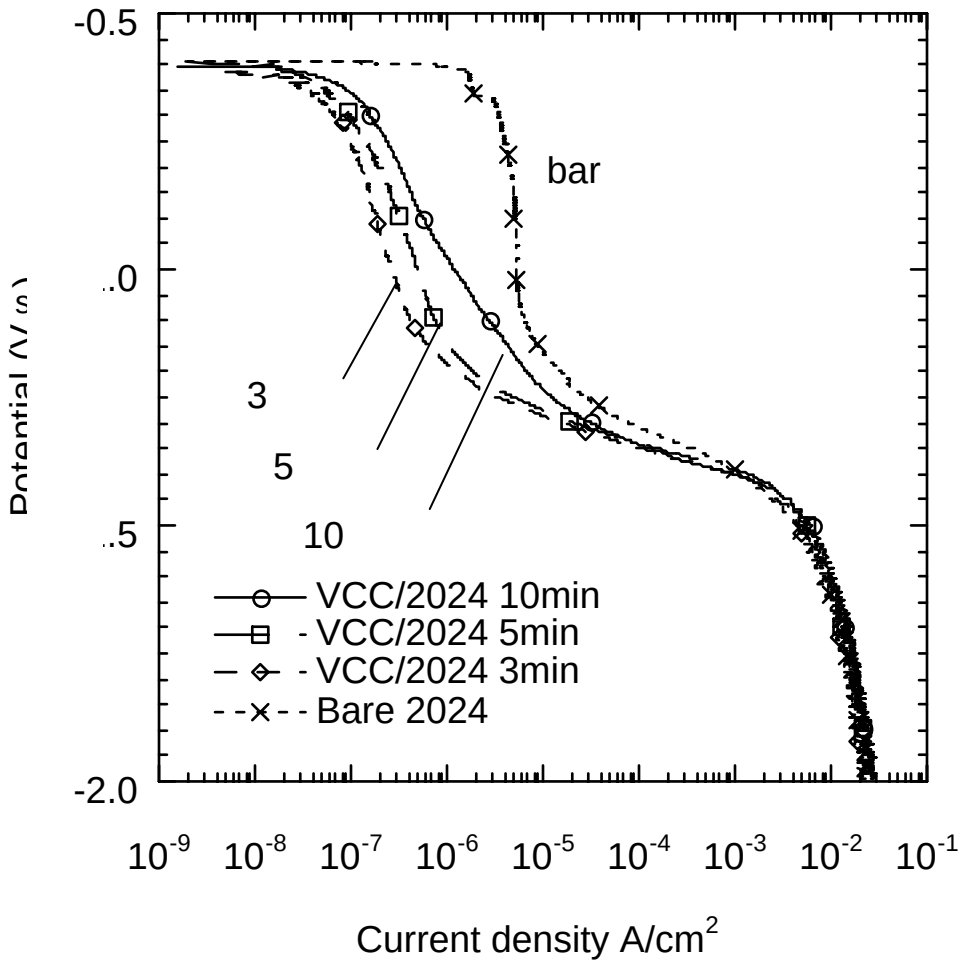

Figure 13. Cathodic polarization curves for VCC coated 2024-T3 collected in aerated 0.5M NaCl. The time notations refer to the length of time the samples were immersed in the coating bath. The "bare" sample was uncoated.

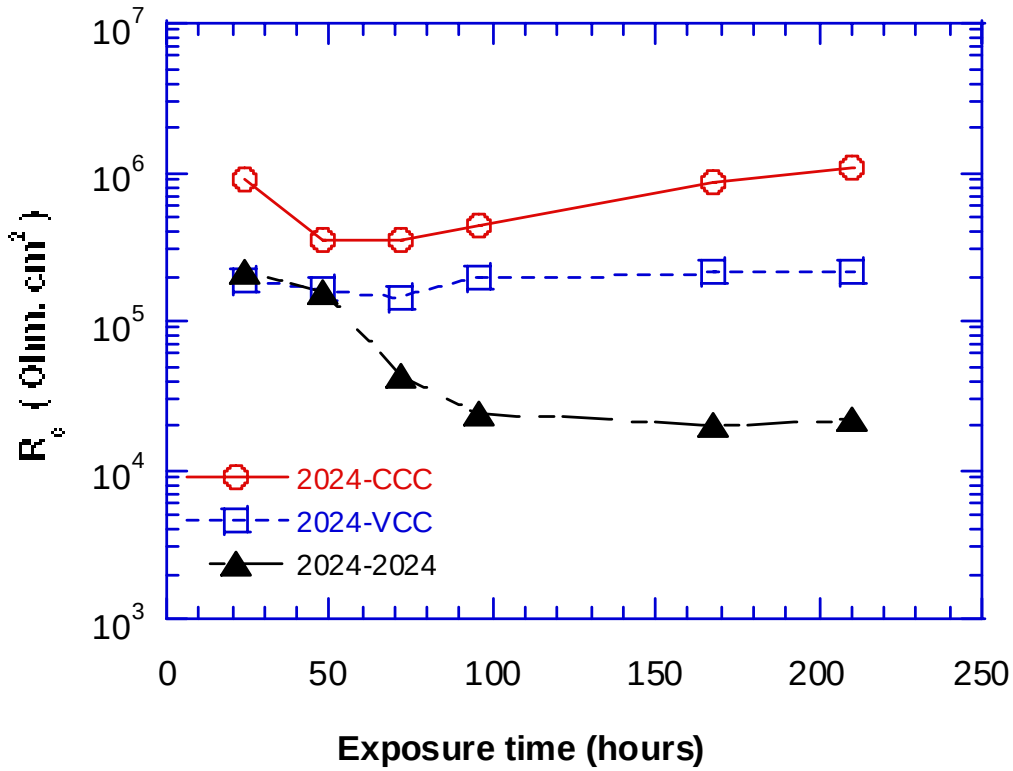

Figure 14. Corrosion resistance of bare 2024-T3 surfaces exposed in a simulated scratch cell with VCC, CCC or uncoated 2024-T3 surfaces. Corrosion resistance is expressed as R_c determined by EIS. The cells were filled with 0.1M NaCl solution. 2024-CCC refers to a cell constructed with a bare 2024-T3 surface and a chromate conversion coated 2024-T3 surface. 2024-VCC refers to a cell constructed with a bare 2024-T3 surface and a vanadate conversion coated 2024-T3 surface. 2024-2024 refers to a cell constructed with two bare 2024-T3 surfaces.

samples were collected from five cells at different exposure times ranging from 24h to 264h. Results indicate that vanadium is, in fact, released from VCCs into solution (Figure 15), and that its concentration in solution generally increases with time in amounts ranging from 0.7 to 8.2ppm. For comparison, identical experiments were carried out in cells fabricated with chromate conversion coatings (CCC) and an uncoated control surfaces. As expected, there was no detectable vanadium release in the control cell. About 1.8ppm chromium was detected after 24 hours of simulated scratch cell exposure and 4.9ppm Cr was detected after 264 hours of exposure in that particular experiment.

Both the vanadium and chromium concentrations are reported here on an elemental basis and do not account for how the oxoanions might be speciated in solution. In the near-neutral solutions existing in the cell, vanadium is present as one of several possible metavanadate species that contain one to four vanadium metal centers per ion [27]. As a result, the concentration of vanadate oxoanions in solution may be lower than that suggested in the figure. In comparison, chromium is speciated as bichromate, $HCrO_4^-$, which has a single chromium metal center in it.

Vanadium is deposited on the bare alloy side of the simulated scratch cell indicating an interaction with the surface and possibly accounting for the increase in corrosion protection observed. The interaction of vanadium with the surface is significant enough that it can be detected by energy dispersive spectroscopy. Detailed surface analysis has not yet been performed, and information regarding the thickness and coverage of the surface layer and the oxidation state of vanadium in the layer have not yet been established.

DISCUSSION

Coating formation. Many chromate-free coating approaches have been developed around the idea that it is necessary to form an oxide film that is insoluble over a wide range of pH and environmental conditions. On this basis, certain transition metal chemistries have not received in-depth consideration as chromate conversion coating replacements. Vanadium may be in this category due to the high solubility of crystalline vanadium oxides [29]. Despite the versatility of vanadium inhibition there are relatively few coating chemistries in which vanadium or its compounds is the primary film-forming agent.

Coating development approaches focussed on oxide precipitation and solubility exclude an important aspect of vanadium chemistry—namely the ability of hydrolyzed vanadium species to behave as a sol, which rapidly condenses and polymerizes to form a hydrated amorphous oxide. In this respect, the understanding of chromate conversion coating formation as a sol-gel-like process is significant. While the use of sol-gel coating methods as chromate conversion coating replacements is not new, the present results show that stimulating gelation of transition metal sols in aqueous solutions at the solution-metal interface using supplemental ingredients can lead to new conversion coatings with desirable properties.

An essential part of the VCC formation process is gelation of a hydrated vanadium oxide. The formation of pentavalent vanadium oxides by condensation and polymerization has been described quite thoroughly [16, 30], and elements of this process appear to be operating in VCC

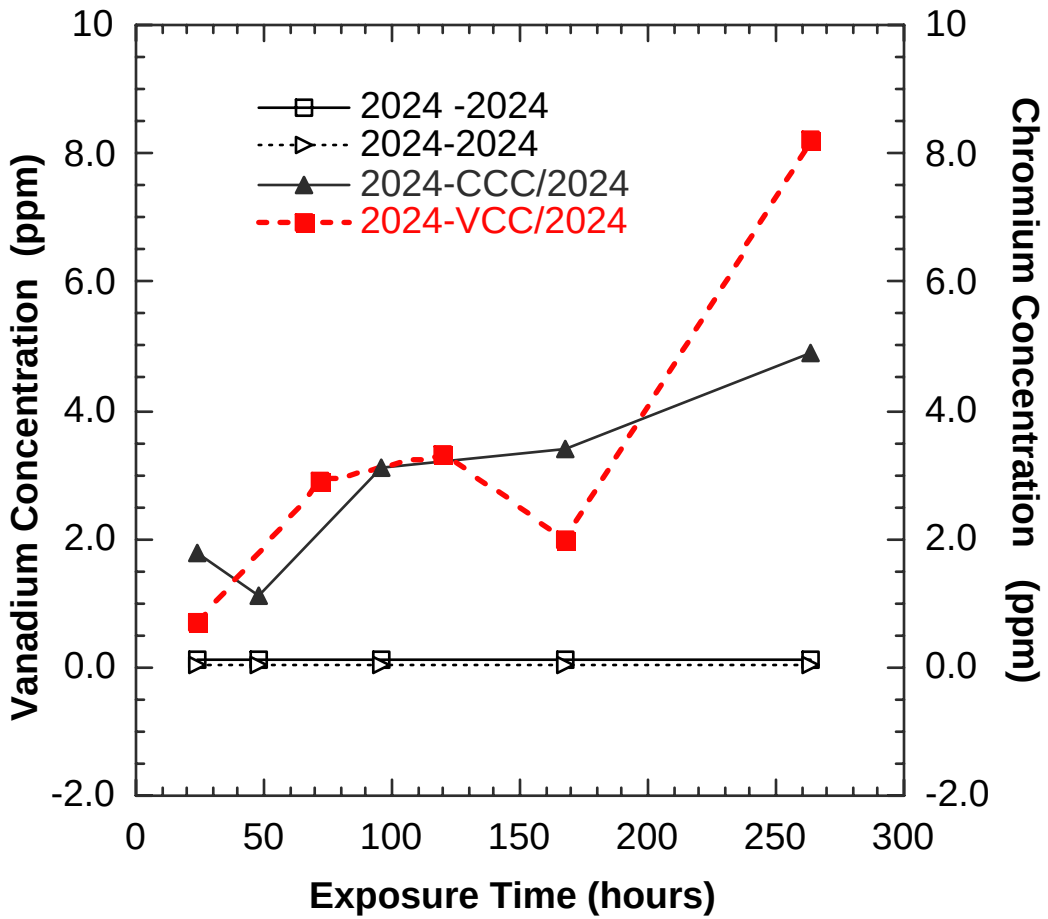

Figure 15. Evolution of the vanadium and chromium concentrations in the simulated scratch cell solutions as determined by ICP-OE. 2024-CCC refers to a cell constructed with a bare 2024-T3 surface and a chromate conversion coated 2024-T3 surface. 2024-VCC refers to a cell constructed with a bare 2024-T3 surface and a vanadate conversion coated 2024-T3 surface. 2024-2024 refers to a cell constructed with two bare 2024-T3 surfaces.

formation. Vanadium oxide gel formation involves olation of octahedrally coordinated $VO(OH)_3(OH_2)_2$ (Figure 16). All the OH ligands lie in the equitorial plane of the molecule giving rise to highly anisotropic rates of polymerization. Rapid polymerization occurs along the equitorial plane of these molecules leading to the formation of long ribbon structures in the resulting gel. Ribbon-like structures are not evident in any of the VCC characterization conducted so far, but the reaction rates for this process are sufficiently high to account for film formation in the time frames observed in these experiments.

The ability to trigger the olation reaction during VCC formation appears to depend on the interplay among the speciation of soluble vanadate ions, pH of the coating bath, and changes in the solution pH at the solution-metal interface. At millimolar concentrations of V^{5+}, the predominant species in solution is VO_2^+ when the pH is less than 1.7 to 1.8. This species does not react to produce condensed vanadium oxides (Figure 17) [30]. For this reason, vanadium oxide gels do not form spontaneously in the coating bath. Upon contact of the metal surface with the coating bath, activation occurs due to dissolution of the air-formed oxide film by the low pH and action of F^-. Proton reduction causes the interfacial pH to increase slightly. An increase in pH to the 2.0 to 3.0 range can be detected within 15 seconds using short range pH papers placed on 2024-T3 surfaces wetted with the coating bath. This pH increase triggers formation of $VO(OH)_3$ by hydrolysis of VO_2^+:

$$VO_2^+ + 2H_2O \rightarrow VO(OH)_3 + H^+ \qquad \text{(eq. 1).}$$

At pH values close to 2, coordination of $VO(OH)_3$ changes from tetrahedral to octahedral by a water addition reaction (Figure 16) [30]:

$$VO(OH)_3 + 2H_2O \rightarrow VO(OH)_3(OH_2)_2 \qquad \text{(eq. 2)}$$

enabling spontaneous polymerization and formation of an amorphous surface film comprised of hydrated vanadium oxides. The resulting film morphology, as it has been characterized so far, is consistent with this type of a formation process. There is no evidence of crystalline compounds in the coating, and the presence of cracks in the VCCs suggests that the oxide is deposited in a highly hydrated form that is susceptible to dehydration after removal from the coating bath in much the same way that CCCs are.

Results from the coating formation experiments and corrosion resistance measurements show that coating formation is critically dependent on the pH of the bath solutions. Table I shows the intensity of coating formation judged visually and by the corrosion resistance measured by EIS during exposure to chlorides solutions. These results show that the best coatings are formed in baths with a pH between 1 and 2. In the context of this coating formation mechanism, if the coating bath is too acid, proton reduction may not be able to shift the pH enough to cause VO_2^+ hydrolysis to any great extent. This would inhibit $VO(OH)_3$ formation and limit subsequent VCC formation. At bath pH values greater than 3, surface activation of Al becomes difficult due to the stability of the Al oxide film, and the concentration of $VO(OH)_3$ becomes too small for meaningful film formation.

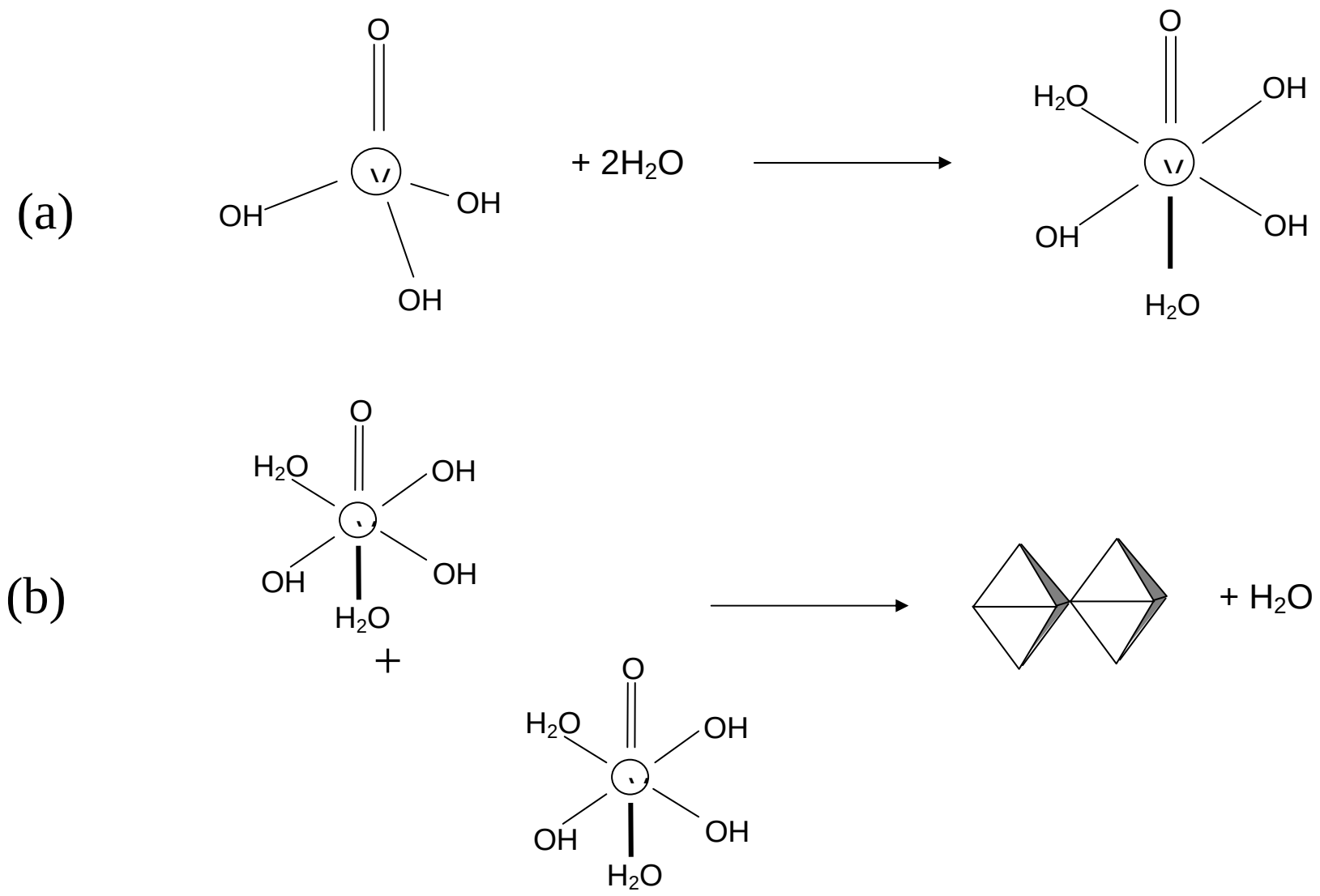

Figure 16. Possible reaction processes involved in VCC formation. (a) water addition to the primary coordination sphere for $VO(OH)_3$ to form $VO(OH)_3(OH_2)_2$. (b) Olation reaction that leads to vanadium oxide gel formation. The octahedra in (b) represent octahedrally coordinated V^{5+}.

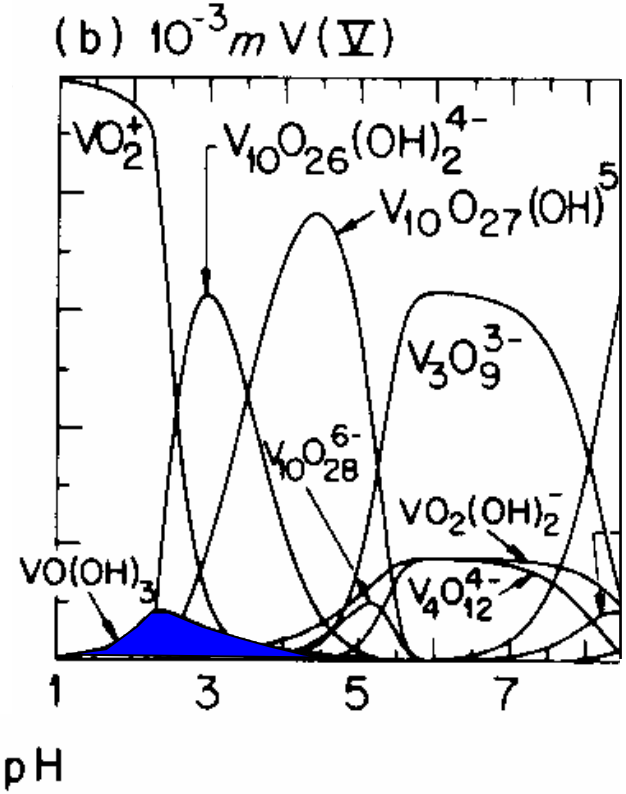

Figure 17. Equilibrium speciation of soluble V^{5+} ions in aqueous solutions at millimolar concentrations. Adapted from C.F. Baes, Jr., R. E. Mesmer, Hydrolysis of Cations, p. 210, Robert E. Krieger Publishing Co., Malabar FL (1986).

In chromate conversion coating formation, $Fe(CN)_6^{3-}$ functions as a redox mediator that catalyzes chromate reduction on Al [21]. Fluoride serves to activate the surface by dissolving the air-formed oxide film permitting intense electrochemical activity to occur. For the formation of corrosion resistant CCCs, F^- has a more significant affect than $Fe(CN)_6^{3-}$ [19]. In VCC formation, $Fe(CN)_6^{3-}$ is the more critical ingredient. Figure 6 shows that over a range of pH, formation of VCCs with high corrosion resistance only occurs when $Fe(CN)_6^{3-}$ is present in the coating bath. The mechanism for the formation of pentavalent vanadium oxides described above does not explicitly account for the critical role of $Fe(CN)_6^{3-}$ in VCC formation and therefore only describes part of the formation process. Additionally, XANES shows that VCCs contain vanadium in oxidation states lower than 5+. The relation of vanadium oxides in oxidation states lower than 5+ to VCC formation and breakdown is not yet understood.

VCC corrosion resistance. On the basis of salt spray exposure testing and EIS carried out in aerated 0.5M NaCl solution, overall VCC corrosion resistance closely approaches that of CCCs. VCC corrosion resistance appears to be degraded by immersion in the coating bath for times greater than about 3 to 5 minutes. This may be due to the fact that once the alloy surface is passivated, the increase in interfacial pH that leads to film formation diminishes, and the vanadium oxide network in the VCC is attacked by the acidic bath chemistry.

Like CCCs and many thickened oxide layers on Al alloys, VCCs inhibit reduction reaction kinetics. The extent of cathodic inhibition cannot be quantified on the basis of the results shown here. However, the limiting current densities of about 10^{-7} A/cm^2 measured in the cathodic polarization curves shown in Figure 13 are as low or lower than the limiting current density measured on chromate conversion coated 2024-T3 [31, 32].

CCCs have been observed to ennoble the pitting potential of 2024-T3 measured by anodic potentiodynamic polarization [33]. Increases in the pitting potential appear to be derived both from the presence of the coating itself and from chromate leached from the coating. Results from this study show that both vanadates in solution and VCCs ennoble the pitting potential of 2024-T3. Whether vanadate leached from the VCC contributes to increases in the pitting potential has not been established.

Vanadate is leached from VCCs as shown by color changes in coupons during salt spray testing and by analysis of solutions from simulated scratch cell experiments. This appears to enable a form of self-healing that is similar to self-healing in CCCs. Self-healing and corrosion resistance in CCCs diminishes with age of the coating. Loss in self-healing appears to be closely related to coating dehydration. VCCs are also hydrated coatings. The observation of shrinkage cracks in scanning electron micrographs of VCCs suggests that they are susceptible to dehydration, however the kinetics of dehydration and the concomitant influence on self-healing has not yet been characterized.

Toxicity. Vanadium is not a cancer-causing agent in mammals, but it is known to produce some adverse health effects [34-37]. The main hazard associated with vanadium is inhalation of airborne particulate and damage to the respiratory system. Acute exposure results in inflammation in the

lungs and mucous linings of the respiratory tract. Reports on the effects of chronic vanadium exposure vary from no observable symptoms to decreased immunity to pulmonary diseases and respiratory failure. Vanadium is absorbed poorly by the gastrointestinal tract, and vanadium ingestion is not considered a significant route of entry into the body. The effects of vanadium on reproductive health have not been established with certainty. Older reports suggest that vanadium is not reproductive toxin [38], however, more recent studies indicate an increased rate of birth defects and infant mortality in animal studies [39].

CONCLUSIONS

Electrochemical testing was used to confirm earlier reports of Al corrosion inhibition by soluble vanadates. In near-neutral solutions vanadate increases the pitting potential and decreases the oxygen reduction reaction rate on 2024-T3. Impedance experiments suggest that slow film formation may be occurring on Al in contact with vanadate-bearing solutions. Vanadate conversion coatings can be produced by immersion in a $NaVO_3/K_3Fe(CN)_6/NaF$ solution with a pH of about 1.7. Coatings form spontaneously at room temperature in a matter of minutes. Coating formation appears to involve hydrolysis, condensation and polymerization to produce a hydrated vanadium oxide, which is triggered by a slight increase in the pH of the metal-solution interface. The resulting coating is yellow in appearance and continuous across the sample surface. The coating is non-crystalline and consists of vanadium in several oxidation states as well as other ingredients in the coating bath. Coating formation is very sensitive to bath pH and the presence of $K_3Fe(CN)_6$. VCCs provide excellent corrosion protection in salt spray and constant immersion tests. Polarization experiments show that VCCs increase resistance to pitting and suppress oxygen reduction reactions. Simulated scratch cell experiments suggest that VCCs are also self-healing in a manner that closely resembles this characteristic in chromate conversion coatings.

REFERENCES

1. D. Bienstock, J.H. Field, *Corrosion*, 17, 87-90 (1961).
2. D. Bienstock, J.H. Field, *Corrosion*, 17, 89-91 (1961).
3. B.R.W. Hinton, *Metal Finish.*, 89, 55-61 (1991).
4. B.R.W. Hinton, *Metal Finish.*, 89, 15-20 (1991).
5. R.L. Cook, S.R. Taylor, *Corrosion*, 53, 321-333 (2000).
6. A.J. Sedricks, *Corrosion of Stainless Steels*, p. 118, New York, John Wiley&Sons, 1996.
7. M.H. Ras, P.C. Pistorius, *Corrosion Sci.*, 44, 2479-2490 (2002).
8. R.D. Davies, *Corrosion*, 49, 544-549 (1993).
9. G.S. Frankel, R.C. Newman, C.V. Jahnes, M.A. Russak, *J. Electrochem. Soc.*, 140, 2192-2197 (1993).
10. C.S. Kumar, V.S. Rao, V.S. Raja, A.K. Sharma, S.M. Mayanna, *Corrosion Sci.*, 44, 387-393 (2002).
11. A.S. Hamdy, A.N. Beccaria, T. Temtchenko, *Surface and Coatings Technology*, 155, 184-189 (2002).

12. D.P. Buxton, P.J. Riley, Anticorrosion Treatment of Metal Coated Steel Having Coatings of Aluminium, Zinc or Alloys Thereof, U.S.Patent no. 5,985,047, 1999.
13. H.E. Hager, C.J. Johnson, K.Y. Blohowiak, C.M. Wong, J.H. Jones, S.R. Taylor, R.L. Cook, Chromate-free Protective Coatings, U.S. Patent no. 5,866,652, 1999.
14. M. Inoue, T. Ohnuma, T. Yamamoto, Liquid Rust Proof Film-forming Composition and Rust Proof Film-forming Method, U.S. Patent no. 5,743,971, 1998.
15. P.J. Riley, Anti-Corrosion Treatment of Aluminium or Aluminium Alloy Surfaces, U.S. Patent no. 5,520,750, 1996.
16. J. Livage, *Solid State Ionics*, 86-88, 935-942 (1996).
17. J.H. Osborne, *Prog. Org. Coatings*, 41, 280 (2001).
18. L. Xia, R.L. McCreery, *J. Electrochem. Soc.*, 145, 3083 (1998).
19. W. Zhang, R.G. Buchheit, *J. Electrochem Soc.*, 149, B357 (2002).
20. W.J. Clark, R.L. McCreery, *J. Electrochem. Soc.*, 149, B379 (2002).
21. L. Xia, R.L. McCreery, *J. Electrochem. Soc.*, 146, 3696 (1999).
22. M.W. Kendig, A.J. Davenport, H.S. Isaacs, *Corros. Sci.*, 34, 41 (1993).
23. F.W. Lytle, R.B. Greegor, G.L. Bibbins, K.Y. Blowhowiak, R.E. Smith, G.D. Tuss, *Corros. Sci.*, 37, 349 (1995).
24. M. Ruitenbeek, A.J. vanDillen, F.M.F. deGroot, I.E. Wachs, J.W. Geus, D.C. Koningsberger, *Topics in Catalysis*, 10, 241-254 (2000).
25. J. Wong, F.W. Lytle, R.P. Messmer, D.H. Maylotte, *Phys. Rev. B*, 30, 5596-5610 (1984).
26. J. Zhao, G.S. Frankel, R.L. McCreery, *J. Electrochem. Soc.*, 145, 2258 (1998).
27. C.F. Baes, R.E. Mesmer, *Hydrolysis of Cations*, p. 197, Malabar, FL, Robert E. Kreiger Publishing Co., 1986.
28. M. Nabavi, F. Tauelle, C. Sanchez, M. Verdaguer, *J. Phys. Chem.*, 51, 1375-1382 (1990).
29. M. Pourbaix, *Atlas of Electrochemical Equilibria in Aqueous Solutions*, p. 234, Houston, TX, NACE, 1974.
30. M. Henry, J.P. Jolivet, J. Livage, *Aqueous chemistry of metal cations: hydrolysis, condensation and complexation*, p. 157-206 in *Structure and Bonding*, Springer-Verlag, Berlin, 1992.
31. G.O. Ilevbare, J.R. Scully, *J. Electrochem Soc.*, 148, B196-B207 (2001).
32. X. Sun, R. Li, C. Wong, K.A.R. Mitchell, *J. of Materials Sci.*, 36, 3215-3220 (2001).
33. G.O. Ilevbare, J.R. Scully, J. Yuan, R.G. Kelly, *Corrosion*, 56, 227-242 (2000).
34. G.M. Grabowski, J. Paulauskis, J. Godleski, *Toxicology and applied Pharmacology*, 156, 170-178 (1999).
35. L.M. Pierce, F. Alessandrini, J. Godleski, *toxicology and Applied Pharmacology*, 138, 1-11 (1996).
36. M.M. Shi, I.Chong, N.C. Long, A. Love, J. Godleski, J. Paulauskis, *Inflammation*, 22, 29-43 (1998).
37. C.S. Tsai, M.M. Shi, I. Chong, J. Godleski, J. Paulauskis, *American Journal of Respiratory and Critical Care Medicine*, 155, A960 (1997).

38. D.M. Opresko, *Toxicity Summary for Vanadium*, Oak Ridge National Laboratory, Oak Ridge, TN, 1991.
39. J.L. Domingo, *Reproductive Toxiciology*, 10, 175-182 (1996).

Table I. VCC Color and corrosion resistance as a function of bath pH. Corrosion resistance is reported as R_c determined by EIS after a 3 h exposure in 0.1M NaCl solution.

pH	Coating color	R_c(kohm·cm^2)
8.5	None	25.9
6.2	None	12.9
4.5	None	79.7
2.5	Pale yellow	118
1.7	Yellow	1330
1.0	Yellow	222

Results and Accomplishments Part III:

Active Corrosion Protection and Corrosion Sensing in Chromate-Free Organic Coatings[3]

ABSTRACT

In this study it is shown that anion-exchanging hydrotalcite compounds dispersed as a particulate additive in organic resins leads to potent corrosion inhibition of an underlying aluminum alloy substrate. The use of this additive also imparts the ability to detect environmental changes in the coating that are a prelude to substrate corrosion. Corrosion inhibition is derived from release of a decavanadate from crystalline Al-Zn hydroxide-based hydrotalcite particles into electrolyte that has permeated the pore space of the coating. Decavanadate release is accompanied by uptake of chloride ion in an exchange reaction. The exchange of the large decavanadate anion for the smaller chloride ion in the hydrotalcite structure results in a predictable change in crystal structure, which can be detected by x-ray diffraction. The occurrence of the decavanadate-chloride exchange reaction indicates that aggressive electrolyte has invaded the coating and that corrosion may be imminent. In this paper, methods for synthesizing an Al-Zn-decavanadate hydrotalcite particulate suitable for dispersion in an epoxy resin are described. Results from exposure and electrochemical tests illustrating corrosion protection by the hydrotalcite pigmented coatings are presented. Additionally, the characteristic changes in the x-ray diffraction pattern of hydrotalcite associated with the decavanadate-chloride exchange are presented. Diffraction patterns collected from coated Al substrates are also presented, indicating that diffraction-based interrogation of coatings is possible.

INTRODUCTION

Protection of aircraft airframes depends heavily on corrosion inhibiting primer coatings. The prototypical coating is a polyamide-cured bisphenol epoxy resin containing about 30wt.% $SrCrO_4$ as a leachable inhibiting pigment [1]. Due to the high volume fraction of solid pigment, these coatings take up environmental water rapidly and can become water-saturated. Under these conditions, the $SrCrO_4$ pigment will dissolve up to a concentration determined by its solubility limit (about 5 mM CrO_4 at near-neutral pH [2]). In these solutions, the primary inhibiting species is the CrO_4^{2-} anion [3]. The inhibitor-saturated electrolyte in the pore space of the coating is very effective in suppressing corrosion of the underlying aluminum alloy substrate.

Soluble inhibitors can also be leached into solution outside of the coating. If mechanical defects exist exposing bare metal, corrosion may be stifled if a critical concentration of inhibitor in the vicinity of the defect can be achieved. Inhibitor transport

[3] Published in Progress in Organic Coatings, 47, 174 (2003).

and corrosion inhibition at mechanical defects, which is colloquially referred to "throwing power", is the signature attribute of chromate-bearing epoxy primers.

As is now well documented, chromate must be eliminated from metal finishing processes due to its toxic nature [4-7]. A range of alternate pigments have been explored and some perform as well or better than $SrCrO_4$ in laboratory testing [8]. Some of these pigments have been incorporated into primer coating formulations exist as products qualified for use in military systems [9]. In service, these chromate-free coatings perform well, but usually are not better than $SrCrO_4$-bearing primers. In comparative exposure testing, Cr-free organic coating performance is generally observed to be unsatisfactory unless coatings are applied over a chromate conversion coating [10].

In the absence of a clear-cut alternative to $SrCrO_4$, continued research and development of new inhibiting compounds is warranted. The desire to move to low cost condition-based maintenance of aircraft in the U.S. Air Force has spawned efforts aimed at early detection of corrosion under coatings, or coatings that sense corrosion of the underlying substrate. In this latter regard, attempts to formulate corrosion-sensing coatings have been made based on the use of pH indicators that have been added to organic resins for the purpose of detecting the alkaline pH associated with cathodic activity under the coating [11]. In this sensing scheme, visual indications of a pH increase are taken as an indication of anodic activity nearby in pits or in crevices. This technique is potentially quite sensitive in that it can detect small amounts of corrosion damage. However it depends on the ability to visually interrogate the pH indicator added to the coating. This is problematic in most aircraft coatings, which are opaque.

In this paper, the use of crystalline hydrotalcite (HT) particulate additives to organic coatings for corrosion inhibition and corrosion sensing is described. HTs are layered clay materials used for a variety of industrial purposes [12, 13]. Specifically, HTs are being synthesized with vanadates, which have been shown to be excellent inhibitors of Al corrosion [14]. The ion exchange characteristic of HTs is being used to release vanadates into an attacking electrolyte to stifle corrosion. When this occurs, potent corrosion protection is observed. Upon vanadate release, chloride or sulfate in the attacking electrolyte is taken up by the HT inducing a change in the crystal structure that can be detected by x-ray diffraction methods. This change in structure can be detected in HT-bearing coatings applied to metal surfaces indicating that this approach may be viable as a means for detecting environmental changes in a coating that are a prelude to corrosion of the underlying substrate.

EXPERIMENTAL PROCEDURES

Hydrotalcite Synthesis. The Al-Zn-decavanadate hydrotalcite (HT-V) compound used in this study was prepared using a coprecipitation method described by Kooli [15]. A 20 g sample of sodium metavanadate ($NaVO_3$) was dissolved in 500 ml of boiled (to remove CO_2) and distilled water under stirring. The pH of the solution was reduced to 4.5 by the dropwise addition of 2M hydrochloric acid (HCl). At this pH, metavanadate VO_3^- speciated to decavanadate ($V_{10}O_{28}^{6-}$) resulting in an orange-yellow solution. The solution

pH was then adjusted to about 6.3 by dropwise addition of 2M NaOH. Decavanadate is unstable at pH 6.3, but the transformation to the thermodynamically stable metavanadate species is inhibited by sluggish reaction kinetics [16]. As a result, metastable decavanadate persists in solution long enough for HT-V synthesis to be carried out. The decavanadate solution was then titrated with a solution consisting of 13.4 g anhydrous $ZnCl_2$, and 11.8 g of aluminum chloride hexahydrate ($AlCl_3 \cdot 6H_2O$), which were dissolved in 250 ml of boiled and deionized water. The addition took approximately 40 minutes and the pH was maintained between 6.3 and 6.5 with additions of NaOH. Upon titration, solid HT-V was observed to form. After titration, the mixture was aged at 55°C overnight under constant stirring. The solid material was then collected in a Buchner funnel using water aspiration. This process yielded a solid clay cake with a distinctive yellow color. The cake was washed with at least 500 ml of deionized water to remove unreacted components—primarily chlorides. After washing, the cake was dried in air at 40°C for 12 hours and then ball milled for 4 hours to produce a powder that was suitable for mixing with epoxy. This process yielded about 25 g of particulate. The powder was not sieved, and the particle size distribution was not characterized. Similar procedures were used to synthesize an Al-Zn-chloride hydrotalcite (HT-Cl). In this case a sodium chloride solution was substituted for the sodium vanadate solution in the initial titration.

Coating Synthesis and Application. HT pigmented coatings were made by mixing milled HT powder into an amide-cured bisphenol epoxy resin conforming to MIL-P-23377. HT was added to the resin component of the coating in amounts ranging from 25 to 30% by weight. The mixture was stirred until a uniform consistency was achieved. At that point hardener was added and the coating was promptly applied to the substrate.

Coatings were applied to 2024-T3 (Al-4.4Cu-1.5Mg-0.6Mn) sheet stock coupons using a drawdown bar. Two coats were normally applied with the second coat being applied several hours after the first. Coatings produced in this way were uniform in color and visually masked the underlying substrate. Coatings were allowed to cure for 48 hours at room temperature and humidity before any corrosion testing.

Instrumental Procedures. X-ray diffraction patterns were collected from powder samples using a Sintag Pad-V^{TM} diffraction measurement system. Patterns were collected at a scan rate of 0.2^o/minute using Cu K_α radiation (λ = 1.54Å).

Inductively coupled plasma-optical emission spectroscopy (ICP-OES) was used to analyze solutions for the presence of inhibitors released from the hydrotalcite pigment. Aliquots of solution of known volume were acidified with nitric acid, converted to an aerosol, and fed into a plasma chamber. Photon emission from the plasma was analyzed to determine quantitatively the composition of the plasma and the solution from which it was produced with part-per-billion sensitivity.

Corrosion testing of coated surfaces was carried out using electrochemical impedance spectroscopy (EIS)-based methods. Tests were conducted in cells filled with 0.5M NaCl solution that was open to air, but quiescent. Cells were also fitted with a saturated calomel counter electrode and graphite counter electrode to enable three

electrode measurements to be made. Impedance spectra were collected every 24 hours over 200 hours of total exposure using a 10mV sine wave voltage perturbation, which was varied in frequency from 10^5 to 10^{-2} Hz. The experiments were carried out using a Princeton Applied Research 273A potentiostat, and a Solartron Model 1255 frequency response analyzer. The experiment and data logging were coordinated by Scribner Associate's Zplot™ impedance software.

RESULTS AND DISCUSSION

Hydrotalcite structure. HT synthesis was verified by powder x-ray diffraction (XRD). Figure 1 shows the x-ray diffraction patterns for an HT-V and HT-Cl. The positions of peaks and their relative intensities compares well with patterns reported in the literature [15, 17], and indicate successful synthesis of a compound with a Zn to Al ratio of 2 to 1.

At 2θ values between 10° and 35°, HT XRD patterns are characterized by reflections originating from their layered structure. At larger 2θ values reflections are due to structure within the mixed metal hydroxide layer in the compound. Figure 2 shows schematically the structure of an Al-Zn HT, which is characteristic of most HT compounds. The structure consists of layers of mixed Al-Zn hydroxide separated by layers of anions and water. A HT unit cell contains three hydroxide layers, hence every third layer represents a repeat of the unit cell in that direction. The most intense reflection in hydrotalcite patterns typically originates from diffraction from these hydroxide layers, and this reflection occurs at the lowest 2θ values due to the large interplanar spacings. These reflections are referred to as the 003 reflection. Diffraction from 003 multiples (e.g., 006, 009, etc.) is often sufficiently intense to be observed in XRD patterns. The unit cell height can be estimated directly using the 003 peak positions and Bragg' s Law where the unit cell dimension perpendicular to the layers, d, is given by:

$$d = \frac{n\lambda}{2\sin\theta} \qquad \text{(eq. 1).}$$

The thickness of the mixed Zn-Al hydroxide layer has been determined to be 4.77Å [17]. Subtracting this value from the total layer thickness enables a determination of the anion layer thickness. The anion layer is referred to as the "gallery" because anions can be exchanged into or out of this layer with relative ease while the Al-Zn hydroxide structure serves as a host structure that retains its structure. Using this calculation, gallery heights of 6.89Å and 2.92Å are estimated for HT-V and HT-Cl respectively. These values are in good agreement with values available in the literature [15, 17].

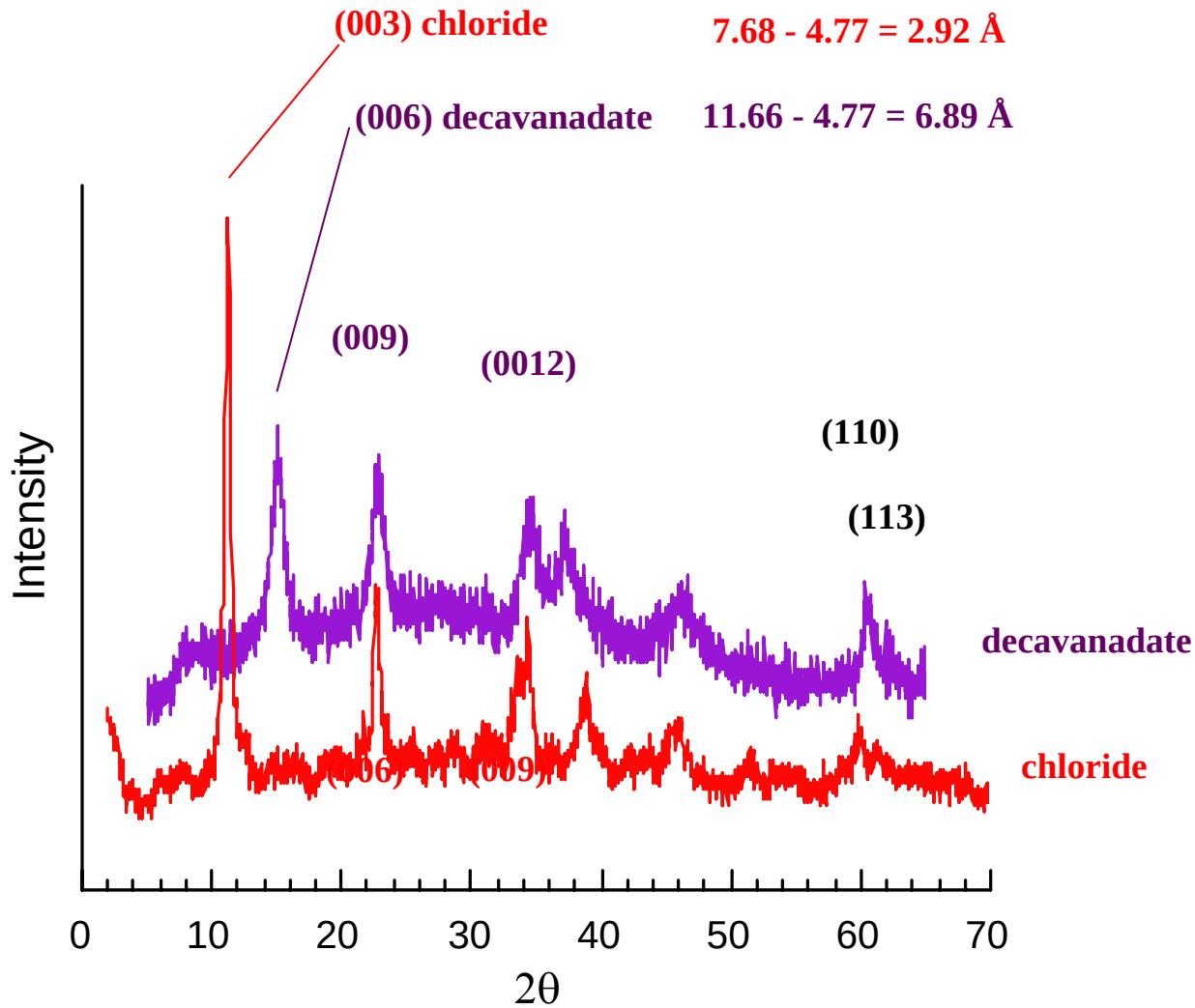

Figure 1. X-ray diffraction patterns for Al-Zn-decavanadate and Al-Zn-chloride hydrotalcite compounds. The approximate ratio of Zn to Al in these compounds is 2 to 1. Gallery heights are calculated from the difference between the basal plane spacing and the thickness of the Al-Zn-hydroxide layer (4.77Å).

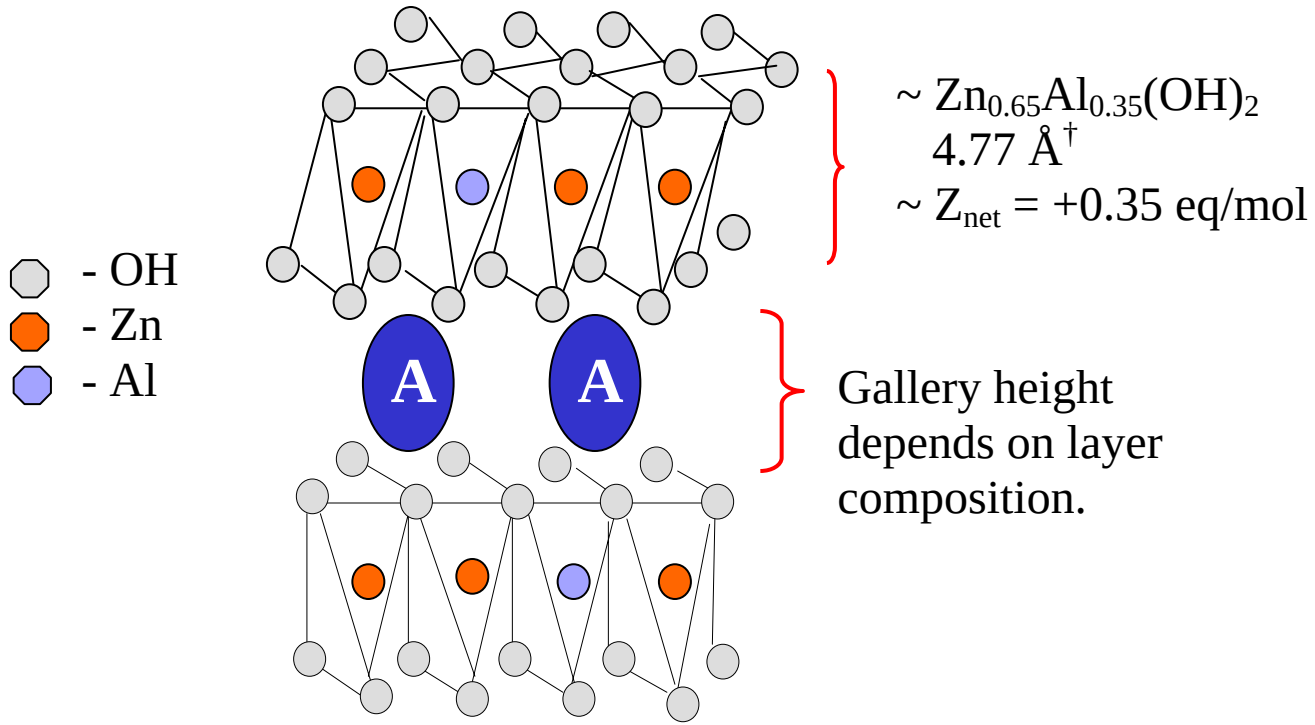

Figure 2. Schematic illustration of the layered structure in hydrotalcite compounds. The structure consists of alternating layers of positively charged mixed metal hydroxide sheets and anions.

In the x-ray diffraction patterns shown in Figure 1, the 003, 006 and 009 basal plane reflections of the Al-Zn-chloride HT can be clearly distinguished from the 006 and 009 reflections of the Al-Zn-vanadate HT. This is the basis for corrosion sensing. As chloride exchanges for decavanadate in the compound, a phase transformation is induced and small cyrstallites of HT-Cl nucleate in the particulate.

The 003 reflection from the HT-V compound is not observed in this pattern. Due to large d-spacing of the 003 planes, the diffraction peak occurs at a 2θ value less than 4°, which cannot be resolved with the diffractometer and experimental protocol used in these experiments.

Inhibitor release from HT particulate. In this corrosion protection scheme, the HT particulate serves as an inhibitor reservoir from which inhibitor can be released when necessary. For the particulate to be useful in this regard it must preserve the inhibiting species until needed, it must have a sufficient inhibitor capacity to render effective protection for the intended life of the coating, and it must release the inhibitor at a sufficient rate and achieve a sufficient concentration to protect the substrate against aggressive service environments. All of these functions are achieved by HT-V particulate.

Hydrotalcites are anion exchange compounds. In general, ion exchange compounds consist of a host structure with a fixed charge. In the case of HT-V, the host is a mixed Al-Zn hydroxide that is positively charged. The positive charge originates from the substitution of Al^{3+} on Zn^{2+} sites in the structure. For an estimated host composition of $Zn_{0.65}Al_{0.35}(OH)_2$, the net positive charge is +0.35 eq/mol.

Within the host are open channels or “galleries”, discussed above, which can accommodate anions and solvent molecules. Cations may also be incorporated into the gallery provided that overall electroneutrality is maintained in the solid. In the initial state, HT-V contains inhibiting anions in the gallery. As is depicted schematically in Figure 3, on contact with an aggressive electrolyte containing chloride ions, an exchange reaction will occur in which the inhibitor anion will be released, and chloride will be adsorbed into the HT gallery. The exchange reaction is chemical in nature and is governed by and equilibrium constant and an exchange isotherm, which can be measured [18]:

$$\underline{\mathrm{HT}\mathit{Inh}} + \mathrm{NaCl}_{(aq)} \leftrightarrow \underline{\mathrm{HTCl}} + \mathrm{Na}\mathit{Inh}_{(aq)} \qquad \text{(eq.2).}$$

In this expression HTInh and HTCl refer to inhibitor and Cl^- in the gallery of the HT compound respectively. Anion storage capacity for hydrotalcites ranges from 2 to 4 meq/gram[19]. Exchange kinetics are not widely reported [20-22], but appear to be fast enough to be useful for corrosion inhibition as will be shown below.

Figure 4 shows the concentrations of vanadium and zinc detected in a 0.5M NaCl solutions containing an excess of solid HT-V particulate. The plot shows the

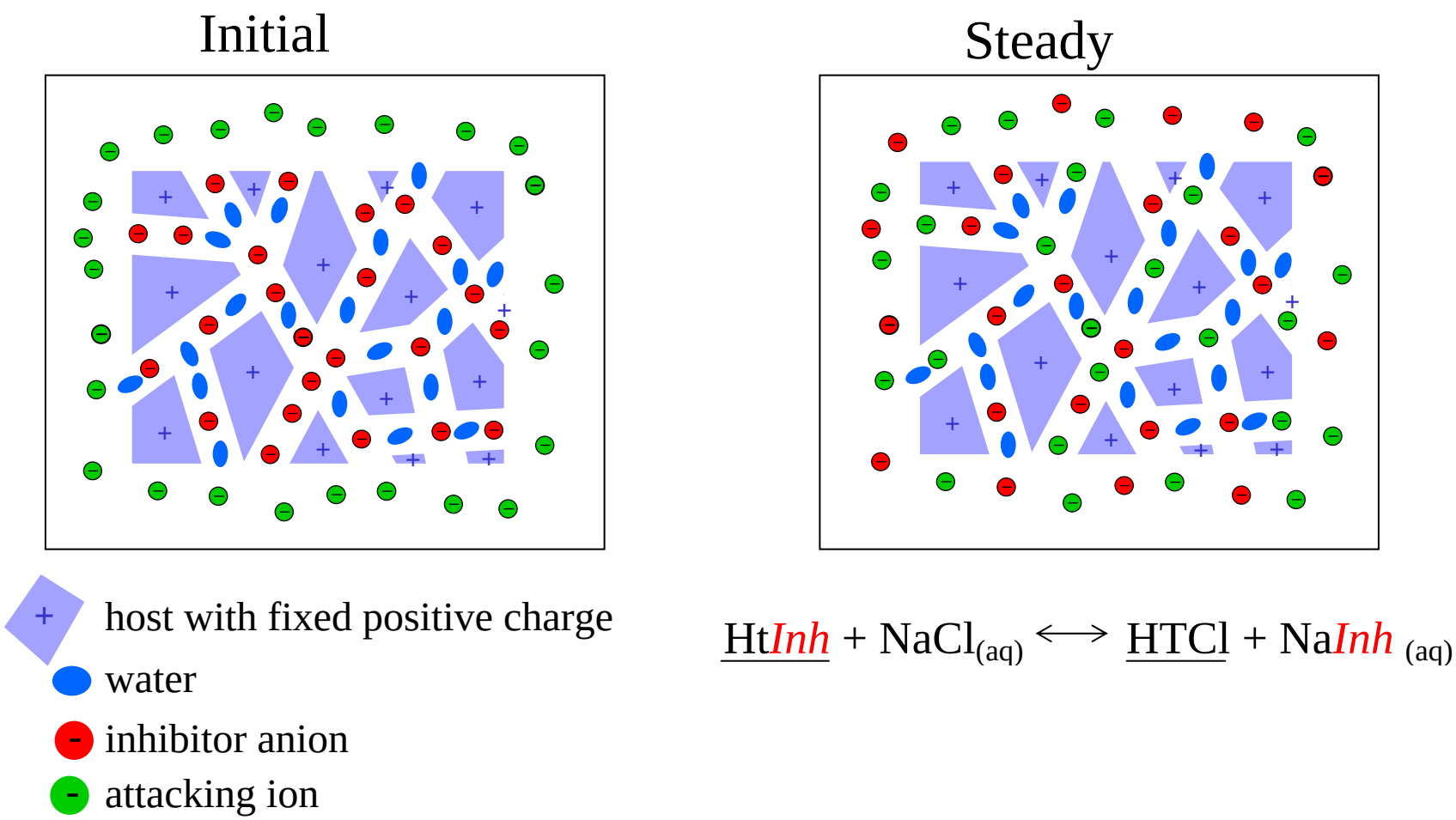

$$\underline{\mathrm{Ht}\mathit{Inh}} + \mathrm{NaCl}_{(aq)} \longleftrightarrow \underline{\mathrm{HTCl}} + \mathrm{Na}\mathit{Inh}_{(aq)}$$

Figure 3. Schematic illustration of anion exchange in hydrotalcite compounds.

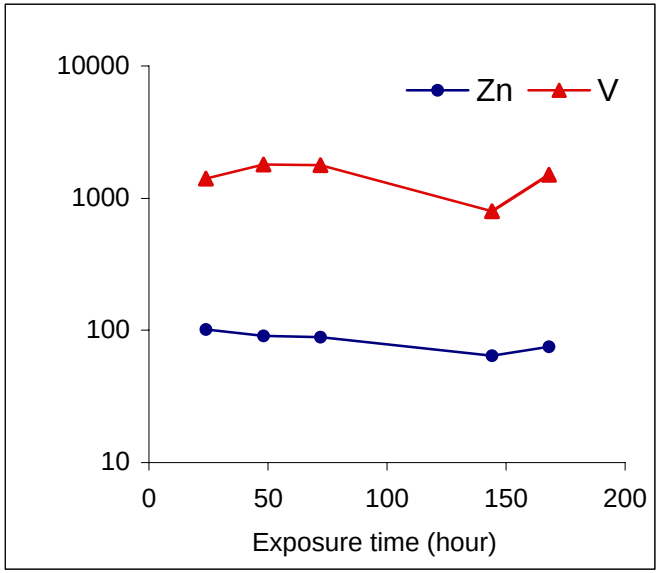

Figure 4. Concentration as a function of exposure time for vanadium and zinc in 0.5M NaCl solution in contact with an excess of Al-Zn-decavanadate hydrotalcite powder.

concentrations of V and Zn expressed as parts per million by weight (ppmw) as a function of exposure time. These data show that appreciable concentrations of both Zn and V accumulate rapidly in solution and that there is not a significant variation in concentration beyond 24 hours. Information on vanadate speciation is not available from ICP-OES measurements, however the steady state pH in these solutions was found to range from 5.97 to 6.30. At this pH, vanadium in solution should exist primarily as metavanadate (e.g., $V_3O_9^{3-}$, or $V_4O_{12}^{4-}$) under equilibrium conditions. Metavanadates have been shown to be good inhibitors of Al corrosion in this and other studies [14]. In experiments carried out in a related study in our laboratories, we have used a combinatorial chemistry approach to show that Al alloy corrosion is significantly inhibited in solutions produced by leaching vanadates and Zn^{2+} from HT-V particulate [23]. In a direct experimental comparison, this solution was found to be more inhibiting than a 1 mM chromate solution in terms of the effect on the pitting potential distribution for 2024-T3.

While the release of vanadates from the HT-V particulate by anion exchange was expected in these experiments, the release of Zn^{2+} was not. As indicated by XRD (shown later) of HT-V particulate after exposure to solutions, Zn^{2+} release does not occur due to large-scale breakdown of the Al-Zn host; structural integrity of the hydrotalcite is retained. The origins of Zn^{2+} release are not obvious based on experiments conducted so far. However, there are several possible routes for Zn^{2+} into solution. First, Zn^{2+} may reside in the galleries of the compound. Cations can be present in the galleries provided that overall charge neutrality of the hydrotalcite compound is maintained. In this case, Zn^{2+} release would be expected to occur in conjunction with decavanadate release. a second possibility is that during HT-V synthesis a hetero-polyoxometallate of Zn and V may form and be incorporated into the gallery of the compound. Release of the Zn-V metallate would result in release of Zn and detection by ICP-OES. This does not appear likely, as XRD measurements of the gallery height are consistent with the presence of decavanadate and not a presumably larger Zn-V metallate. More likely is the possibility of selective dissolution of Zn^{2+} from Zn-Al-vanadate hydrotalcites, which has been reported on several occasions [24, 25]. These reports indicate Zn^{2+} dissolution without structural decomposition of the compound during exposure to mildly or strongly acidic solutions.

<u>Corrosion Inhibition</u>. HT-V pigments are good corrosion inhibitors. Figure 5 is a set of optical macrographs showing 2024-T3 coupons before and after exposure to ASTM B117 salt spray. In these experiments, 2024-T3 coupons were coated with 3 wt. % HT-V pigment dispersed in 10wt % polyvinyl alcohol (PVA) solution $[(-CH_2-CH(OH)-]_n$ (n= 13,000 - 23,000). This mixture was then cast onto degreased and deoxidized 2024-T3 substrates. The coating was allowed to dry and was then cured for 2 hours at 150°C to remove residual water and form a three-dimensional polymer network. During curing the PVA polymerizes becomes insoluble in water. The use of PVA as the resin component in coatings is an experimental convenience only. PVA is quite water permeable, and as such is not necessarily a good resin for durable coatings. However, it allows for ready observation of the behavior of corrosion inhibition of pigments in laboratory experiments, and for this reason, it was used in these experiments.

PVA/HT-V no exposure | PVA/HT-V after 240h | PVA only after 240h

Figure 5. Optical macrographs of 2024-T3 coupons coated with PVA with and without HT-V inhibitors before and after exposure to ASTM B117 salt spray.

The leftmost panel shows the appearance of the coated panel prior to exposure. The coating is not opaque and the coupon exhibits a yellow-brown coloration due to the presence of the HT-V pigment in the PVA. Examination of coating cross sections by scanning electron microscopy revealed the coating thickness to be on the order of 3 µm. The center panel shows a coupon that had been exposed to salt spray for 240 hours. The rightmost sample was coated only with PVA then exposed to salt spray along side the sample with the HT-V pigment. Comparison of the center and right sample illustrates the high level of corrosion protection associated with the presence of the HT-V pigment in the coating.

Evidence of corrosion protection by HT-V pigment can also be detected in the EIS response of coated samples. In EIS experiments, coupons were coated with PVA only, PVA plus 3 wt.% HT-V pigment and PVA plus 3 wt.% $NaVO_3$. Coated coupons were fixed in a cell that permitted exposure of 16 cm^2 of the coupon surface.

In most cases, the impedance response was that of a distributed single time constant, which yielded a partially resolved semi-circular arc in a complex plane plot of the data. These spectra were analyzed by equivalent circuit modeling and complex non–linear least squares fitting of the measured spectrum to the equivalent circuit model response. This procedure was carried out using Scribner Associate's Zview™ software. The equivalent circuit model used was a Simplified Randles circuit, which consisted of a parallel resistor-constant phase element combination [26]. This two-element network was then placed in series with a solution resistance. The fitting routine minimized the residual error between the measured spectrum and a model response by adjusting the numerical values of the circuit elements in the equivalent circuit model. The fit was optimized when a root mean square error of less than 5% between the experimental data and the model-generated fit was obtained. The numerical value of the series resistance determined from this analysis was taken as a figure of merit for ranking the relative corrosion resistance of the various coated surfaces. This value is referred to as "R_c". The samples coated with PVA exhibited poor corrosion resistance sometimes exhibited a two time constant impedance response. In these cases, the total impedance at the lowest measured frequency was taken as the value of R_c.

Figure 6 shows the variation in single point measurements of R_c as a function of exposure time to aerated 0.5 M NaCl solution. The PVA-only control sample yields an R_c value of about 10^6 ohm-cm^2 after 24h exposure, but this decreases to a value of 10^4 ohm-cm^2 after 100h. This value of R_c is similar to that observed for unprotected Al alloys exposed to aerated chloride solutions. By comparison, the PVA coatings dosed with $NaVO_3$ and HT-V pigment maintain very high values of R_c over the entire duration of the experiment. The range of R_c values for the HT-V pigmented coatings are consistently 5 to 10 times greater than those of the $NaVO_3$ pigmented coating. The increased corrosion resistance of the HT-V bearing coatings is attributed to the release of Zn^{2+} ions by the pigment.

Figure 7 shows anodic and cathodic polarization curves for 2024-T3 exposed to 0.124 M NaCl solution at pH 6. In figure 7a, anodic polarization curves are shown for

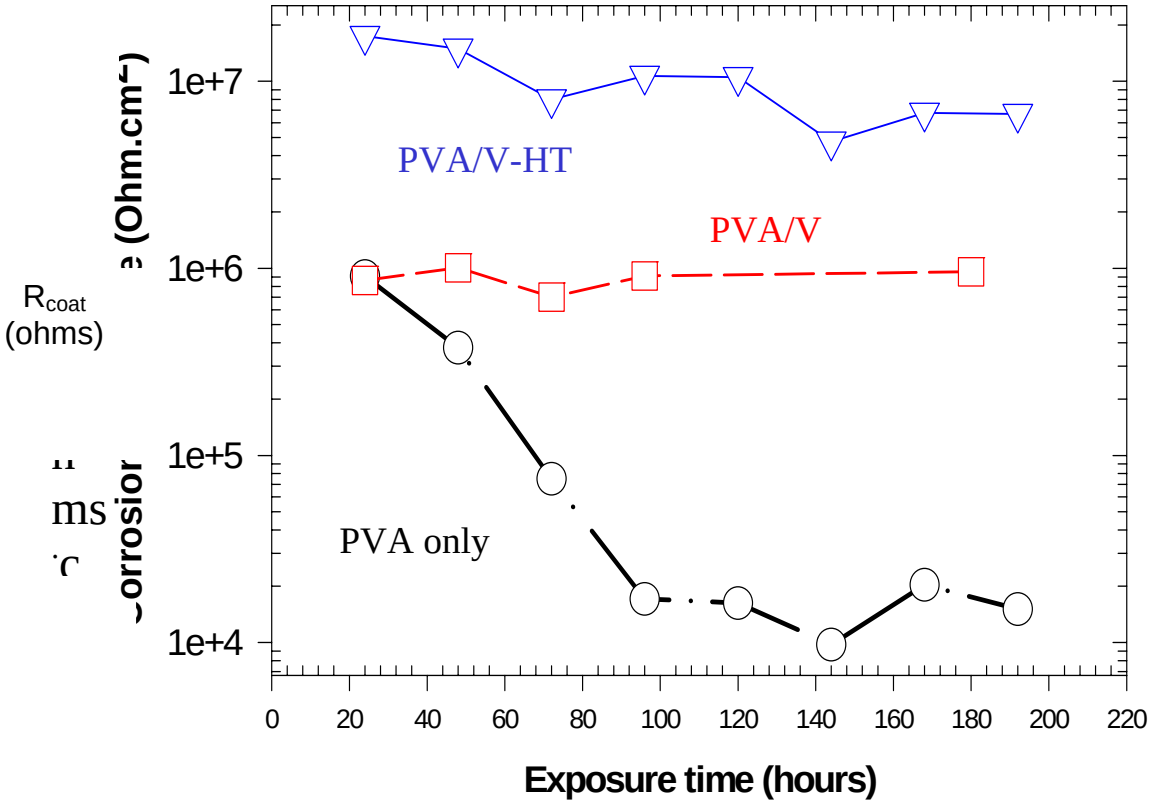

Figure 6. R_c (R_{coat}) for PVA coated 2024-T3 substrates as a function of exposure time to aerated 0.5M NaCl solution. (PVA/V-HT) PVA resin containing 3 wt.% Al-Zn-decavanadate particulate additive, (PVA/V) PVA resin with 3wt.% $NaVO_3$ added, (PVA only) PVA resin with no additives.

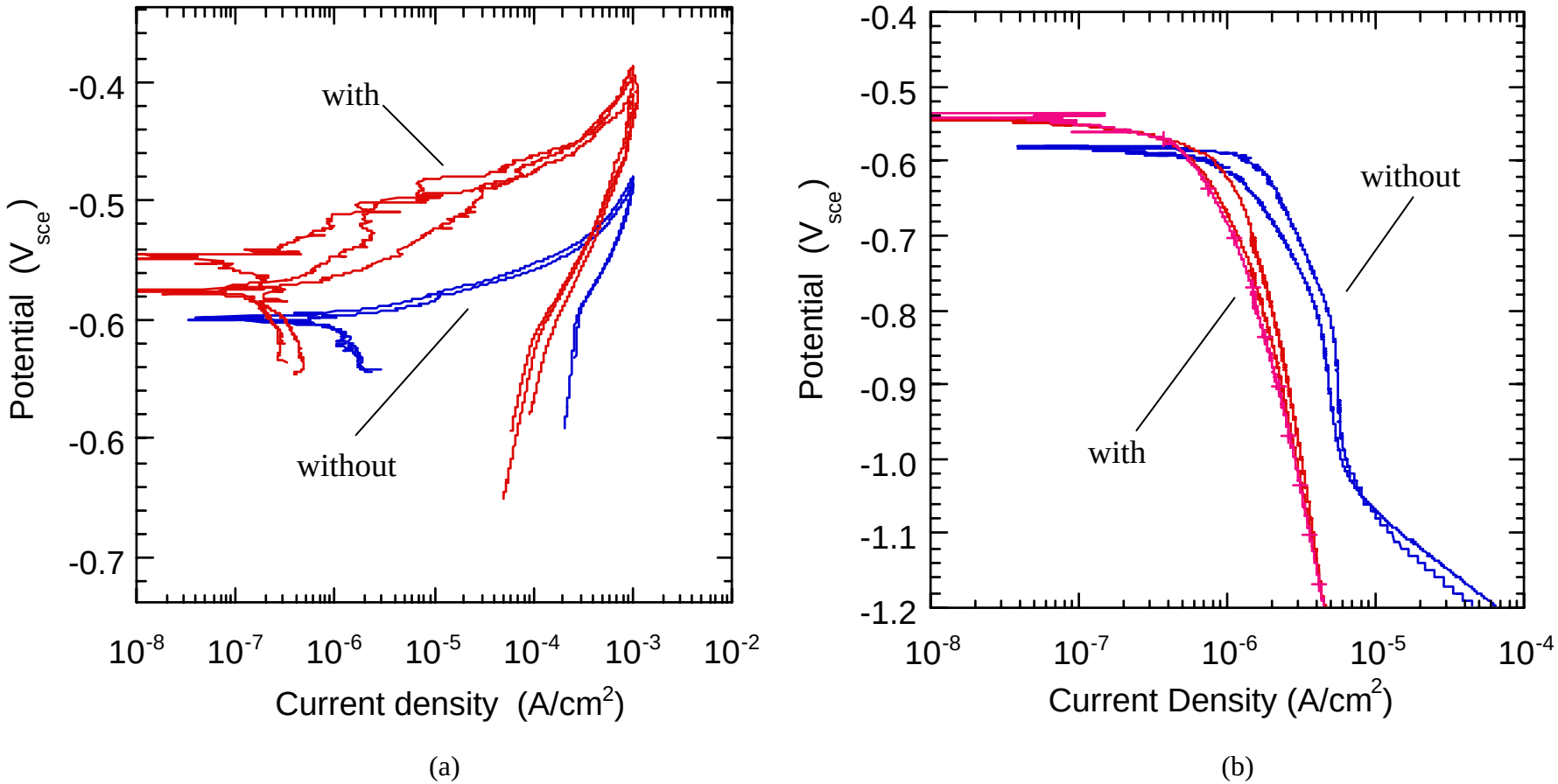

Figure 7. (a) Anodic and (b) cathodic polarization curves for 2024-T3 in 0.124M NaCl solution open to air with and without additions of 0.1M $NaVO_3$.

experiments with and without 0.1M $NaVO_3$ in solution. In the presence of $NaVO_3$, the pitting potential of the alloy is increased by about 100 mV indicating the vanadates inhibit anodic reactions on this alloy. Figure 7b shows cathodic polarization curves in the presence and absence of $NaVO_3$. This figure shows the region of the polarization response where diffusion limitation dominates the rate of oxygen reduction on bare Al alloys. Comparison of these curves shows that the presence of $NaVO_3$ at a 0.1M concentration has only a minor effect on reducing the rate of oxygen reduction on 2024-T3.

To put these results in perspective, sub-millimolar concentrations of $NaCrO_4$ dissolved in aqueous chloride solutions have been observed to strongly reduce cathodic kinetics on Al alloys [27]. In terms of anodic kinetics, increases in the pitting potential of aluminum are detected in anodic polarization responses when the chromate:chloride ratio exceeds 0.1 to 10 depending on the concentration range [28]. In this respect, vanadates are not as good cathodic inhibitors as chromates, but are as good, if not better anodic inhibitors than chromates.

The release of Zn^{2+} from HT-V may be significant with respect to cathodic inhibition by HT-V pigments. Figure 8 shows the cathodic polarization curves for 2024-T3 in 0.124 M NaCl solutions with various amounts of Zn^{2+} added. These curves show that cathodic kinetics are reduced in the diffusion-limited oxygen reduction reaction regime as the Zn^{2+} concentration increases. The affect Zn^{2+} on cathodic kinetics is not as strong as that observed for chromates, but it contributes to the overall corrosion protection afforded by HT-V pigments in PVA resins. The action of Zn^{2+} on cathodic kinetics is unusual in the sense that the diffusion limited current density is reduced without an apparent transition to activation control. This is likely due to the fact that oxygen reduction occurs locally at points on the surface defined by intermetallic particles. As a result, spherical diffusion rather than planar diffusion controls the limiting current density. Zn^{2+} may act at some fraction of these sites to stifle their ability to support reduction reactions. In this case, the diffusion limitation evident in the polarization response is retained, albeit at a lower overall current density.

HT-V pigmented epoxy primers prepared as described in the experimental procedures are sufficiently corrosion resistant to protect against significant corrosion in scribes. Figure 9 shows several optical macrographs of scribes exposing underlying substrate through a neat epoxy resin, an epoxy resin containing 1 µm alumina particulate, HT-V pigment, and $SrCrO_4$ pigment. These coatings were applied using a drawdown bar and were allowed to cure for 48 hours before exposure testing. Once cured, the surfaces were exposed to aerated 0.5M NaCl solution for approximately 400 hours. Inspection of the macrographs shows varying degrees of corrosion damage. Significant corrosion is evident in the scribe in the neat resin coating and the alumina-filled coating. No corrosion is observed in the $SrCrO_4$-bearing coating. However, the coating was leached of chromate so significantly that the contacting solution in the exposure cell turned yellow. This solution was probably inhibited enough so that corrosion of the substrate was not possible. In the case of the HT-V pigmented coating, a small amount of corrosion was detected in one leg of the scribe. The small amount of corrosion damage is consistent

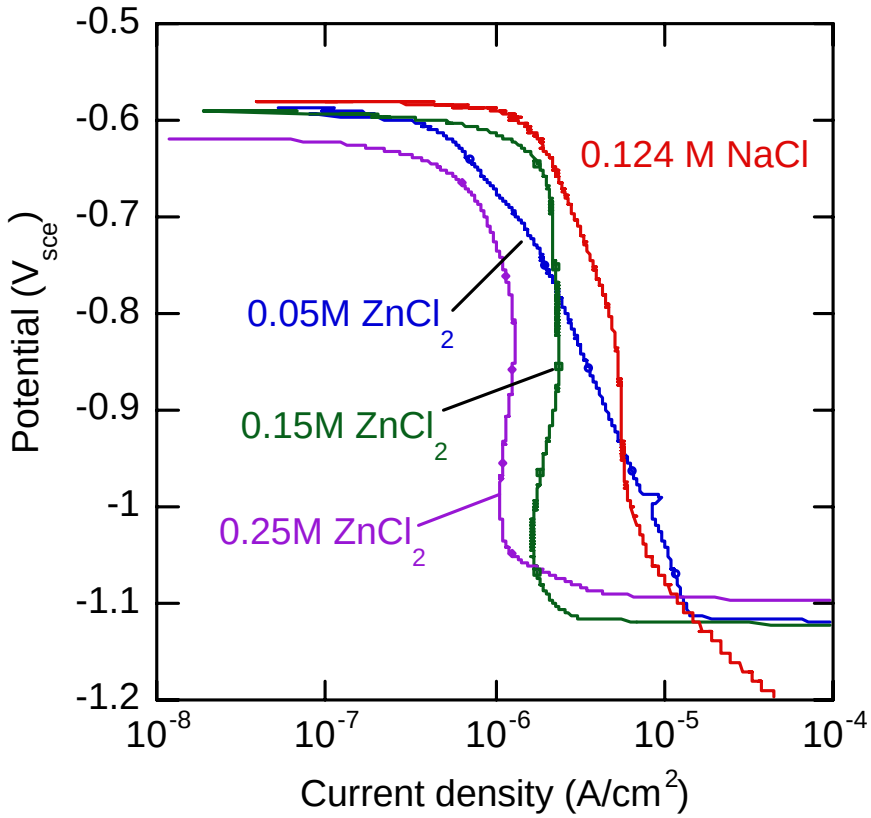

Figure 8. Cathodic polarization curve for 2024-T3 in aerated 0.124M NaCl solution with increasing amounts of Zn^{2+} added as $ZnCl_2$.

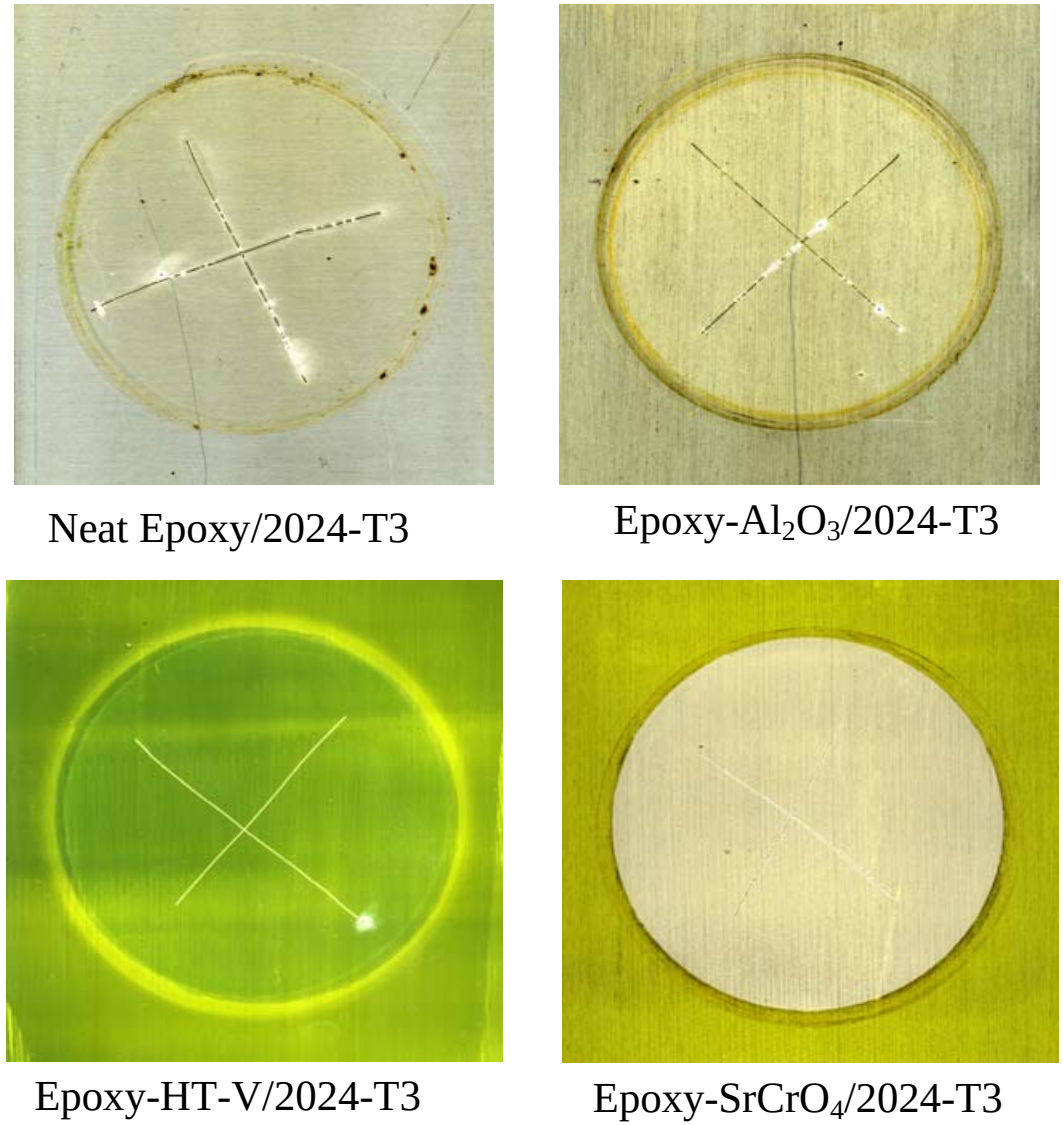

Figure 9. Optical macrographs of coated and scribed samples exposed to aerated 0.5M NaCl solution for 400 hours. Exposed circular areas are 32 cm^2.

with leaching of vanadates and Zn^{2+} to inhibit corrosion. Further experiments examining self-healing using a simulated scratch cell [29] have been conducted that show that HT-V epoxy coating do leach vanadates and Zn^{2+} and can protect bare surfaces in close proximity to the coating [30].

Corrosion sensing. Corrosion sensing with hydrotalcite pigments dispersed in organic resins is based on the change in the crystal structure that is associated with inhibitor anion release and chloride ion uptake. This is expected to occur when electrolyte penetrates into the coating. Remote detection is accomplished by x-ray diffraction. This strategy does not sense corrosion directly, but would indicate an environmental change in the coating that is a prelude to corrosion.

As discussed earlier, hydrotalcites are layered compounds comprised of alternating sheets of mixed metal hydroxides and sheets of anions. The primary indicator of electrolyte permeation in the coating is the appearance of a new basal plane diffraction peak associated with the nucleation of a new hydrotalcite phase containing chloride or sulfate from the electrolyte. Since both of these ions have smaller sizes that decavanadate, the basal plane spacing of the new hydrotalcite phase will be smaller than that of the HT-V compound causing a new diffraction peak to appear.

Figure 10 shows a series of diffraction patterns for the HT-V hydrotalcite powder exposed for 22 days to deionized water, 0.5M NaCl solution and a saturated NaCl solution. The diffraction pattern for unexposed HT-V is shown for comparison. In each of the diffraction patterns from samples exposed to chloride solutions there is a distinctive diffraction peak from the 003 basal plane of HT-Cl hydrotalcite at about 12° 2θ. The very weak peak at this position in the unexposed sample is due to slight chloride contamination of the HT-V powder.

Solution exposure-induced changes in the HT-V diffraction pattern when the pigment is dispersed in epoxy and applied to a 2024-T3 substrate are shown in Figure 11. In this experiment, two coats of 25 wt.% HT-V epoxy primer were applied to degreased and deoxidized 2024-T3. After drying or 48 hours, x-ray diffraction patterns were collected from the surface. These patterns appear in Figure 11a. Only 35° of the pattern are shown, but broad 006 and 009 basal plane reflections are evident at about16^o and 24° respectively. A diffraction pattern was then collected after 456 hours of exposure to aerated 0.5M NaCl solution. This pattern is shown in Figures 11a against the diffraction pattern of the unexposed coating, and in Figure 11b against the diffraction patterns for HT-V and HT-Cl hydrotalcite powders. The pattern from the exposed coating contains of a very broad peak centered at about 15° that appears to be comprised of overlapping 006 HT-V and 003 HT-Cl peaks. Other possible contributions to broadening include exchange of carbonate into the anion layer of the hydrotalcite, and peak broadening due to the presence of very fine HT-Cl crystallites. The 009 HT-V reflection is still present in the pattern indicating that the HT-V pigment has retained structural integrity. In any case, the profound changes in the diffraction pattern of HT-V occur upon exposure to solution indicating that x-ray diffraction can be used to remotely detect environmental changes in the coating due to exposure to aggressive environments.

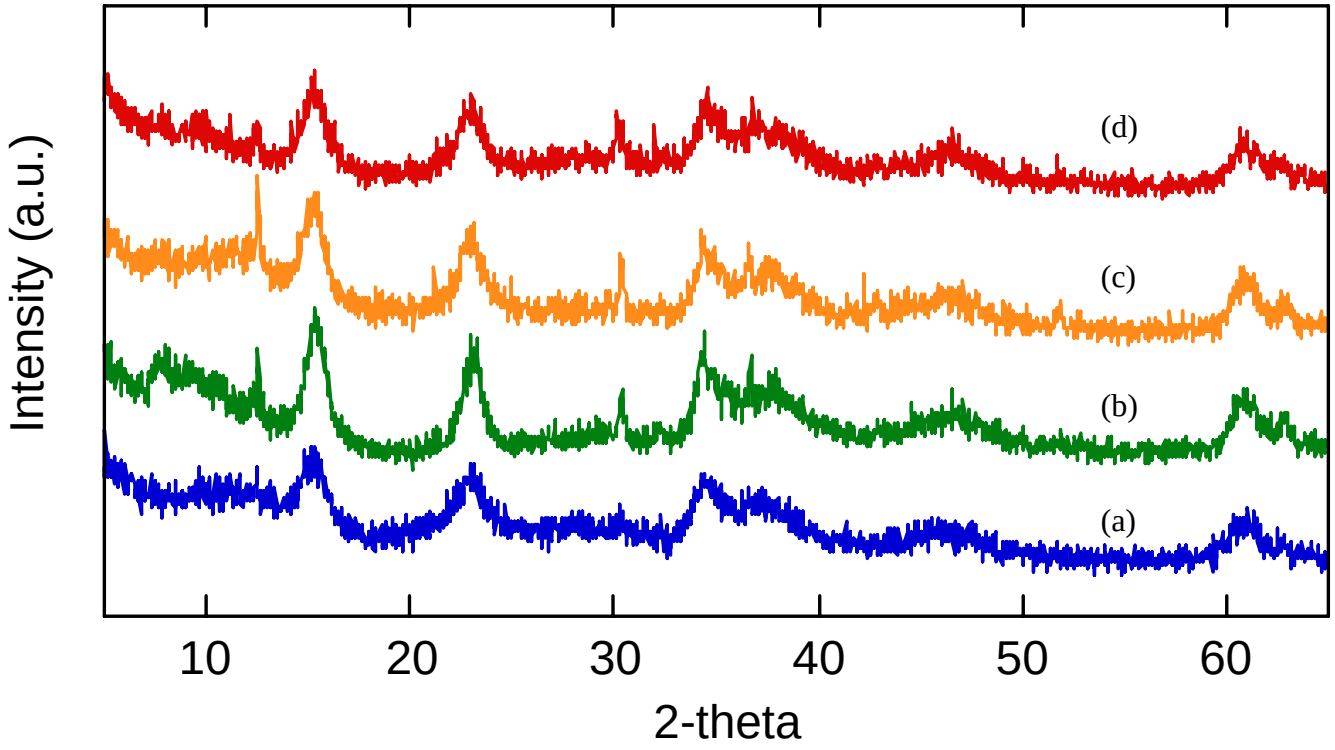

Figure 10. X-ray diffraction patterns from Al-Zn-decavanadate hydrotalcite powder specimens. (a) unexposed. (b) exposed to deionized water for 22 days. (c) exposed to 0.5M NaCl solution for 22 days. (d) exposed to saturated NaCl solution for 22 days. Boxed region contains the HT-V 006 reflection at about 16° and the 003 HT-chloride reflection at about 12°.

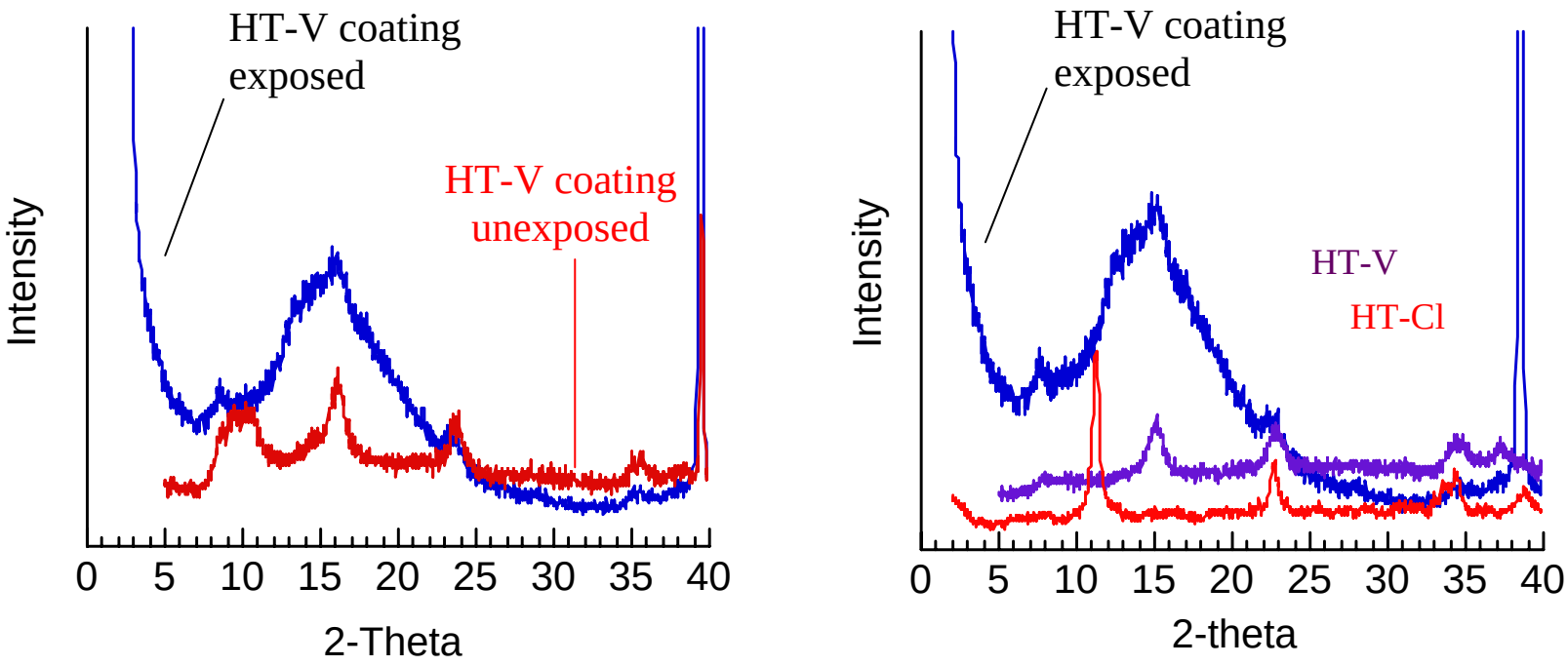

Figure 11. X-ray diffraction patterns from HT-V dispersed in epoxy resin and exposed to aerated 0.5M NaCl solution for 450 hours.

SUMMARY

In this paper, the basic aspects of corrosion protection and corrosion sensing enabled by Al-Zn-decavandate hydrotalcite pigments in epoxy are demonstrated. Corrosion protection originates from release of vanadates and Zn^{2+}, which are anodic and cathodic inhibitors respectively for Al alloys. Corrosion protection due to leaching of these two inhibitors is sufficient to suppress corrosion in scribes exposing underlying bare metal during exposure to salt spray testing. Corrosion sensing consists of detection of electrolyte permeation into coatings, which is often a prelude to corrosion under coatings. This is achieved by exploiting the change in basal plane spacing in hydrotalcites that accompanies ion exchange. In this case, inhibiting decavanadate ion is exchanged for chloride or sulfate contained in the attacking electrolyte. Inhibitor is released, attacking ions are taken up and nucleate a new hydrotalcite phase with a different basal plane spacing. The presence of this new phase can be detected remotely by x-ray diffraction. Taken together, these results show that the use of hydrotalcite pigments in organic coatings may lead to new coatings with useful levels of corrosion protection for Al alloys and can enable a new means for determining when coating replacement is warranted.

REFERENCES

1. Primer Coatings: Epoxy, High Solids,MIL-PRF-23377, Naval Air Warfare Center Aircraft Division., Lakehurst NJ, 1994.
2. Sinko, J., *Prog. Organic Coat.*, **42**, 267 (2001).
3. C.F. Baes, J. and R.E. Mesmer, *Hydrolysis of Cations*220. ed., Malabar, FL: Robert E. Kreiger Publishing Co. 1986
4. *Chromium and Nickel Welding*, in *IARC, Monograph on the Evaluation of the Carcinogenic Risk of Chemicals to Humans*. 1990, International Agency for the Research on Cancer: Lyon.
5. O'Brien, P.O. and A. Kortenkamp, *Transition Metal Chemistry*, **20**, 636 (1995).
6. Suzuki, Y., *Ind. Health*, **28**, 9 (1990).
7. Suzuki, Y. and K. Fukuda, *Arch. Toxicol.*, **64**, 169 (1990).
8. Kendig, M., et al., *J. Electrochem. Soc.*, **144**, 3721 (1997).
9. Primer, Epoxy Coating, Corrosion Inhibiting, Lead and Chromate Free,MIL-P53022A,USA Belvoir Research, Development, and Engineering Center., Fort Belvoir, VA, 1983.
10. Osborne, J.H., et al., Advanced Corrosion Resistant Aircraft Coatings,prepared under contract no. F33615-96-C-5078,Air Force Materiel Command., Wright-Patterson AFB, OH, October, 2000.
11. Zhang, J. and G.S. Frankel, *Corrosion*, **55**, 957 (1999).
12. Anon., *Chemical Week*, **161**, 27 (1999).
13. Anon., *Chemical and Engineering News*, **77**, 12 (1999).
14. R.L. Cook, J. and S.R. Taylor, *Corrosion*, **56**, 321 (2000).
15. Kooli, F. and W. Jones, *Inorg. Chem.*, **34**, 6237 (1995).
16. C.F. Baes, J. and R.E. Mesmer, *Hydrolysis of Cations*205. ed., Malabar, FL: Robert E. Kreiger Publishing Co. 1986

17. Velu, S., et al., *J. Mater. Sci.*, **32**, 957 (1997).
18. Miyata, S., *Clays and Clay Miner.*, **31**, 305 (1983).
19. Kooli, F., V. Rives, and M.A. Ulibarri, *Inorg. Chem.*, **34**, 5122 (1995).
20. Goswamee, R.L., P. Sengupta, and K.G. Bhattacharyya, *Applied Clay Sci.*, **13**, 21 (1998).
21. Hussein, M.Z.B., Z. Zainal, and E.M. Choong, *J. Porous Materials*, **8**, 219 (2001).
22. Shin, H.S., et al., *Wat. Sci. Tech.*, **34**, 161 (1996).
23. Zhang, W., et al., *Proceedings of the 201st meeting of the Electrochemical Society*, **Salt Lake City UT**, in press (2002).
24. Barriaga, C., et al., *Inorg. Chem.*, 1812 (1998).
25. Weir, M.R. and R.A. Kydd, *Inorg. Chem.*, **37**, 5619 (1998).
26. Buchheit, R.G., et al., *Corrosion*, **54**, 61 (1998).
27. Sehgal, A., D. Lu, and G.S. Frankel, *J. Electrochem. Soc.*, **145**, 2834 (1998).
28. Kaesche, H. *Pitting Corrosion of Aluminum and Intergranualr Corrosion of Al Alloys*. in *Localized Corrosion*. 1971. Williamsburg, VA: NACE, Houston, TX.
29. Zhao, J., G.S. Frankel, and R.L. McCreery, *J. Electrochem. Soc.*, 2258 (1998).
30. Mahajanam, S. and R.G. Buchheit, *Corrosion*, in preparation (2002).

Results and Accomplishments Part IV:

Integrated Coating System Evaluation

OBJECTIVE AND APPROACH

The objective of this task was to evaluate properties related to corrosion resistance of several Cr-free coating systems comprised of selected Cr-free pretreatments and an epoxy primer coating containing a hydrotalcite corrosion-inhibiting pigment. The performance of these coatings systems was evaluated against positive control sample comprising a chromate conversion coatings and a $SrCrO_4$-pigmented epoxy primer (MIL-P-23377), and a negative control comprising an epoxy neat resin applied on an aluminum alloy surface that was cleaned and deoxidized only.

All the samples were exposed for 1344h according to ASTM B117 salt fog exposure, and to condensing ultraviolet exposure using a Q-UV exposure chamber per ASTM G 154-00a conditions. Paint adhesion was examined using a Pneumatic Adhesion Tensile Test Instrument (PATTI). Electrochemical Impedance Spectroscopy (EIS) and XRD were carried out to assess corrosion protection of the samples during salt spray and UV exposures.

MATERIALS AND METHODS

Substrates. Aluminum alloy 2024-T3 Substrates were used as substrates for all coatings. Commercial 2.0-mm thick AA2024-T3 sheet stock was purchased from Midwest Metals, Inc. The alloy had the following composition: All-3.8-4.9Cu, 1.2-1.8 Mg, 0.3-0.9 Mn, 0.5 Si and Fe, 0.15 Zn and Ti, and 0.1 Cr wt%.

Substrate Cleaning. All coupons were cleaned using Alconox and rinsed using tap water. Immediately following the cleaning rinse, coupons were immersed in a bath containing 48.0 g $Na2CO_3$, 32.4g Na_2SiO_3, 1000.0 ml deionized (DI) H_2O at about 65^oC for 2 min. The coupons were cleaned by two DI-water rinses. The degreased coupons were deoxidized by 3-min immersion in a bath containing 30.0 g Sanchem 1000, 72.0 ml HNO_3 (concentrated) and 1000.0 ml DI-H_2O at about 55^oC. Coupons were subject to a final clean by DI-water rinsing.

Pretreatments. Sample pretreatments (conversion coatings) were carried out on substrate immediately following the deoxidizing. Five potential nonchromated pretreatment alternatives were used. They included vanadate conversion coating (VCC), silane adhesive protection with and without cerium, cerium conversion coating and with and without molybdenum modification.

The coatings were then allowed to stand overnight with subsequent primer application. The primer coatings were applied within 24h after the pretreatment. The coating systems were cured at ambient conditions for 5 days before testing.

Chromate conversion coating (CCC). CCCs were applied according to the Alodine 1200S, process: 7.55g/L, pH 1.55 CrO_3/HNO_3 bath. The bath solution was stirred for 3 hours at room temperature prior to use. Deoxidized 2024-T3 panels were exposed in the bath at RT for 1min. Panels were then subject to two DI-water rinses for 1min.

Vanadate conversion coating (VCC). VCCs were applied using an internally developed process. The coating bath chemistry used was: 10 mM $NaVO_3$, 9 mM NaF , 12 mM KBF_4, 1 mM K_2ZrF_6, 3 mM $K_3Fe(CN)_6$. The bath solution was adjusted to pH 1.69 using concentrated HNO_3 and stirred for 3 hours at room temperature.

Deoxidized 2024-T3 panels were exposed in the bath at RT for 1min. Panels were then subject to two DI-water rinses for 1min.

Cerium conversion Coating. Cerium conversion coatings are a potential a non-toxic alternative to chromate conversion coating. The coating bath consisted of 10g/l $CeCl_3 \cdot 7H_2O$ + 40ml/l (30 wt%) H_2O_2, pH ~ 2.0.

Cerium/Molybdenum conversion coating (Ce-Mo). Expose the samples in water saturated environment for 3hrs at 90°C then rinsed. Expose the samples in 10mM $Ce(NO_3)_3$ at ~ 90°C for 2hrs and rinsed. The samples were then exposed in 10mM $CeCl_3 \cdot 7H_2O$ at ~ 90°C for 2hrs and rinsed. Another set was prepared by degreasing, deoxidizing, step 1 to step 3 (above) followed by anodic polarization of samples at +500mV in Na_2MoO_4 for 2hrs.

Silane pretreatment. Two silanes, a nonfunctional silane and an organo-functional silane were used as pretreatments. The two silanes used were: 1,2-bis-(triethoxysilyl)ethane (BTSE), and 3-aminopropyltriethoxysilane (3-APS).

The BTES solution chemistry (by volume) was 4% BTSE, 6% water, 90% methanol pH = 6. Solution pH was adjusted using acetic acid or sodium hydroxide. The solution was stirred for 4-5 hours to hydrolyze the silane completely. Degreased and deoxidized Al-2024-T3 panels were dipped in the first solution for 2 minutes, air dried and then dipped in the solution again for 2 minutes. Finally, the panel was blow dried and cured at room temperature for 24 hours.

Cerium-inhibited silane pretreatment. Conversion coatings were made by deposition of hydrated cerium oxide from acidified cerium solutions. Silane/Cerium coatings were made and under investigation at the University of Cincinnati (Prof. Van Ooij's group). Ce^{3+}-doped inorganic-organic material hybrid material was prepared using functionalized silanes by sol-gel process. Functionalized Silane/Cerium molar ratio is an important variable in coating formation. Though it is not clearly established in this study, it seems there is an optimal value of this ratio. Beyond that ratio, corrosion performance of these coatings decreases drastically. A 0.1 M $Ce(NO_3)_3$ solution was prepared and 1.5 ml. of this solution was dissolved in 3-APS solution. Again, a 2-step coating was

prepared on degreased and deoxidized Al-2024-T3 panel using BTSE solution and 3-APS / $Ce(NO_3)_3$ solution as described before.

Synthesis of hydrotalcite (HT-V) corrosion-inhibiting pigment. HT-V pigment was prepared using direct synthesis by co-precipitation in the presence of exchangeable anion. In this process, a $NaVO_3$ solution was acidified to pH 4.5 using HCl. Decavanadate anion $[V_{10}O_{28}]^{6-}$ formed and was stable up to pH 6.5 and a solution color change to orange was observed. This solution was then titrated using $ZnCl_2$, $AlCl_3 \cdot 6H_2O$ and NaOH. The solution was aged overnight at 55°C. The resulting precipitate was filtered and dried overnight at 400°C. It was then ground to get fine Zn-Al-$[V10O_{28}]^{6-}$ (HT-V) powder.

HTV epoxy coating preparation. A two-part epoxy resin was used to form coatings (component A was an unpigmented epoxy. Component B was curing agent based on a polyamide-amine mixture. (Deft Inc. Irvine, CA, satisfying MIL-P-23377G Primer specification, type 02-Y-40). The mix ratio (A:B) was 10: 4.15 by weight. 42.45g HT-V powder was mixed with 90g component A. The mixture was stirring using a magnetic bar for 1 h at room temperature. 37.35 g component B then was added into the mixture and stirred for 0.5 hour before forming coatings.

Forming of HT-V Epoxy primer coatings. Pretreated 2024-T3 coupons were coated using HTV pigmented epoxy by rolling method. A RDS 09 rolling coating bar was used. Single layer coatings were applied on each sample. Samples were cured for 5 days in ambient air at 250°C before UV and salt spray exposure.

Salt spray exposure testing. Salt spray exposure was carried out in a salt fog chamber under conditions specified by ASTM B 117. A 5 wt.% NaCl solution at pH 6.8 and 35°C was used. The exposure period was 1344 hours. Sample edges were sealed using red lacquer to suppress edge corrosion. Sample labels were protected by salt fog resistant tape. Samples were racked at a 15-30° angle from the vertical.

UV exposure testing. UV exposure was carried out in a QUV accelerated weathering tester. Q-panel products. Exposure was carried out according to ASTM G 154-00a. A 340 nm UV light was used for illumination (recommended by ASTM G 154 for direct solar UV radiation). The exposure cycle was 8h UV exposure at 70 (± 3)^{o}C followed by 4h water condensation at 50 (± 3)^{o}C .

Adhesion Testing. To determine the adhesive strength of the coating this test was performed. Adhesion testing was carried out using Elcometer 110 PATTI (Pneumatic adhesion tensile test instrument). An aluminum pull stub was glued tot he test surface and then a pulling piston was attached to the pull stub. A pulling force was applied by pulling piston and recorded as the figure of merit.

Electrochemical Impedance Spectroscopy (EIS). EIS was carried out to characterize coating corrosion protection. EIS was performed using a Solartron Model 1255 frequency response analyzer, an EG&G PAR 273 potentiostat. Data collection and analysis was performed using Z-plot software$^{(TM)}$. Spectra were collected at the sample open circuit

potential using an voltage signal with an amplitude of 10 mV. The frequency of the signal was swept from 10 kHz to 10 mHz at a rate of 7 points per decade frequency.

RESULTS

Salt spray exposure testing. Figures 1 through 9 are optical macrographs of coated sample replicates at selected exposure times ranging from no exposure (as-coated) up through 8 weeks. Figure 1 shows positive control samples conforming to MIL-P-23377. These coatings comprise a chromate conversion coating and a $SrCrO_4$-pigmented primer coating. Figure 4 shows the negative control samples. These samples were deoxidized and coated with an unpigmented (neat) epoxy resin. There is no active inhibitor in these coatings and any corrosion protection is derived only from the barrier properties of the epoxy coating. The remaining samples are the experimental Cr-free coating systems. As suggested by the figures, samples were scribed with an "X" across the face to expose underlying bare metal prior to exposure.

Corrosion damage manifested itself on these samples in three main modes: 1) corrosion in the scribe, 2) blistering or filiform corrosion under the coating that initiated at the scribe, and 3) blistering away from the scribe or sample edges. Blisters were localized regions over which the coating was forcibly separated from the underlying substrate by corrosion product. This corrosion product was visible through the coating and was usually red or rusty in color. In some cases, blisters were ruptured and the uncoated surface was covered with red and white corrosion product.

The mode and intensity of corrosion on replicate samples of a given type was remarkably consistent—even as corrosion damage accumulated as a function of exposure time. This suggests that any variability due to coating application methods was minimal compared to factors driving the corrosion process such as environment aggressiveness or coating chemistry.

The positive control sample did not exhibit significant corrosion of any type during the exposure experiment. There was some loss of color intensity with time due to leaching of soluble $SrCrO_4$ pigment from the epoxy primer coating. Performance of this set of samples represents an upper performance benchmark for the experimental Cr-free samples.

In order to chronicle the corrosion, specimens were numerically rated as per ASTM D 1654 method A and B for damage at the eight-week exposure point. Tables 1 and 2 detail corrosion performance for each coating.

Among Cr-free coating candidates, the pretreatment with the best performance is the Ce and Ce-Mo based conversion coating. Except a slight lifting started at the end of scribe, the Ce-Mo pretreated coupons performed well during 8 weeks of salt fog exposure with the highest ratings among the coating systems. The small delamination formed on two Ce-Mo coupons at the 2nd week had no significant increase in size until 8 weeks of exposure. Compared to Ce-Mo pretreated coupons, Ce-only pretreated coupons

Fresh Samples

170h SST

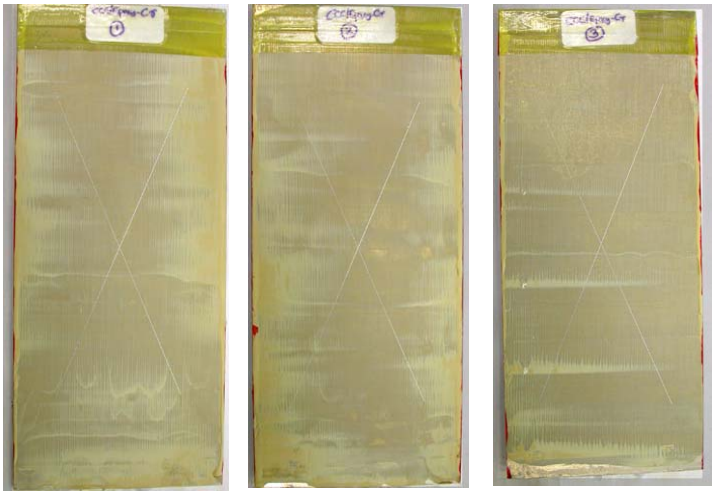

Two weeks SST

Eight weeks SST

Figure 1. Optical macrographs of the chromate-coated positive control samples at selected times during the experiment. Three replicate panels are shown. Exposure times are noted under each set of replicates.

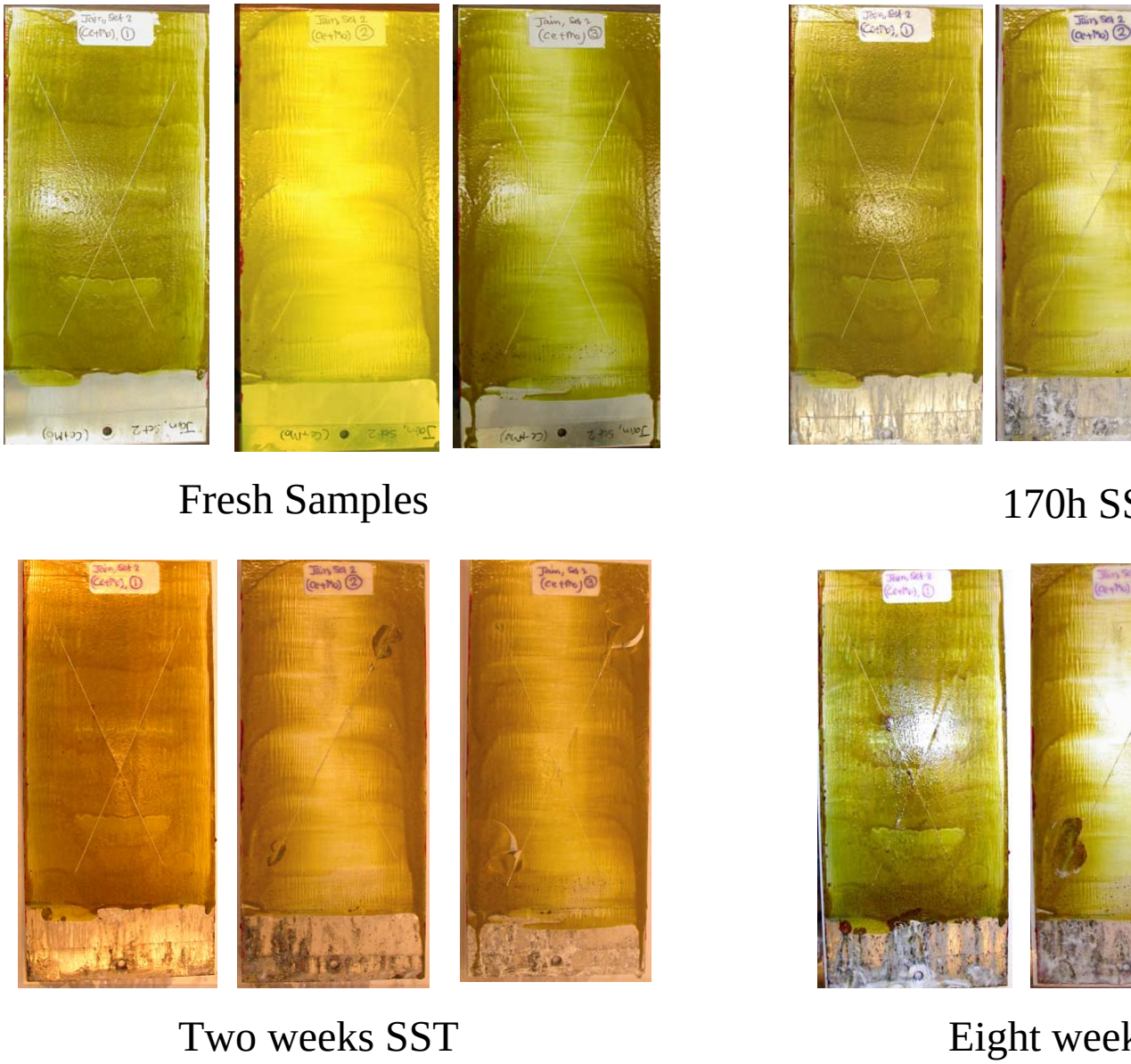

Figure 2. Optical macrographs of the samples with the HT-V-pigmented primer over a Ce/Mo conversion c during the salt spray exposure experiment. Three replicate panels are shown. Exposure times are noted unde

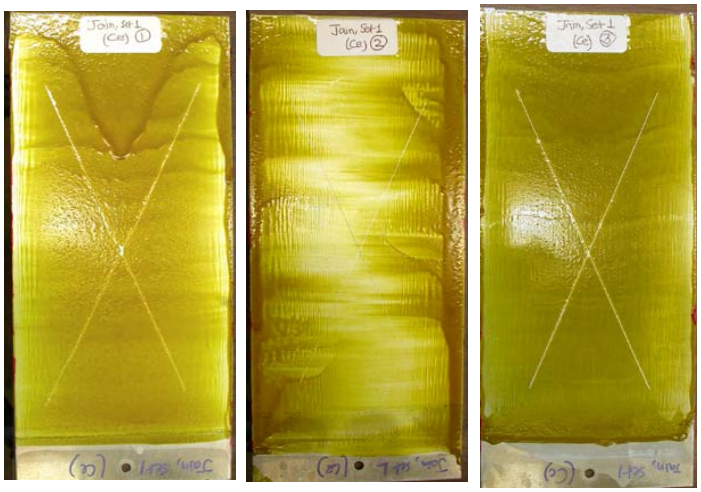

Fresh Samples

170h SST

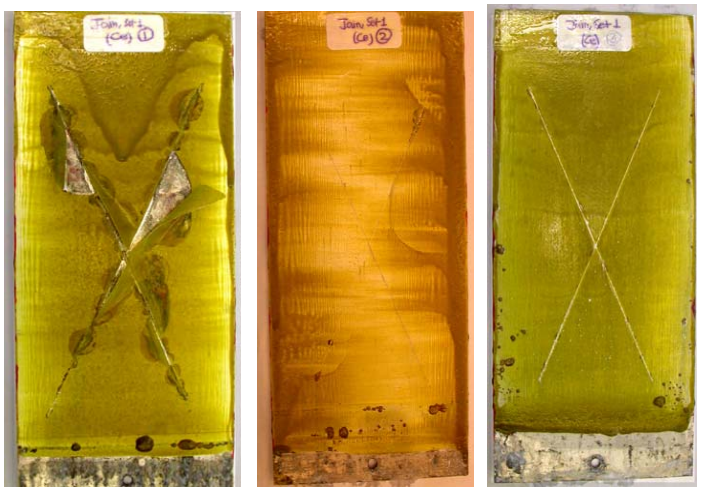

Two weeks SST

Eight week

Figure 3. Optical macrographs of the samples with an HT-V-pigmented primer over a Ce conversion coatin
the salt spray exposure experiment. Three replicate panels are shown. Exposure times are noted under each s

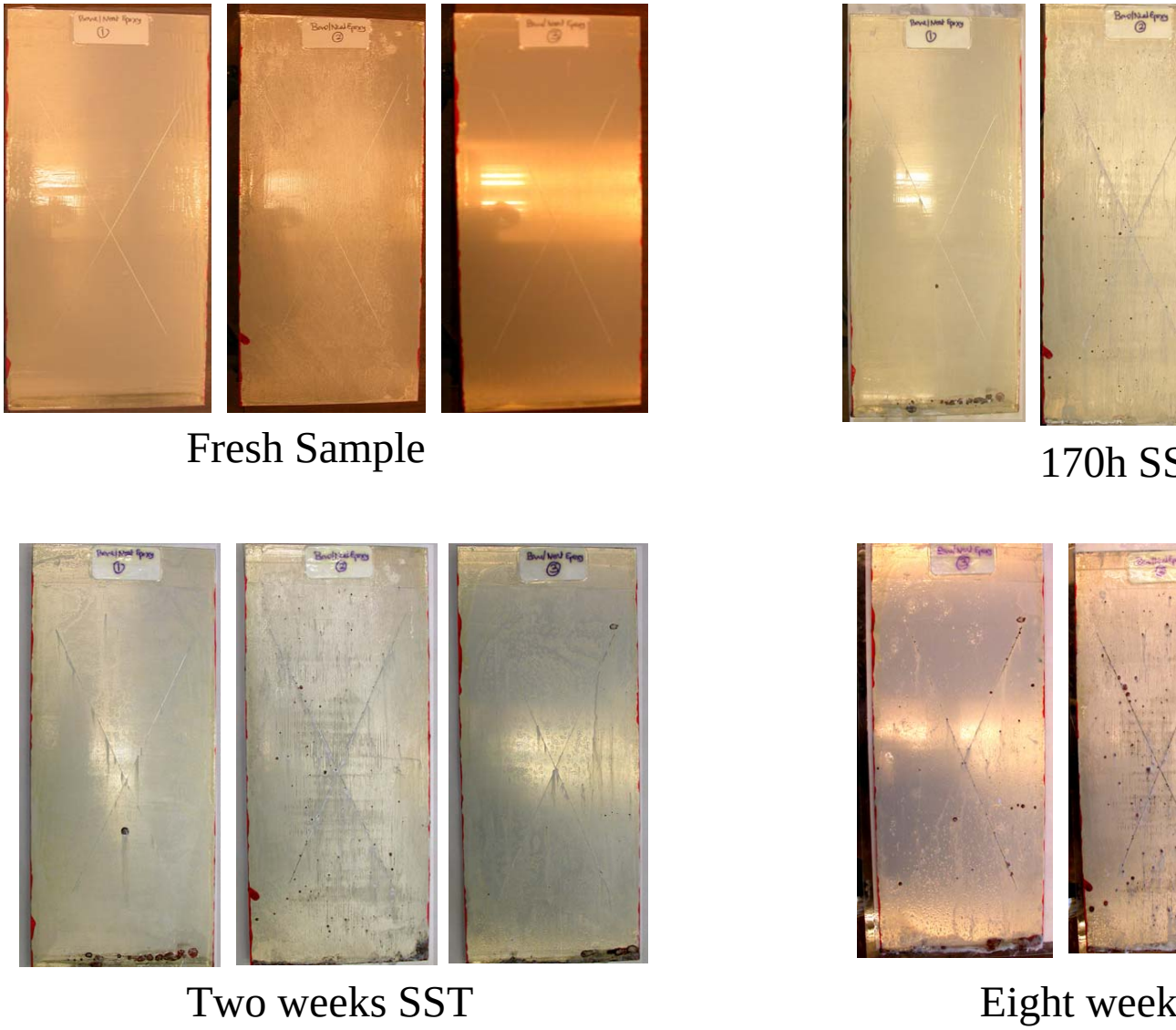

Figure 4. Optical macrographs of the neat epoxy negative control samples at selected times during the salt s
Three replicate panels are shown. Exposure times are noted under each set of replicates.

Fresh Samples

170h SST

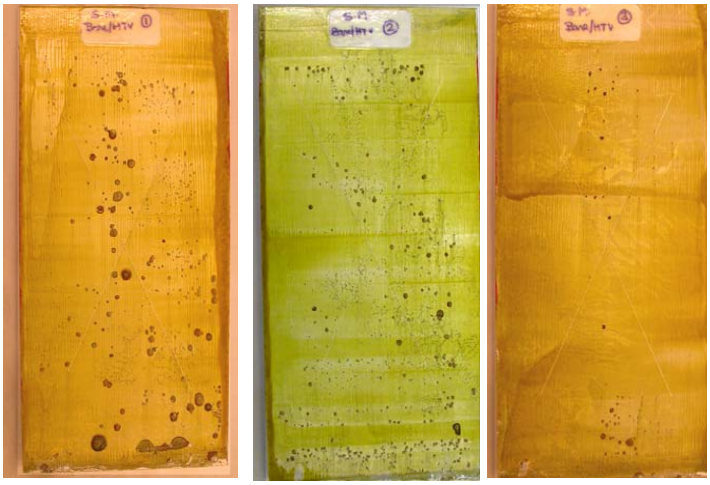

Two weeks SST

Eight weeks S

Figure 5. Optical macrographs of the HT-V-pigmented epoxy coatings applied to deoxidized 2024-T3 surfa
the salt spray exposure experiment. Three replicate panels are shown. Exposure times are noted under each s

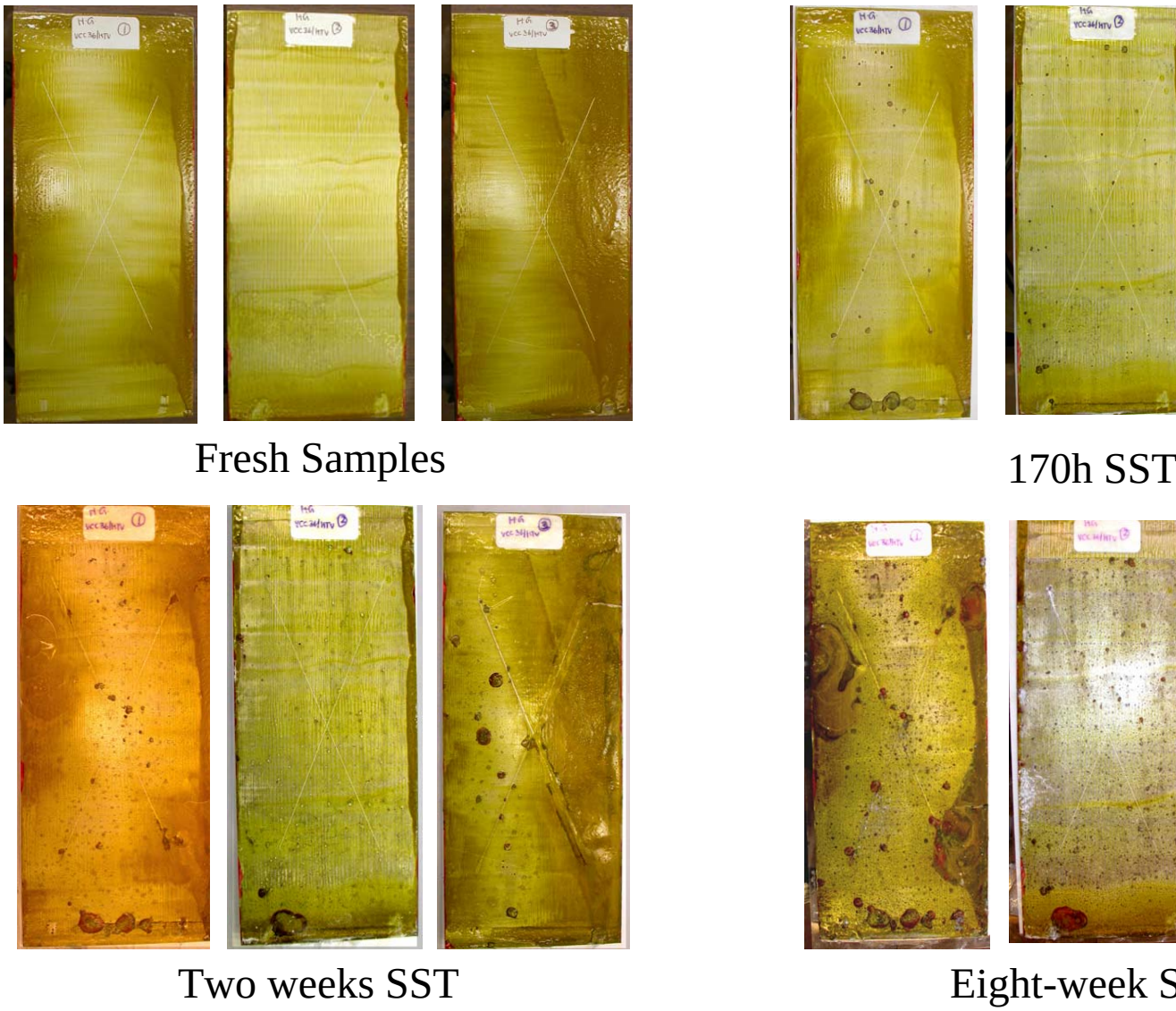

Figure 6. Optical macrographs of HT-V-pigmented epoxy over a vanadate conversion coating at selected tim
exposure experiment. Three replicate panels are shown. Exposure times are noted under each set of replicate

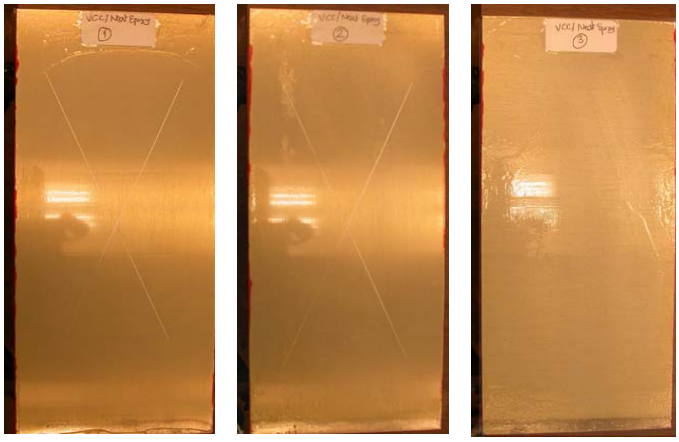

Fresh Samples

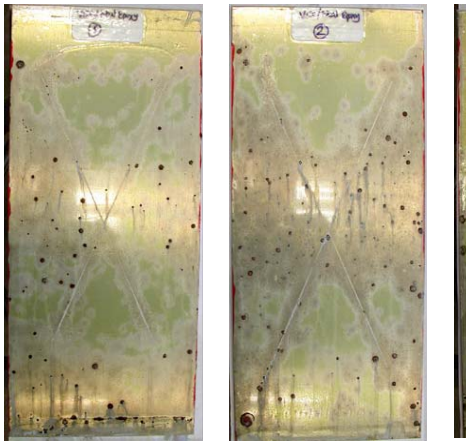

170h SST

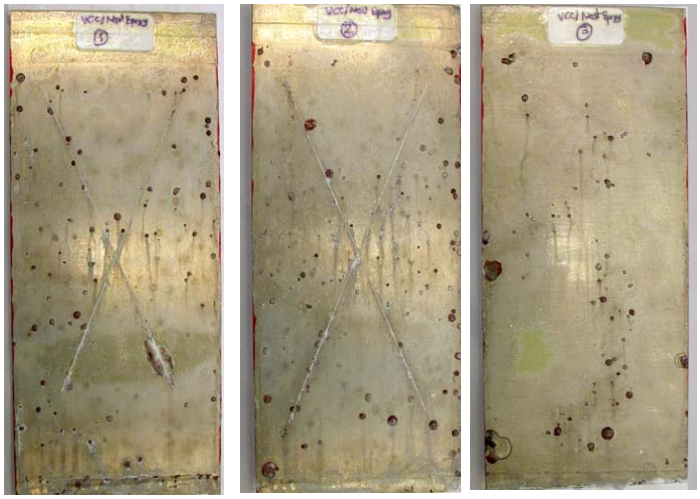

Two weeks SST

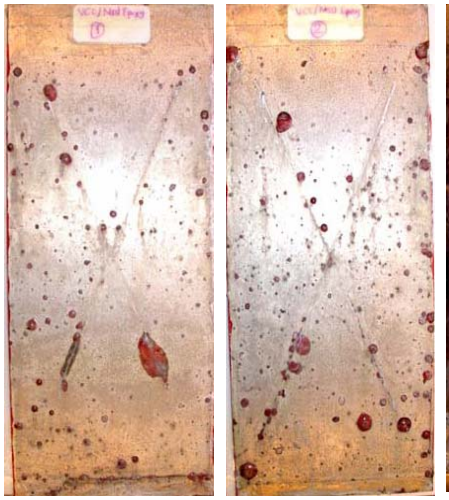

Eight weeks S

Figure 7. Optical macrographs of neat epoxy coatings applied to vanadate conversion coated samples at sele
spray exposure experiment. Three replicate panels are shown. Exposure times are noted under each set of re

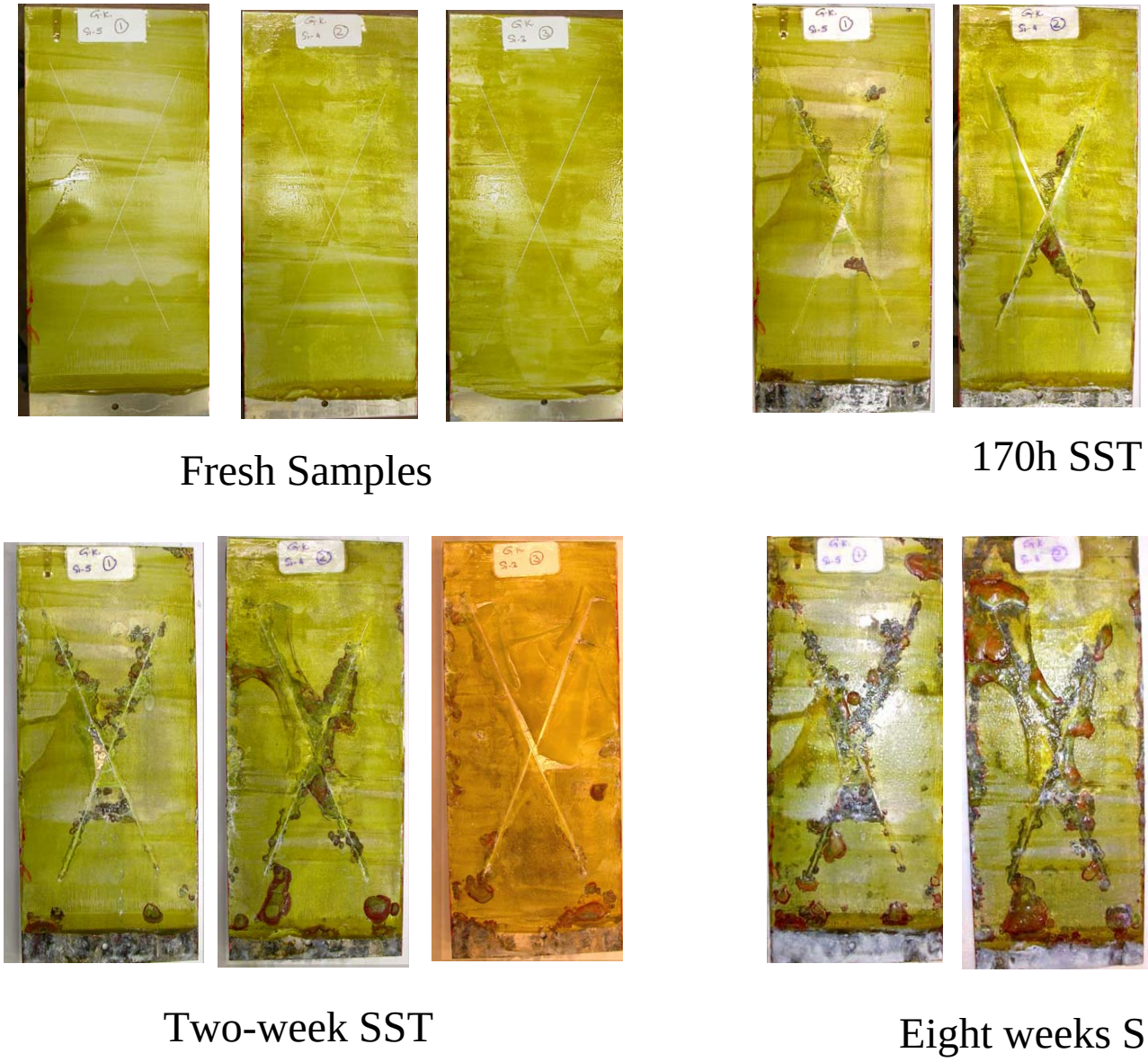

Figure 8. Optical macrographs of the HT-V-pigmented epoxy over a silane pretreatement at selected time
exposure experiment. Three replicate panels are shown. Exposure times are noted under each set of replica

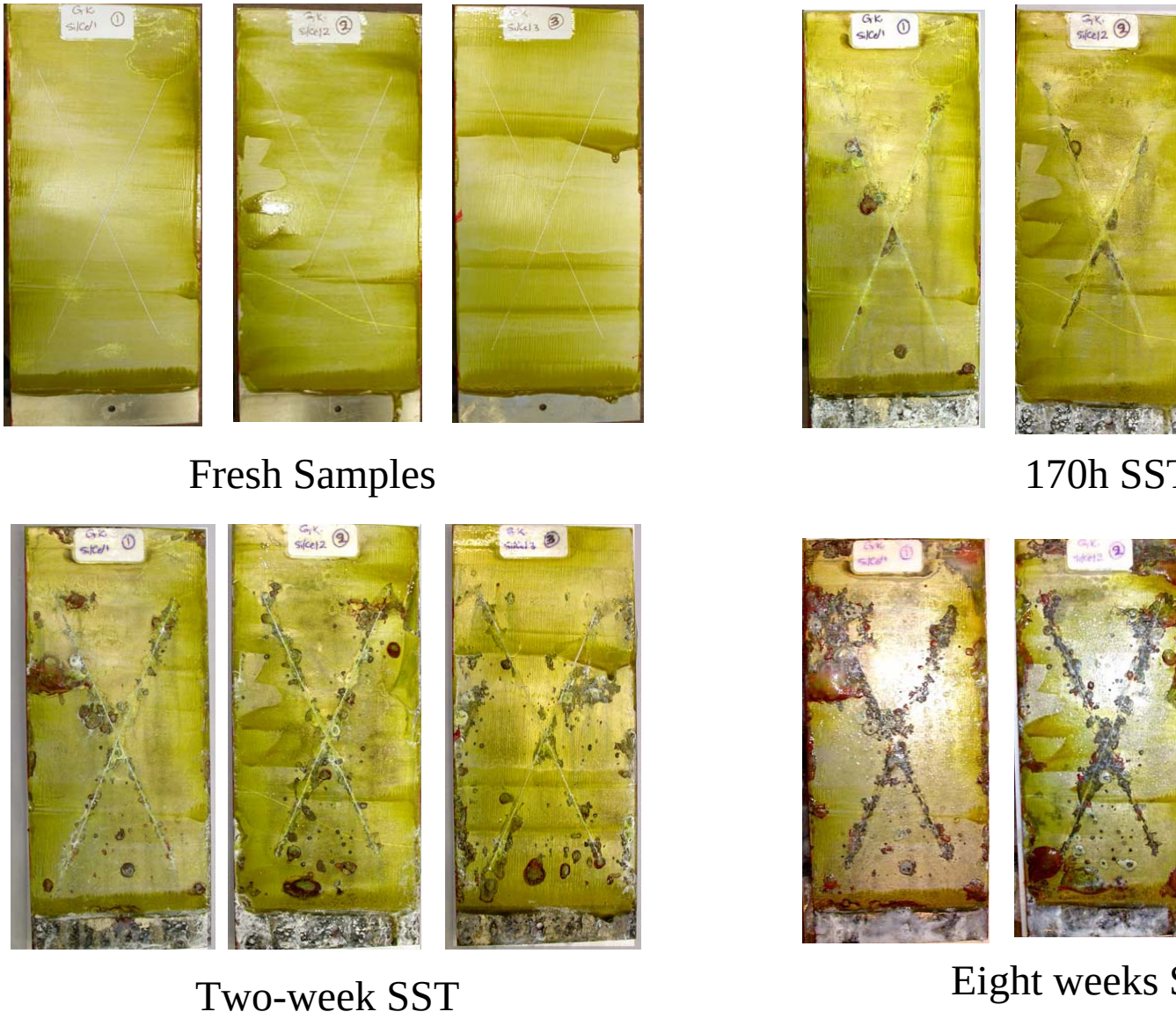

Figure 9. Optical macrographs of HT-V-pigmented epoxy coatings applied to Ce-inhibited silane pretreated
selected times during the salt spray exposure experiment. Three replicate panels are shown. Exposure times
replicates.

performed slightly worse. One of the coatings was delaminated after 2 weeks of exposure, initiated from the scribed area. The other two showed some blistering after 2 weeks exposure.

Vanadium based coatings showed some extent protection on scribed areas during the 8 weeks exposure as compared to the untreated coupons and the coupons pretreated with silane, although all of these coupons have similar performance rating based on unscribed area percentage failure. For bare surface with HTV primer coating, the scribed areas were still shiny after 4 weeks of exposure, which might be an indication of vanadium self-healing. But the VCC pretreated coupons with HTV primer coating showed more delamination (lifting) then that of un-pretreated surface.

For the silane-pretreated coupons, the prevalent failure mode was blistering along the scribe. The corrosion damages started at 24 hours and significantly increased with increasing exposure time. It appeared that the addition of Ce gave no improvement on the coating performance in salt fog exposure.

Table 3 characterizes the corrosion protection of the various coating systems on the basis of the presence or absence of the three modes of corrosion indicated above. It also gives a ranking of the coating systems in terms of the total impedance derived from EIS measurements made after 8 weeks of exposure. A range of performance was exhibited by the group of coatings examined, although there is general agreement between observations of corrosion damage and EIS ranking.

Overall corrosion protection was a strong function of the type of pretreatment used. The best overall performance among the Cr-free coating systems was demonstrated by the samples with the Ce/Mo conversion coatings. Silane pretreated samples shows a great deal of corrosion damage. This behavior is uncharacteristic of these types of pretreatments in our previous experience suggesting a processing or application flaw in these samples.

The effect of leachable vanadate from the HT-V-pigmented primers was evident in the nearly complete absence of scribe corrosion in these types of samples. The only HT-V-bearing coating system that exhibited scribe corrosion was the system using a Ce-inhibited silane pretreatment. In this case corrosion had progressed sufficiently that it was unclear if the scribe had corroded, or if under coating corrosion had migrated into the scribed area.

Ultra-violet condensing-moisture exposure testing (UV exposure). UV exposure is damaging to may organic resins used in primer coatings including MIL-P-23377 epoxy resins. Over long exposure periods, substrate corrosion can be induced, but this test may be considered to be less of corrosion test than ASTM B117 salt spray exposure, and more a test of a coating resistance to UV exposure. As such, coating degradation observed in this test did not depend on the nature of the pretreatment used.

Figures 10 through 18 show optical macrographs of coated samples subject to UV exposure. These images show an apparent progressive loss of coating thickness during the exposure period. In some cases the bare underlying aluminum substrate could be observed. In other cases there was corrosion product that was detected on the sample. This was induced by a combination of the condensing conditions developed in the UV chamber and the use of a sodium chloride electrolyte in the periodic EIS tests that were conducted on these samples.

The HT-V pigmented primer coatings developed a distinctive green coloration during the course of the exposure period. This type of discoloration has been noted in other studies and can be induced by exposure to natural sunlight. Presently, the origin of this discoloration is unknown, but it has been observed that this can be reversed by exposure to oxidizing agents such as peroxide and persulfate. Exposure of coatings to dilute solutions containing these oxidizers restores a deep orange-yellow coloration to the coating. No decrease in corrosion resistance of the coating has been associated with this UV-induced color change.

Adhesion testing. The pneumatic adhesion testing apparatus measured adhesive strength by pulling a stub glued onto the coated substrate surface (Figure 19). This test measured the nominal normal adhesion strength of the coating to the substrate. Figure 20 shows pull-off adhesion strengths for the various coating systems examined in this study. Overall the adhesion strength varies by about a factor of 4 from lowest to highest strengths. The coatings systems roughly break into three groups. On the low end were samples with Ce conversion coating and Ce-inhibited silane pretreatment. Of these the Ce conversion coated sample exhibited good corrosion resistance in salt spray testing, while the Ce-inhibited silane demonstrated the worst corrosion protection.

The middle group contained the vanadate conversion coated samples., the Ce-Mo conversion coated samples and the sample that were simply deoxidized prior to application of the epoxy coating. In salt spray testing the vanadate conversion coated samples exhibited good corrosion resistance. The Ce-Mo conversion coated samples exhibited excellent protection.

The high pull-off strengths were demonstrated by the chromate positive control samples and the silane pretreated sample. Here the chromated sample provided high levels of corrosion protection, but the silane pretreated samples did not.

Adhesion of a coating system to the underlying substrate is an essential element of corrosion protection. However, in the comparison of salt spray exposure test results to pull of adhesion strength, a strong correlation is not evident. This may be due in part to the strong role of chemical corrosion protection from releasable inhibitors in these systems. This effect may mask the effects of lower adhesion in some of the samples examined in this study.

Electrochemical impedance. Electrochemical impedance spectroscopy (EIS) was performed on samples subject to salt spray and UV exposure. In the case of the samples

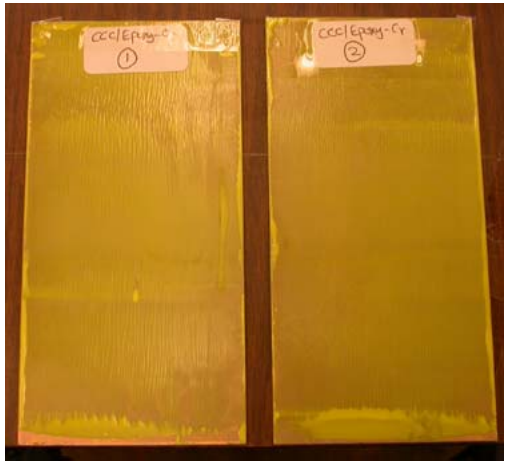

Fresh samples

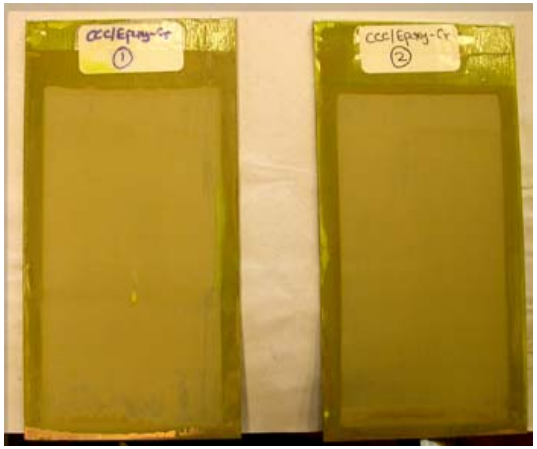

170h UV exposure

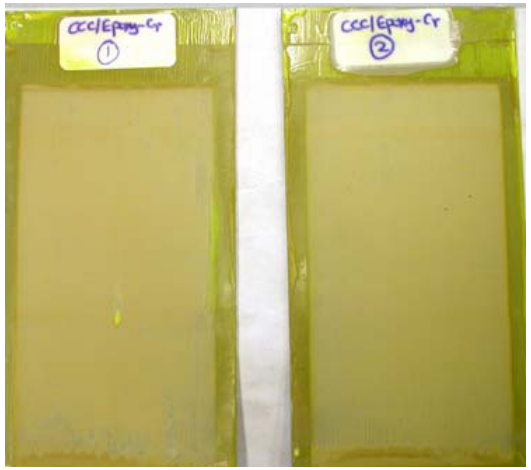

Two weeks UV exposure

Eight weeks UV exposure

Figure 10. Optical macrographs of CCC-$SrCrO_4$-epoxy coating after selected exposure times during UV exposure. Three replicate panels are shown. Exposure times are noted under each set of replicates.

\

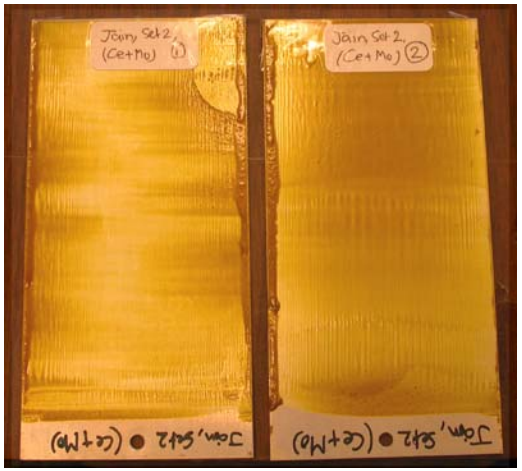

Fresh samples

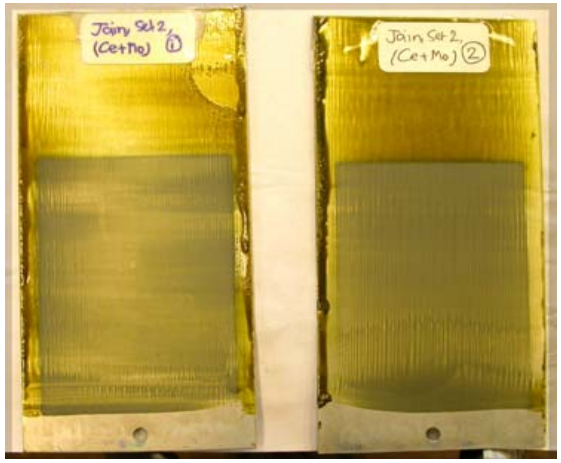

170h UV exposure

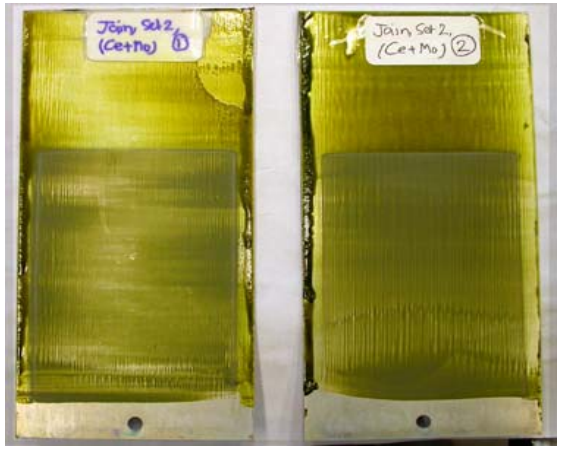

Two weeks UV exposure

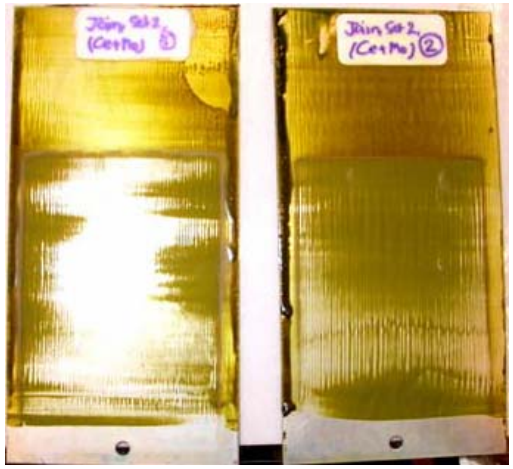

Eight weeks UV exposure

Figure 11. Optical macrographs of HT-V-pigmented epoxy coatings applied to Ce-Mo conversion coated 2024-T3 surfaces after selected times during the UV exposure experiment. Three replicate panels are shown. Exposure times are noted under each set of replicates.

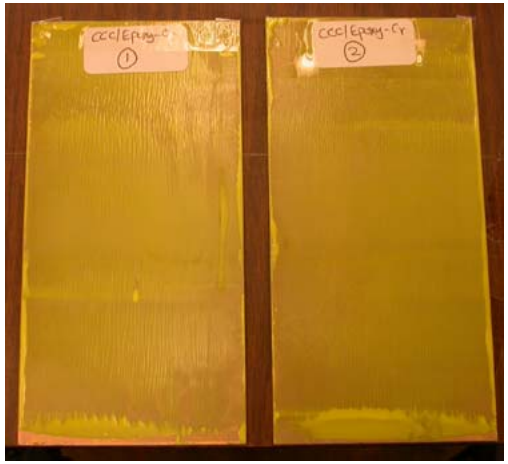

Fresh samples

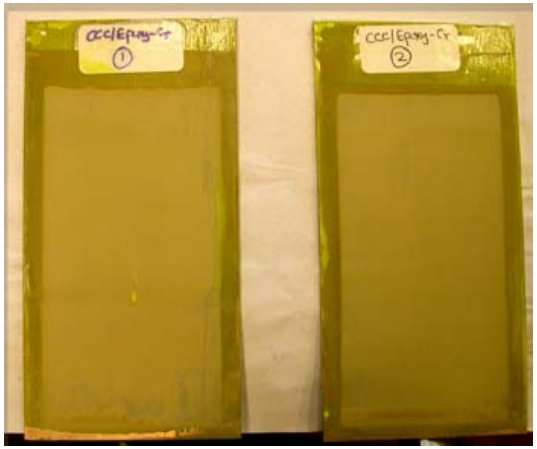

170h UV exposure

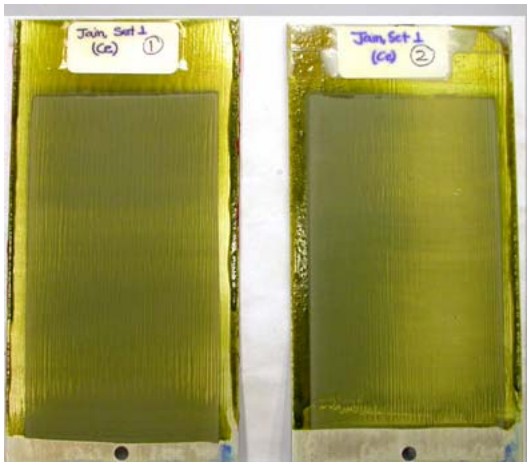

Two weeks UV exposure

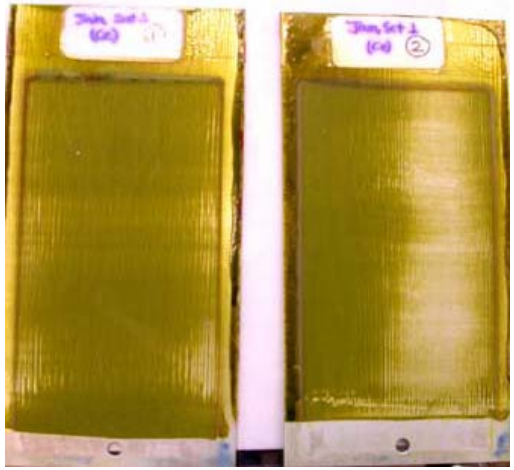

Eight weeks UV exposure

Figure 12. Optical macrographs of HT-V-pigmented epoxy coatings applied to Ce conversion coated 2024-T3 surfaces at selected times during the UV exposure experiment. Three replicate panels are shown. Exposure times are noted under each set of replicates.

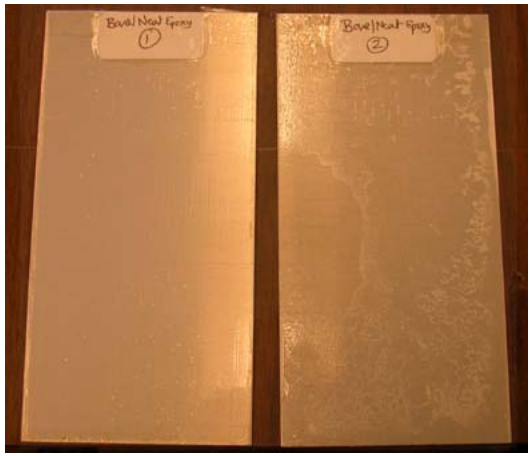

Fresh samples

170h UV exposure

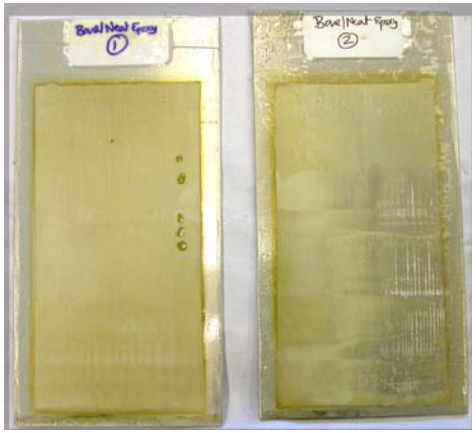

Two weeks UV exposure

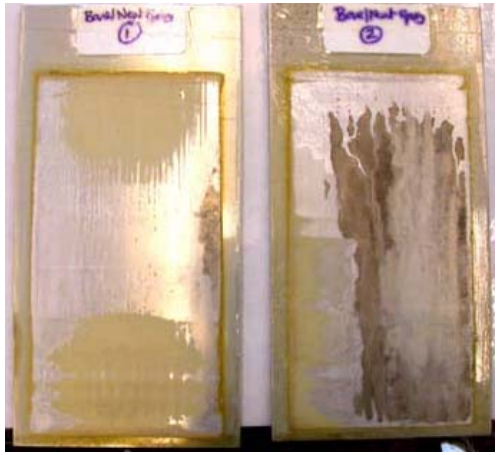

Eight weeks UV exposure

Figure 13. Optical macrographs of neat epoxy coatings applied to deoxidized 2024-T3 surfaces at selected times during the UV exposure experiment. Three replicate panels are shown. Exposure times are noted under each set of replicates.

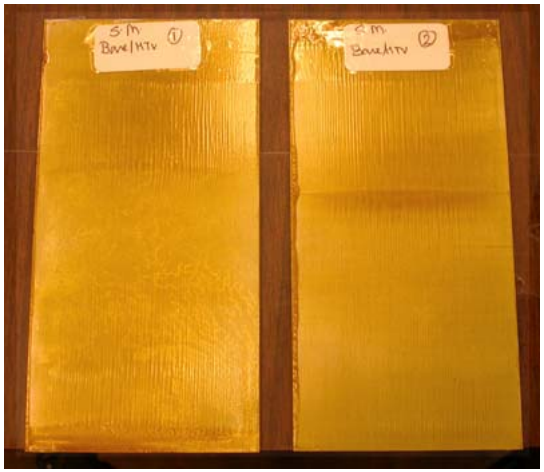

Fresh samples

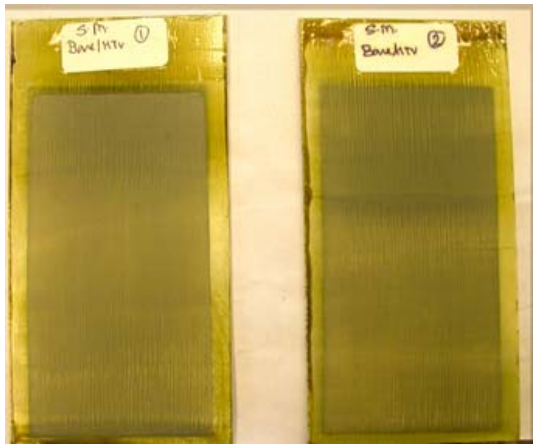

170h UV exposure

Two weeks UV exposure

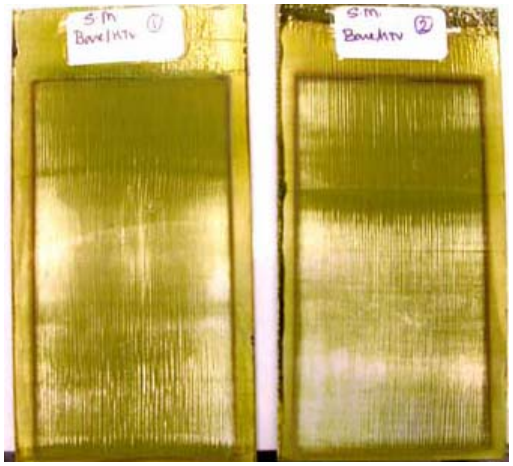

Eight weeks UV exposure

Figure 14. Optical macrographs of HT-V-pigmented epoxy coatings applied to deoxidized 2024-T3 surfaces at selected times during the UV exposure experiment. Three replicate panels are shown. Exposure times are noted under each set of replicates.

Fresh samples

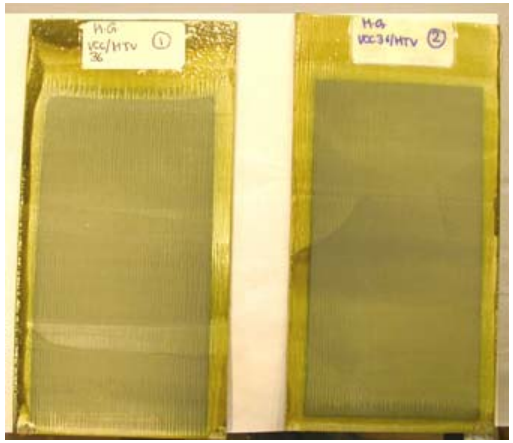

170h UV exposure

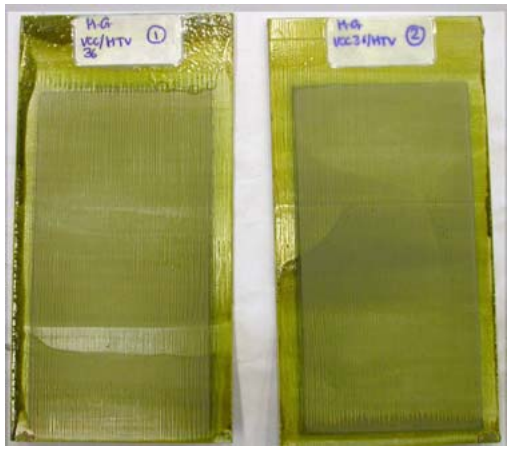

Two weeks UV exposure

Eight weeks UV exposure

Figure 15. Optical macrographs of HT-V-pigmented epoxy coatings applied to mandate conversion coated 2024-T3 surfaces at selected times during the UV exposure experiment. Three replicate panels are shown. Exposure times are noted under each set of replicates.

Fresh samples

170h UV exposure

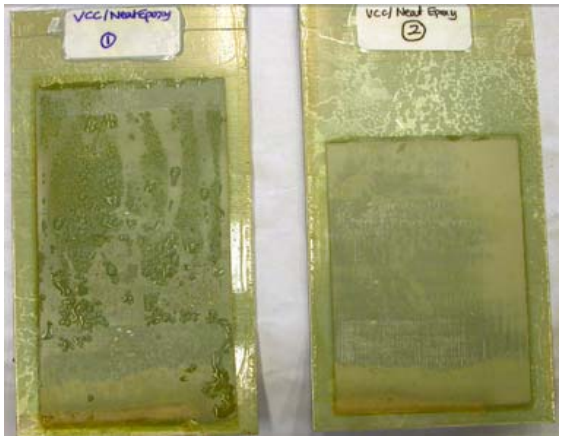

Two weeks UV exposure

Eight weeks UV exposure

Figure 16. Optical macrographs of neat epoxy coatings applied to vanadate conversion coated 2024-T3 surfaces at selected times during the UV exposure experiment. Three replicate panels are shown. Exposure times are noted under each set of replicates.

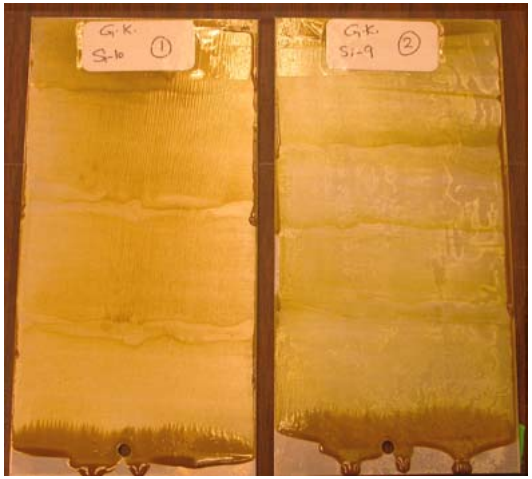

Fresh samples

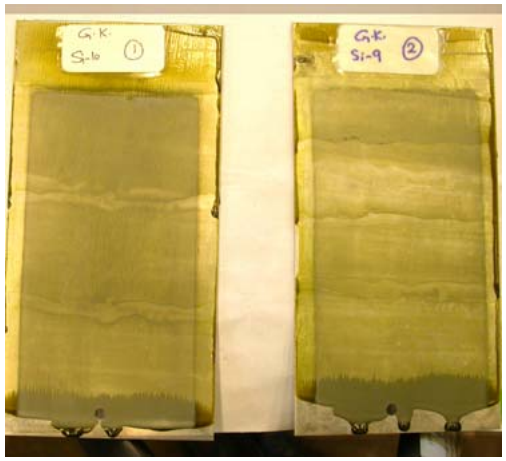

170h UV exposure

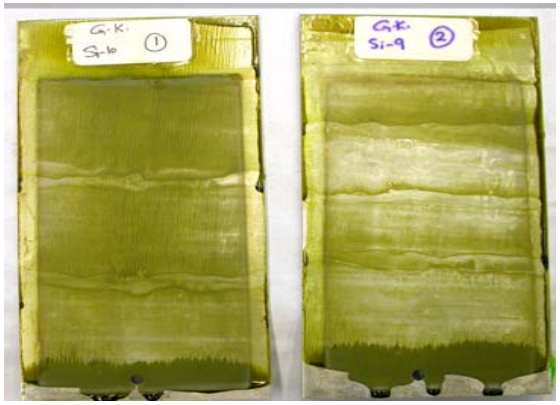

Two weeks UV exposure

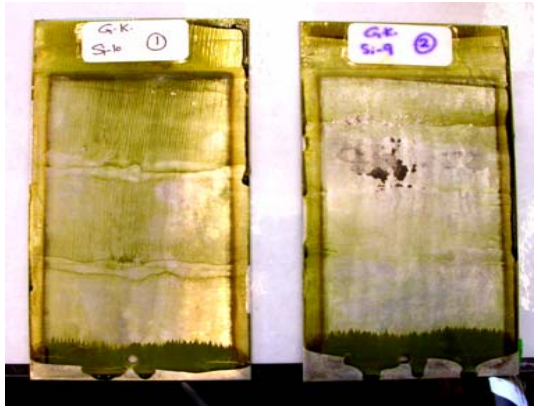

Eight weeks UV exposure

Figure 17. Optical macrographs of HT-V-pigmented epoxy coatings applied to silane pretreated 2024-T3 surfaces at selected times during the UV exposure experiment. Three replicate panels are shown. Exposure times are noted under each set of replicates.

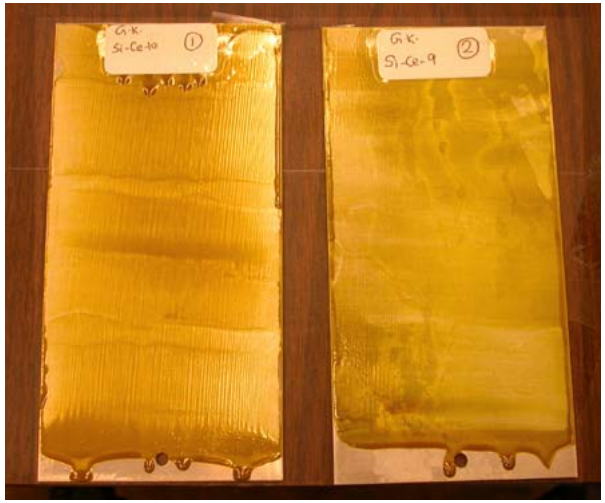

Fresh samples

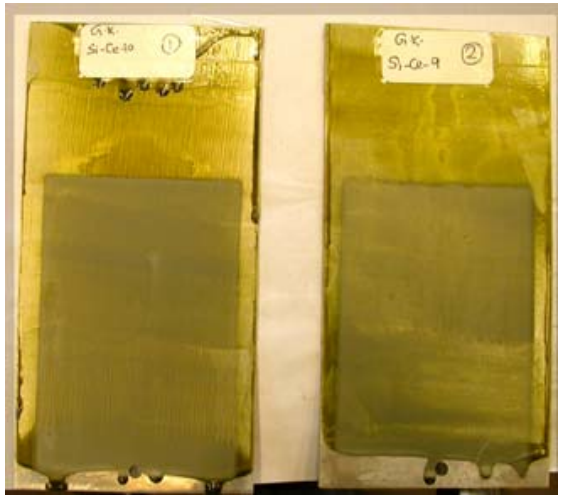

170h UV exposure

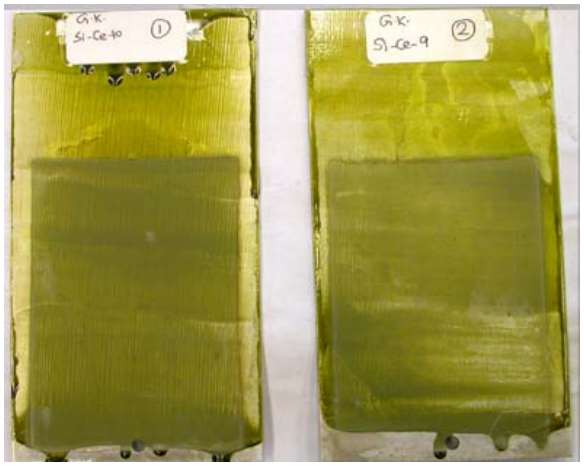

Two weeks UV exposure

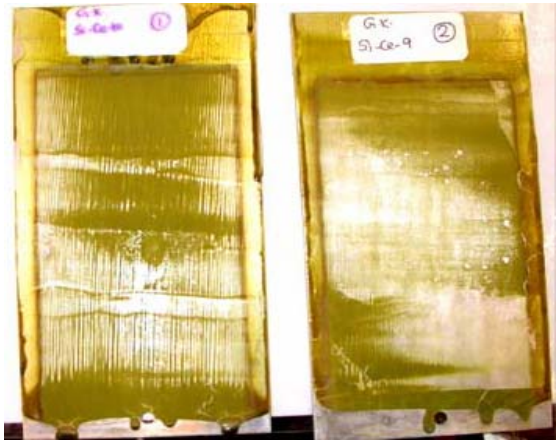

Eight weeks UV exposure

Figure 18. Optical macrographs of HT-V-pigmented epoxy coatings applied to Ce-inhibited silane pretreated 2024-T3 surfaces at selected times during the UV exposure experiment. Three replicate panels are shown. Exposure times are noted under each set of replicates.

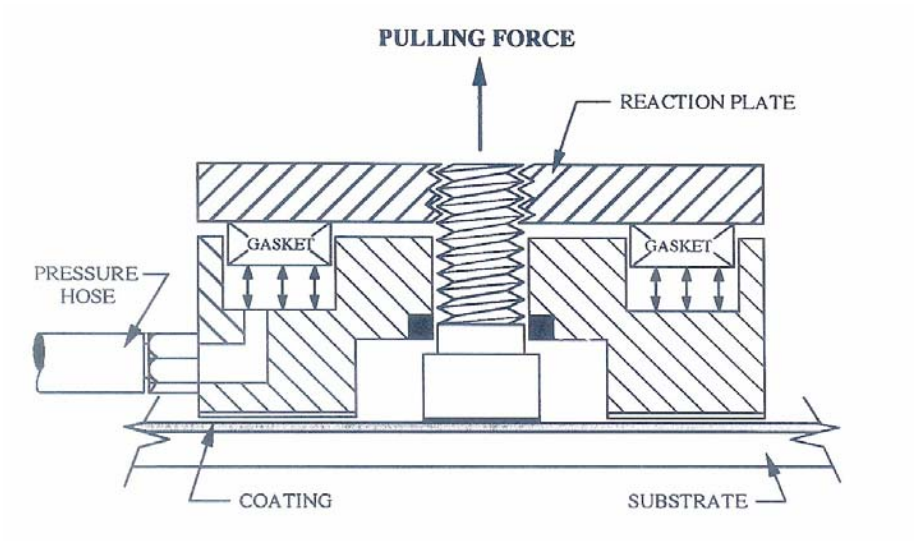

Figure 19. Schematic illustration of the pull-off adhesion test apparatus.

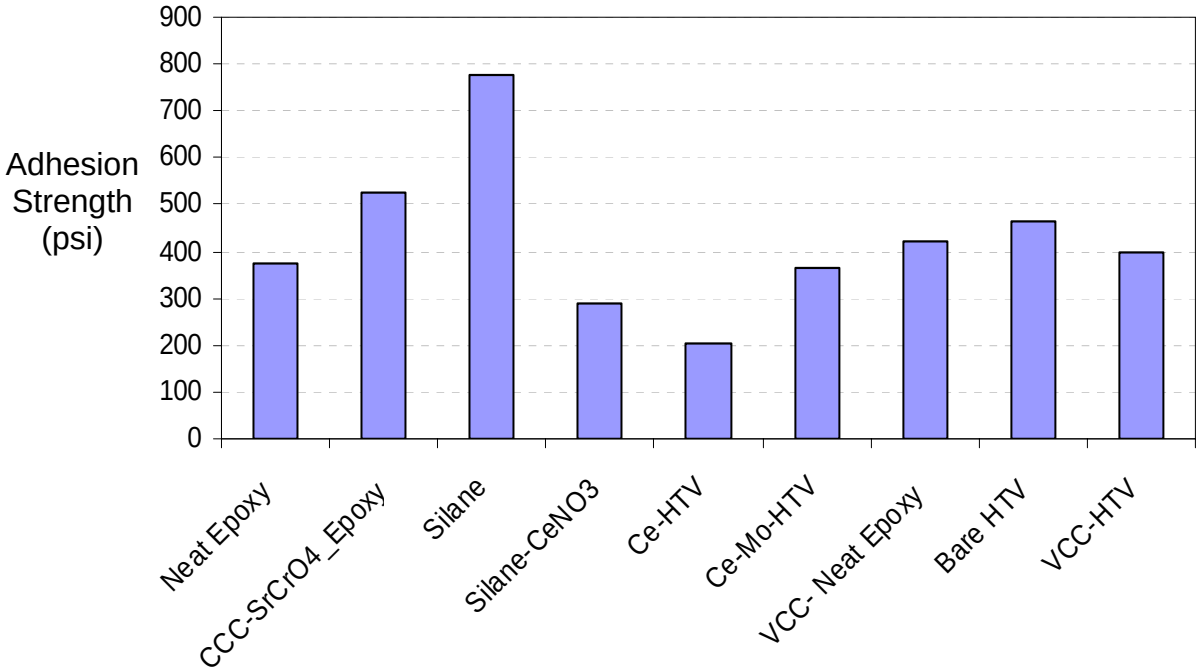

Figure 20. Pull-off adhesion strengths of coating system used in this study. Coating systems are identified by the pretreatment and organic coating used.

exposed in salt spray, EIS measurements were made on areas of the coating away from the scribe and characterize corrosion protection by nominally intact coatings.

Several different figures of merit were extracted from the impedance. The time dependence of these was plotted and analyzed to characterize coating system corrosion protection. These figures of merit included the total impedance measured at low frequency, the pore resistance (resistive plateau at intermediate frequencies), the phase angle at the lowest measured frequency and the coating capacitance.

EIS of salt spray exposure samples. Figures 21-24 show the time dependence in the EIS parameter collected. The samples exposed to salt spray demonstrate a wide range of performance with total impedances ranging over two orders of magnitude (Figure 21). As a group, the total impedances decrease gradually over the exposure period suggesting a gradual increase in overall corrosion damage.

Figure 22 shows the variation in the pore resistance with exposure time. The pore resistance for the chromated positive control sample exhibits very low pore resistances for all exposure times. This is due to the fact that this coating saturates with electrolyte very quickly. In other experiments, we have found that this coating saturates in a matter of hours in salt spray exposure conditions. Corrosion protection is afforded because the electrolyte trapped in the coating is rich in chromate and is therefore inhibits corrosion of the substrate. The pore resistance is relatively high for samples with Ce, Ce-Mo and vanadate conversion coatings. It is lower for samples prepared with the silane and Ce-inhibited silane pretreatments. With the exception of the chromated samples, the magnitude pore resistance seems to generally scale with the extent of corrosion induced during salt spray.

Figure 23 shows the variation in the phase angle at the lowest measured frequency in the impedance spectrum. The rational for examining this parameter is to understand the nature of the impedance at low frequency. A high (negative) phase angle is characteristic of a passivated surface or a diffusion-controlled corrosion process. A low (negative) phase angle is characteristic of a resistive faradaic process such as charge transfer-controlled substrate dissolution. Therefore examining the magnitude of the phase angle give an additional characterization that can be used with the total impedance at low frequency to evaluate the state of corrosion protection provided by the coating. Figure 23 shows that the chromate positive control exhibits a large negative phase angle, about –80 degrees, which is consistent with a passivated surface. The low pore resistance shown in Fig. 22 suggests that the coating is saturated with electrolyte. The high phase angle in Fig. 23 indicates that this environment protects the substrate. This is an essential element of how $SrCrO_4$ primer coatings provide corrosion protection. The phase angle values for all the other coatings range from about -20 to -40 degrees. These values suggest that interfacial reactances are still contributing to the impedance at the lowest measured frequencies. However, none appear to be establishing the passive conditions that are developed in the chromate primer.

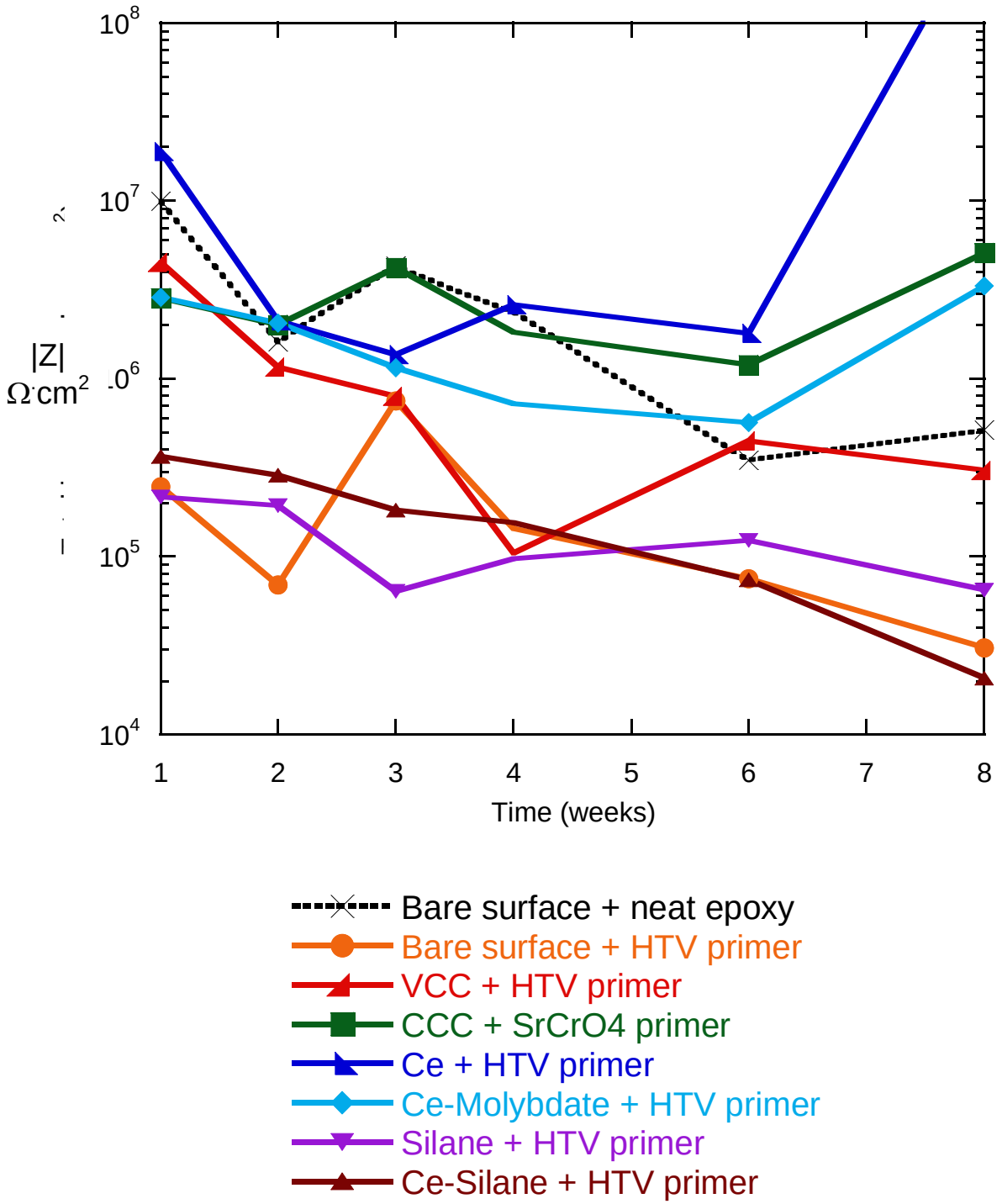

Figure 21. Variation of total impedance, |Z|, with time for salt spray tested coatings.

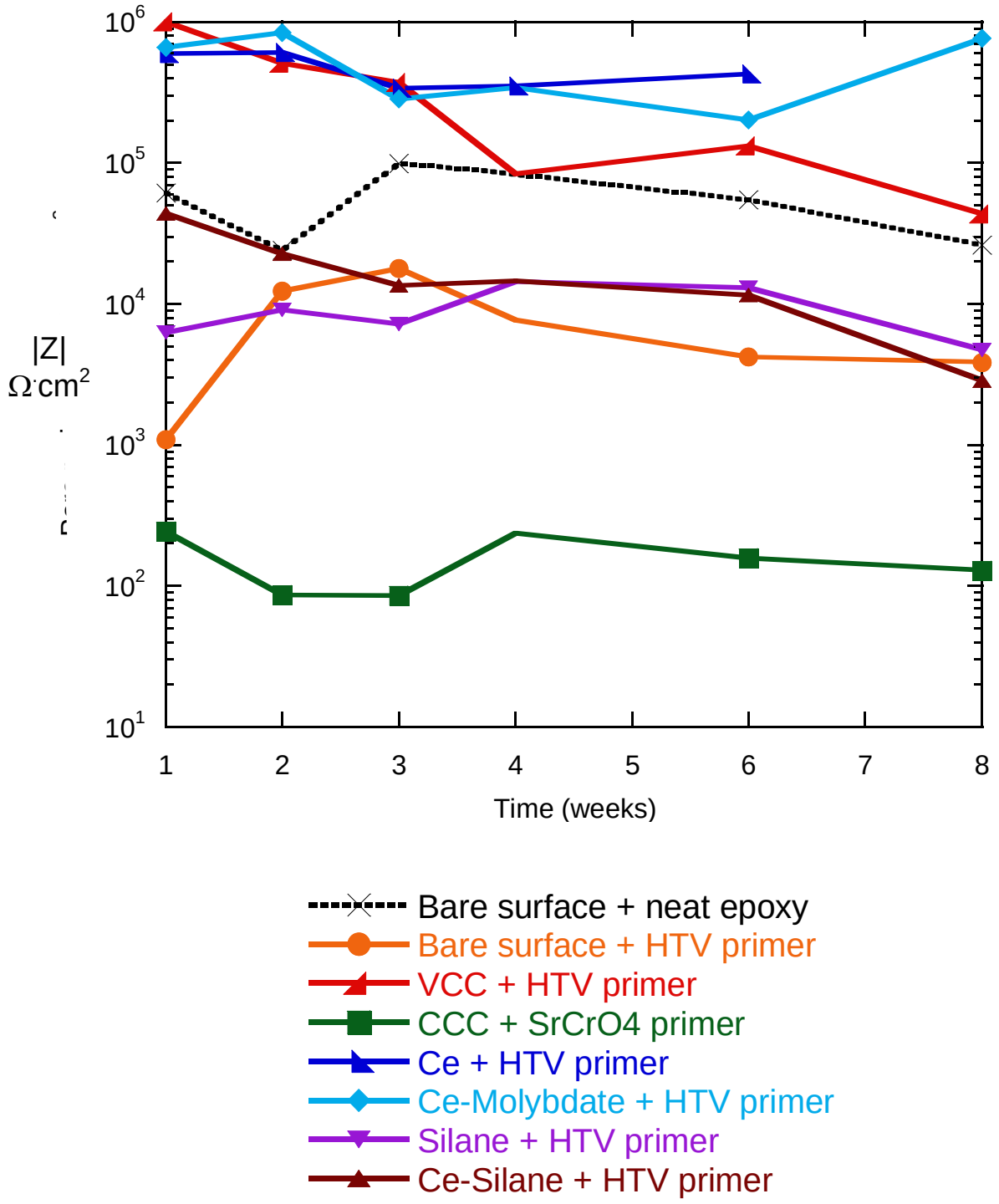

Figure 22. Variation of pore resistance, R_p, with time for salt spray tested coatings.

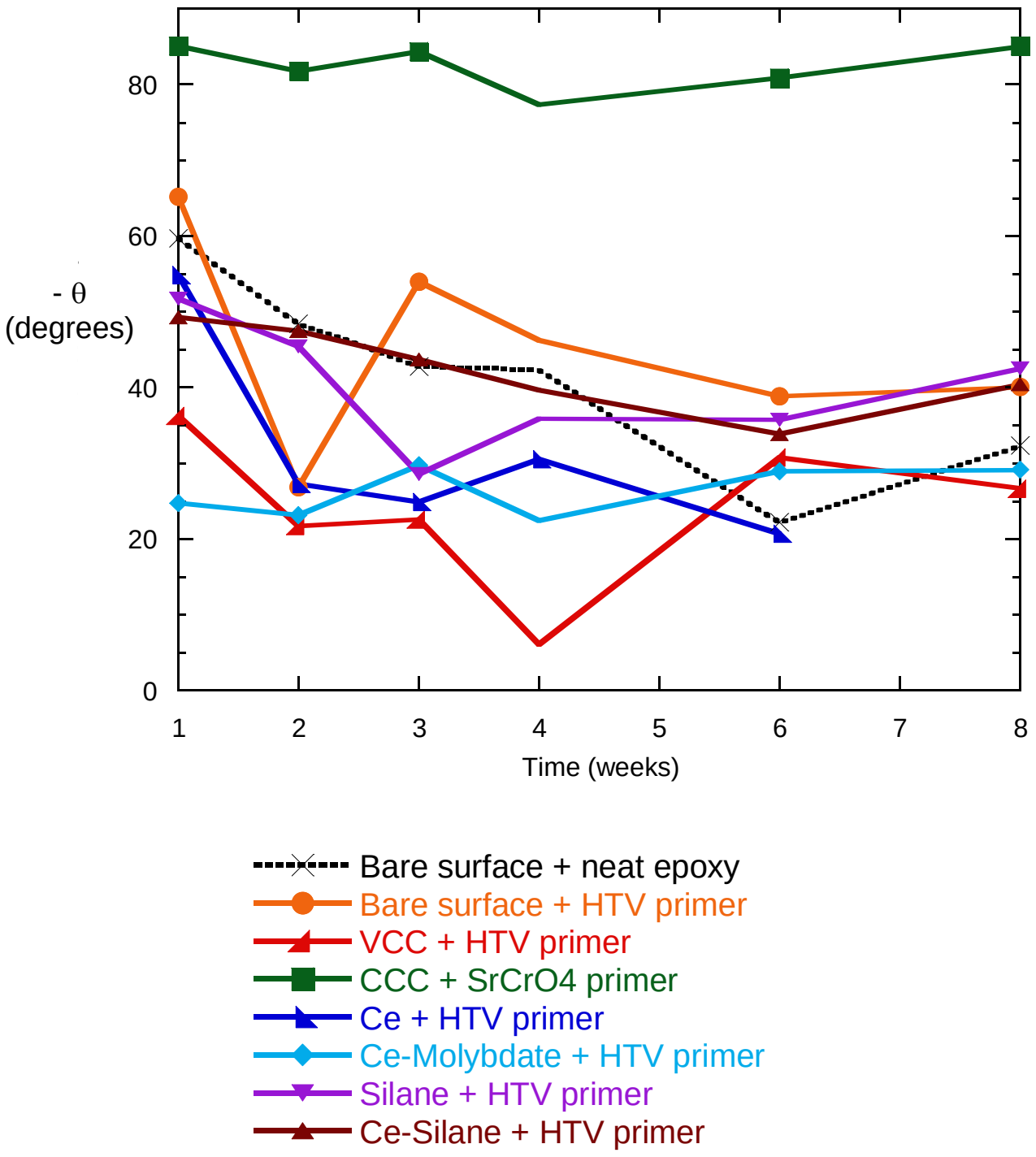

Figure 23. Variation of low frequency phase angle, -θ, with time for salt spray tested coatings.

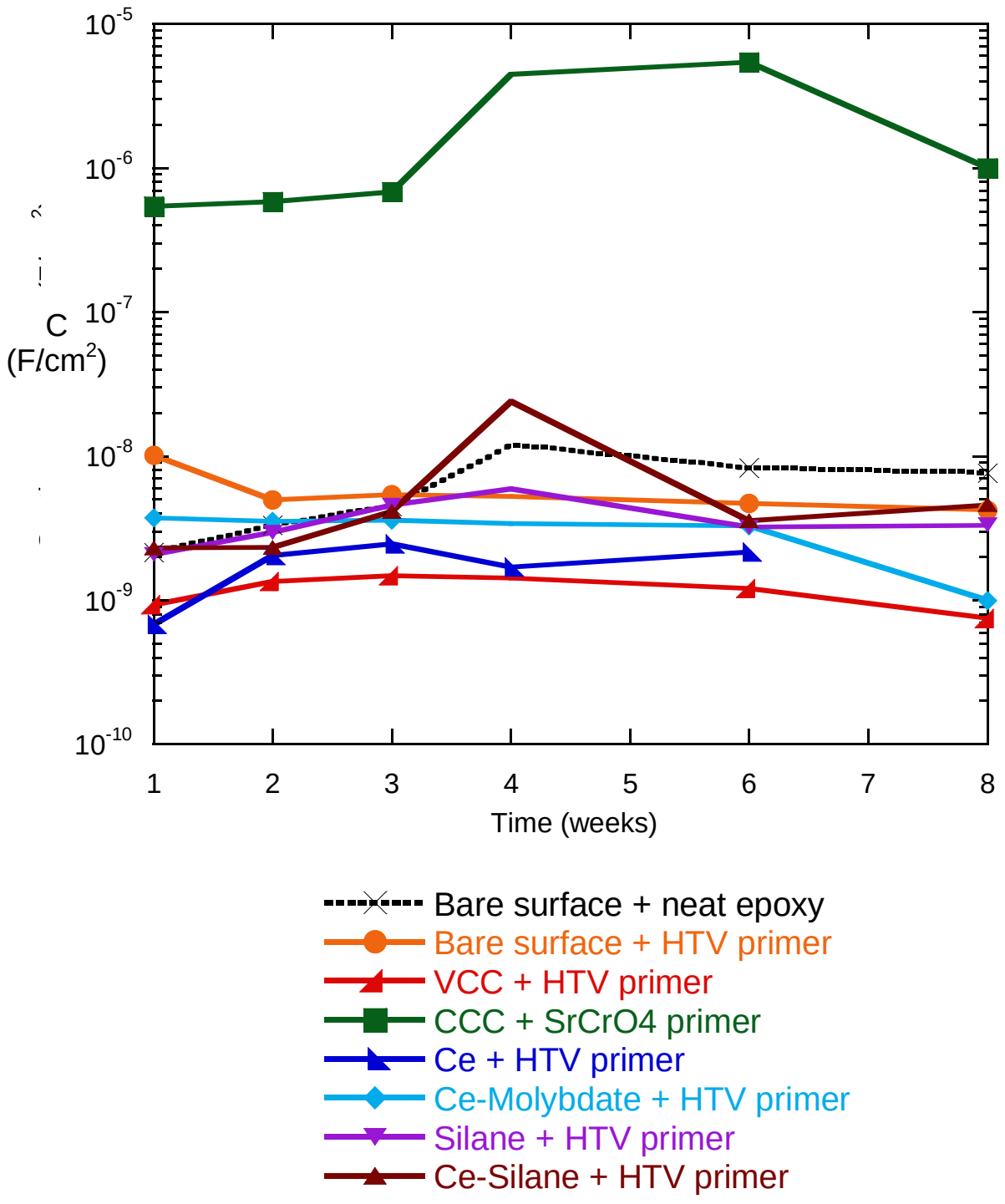

Figure 24. Variation of coating capacitance, C, with time for salt spray tested coatings.

Figure 24 shows the variation in coating capacitance among all the samples tested. In this case, the coating capacitance of the chromate control sample is much greater than that of any of the other samples and varies around several $\mu F/cm^2$ over the exposure period examined. This is consistent with the notion of a water-saturated coating and a passivated coating-metal interface. The coating capacitances for all the other coatings range from 1 to 10 nF/cm^2. These capacitances are consistent with what is expected for epoxy coatings of this thickness. The fact that these capacitances are not increasing with exposure time suggest that the coatings are not taking up water during the exposure period. They have either saturated before the first measurement taken after one week's exposure, or they are not taking up much water at all.

EIS of UV exposure samples. UV exposure degrades the epoxy resin in the organic part of the coating system. The samples are exposure to humidity during exposure and they are periodically exposed to chloride solutions when the EIS measurements are made. However, overall, the amount of corrosion damage experience by the substrates is much less than occurs in salt spray exposure. These facts are important in the interpretation of the EIS parameters collected from samples subject to UV exposures.

Figure 25 shows the variation in total impedance measured at low frequency. Generally, there is little systematic variation in the total impedance of any of the samples. This reflects the fact that none of the samples experiences much corrosion during this test.

Figure 26 shows the variation in pore resistance with exposure time. Pore resistances are either steady or decreasing with exposure time. These trends reflect decreasing coating thickness and an increase in defect sites in the coating as it is degraded.

The low frequency phase angle data in Figure 27 all trend towards large negative values indicating that the samples are largely passive. This is direct reflection of the fact that the UV test is not a test of corrosion of the substrate.

The coating capacitance data in Figure 28 show an increasing trend with increasing exposure time. This trend is consistent with UV-induced thinning and gradual loss of the organic coating layer.

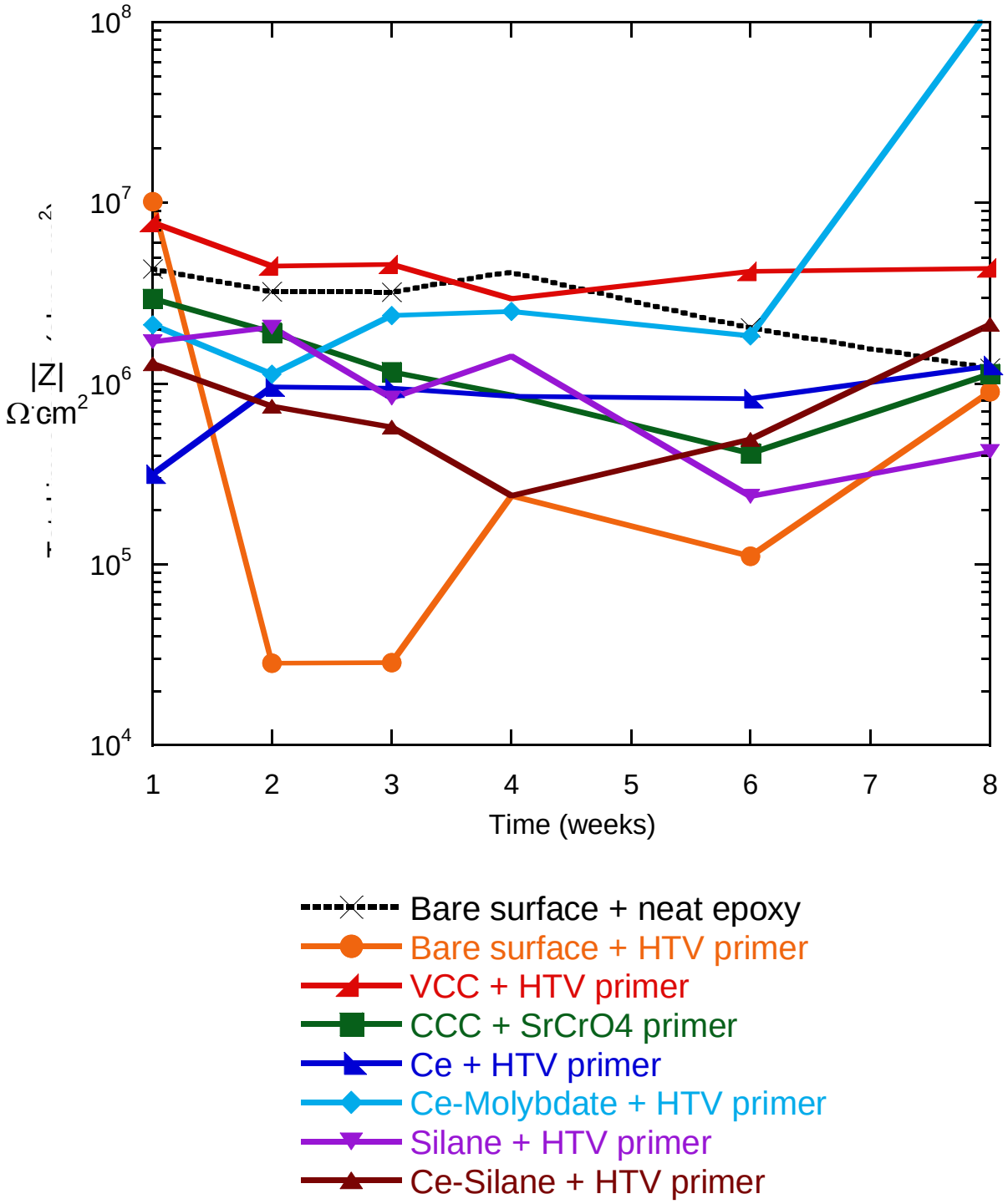

Figure 25. Variation of total impedance, |Z|, with time for UV-exposed coatings.

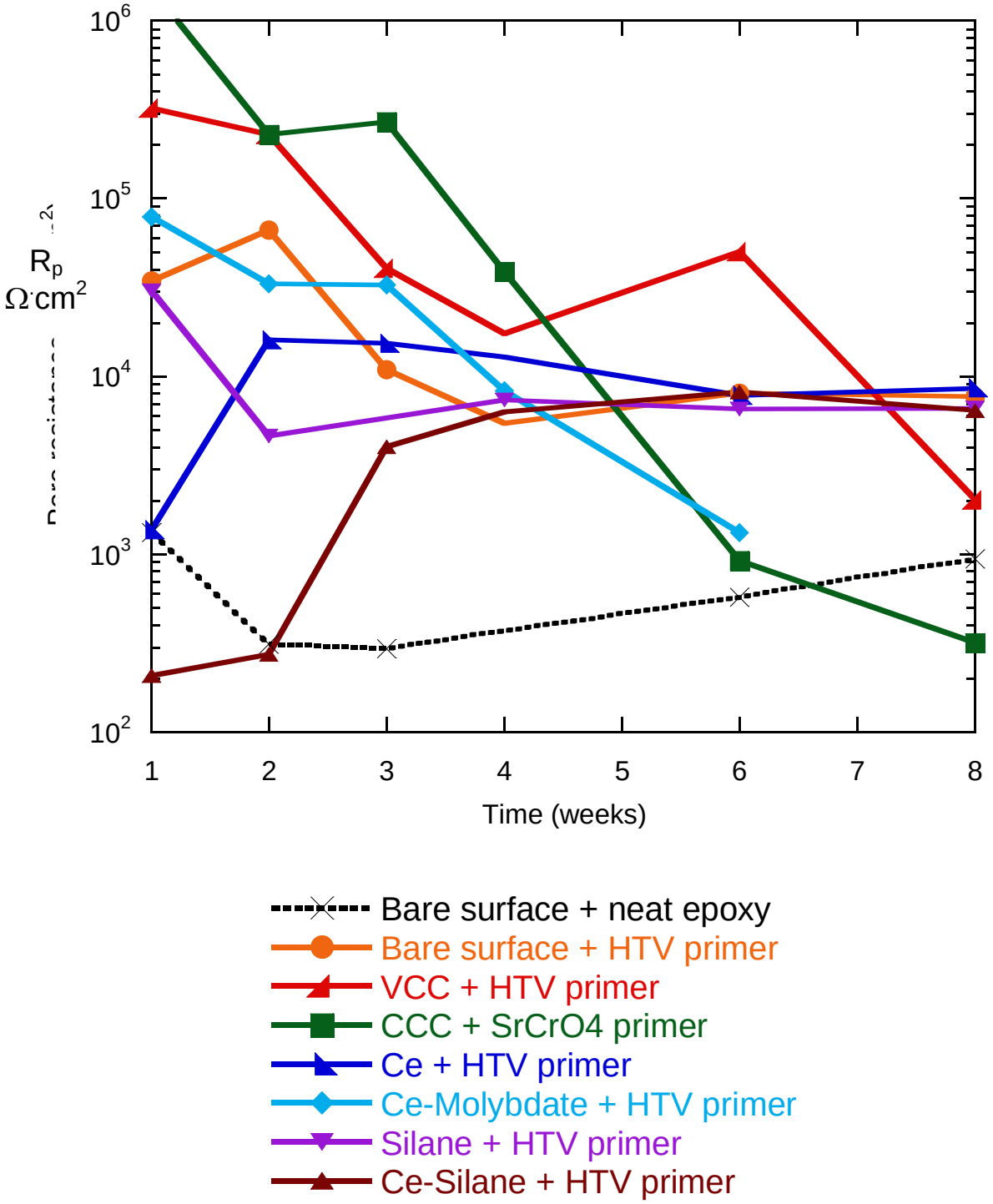

Figure 26. Variation of pore resistance, R_p, with time for UV-exposed coatings.

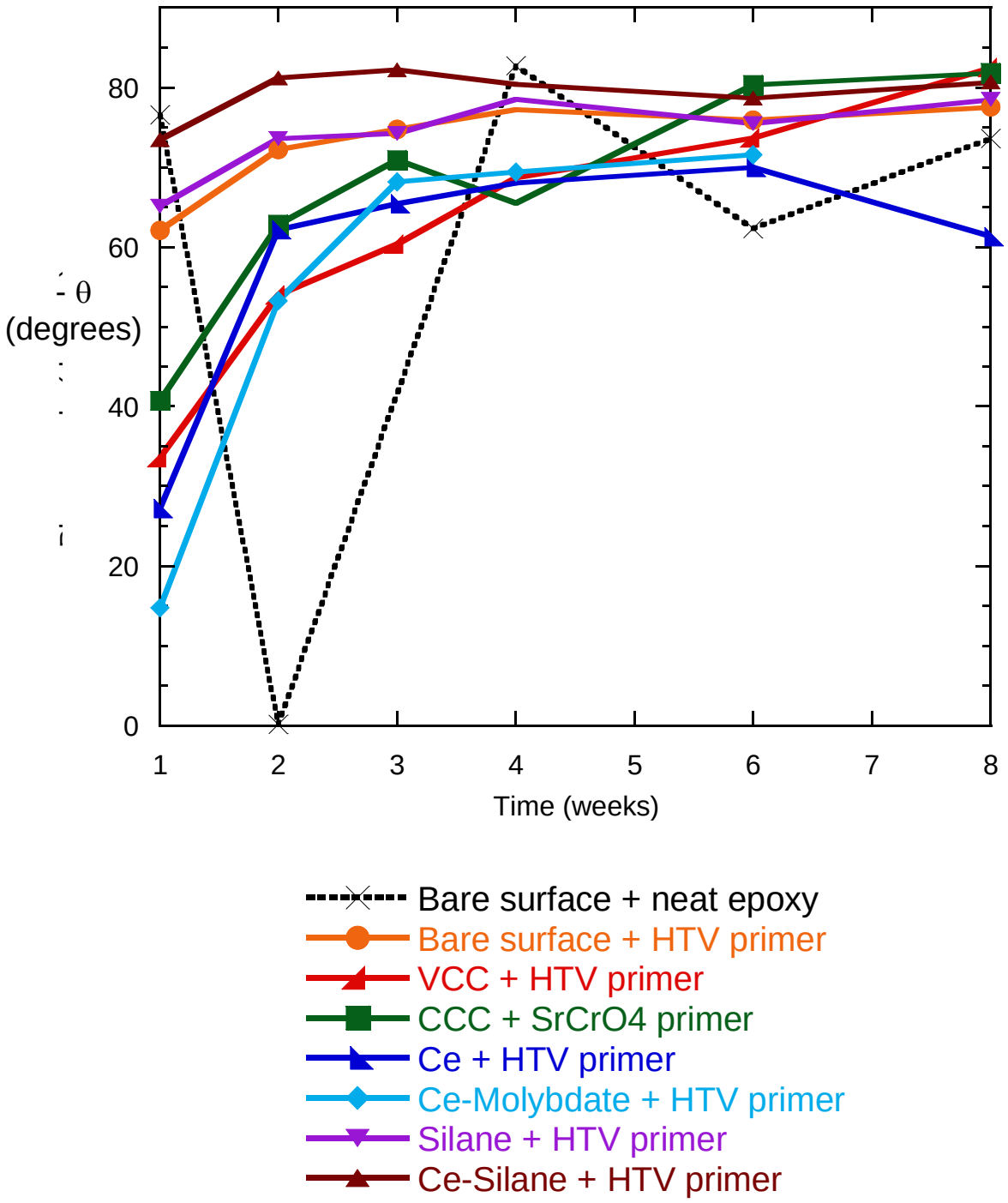

Figure 27. Variation of low frequency phase angle, -θ, with time for UV-exposed coatings

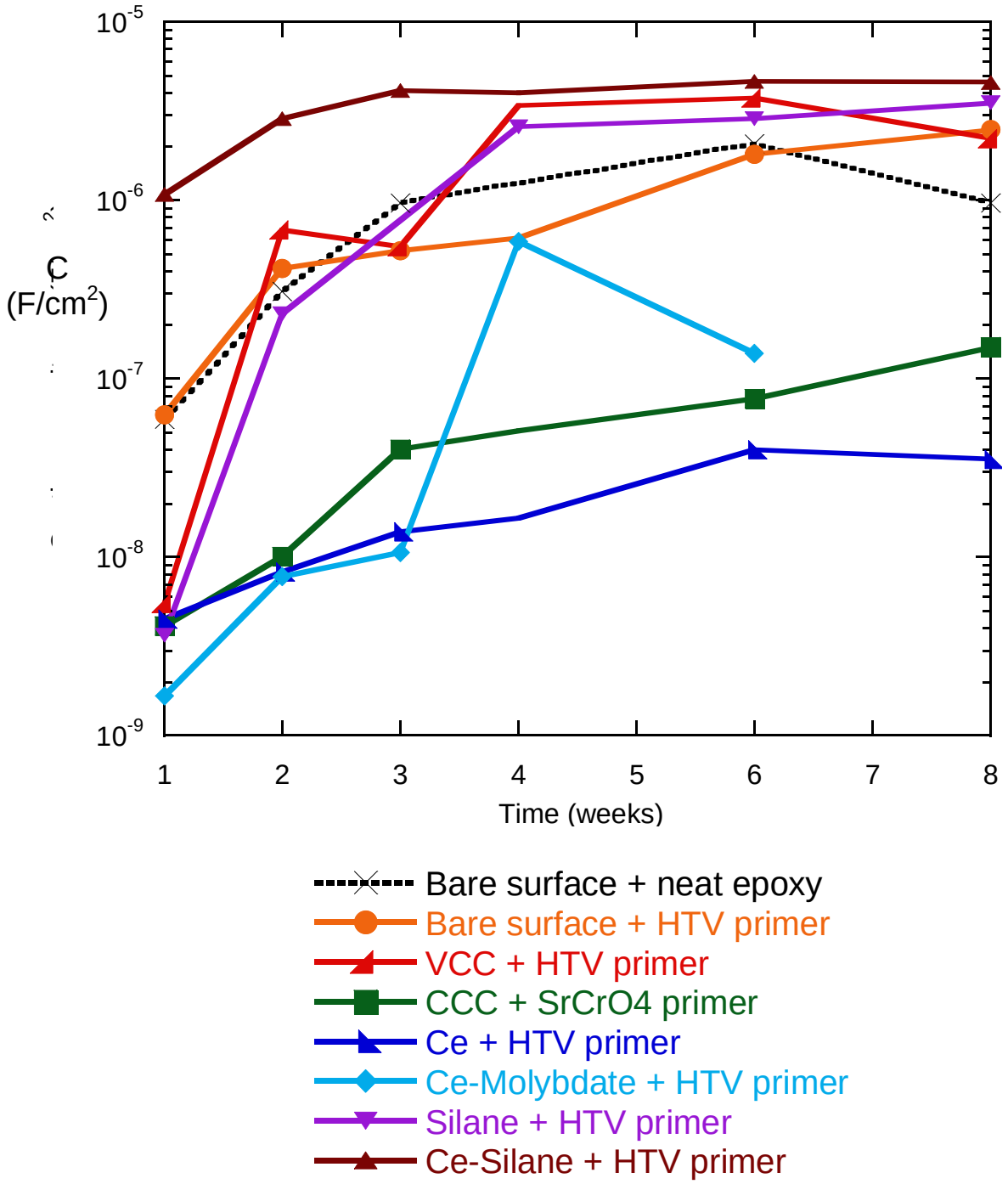

Figure 28. Variation of coating capacitance, C, with time for UV-exposed coatings.

SUMMARY

This exercise demonstrates that high levels of coating performance can be achieved with novel coatings systems. Corrosion resistance and adhesion levels of these simple and rudimentary coatings approach that of incumbent chromate-bearing coating systems. It should be noted that no attempts to optimize coating formulation or application were made in this study. Optimization in this regard can be expected to result in considerable improvements in coating performance.

Coatings and releasable inhibitors based on Ce, V and Mo all show benefit in terms of corrosion protection.

Future efforts dedicated towards optimization of formulations and application using chemistries based on those examined here appear to have a high likelihood of achieving chromate-like coatings system performance.

Table 1. Average scribe failure rating for AA2024-T3 with various pretreatments and HTV primer (ASTM D 1654 Procedure A).

Sample Name	Sample a	Sample b	Sample c	Mean
CCC+ $SrCrO_4$ primer	10	10	10	10.00
Ce/Mo CC+ HT-V primer	9	9	9	9.00
Ce CC + HT-V primer	8	8	7	7.67
Deox + HT-V primer	9	8	9	8.67
Deox + Neat Epoxy	4	5	5	4.67
VCC + HT-V primer	9	6	8	7.67
Vanadate CC + neat epoxy	7	7	-	7.00
Silane pretreat + HT-V primer	2	2	3	2.33
Ce-inhibited silane + HT-V primer	2	2	0	1.33

Table 2. Average unscribed area failure for AA2024-T3 with various pretreatments and HTV primer (ASTM D1654 Procedure B).

Sample Name	Sample a	Sample b	Sample c	Mean
CCC+ $SrCrO_4$ primer	8	10	10	9.33
Ce/Mo CC+ HT-V primer	9	7	6	7.33
Ce CC + HT-V primer	1	7	8	5.33
Deox + HT-V primer	2	2	5	3.00
Deox + Neat Epoxy	2	2	2	2.00
VCC + HT-V primer	2	4	2	2.67
VCC + neat epoxy	2	2	2	2.00
Silane pretreat + HT-V primer	4	2	1	2.33
Ce-inhibited silane + HT-V primer	3	2	1	2.00

Table 3. Summary of corrosion observations from salt spray exposure testing. "x" indicates a positive indication.

Sample	Scribe Corrosion	Filiform or Blister at scribe	Blister away from scribe	EIS rank at 8 weeks
CCC+ $SrCrO_4$ primer				2
Ce/Mo CC+ HT-V primer		x		3
Ce CC + HT-V primer		x	min	1
Deox + Neat Epoxy	x	x	x	4
Deox + HT-V primer			x	7
VCC + HT-V primer		min	x	5
VCC + neat epoxy	x	x	x	--†
Silane pretreat + HT-V primer		x	x	6
Ce-inhibited silane + HT-V primer		x	x	8

Min- present, but minimal

†- not tested.

Publications

Peer-reviewed Articles

Y. Yoon, R.G. Buchheit, “The Effect of Microstructural Heterogeneity on Chromate Conversion Coating Formation on 7x75 Al Alloys”, Corrosion Science, submitted (2005).

H.S. Isaacs, K. Sasaki, C.SW. Jeffcoate, V. Laget, R.G. Buchheit, “Formation of Chromate Conversion Coatings on Aluminum and its alloys: An In Situ XANES Study,” J. Electrochem. Soc., accepted for publication (2005).

W. Zhang, R.G. Buchheit, "Effect of Ambient Temperature Aging in Dehumidified air on the Properties of Chromate Conversion Coatings (CCCs)," Thin Solid Films, accepted for publication (2005).

Y. Yoon, R.G. Buchheit, “The Effect of Cu Content on Chromate Conversion coating Formation of Compositional Analogs of the Phase $Mg(Zn, xCu)_2$”, Electrochem. & Sol. St. Lett. accepted for publication (2005).

Y. Yoon, R.G. Buchheit, “The effect of Chromate Conversion Coating on the Dissolution Behavior of Al_2CuMg (S Phase),” J. Electrochem. Soc., accepted for publication (2005).

H. Guan, R.G. Buchheit, “Corrosion protection of aluminum alloy 2024-T3 by vanadate conversion coatings,” Corrosion 60 (3): 284-296 (2004).

R.G. Buchheit, H. Guan, S. Mahajanam, F. Wong, "Active Corrosion Protection and Corrosion Sensing in Chromate-free Organic Coatings," Progress in Organic Coatings, 47, 174 (2003).

W. Zhang, R.G. Buchheit, "Effect of Ambient Aging of Chromate Conversion Coatings on the Rate Oxygen Reduction," Corrosion, 59, 4, 356 (2003).

F. Di Quarto, M. Santamaria and N. Mallandrino, V. Laget, R. Buchheit, K. Shimizu, "Structural Analysis and Photocurrent Spectroscopy of Chromate Conversion Coatings on 99.99% Aluminum," J. Electrochem. Soc., 150, 10 B462-B472 (2003).

M. W. Kendig, R. G. Buchheit, "Corrosion Inhibition of Al and Al Alloys by Hexavalent Cr Compounds," Corrosion, 59, 379-400 (2003).

V. Laget, C. Jeffcoate, H.S. Isaacs, R.G. Buchheit, "Dehydration-Induced Loss of Corrosion Protection Properties in Chromate Conversion Coatings on Aluminum Alloy 2024-T3", J. Electrochem. Soc., 150, B425-B432 (2003).

W. Zhang, R. G. Buchheit, "Chromate Conversion Coating Characterization Using Multichannel Microelectrode Analyzer (MMA)," J. Electrochem. Soc. 149, B357 (2002).

R. B. Leggat, W. Zhang, R.G. Buchheit, S. R. Taylor, "Performance of Hydrotalcite Conversion Treatments when used in a Coating System on AA2024-T3," Corrosion, 58, 322-328 (2002).

W. Zhang, R.G. Buchheit, "Hydrotalcite Coating Formation on Al-Cu-Mg Alloys from Oxidizing Bath Chemistries," Corrosion, 58, 591 (2002).

R.G. Buchheit, S.B. Mamidipally, P. Schmutz, H. Guan, "Active Corrosion Protection in Ce-Modified Hydrotalcite Conversion Coatings," Corrosion, 58, 1, 3-14 (2002).

R. B. Leggat, S. R. Taylor, W. Zhang, R.G. Buchheit, "Corrosion Performance of Field-Applied Chromate Conversion Coatings," Corrosion, 58, 283-291 (2001).

R. G. Buchheit, R. K. Boger, M. C. Carroll, R. M. Leard, C. Paglia, J. L. Searles, "The Electrochemistry of Intermetallics in the Localized Corrosion in Al alloys," JOM, 53, 7 , 29 (2001).

R. G. Buchheit, R.K. Boger, "Cu Redistribution and Surface Enrichment Due to Dissolution of Al-Cu Alloys," p. 265-292, Localized Corrosion, NACE International, Houston, TX (2001).

W. R. McGovern, P. Schmutz, R. G. Buchheit, R. L. McCreery, "Formation of Chromate Conversion Coatings on Al-Cu-Mg Intermetallic Compounds and Alloys," J. Electrochem. Soc., 147, 4494-4501 (2000).

N.Voevodin, M.Khobaib, S.Balbyshev, A.Khramov, L.Kasten, M.Donley, "Nanostructured Sol-Gel Approach for Corrosion Protection", Progress and Organic Coatings, accepted for publication August (2002).

V. Laget, H.S. Isaacs, C.S. Jeffcoate, R.G. Buchheit, " Thermally Induced Degradation of Chromate Conversion Coatings on Aluminum Alloy 2024-T3," Aluminum Surface Science and Technology 2000, p. 295-300, vol. 40-41, no. 1-4, ATB Metallugie (2000).

R.G. Buchheit, S.B. Mamidipally, P. Schmutz, H. Guan, "Active Corrosion Protection in Chromate and Chromate-Free Conversion Coatings," p. 67-92, Surface Conversion for Aluminum and Ferrous Alloys, NACE International, Houston, TX (2000).

M. Kendig, R. Buchheit, "Corrosion Inhibition of Al and Al Alloys by Hexavalent Cr compounds, A Mechanistic Overview," p. 1-31, Surface Conversion for Aluminum and Ferrous Alloys, NACE International, Houston, TX (2000).

Q. Meng, G. S. Frankel. “Effect of copper content on chromate conversion coating protection of 7xxx-T6 aluminum alloys Corrosion 60 (10): 897-905 (2004).

Q. Meng, G. S. Frankel, “Effect of Cu content on corrosion behavior of 7xxx series aluminum alloys,” J. Electrochem. Soc. 151 (5): B271-B283 (2004).

Q. Meng, G. S. Frankel, “Characterization of chromate conversion coating on AA7075-T6 aluminum alloy” , Surf and Inter. Anal., 36 (1): 30-42 (2004).

B. L. Hurley, R. L. McCreery, “Raman spectroscopy of monolayers formed from chromate corrosion inhibitor on copper surfaces ,”J. Electrochem. Soc., 150 (8): B367-B373 (2003).

Proceedings Articles

S. Jain and R.G. Buchheit, The Effect of Chromates and Chromate Conversion Coatings on the Corrosion of Cast Al-Si Alloy 356 and Al-Si-Cu Alloy 380," p. 214 in the Proceedings of the Electrochemical Society, PV2003-23, The Electrochemical Society, Pennington, NJ (2004).

Y. Yoon, R.G. Buchheit, "The Formation and Breakdown of Chromate Conversion Coatings on AL-Zn-Mg-Cu Alloy Using Electrode Arrays," p. 226 in the Proceedings of the Electrochemical Society, PV2003-23, The Electrochemical Society, Pennington, NJ (2004).

S.P.V. Mahajanam, R.G. Buchheit, "Characterization of Zn-Al-$V_{10}O_{28}^{6-}$ Corrosion Inhibiting Hydrotalcite Pigments in Epoxy Resins," p. 270 in the Proceedings of the Electrochemical Society, PV2003-23, The Electrochemical Society, Pennington, NJ (2004).

R.G. Buchheit, "Historical Perspective on Conversion Coating s for Light Metals," p. 430, ECS PV2002-13, The Electrochemical Society, Pennington, NJ (2002).

Y. Yoon, R.G. Buchheit, The effect of Artificial Heat Treatment on the Chromate Conversion Performance of Al-Xn-Mg-Cu Alloys," Tri-Service Corrosion Conference, January 14-18, 2002, San Antonio TX. (in press).

W. Zhang, R.G. Buchheit, "Aging of Chromate Conversion Coatings", Tri-Service Corrosion Conference, January 14-18, 2002, San Antonio TX.

R. Boger, R. Buchheit, " Copper Release from Corroding Al-Cu Alloys Measured Using a Rotating Ring Disk Electrode," p. 19, ECS PV00-23, The Electrochemical Society, Pennington, NJ (2001).

J. Ramsey, R. McCreery, R.G. Buchheit, "Chromate Inhibitor Interactions with Aluminum Aircraft Alloy Probed with Vibrational Spectroscopy," p. 79, ECS PV00-23, The Electrochemical Society, Pennington, NJ (2001).

N.N. Voevodin, V.N. Balbyshev, A.J. Vreugdenhil, J. A. Johnson, M. S. Donley," Evaluation of Corrosion Protection Performance of Sol-Gel Surface Treatments on AA2024-T3, - Advanced Affordable Materials Technology," Proceedings of 33rd International SAMPE Technical Conference, Seattle, WA, Nov 4-8, 2001.

N.N. Voevodin, M. Donley, "Electrochemical Spectroscopy for Lifetime Prediction Studies," Proceedings of the 198th Meeting of the Electrochemical Society, October 22-27, 2000, Phoenix, AZ.

V. Laget, C. Jeffcoate, H. S. Isaacs, R. G. Buchheit, "Thermal Stability and Aging Characteristics of Chromate Conversion Coatings on Aluminum Alloy 2024-T3,", p. 173, Corrosion and Corrosion Control in Saltwater Environments, P. M. Natishan, S. Ito, D. A. Shifler, and T. Tsuru, Eds., PV 99-26, The Electrochemical Society, Inc., Pennington, NJ (1999).

R. G. Buchheit, R. K. Boger, M. W. Donohue, "Copper Dissolution Phenomena in Al-Cu and Al-Cu-Mg Alloys", p. 205, Corrosion and Corrosion Control in Saltwater Environments, P. M. Natishan, S. Ito, D. A. Shifler, and T. Tsuru, Eds., PV 99-26, The Electrochemical Society, Inc., Pennington, NJ (1999).

M.W. Kendig, S. Jeanjaquet, R. Buchheit, H. Guan, R. Leard," Electrochemical Aspects of Dealloyed (Cu,Mg)Al_2, " p. 1, ECS PV00-23, The Electrochemical Society, Pennington, NJ (2001).

R. K. Boger, R. G. Buchheit, "Copper Release from Corroding Al-Cu Alloys Measured Using a Rotating Ring-Disk Electrode'", p. 205 , Corrosion and Corrosion Control in Saltwater Environments. P. M. Natishan, S. Ito, D. A. Shifler, and T. Tsuru. PV 99-26, The Electrochemical Society, Inc., Pennington, NJ (1999).

Books and Chapters

R.G. Buchheit, "Use of Ion Exchange Compounds as Corrosion Inhibiting Pigments in Organic Coatings", ACS Book Series, May 2005 (in preparation).

R.G. Buchheit, "Corrosion Resistant Coatings and Paints," in Handbook of Environmental Degradation of Materials,' Myer Kutz, Ed., William Andrew Publishing, New York (2005).

R.G. Buchheit, R.G. Kelly, N.A. Missert, B.A. Shaw, Corrosion of Light Metals, ECS PV 2003-23, The Electrochemical Society, Pennington, NJ 2004.

R.G. Kelly, J.R. Scully, D.A. Shoesmith, R.G. Buchheit, Electrochemical Techniques in Corrosion Science and Engineering, Marcel Dekker, New York (2003).

R.G. Buchheit, "Filiform Corrosion," Metals Handbook Vol. 13A, ASM International, in press, anticipated release (2003).

R.G. Buchheit, A.E. Hughes, "Chromate and Chromate-Free Conversion Coatings," p. 720 in Metals Handbook Vol. 13A, S.D. Cramer, B.S. Covino, Eds., ASM International (2003).

R.G. Buchheit, sub-section Chair, "Surface Treatments and Conversion Coatings, SC-4b, Metals Handbook Vol. 13A, ASM International, in preparation, anticipated release (2003).

K. Ogle and R. G. Buchheit, "Conversion Coatings," in *Encyclopedia of Electrochemistry*, edited by A. J. Bard and M. Stratmann, *Vol. 4, Corrosion and Oxide Films*, edited by M. Stratmann and G. S. Frankel, pp. 460-499, Wiley-VCH, Weinheim, Germany, 2003.

B. A. Shaw, R. G. Buchheit, J. P. Moran, Eds., Corrosion and Corrosion Protection of Low Density Metals and Alloys, ECS PV00-23, The Electrochemical Society, Pennington, NJ (2001).

R. G. Buchheit, M. R. Jaworoski, P. D. Chalmer, Eds., Surface Conversion for Aluminum and Ferrous Alloys, Proceedings of the 2000 Research Topical Symposium, NACE International, Houston, TX (2000).

Patents

R.G. Buchheit, H. Guan, V.N. Laget, “Active Corrosion Protection and Corrosion Sensing in Chromate-Free Organic Coatings,” U.S. Provisional Patent Application, 60/606,757, September 1, 2004.

R. G. Buchheit, H. Guan, V. N. Laget, "Corrosion Resistant Coating," Utility U.S. Patent filing, OSU1159-174A, January 2004.

R. G. Buchheit, H. Guan, V. N. Laget, "Corrosion Inhibiting Pigment," Ohio State patent application submitted, 01ID108U, June, 2001.

Appendix A

Science-based Approaches for Cr-free Corrosion Protection PP-1119

Rudolph G. Buchheit
Ohio State University

Final Debrief

June 29, 2005

Background

- This project was initiated in 1999.
- A second phase was initiated in 2003.
- Each phase addressed a different SON.
  - The first was related to reverse engineering chromate corrosion protection.
  - The second was to use lessons learned to develop environmentally friendly coating systems.

Technical Objectives and Approach

Our objective is to use our understanding of corrosion protection by chromates to develop functional equivalents for:

- Conversion coatings based on rapid, spontaneous coating formation due to inorganic polymerization in V, Mo, Fe, W systems.
  Demonstrate performance that is generally consistent with MIL-C-81706/MIL-C5541E conversion coatings.

- Corrosion-inhibiting organic coatings by replacement of $SrCrO_4$ pigments with ion exchange compounds.
  Demonstrate performance that is generally consistent with MIL-P-23377 primer coatings.

Our main focus has been on protection of aluminum alloy substrates.

$Cr(OH)_3$ polymerization plays an important role in CCC formation

Hydrolysis-polymerization-precipitation mechanism for $Cr(OH)_3$ "backbone" formation.

Condensation of Cr(VI) on the Cr(III) backbone by nucleophilic attack of hydroxyl ligands in the backbone.

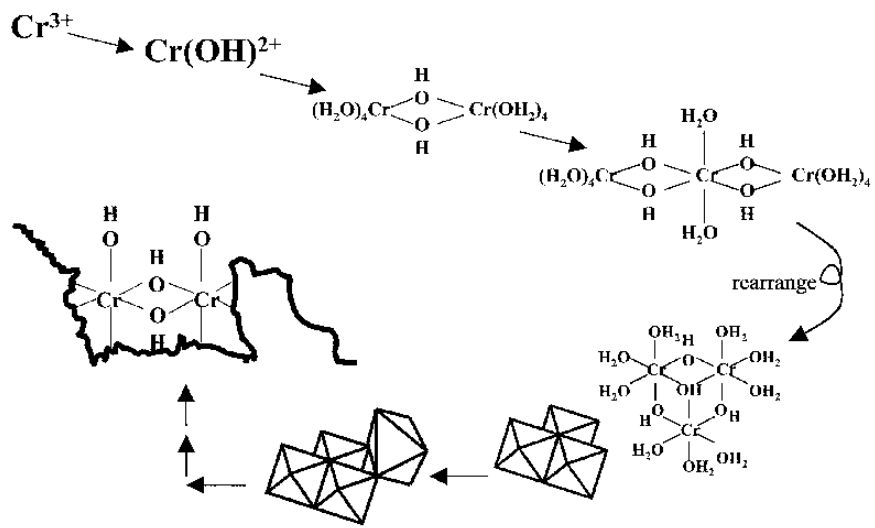

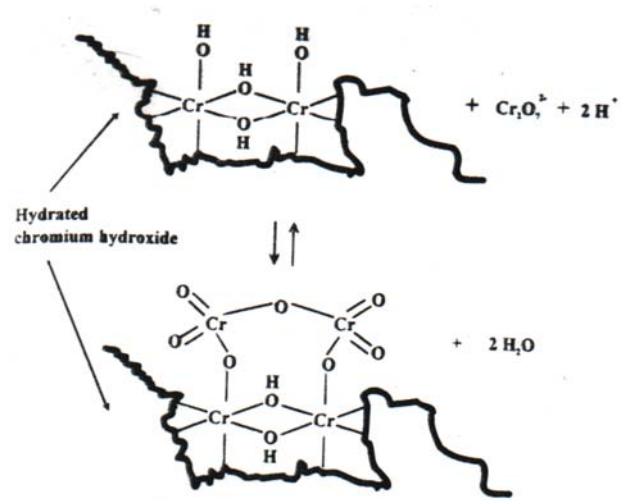

L. Xia, R.L. McCreery, J. Electrohem. Soc., 145, 3083 (1998).

PP-1119 (part I) showed that polymerization of hydrolyzed Cr affects all CCC properties

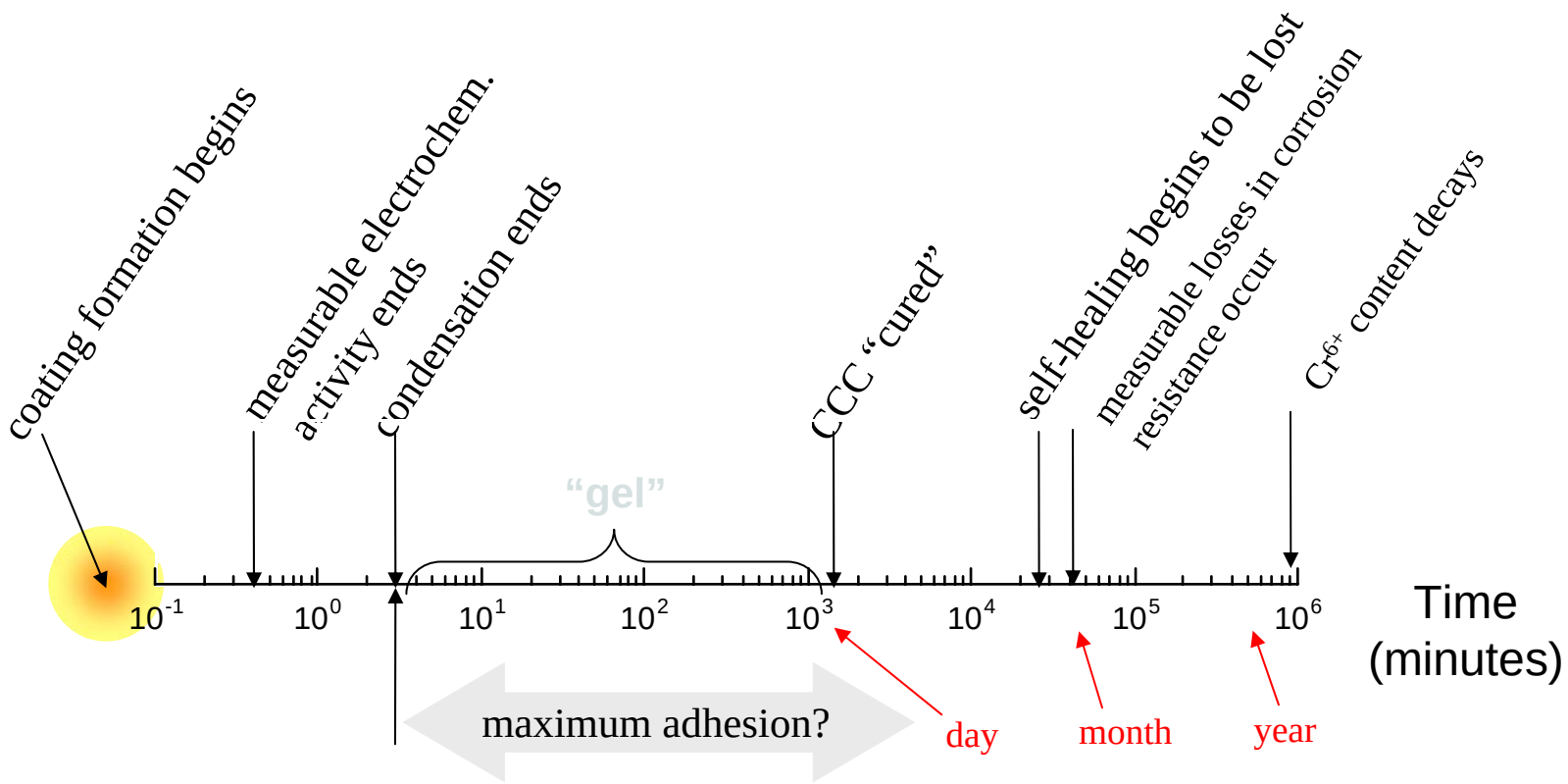

condensation polymerization leads to film formation

dehydration polymerization leads to coating degradation.

PP-1119 (part II) conversion coating work capitalized on vanadium polymerization

- near surface pH increases due to surface-catalyzed proton reduction
- ”rapid” monomeric hydrolysis of V^{5+} is triggered: $VO_2^+ + 2H_2O \rightarrow VO(OH)_3 + H^+$
- At $pH_{pzc} \sim 2$: $VO(OH)_3 + 2H_2O \rightarrow VO(OH)_3(OH_2)_2$
- addition of H_2O leads to olation (OH bridging) and oxolation (O bridging)
- hydrated V^{5+} gel formation ensues.
- V^{3+} or V^{4+} gels may form by a hydrolysis- condensation- polymerization processes analogous to those for Cr^{3+} and Ti^{4+} gels.

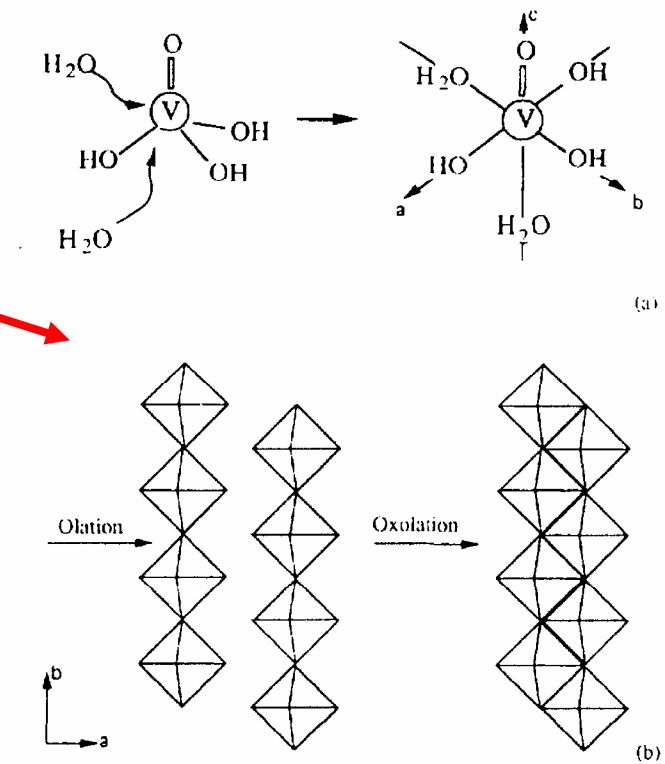

J. Livage, Solid State Ionics, 86-88, 935 (1996).

The VCC process is identical to immersion chromate conversion coating processes

Clean
↓
Alkaline Clean
↓
Rinse
↓
Deoxidation
↓
Rinse
↓
Conversion Coat
↓
Rinse
↓
Dry

- 2024-T3 panels degreased and deoxidized.
- 3 minute simple immersion in coating bath at RT.
- A yellow integral layer was formed on the alloy surface.

VCC

CCC

Vanadium-based conversion coating (VCC) formed on 2024-T3

- 2024-T3 panels degreased and deoxidized.
- 3 minute simple immersion at RT.
- A yellow integral layer was formed on the alloy surface.

VCC Before SST

VCC after 168 h SST

2024-T3

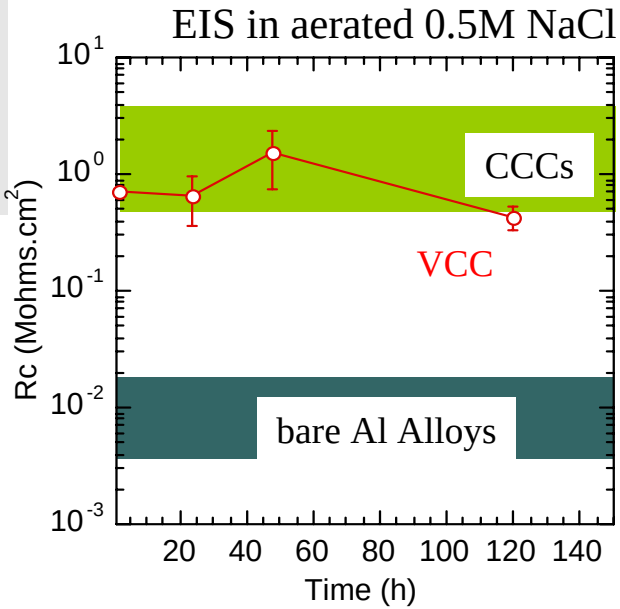

New findings (2004):

- V-Fe interaction is critical for VCCs formed from acidic baths.
- A new Fe-free, neutral pH VCC formulation has been devised.
- BF_4^- and ZrF_6^{2-} additions to acidic VCC formulations improve corrosion resistance.

Mo, W, Fe, Ce-based conversion coating summary

Coating corrosion resistance determined by EIS after exposure to aerated 0.5M NaCl for 24±1 h

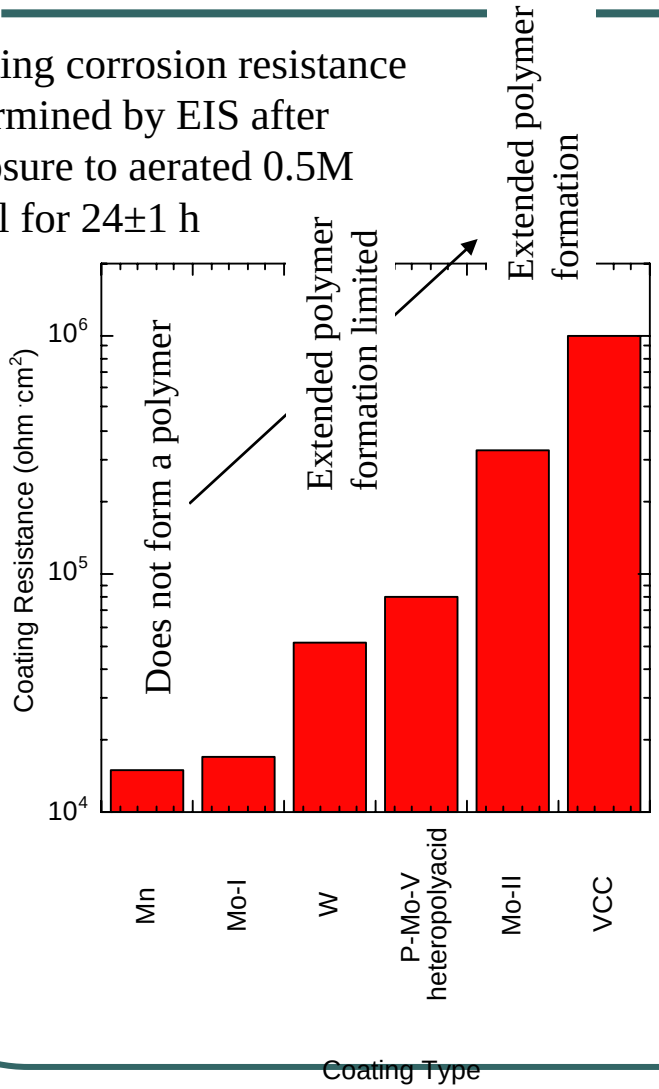

- Corrosion resistant conversion coating formation appears to be related to extended polymer network formation
- Extended polymer formation depends on pH, ion concentration, co-polymer formers
- Fe appears to be an exception to the corrosion resistance-polymerization trend. Prussian blue and Berlin green-type Fe(III)-Fe(II) polymer films are readily formed on Al substrates, but corrosion protection is negligible.
- Ce is also an exception. It is not a polymer former, but confers good corrosion protection to Cu-bearing Al alloys.

$SrCrO_4$-pigmented primers

25 v/o $SrCrO_4$ in polyamide-cross linked epoxy
CrO_4^{2-} inhibitor derived from sparingly soluble $SrCrO_4$.

2 mils
50 µm

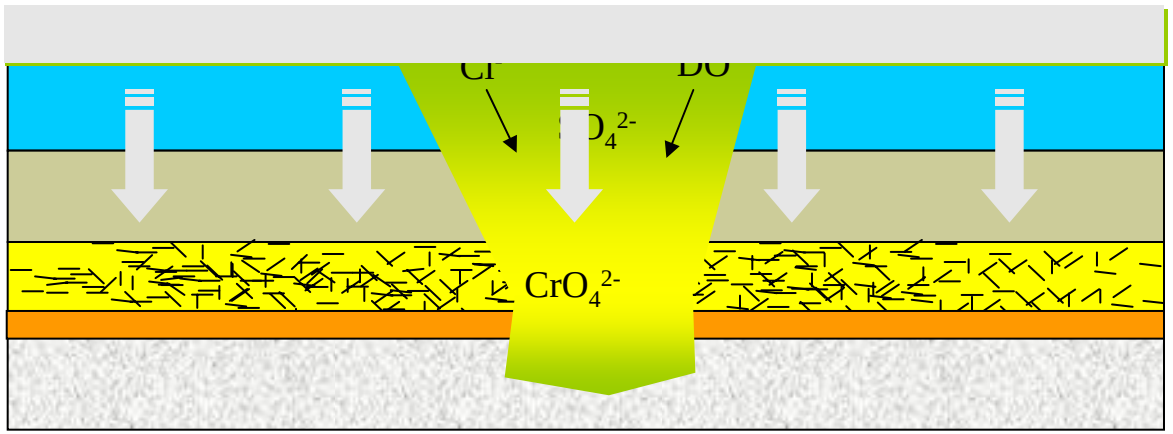

Second topcoat

Topcoat

Primer

Conversion coating

Substrate

Corrosion inhibition occurs when:

$C_{saturation} > C_{coating} > C_{inhibition}$

pH near neutral

To release the proper inhibitor "dose", synthetic ion exchange compounds are used

- Cationic clays (montmorillonites, bentonites)
  Bohm et al.. Werkst. u. Korros., 52, 896 (2001).

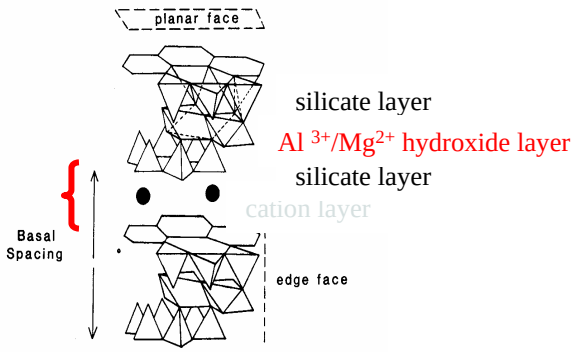

Huang, et al., J. Coll. & Interf. Sci. (2002).

- Anionic clays (hydrotalcites).
  Buchheit, et al., POC, 47, 174 (2003).

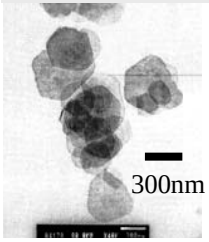

Kloprogge, Appl. Clay Sci.(2001).

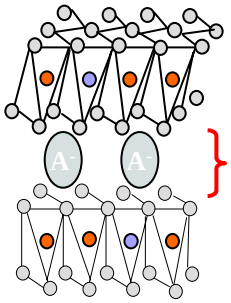

~ $Zn_{0.65}Al_{0.35}(OH)_2$
4.77 Å†
~ Z_{net} = +0.35 eq/mol
Gallery height depends on layer composition.

- OH
- Zn
- Al

Hosts
$Li_2[Al(OH)_3]_2^+$
$Ni[Al(OH)_3]_2^{2+}$
$Zn[Al(OH)_3]_2^{2+}$
$Mg[Al(OH)_3]_2^{2+}$

Exchangable inhibitors
MnO_4^-
VO_3^-
$V_{10}O_{28}^{6-}$
MoO_4^{2-}
$Fe(CN)_6^{4-/3-}$
NO_3^-

- high inhibitor capacity 2-30 meq ions /g.
- enormous chemical diversity--hundreds of synthetic compounds already demonstrated.
- can store organic or inorganic anions or cations. and them with reasonable exchange (inhibitor release) kinetics.
- compatible with organic resins.

NSS exposure reveals differences in protective ability of the pigments

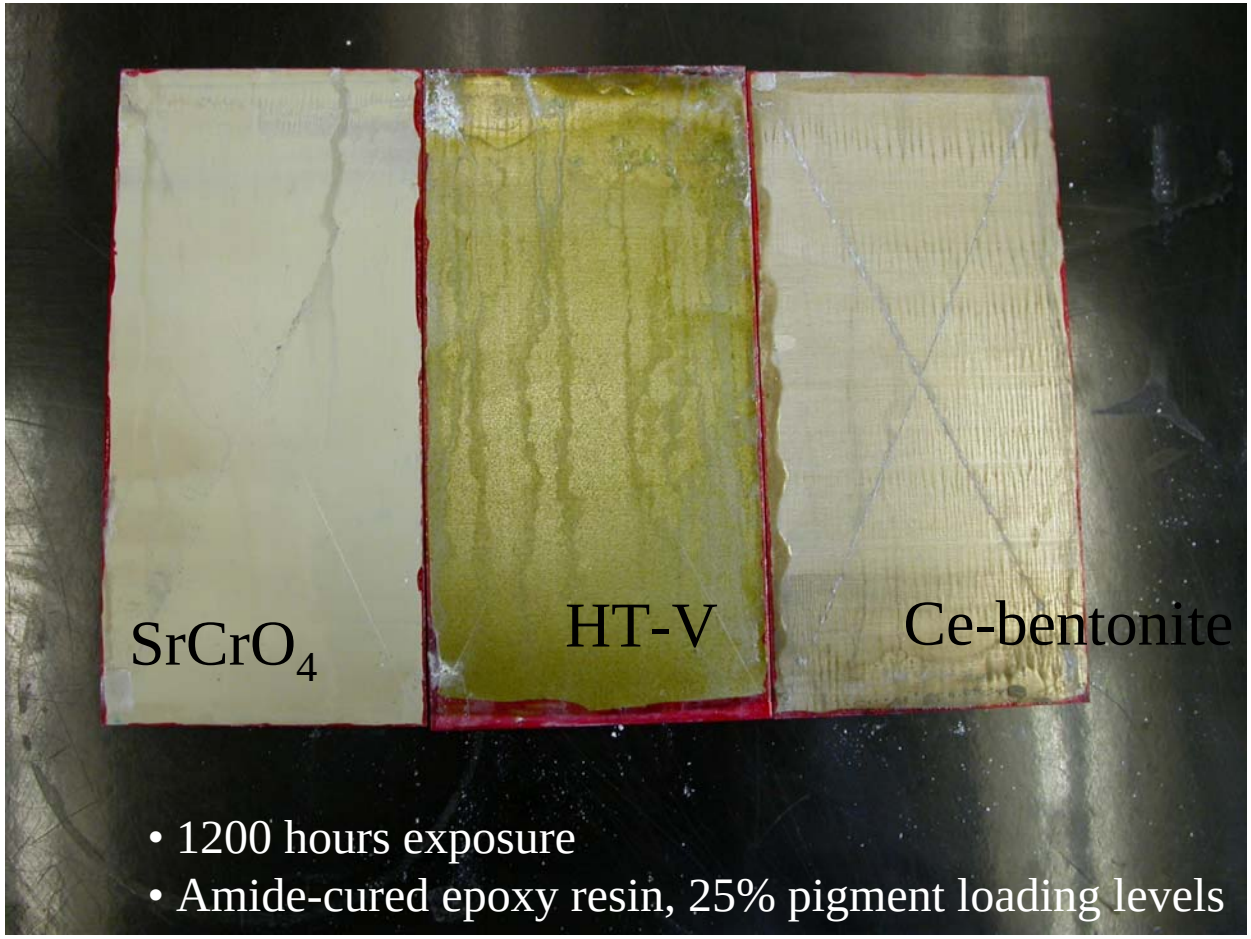

- 1200 hours exposure
- Amide-cured epoxy resin, 25% pigment loading levels

PP-1119 Publications and Research Output

Total publications (as of 10/15/04)	50
Peer reviewed articles	23
Books	1
Edited books	3
Book chapters	4
Proceedings	15
Patent Filings	4
Invited Presentations	16

Post-doctoral researchers supported:

A. Sehgal	1999	Micron, U.S.
V. Laget	1999-2001	Suiza-Aero, France
C. Paglia	2001-2003	Helbling Ing. AG, Switz.

Total Ph.D. Dissertations: 7

Ramsey	Chem	2002	ABQ
Zhang	MSE	2002†	Alcoa TC
Voevodin	MSE	2002	AFRL
Meng	MSE	2003 †, ††	USNA
Hurley	Chem	2004	TBD
Yoon	MSE	2004	TBD
Jain	MSE	2005	

Total M.S. Theses: 4

Boger	MSE	2000†	Ph.D./OSU
Wu	Chem.	2000	
McGovern	Chem.	2000	Ph.D./OSU
Leard	MSE	2001†	AFRL

† earned NACE awards for research
†† Morris Cohen Grad Student Award, ECS

Transition Plan

To transition our work, we must get the word out to prospective customers and vendors. Ohio State issued a press release in late August 2004, which has triggered a number of news stories:

"OSU Engineers Create Anti-corrosion paint"	Columbus Dispatch 9/1/04
"Smart Paint reduces pollution and adds protection at low cost"	Cleveland Plain Dealer 9/9/04.
"Paint's Smart Pigment Stops Corrosion"	www-applesforhealth-com
"Smart Paint"	Waste News, 9/27/04.

TV story in production by the American Institute of Physics

Transition Plan

- We have a formal collaboration with Shepherd Color Company, Cincinnati, OH to begin the commercialization process for some of our Cr-free pigments.

    - Independently verified our findings on corrosion protection
    - We have entered into a mutual non-disclosure agreement
    - SCC is sponsoring H.Guan,our staff chemist to work exclusively on validation and reduction to practice.

- We have briefed another international paint commodities company headquartered in Ohio on our Cr-free corrosion protection work. We are supplying Cr-free pigments for their evaluation.

The Shepherd Color Company is a privately held producer of inorganic pigments, specifically, Complex Inorganic Colored Pigments. These pigments, due to their extreme stability, are used in high performance coatings, plastics, glass enamels, and high heat coatings. They are headquartered in Cincinnati, OH with offices in Belgium and Australia.

Summary

- Chemically-triggered polymerization can lead to formation of conversion coatings that have useful properties:

  - rapid and spontaneous formation
  - self-healing characteristics

- The concept of ion exchange compounds as store-and-release corrosion-inhibiting pigments appears to be viable:

  - pigments are dispersible and compatible
  - useful levels of corrosion protection can be imparted.

Vanadium toxicity

- Vanadium is **not a cancer-causing agent** in mammals, but it is known to produce some adverse health effects .
- Acute over-exposure results in inflammation in the lungs and mucous linings of the respiratory tract.
- Effects of chronic vanadium exposure range from no observable symptoms to decreased immunity to pulmonary diseases.
- Vanadium is absorbed poorly by the gastrointestinal tract, and vanadium ingestion is not considered a significant route of entry into the body.
- The effects of vanadium on reproductive health have not been established with certainty.